High Resolution X-ray Spectroscopy:
An Introduction

Jörn Wilms

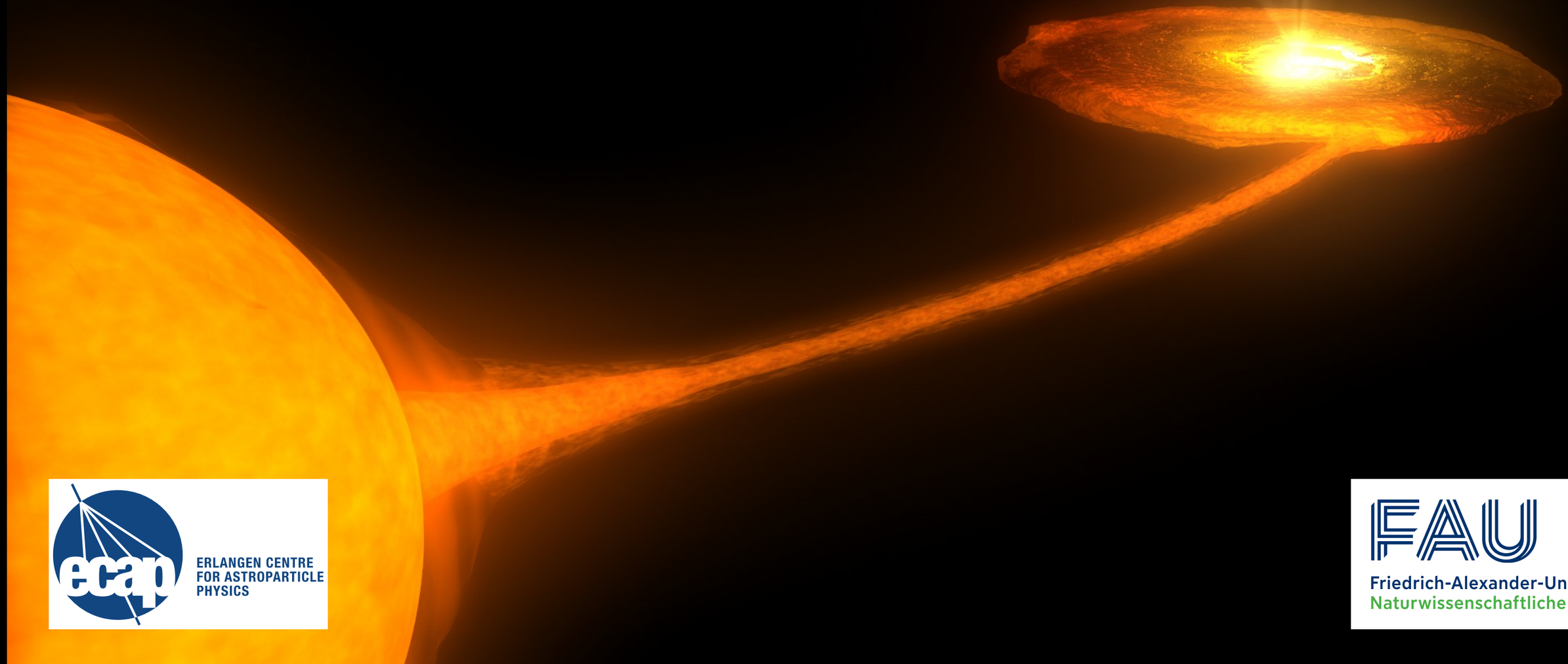

ERLANGEN CENTRE FOR ASTROPARTICLE PHYSICS

Friedrich-Alexander-Universität
Naturwissenschaftliche Fakultät

X-ray Astronomy Today

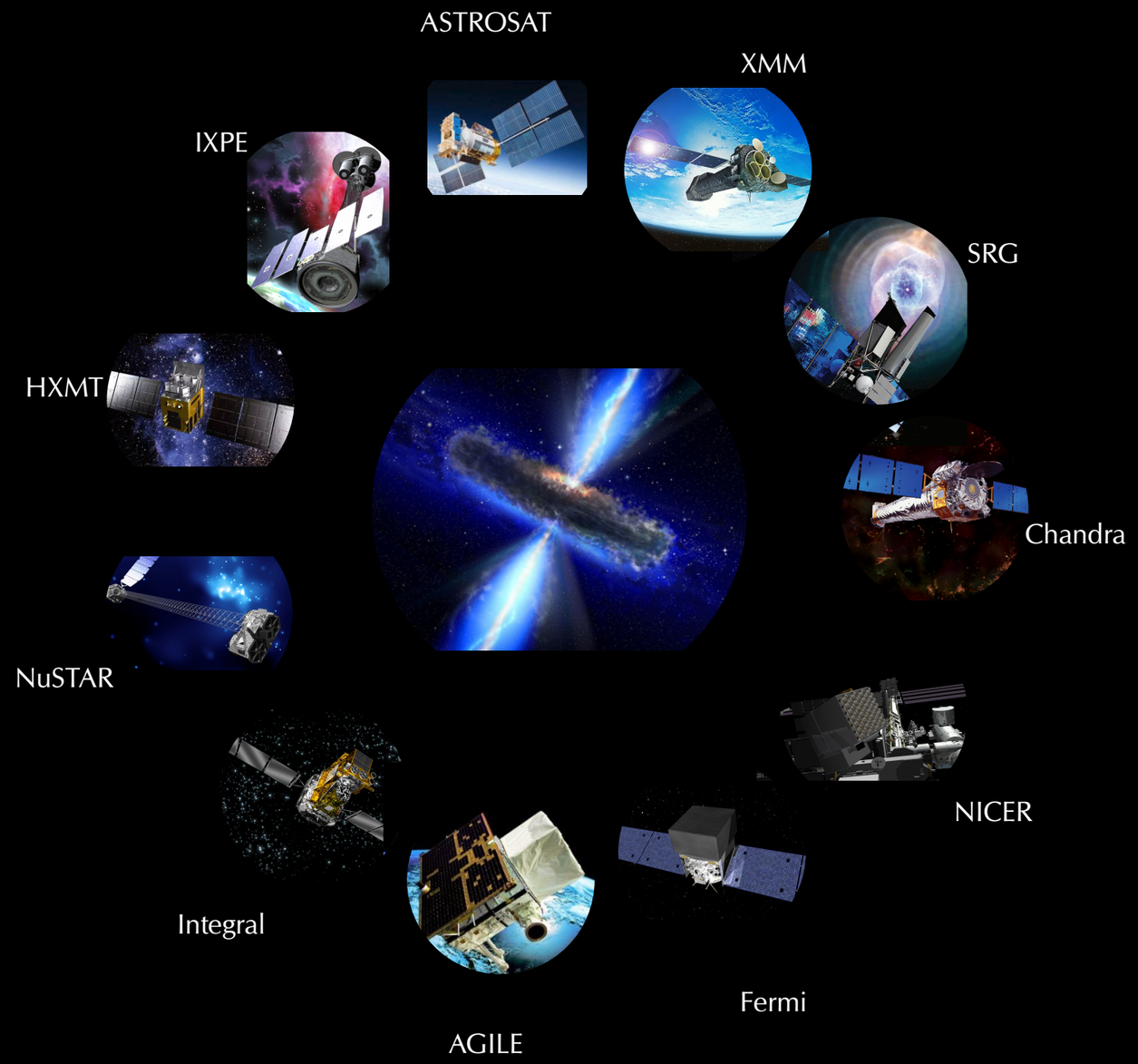

X-ray Astronomical Spectroscopy

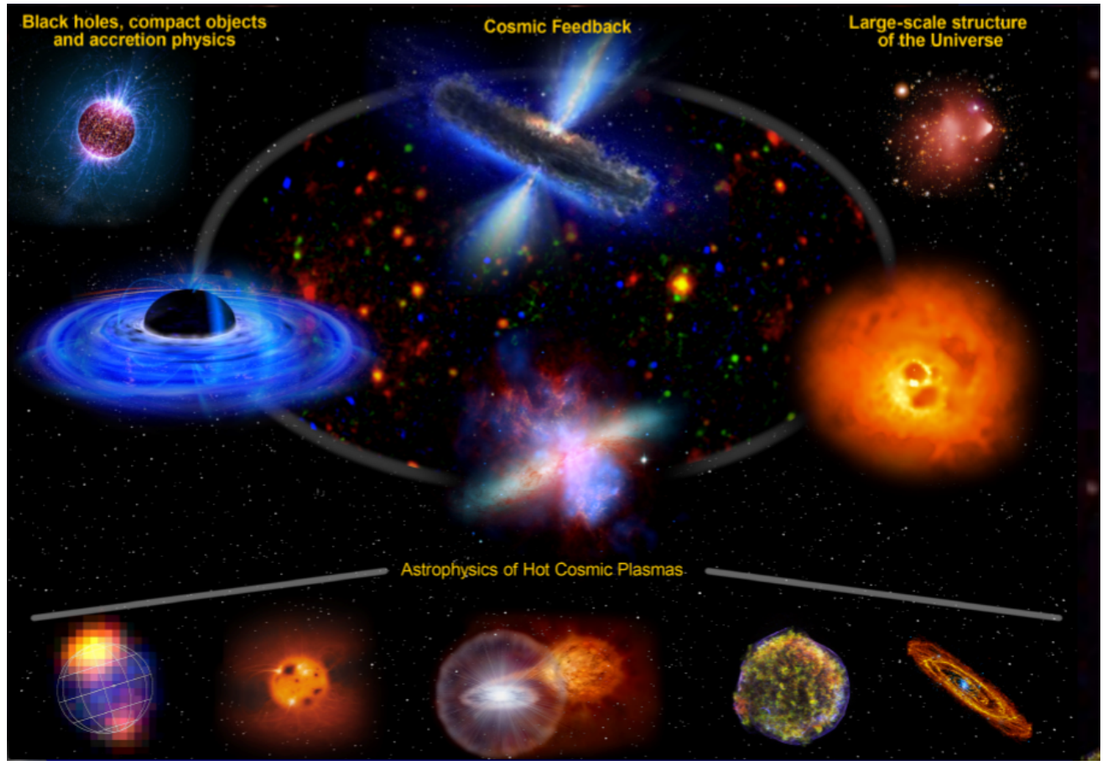

Nandra et al.

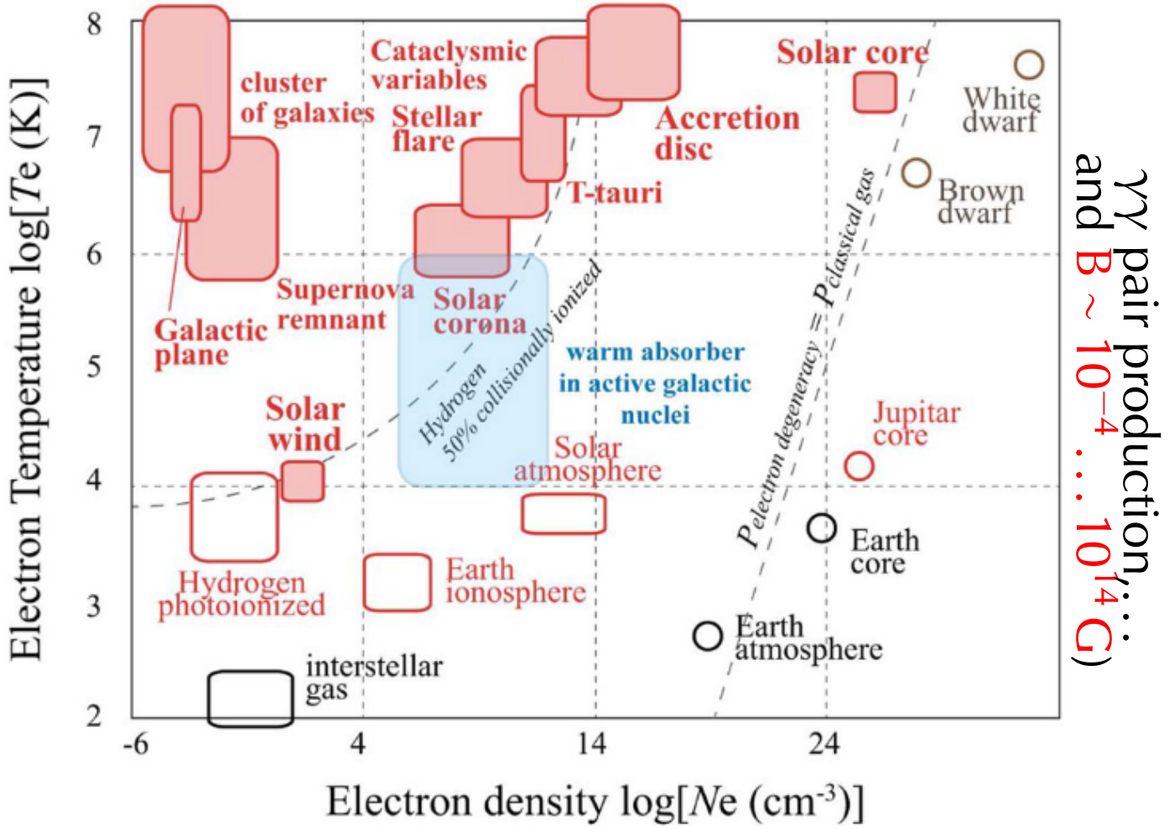

Ezoe et al., 2021, Rev. Mod. Plasma Phys. 5, 4

Pretty pictures are good for PR and, e.g., morphological studies of extended sources, but most X-ray astronomy is spectroscopy of ionized plasmas under conditions not accessible in the lab.

X-ray Astronomical Spectroscopy

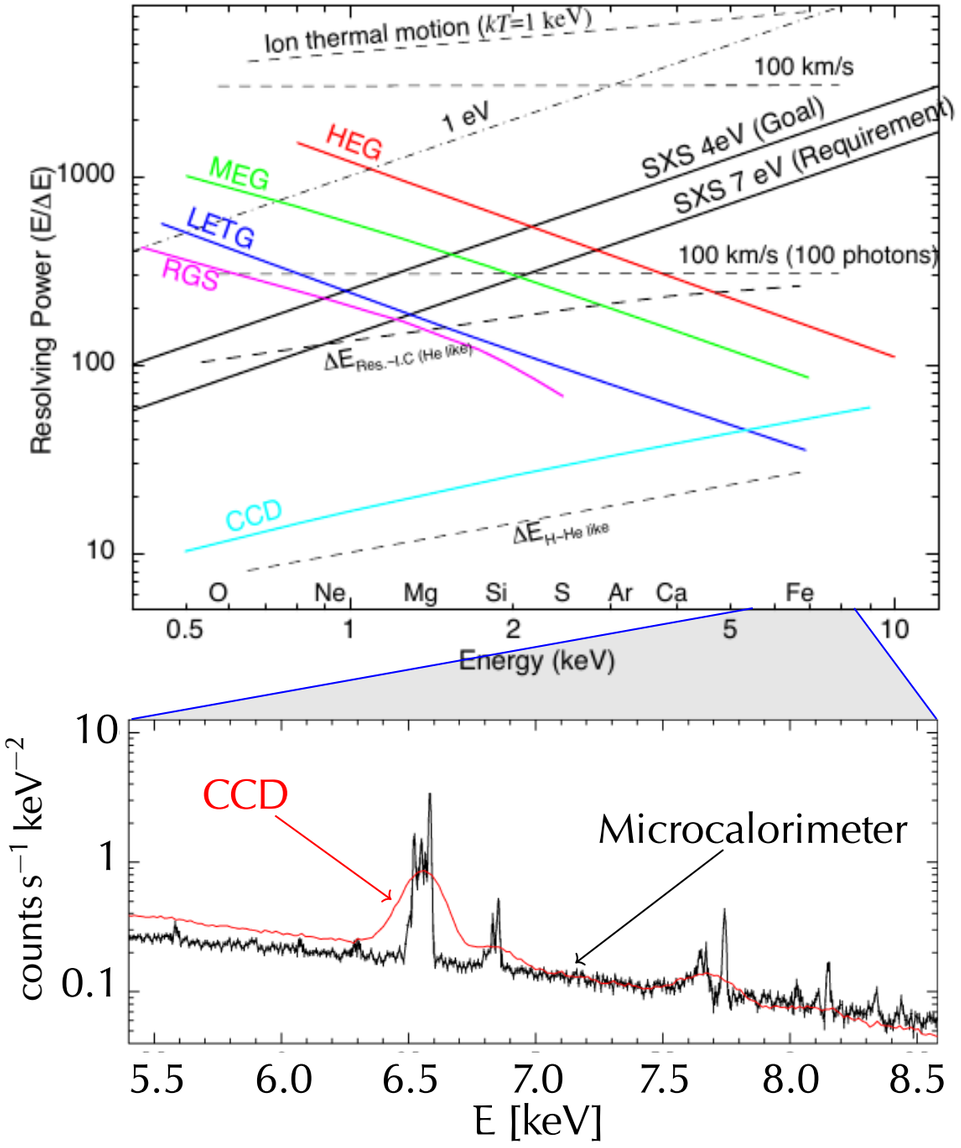

Current X-ray missions carry:

- Silicon detectors
  (at Fano limit, $\Delta E \sim 150$ eV at 5.9 keV)
- Reflection gratings
  (mainly soft X-rays, $R = E/\Delta E \sim 1000$)
- Microcalorimeters
  (0.5–10 keV, $\Delta E \sim 3$ eV; Hitomi [2016, only few spectra], XRISM [2023–], Athena [2035–])

Instruments are typically extremely well calibrated (e.g., Chandra gratings to 13 km s^{-1}, or 5–10 mÅ absolute, and few percent in flux

Count rates: 10^{-5} s … 10^{5} s

To a large extent, current missions have Si-type resolution (or worse) $\Longrightarrow$ X-ray astronomy is mainly multi-color photometry.

(Aharonian et al., 2016, Nature 535, 117)

X-ray Astronomical Spectroscopy

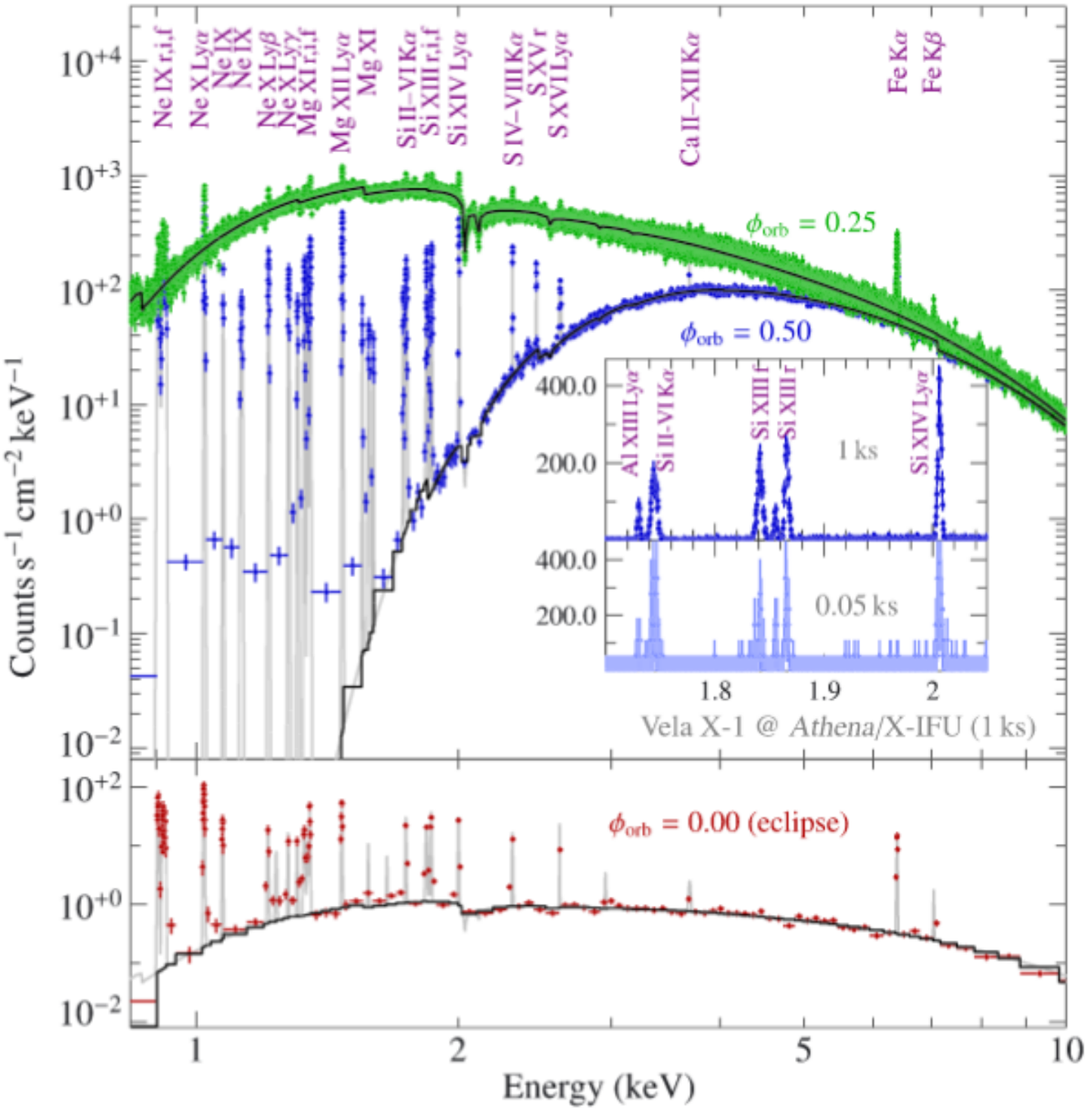

Diagnostics used:

- Density and temperature diagnostics (He-like ions, thermal broadening,...),
- Elemental abundances,
- Velocities via Doppler

and detailed collisional ionization models, photoionization modeling, and hybrid plasmas.

Requires: photoionization cross sections, *gf*-values, highly precise line energies, collisional ionization cross sections,... for all elements with $Z \lesssim 30$ and *all* ionization stages.

Predicted spectral changes for photoionized wind around neutron star Vela X-1 for Athena
(Hell et al., 2020, X-ray spectrometry 49, 218)

Line Energies: AGN Winds

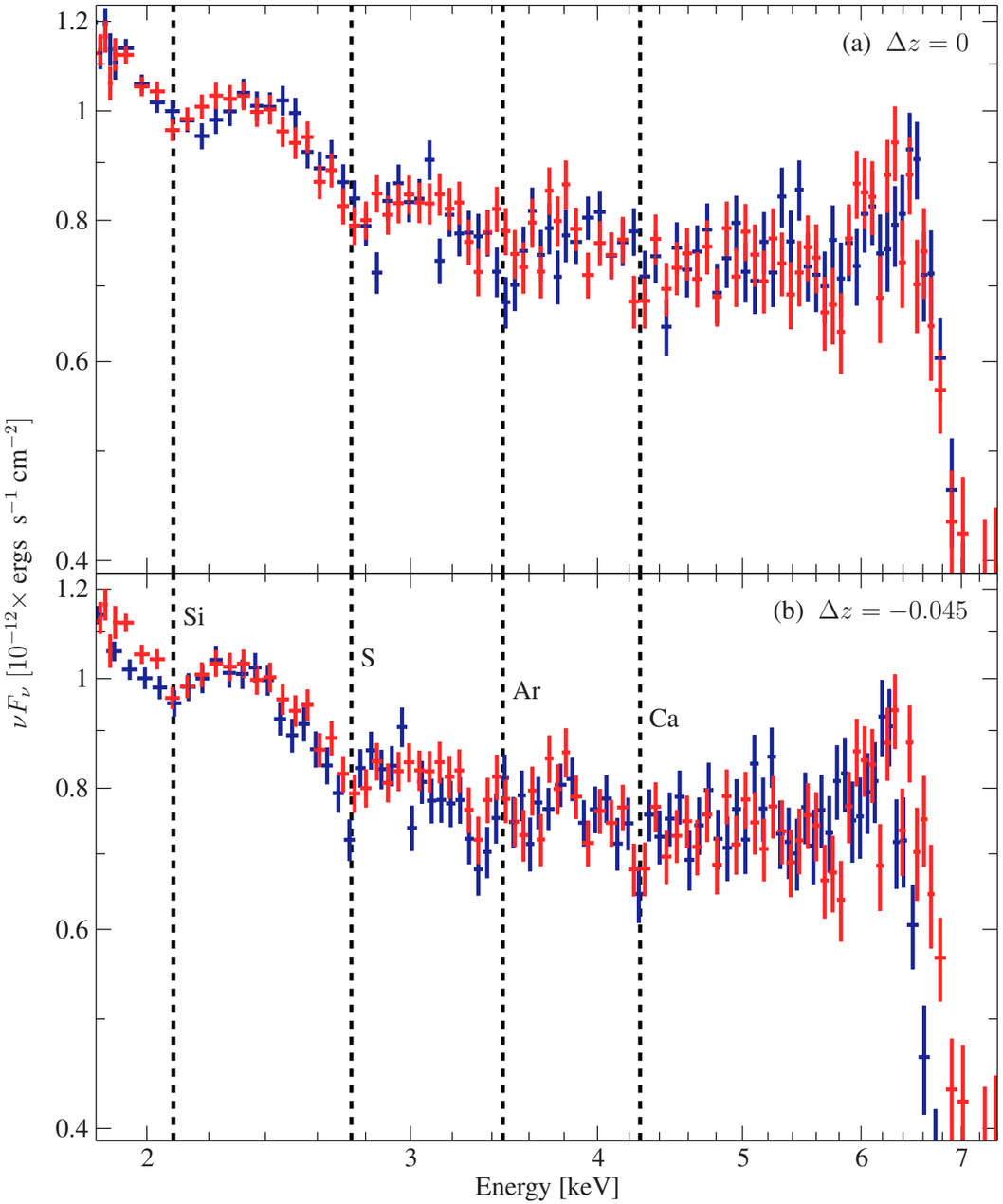

Changing lines from a radiatively driven wind around the supermassive black hole 1H0707−495

wind speeds: $z = 0.11$–0.17, $\Delta z = 0.05$ or $\Delta v = 15000\,\mathrm{km\,s^{-1}}$!

radiatively driven wind: require knowledge of line energies and transition probabilities

Dauser et al. (2012, Mon. Not. R. Astron. Soc. 422, 1914)

Line Energies: AGN Winds

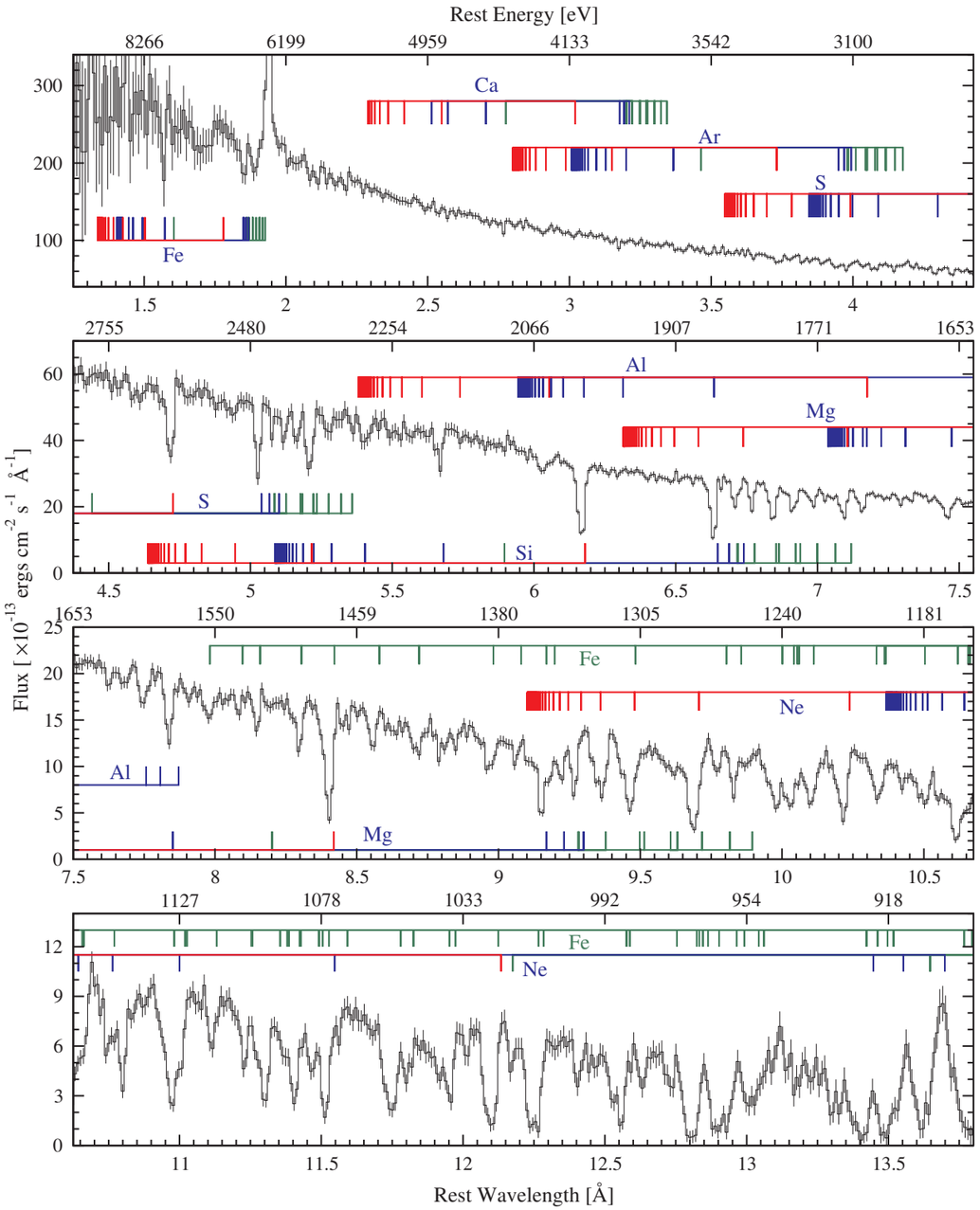

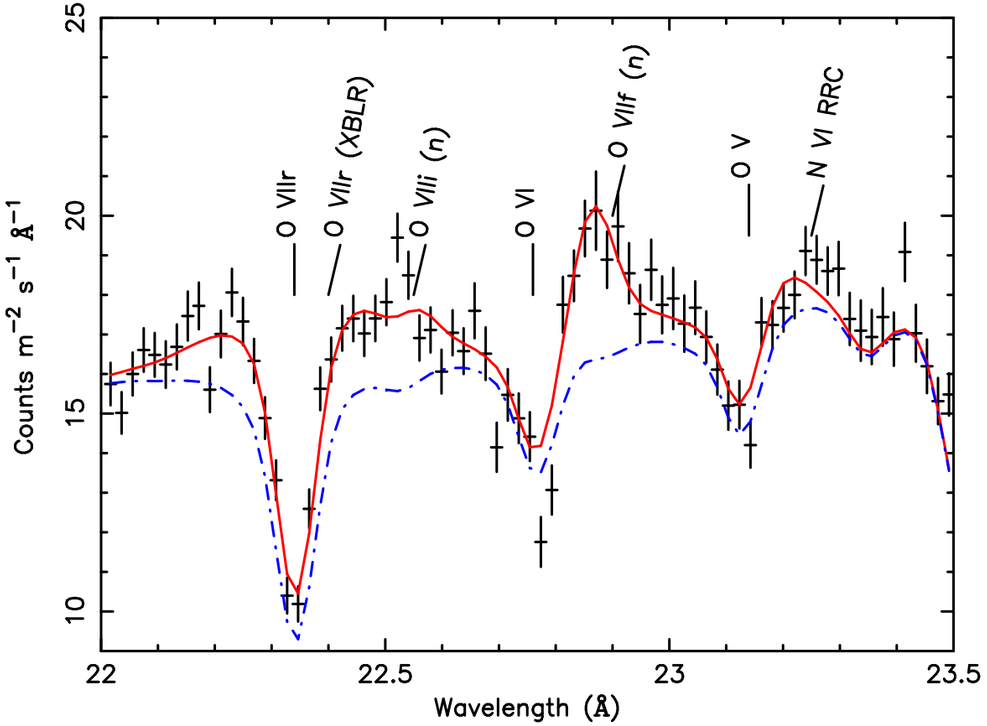

(Mrk 509 [QSO/Sy 1 hybrid]; Detmers et al., 2011, Astron. Astrophys. 534, 38)

Similar winds are seen from many accreting supermassive black holes

Require high precision knowledge of line positions, transition probabilities for photoionization calculations

NGC 3783, Chandra (Kaspi et al., 2002, Astrophys. J. 574, 643)

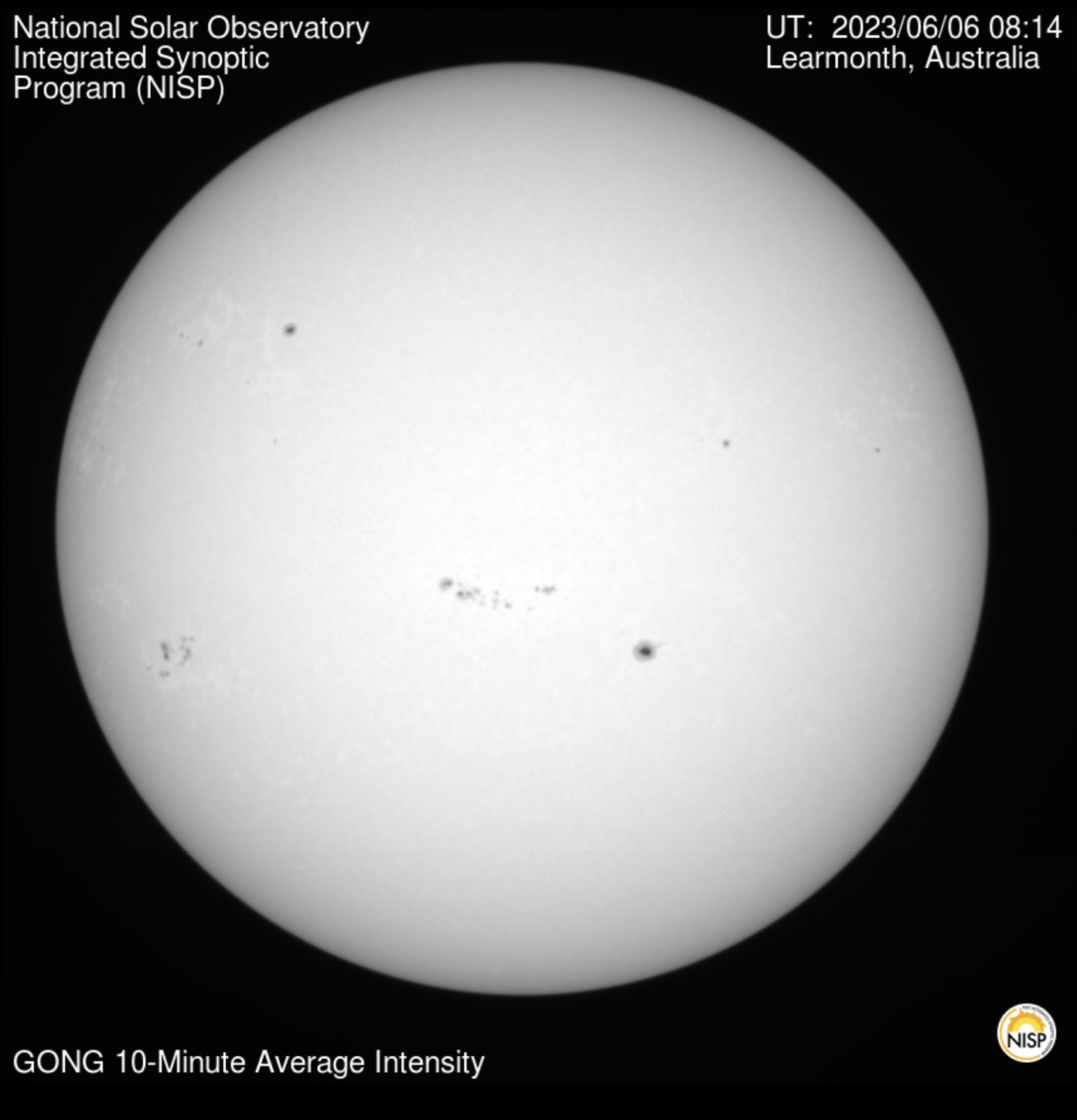

Continuum image of the Sun this Tuesday

Sun: 2023 June 06, Optical

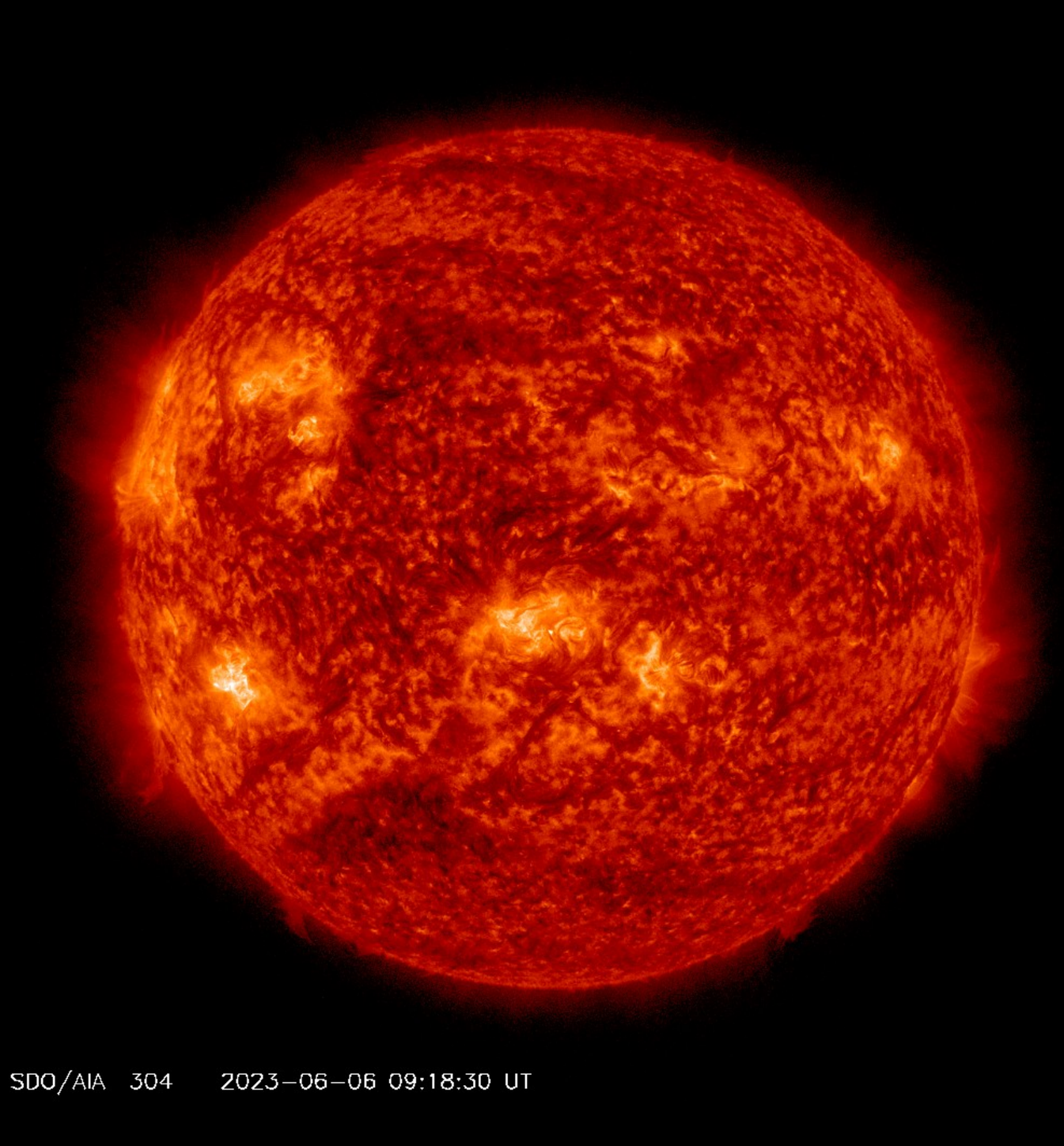

SDO (Solar Dynamics Observatory) Atmospheric Imaging Assembly (AIA) of the EUV Sun at 304 Å, showing chromospheric emission from He II (T ~ 80000 K).

Sun: 2023 June 06, EUV

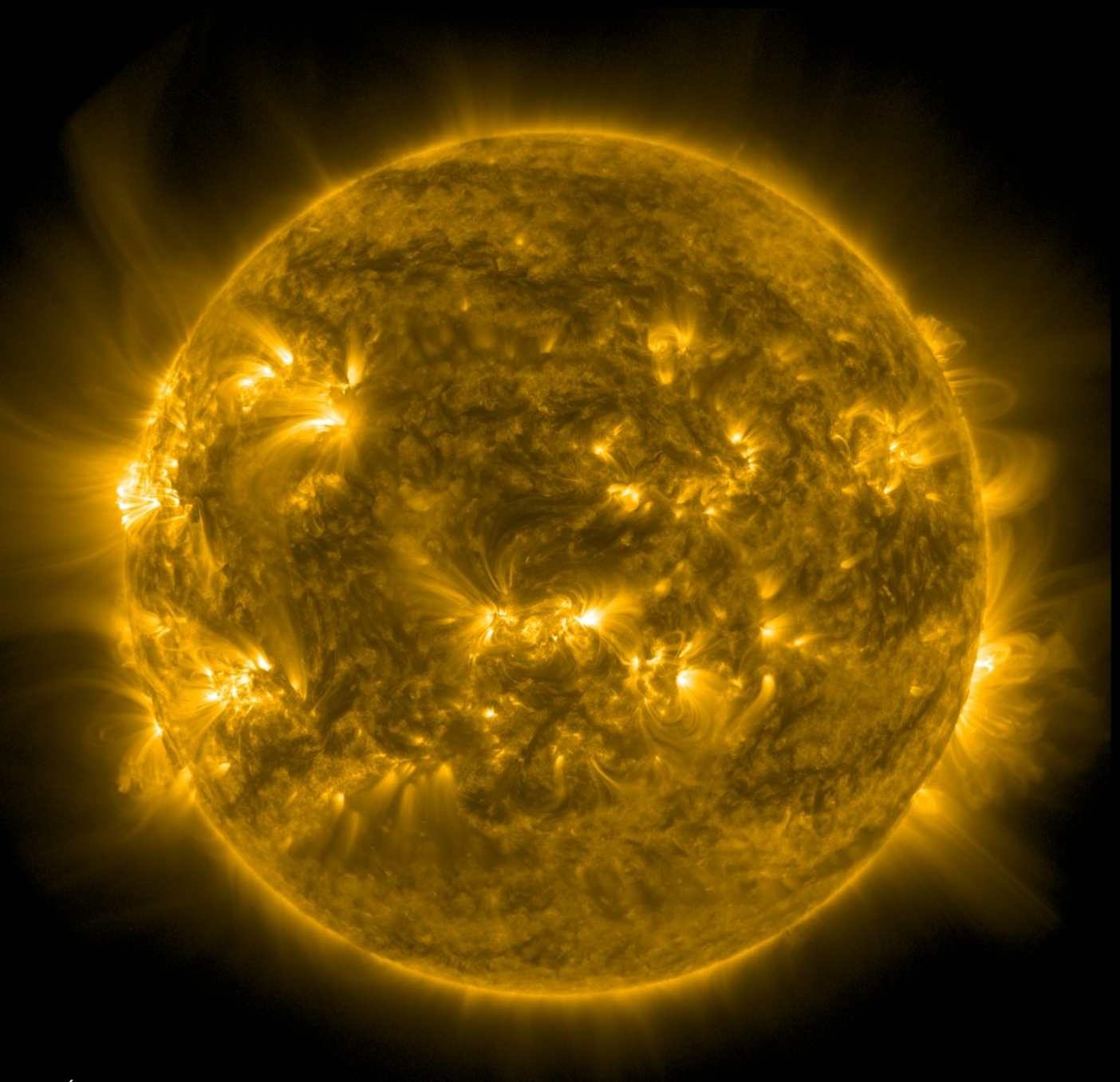

SDO AIA image of the EUV Sun at 171 Å, showing distribution of emission from highly ionized iron ions
(Fe IX/X; T ~ 10^6 K) in the lower corona.

Sun: 2023 June 06, EUV

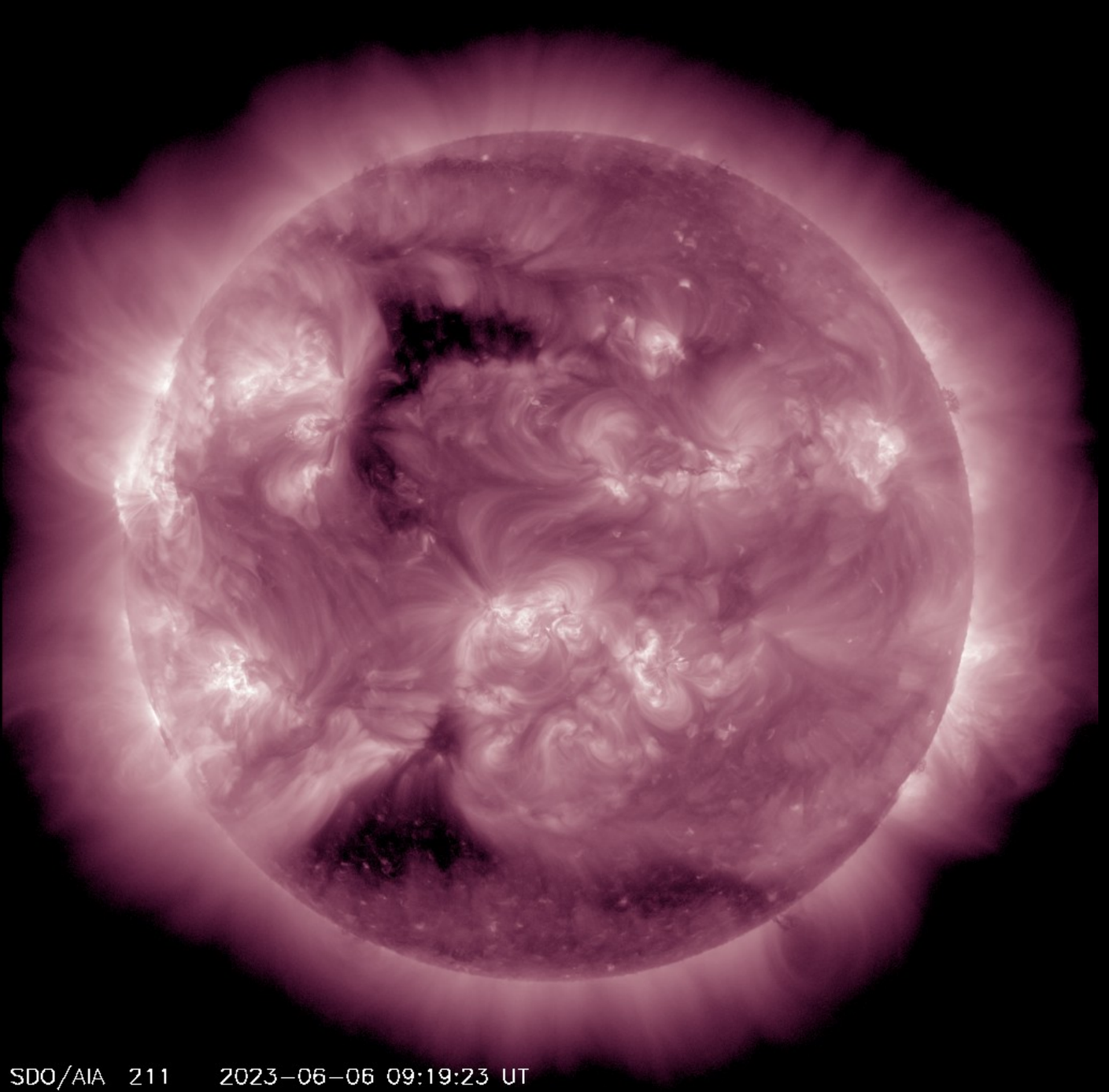

SDO AIA image of the EUV Sun at 211 Å, showing distribution of emission from Fe XIV in the upper corona.

Sun: 2023 June 06, EUV

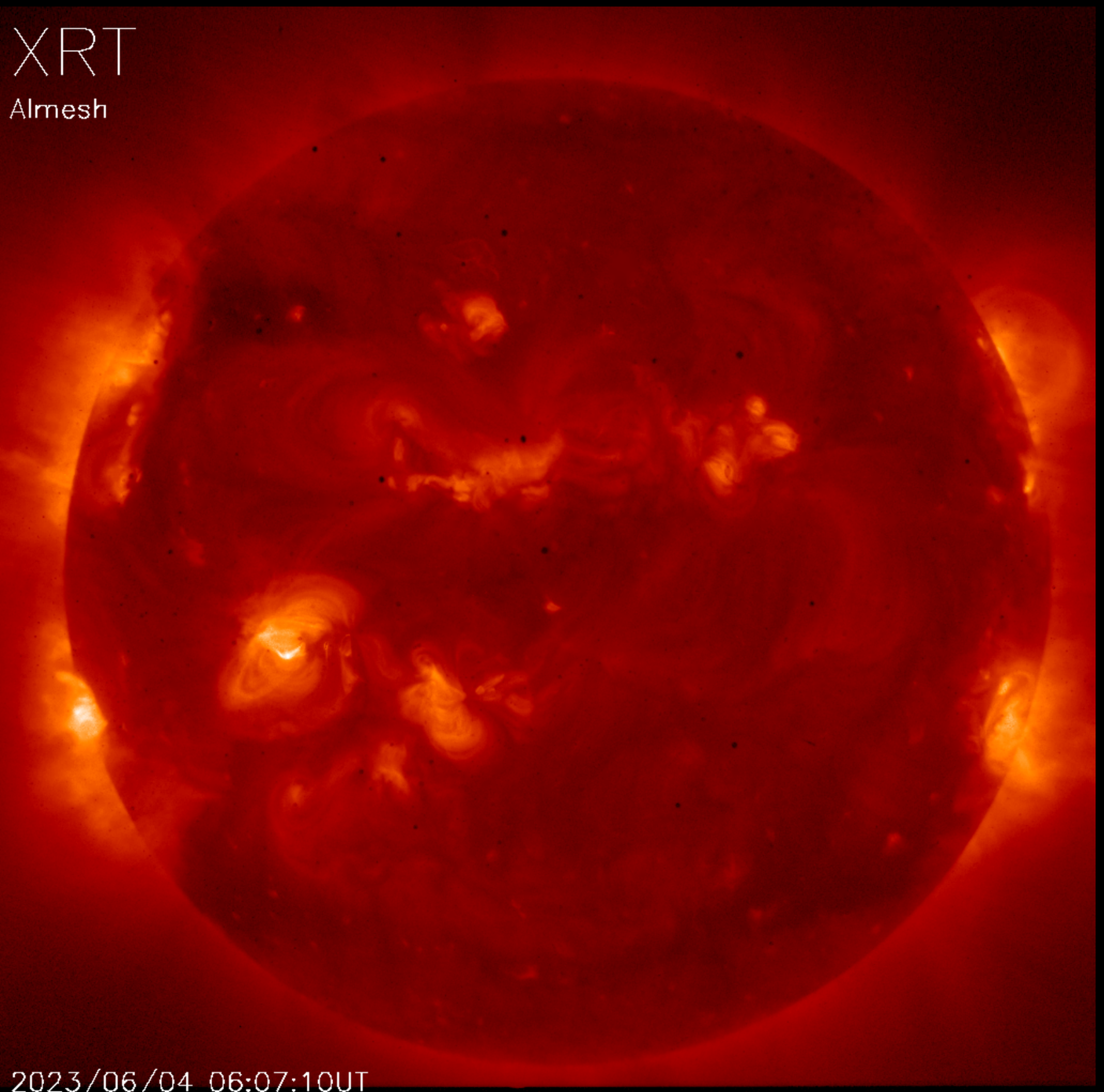

Hinode soft X-ray telescope (SXT) image of the Sun in soft X-rays, showing spatial distribution of the hottest ($T \sim 2 \times 10^6$ K) parts of the outer corona.

Sun: 2023 June 04, X-ray

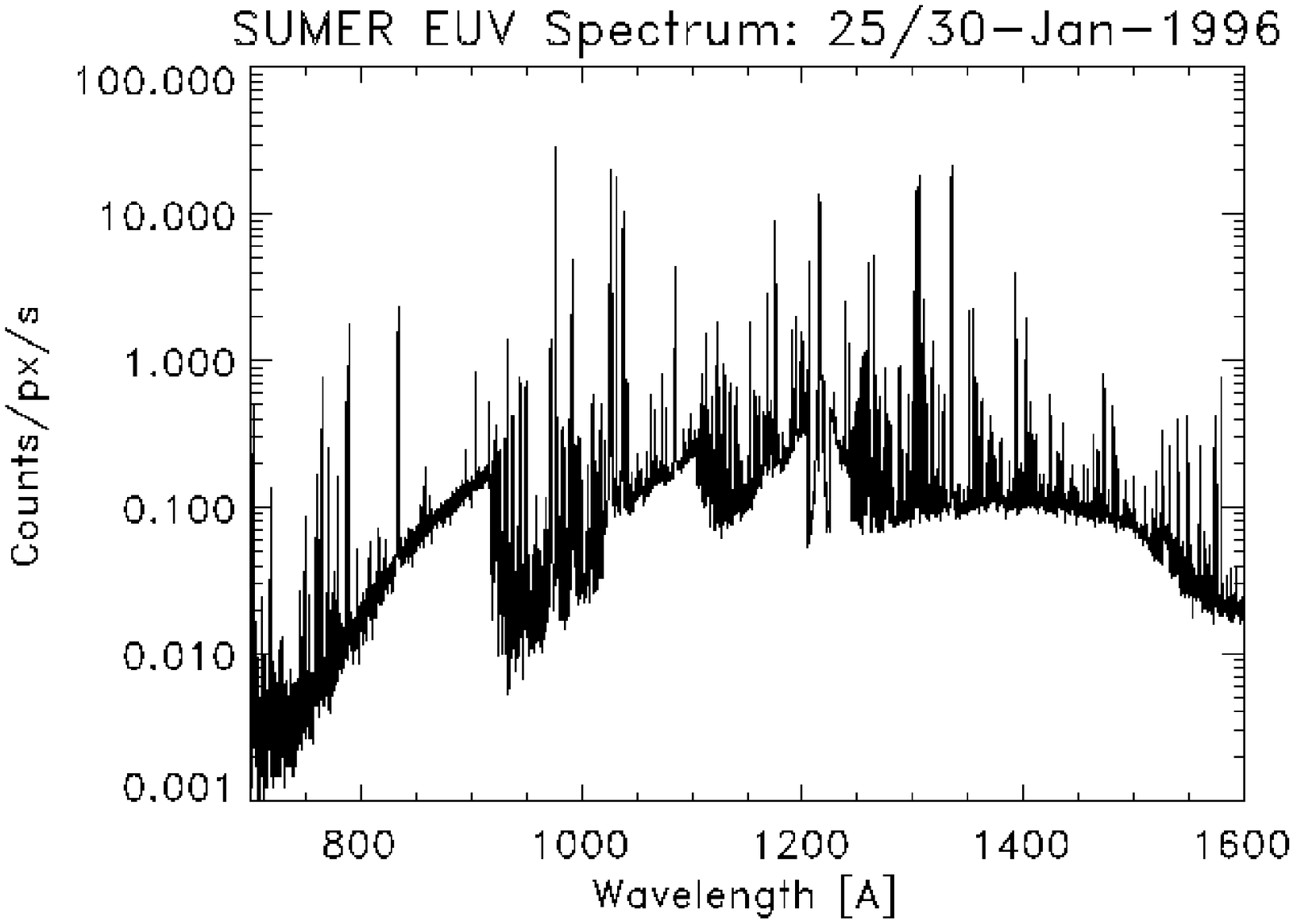

UV spectrum of the solar corona obtained with *SOHO*-SUMER experiment.

$\Longrightarrow$ Optically thin emission line spectrum.

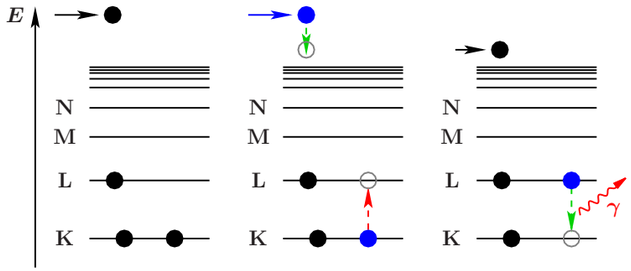

collisional excitation
$E_\gamma = E_{\mathrm{KL}} < E_{\mathrm{kin}}$

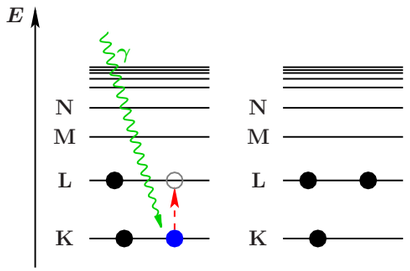

photo-excitation

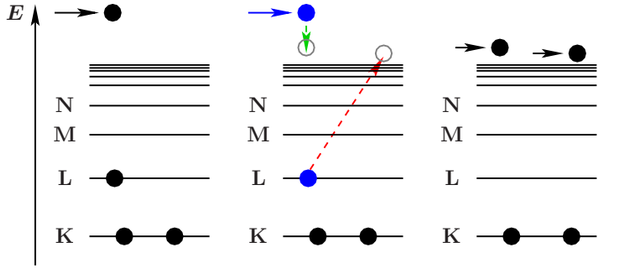

collisional ionization

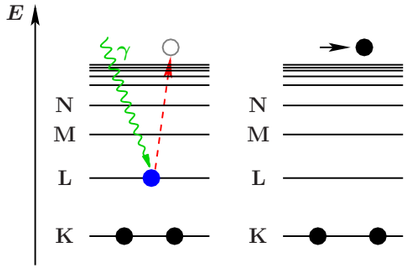

photo-ionization

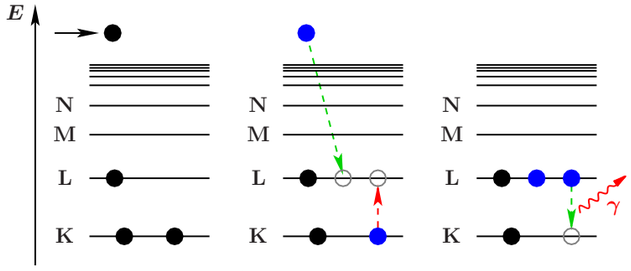

Dielectronic Recombination:
KLL di-electronic resonance
$E_{\mathrm{KL}} = E_{\mathrm{ion.\,pot}} + E_{\mathrm{kin}}$

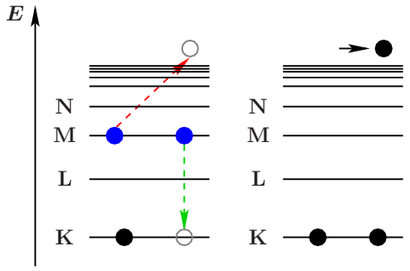

auto-ionization

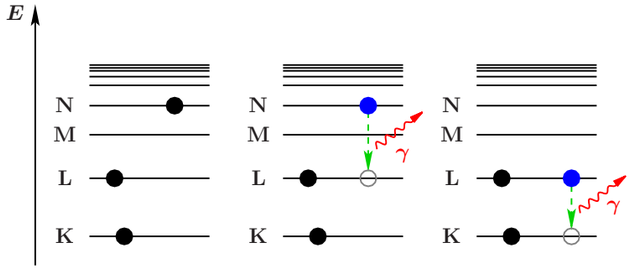

Cascades

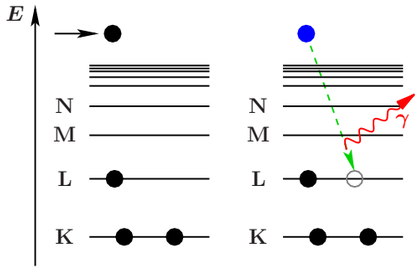

radiative recombination

Selection of atomic/ionic processes relevant for X-ray astronomy

N. Hell, PhD thesis, FAU Erlangen-Nürnberg

Coronal Plasmas

Coronal model for the ionization equilibrium: rate of ionizations by thermal collisional ionizations is balanced by the rate of radiative recombinations (thermal collisional ionization equilibrium; CIE).

$$n_e C_Z(T) n(Z) = n_e \alpha_Z(T) n(Z+1)$$

where:

- n: particle number densities (unit: particles cm^{-3})
- $\alpha_Z(T)$: coefficient for radiative and collisional recombination
  (atomic physics; depends on element Z and temperature T)
- $C_Z(T)$: Collisional ionization coefficient

Therefore

$$\frac{n(Z+1)}{n(Z)} = \frac{C_Z(T)}{\alpha_Z(T)}$$

In CIE, the ionization fractions $n(Z+1)/n(Z)$ are a function of temperature only.

Rate coefficients are tabulated in the literature
(e.g., Sutherland & Dopita 1993 and references therein; not well known)

Typically described with fitting functions:

$$C_Z(T) = A_i T^{3/2} \frac{\exp(-I_Z/kT)}{1 + a_i(T/T_Z)}$$

where $T_Z = I_Z/kT$, I_Z binding energy; A_i and a_i are fitting coefficients.

Recombination: radiative recombination and dielectric recombination are important,

$$\alpha_Z(T) = \alpha_{rad}(T) + \alpha_{diel}(T)$$

with

$$\alpha_{rad}(T) = A_{rad} T^{-\xi_{rad}} \quad \text{where} \quad \xi_{rad} \sim 0.6 \ldots 0.9$$

and

$$\alpha_{diel}(T) = A T^{-3/2} \exp\left(-\frac{T_B}{T}\right)\left[1 + B \exp\left(-\frac{T_i}{T}\right)\right]$$

Coronal Plasmas

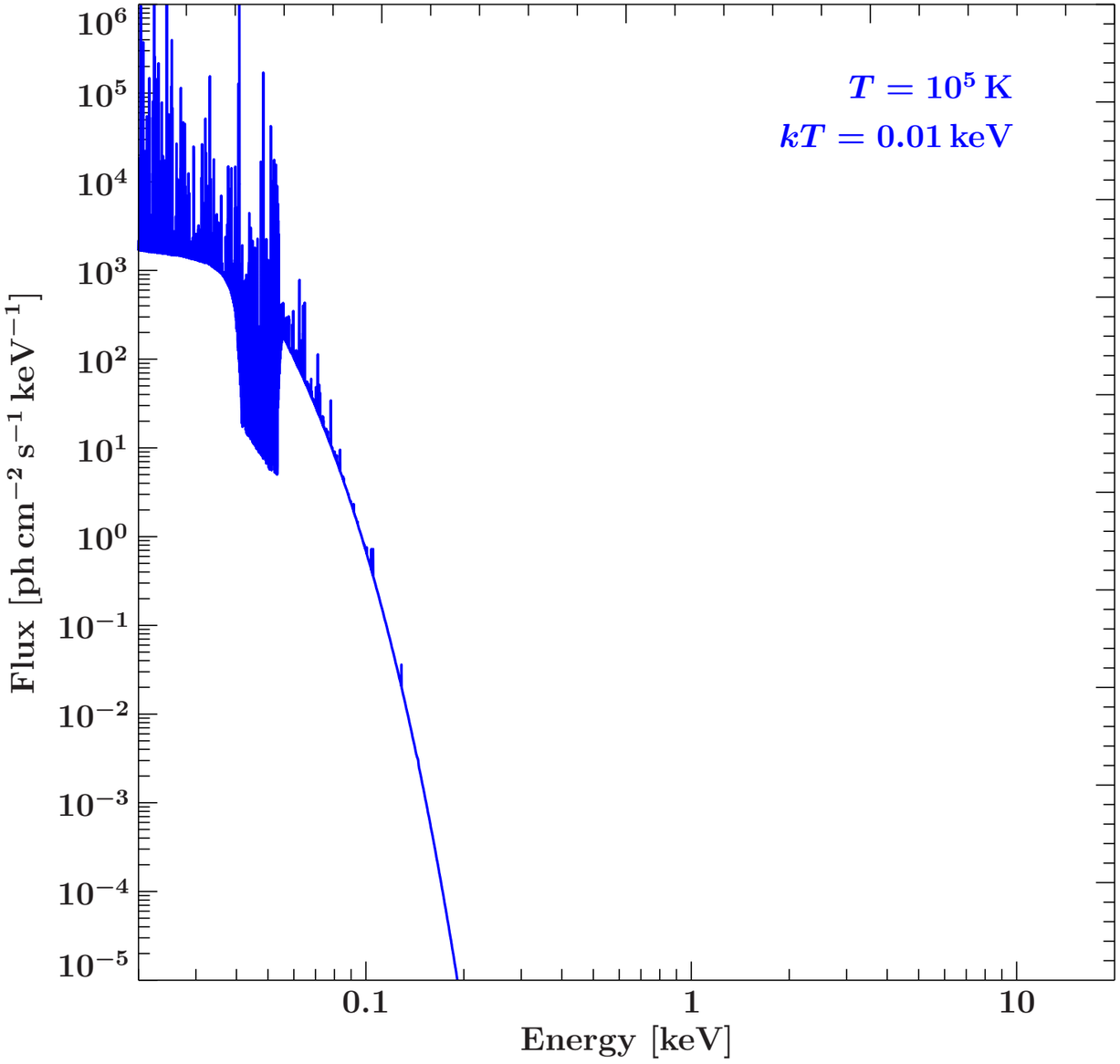

Physics of Corona: Coronal Plasma
(CIE: Coronal Ionization Equilibrium).
Basic assumption: collisional ionization balanced by radiative recombination
Plasma is optically thin
$\Longrightarrow$ Cooling by line emission and thermal bremsstrahlung.

Coronal Plasmas

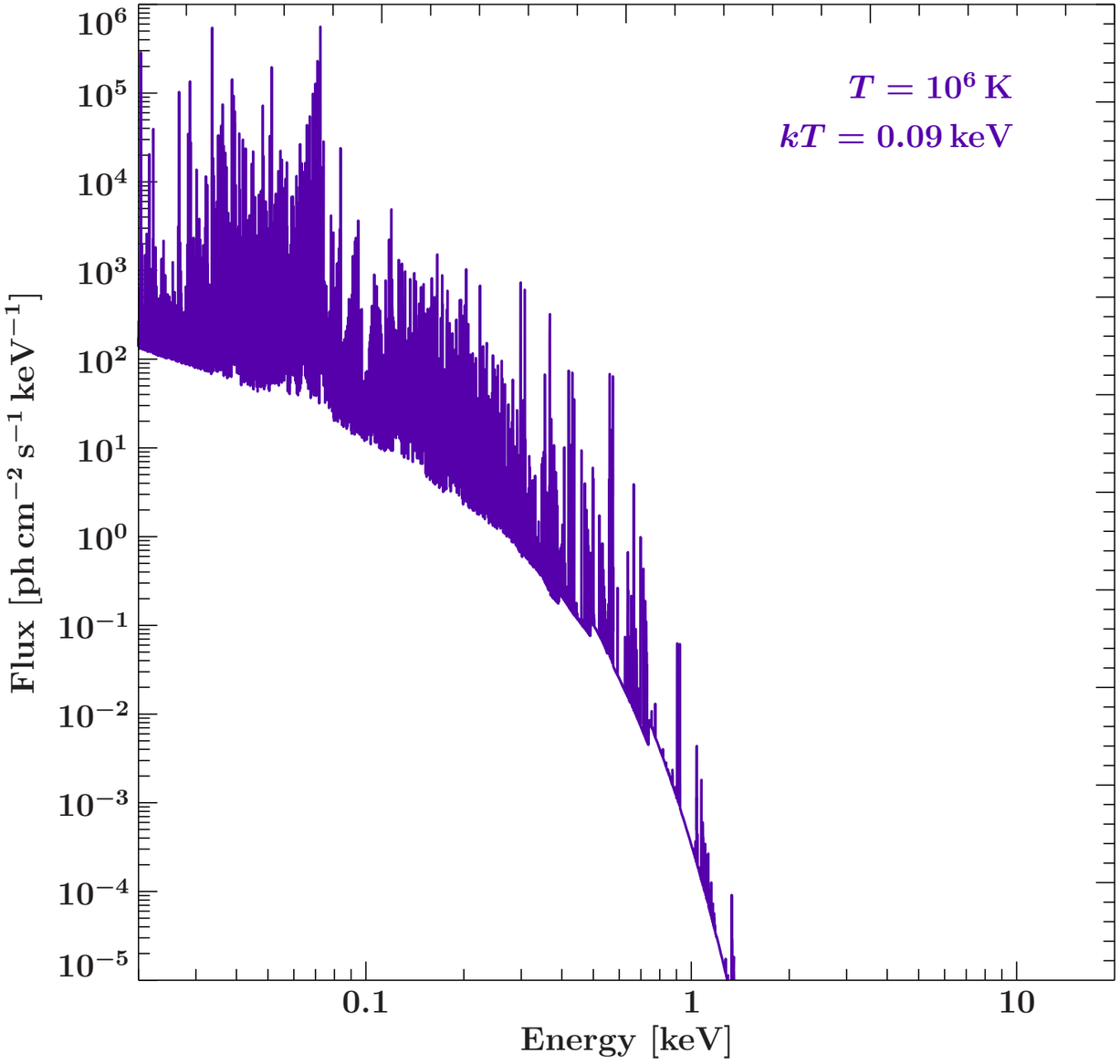

Physics of Corona: Coronal Plasma
(CIE: Coronal Ionization Equilibrium).
Basic assumption: collisional ionization balanced by radiative recombination
Plasma is optically thin
$\Longrightarrow$ Cooling by line emission and thermal bremsstrahlung.

Coronal Plasmas

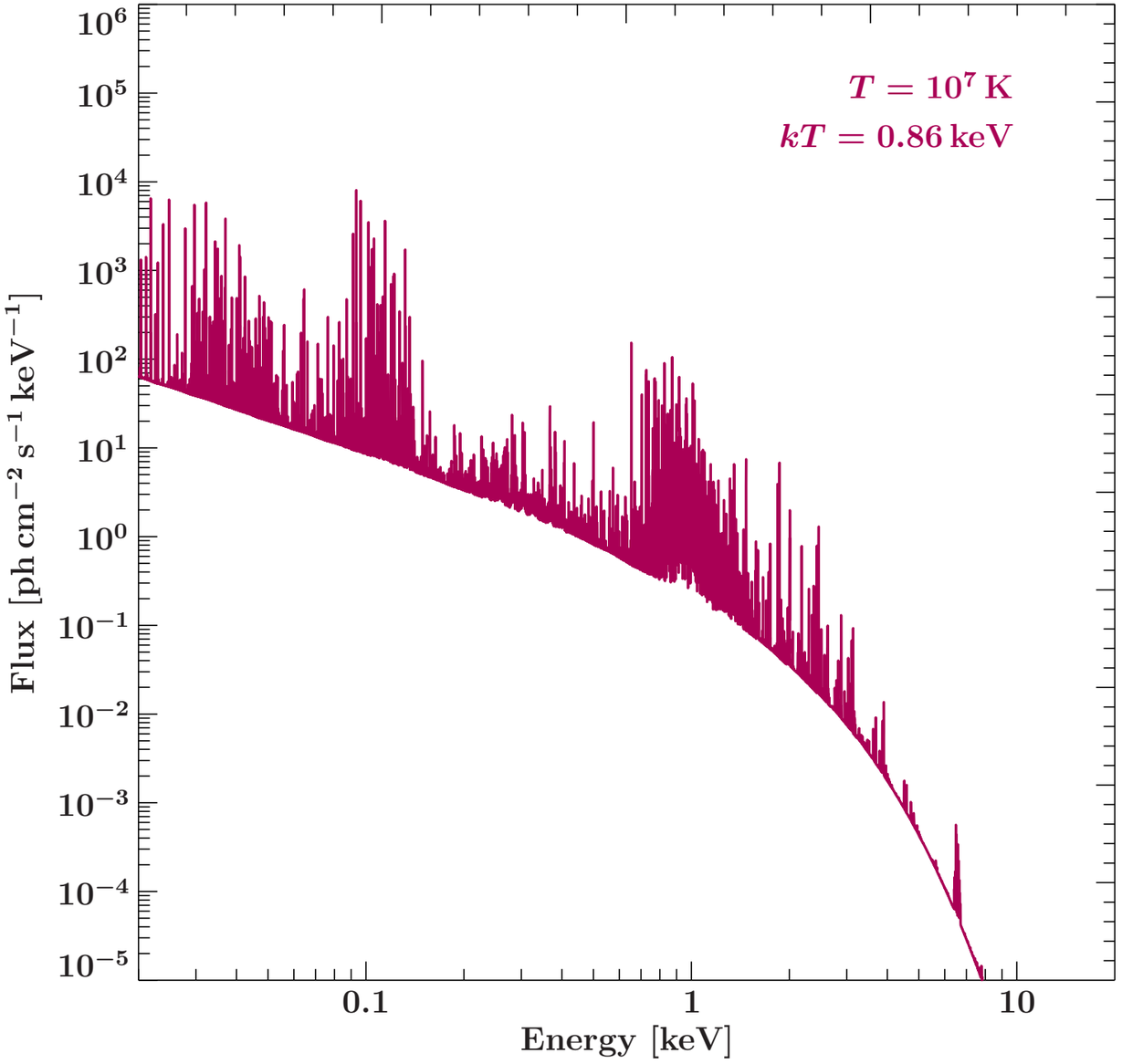

Physics of Corona: Coronal Plasma
(CIE: Coronal Ionization Equilibrium).
Basic assumption: collisional ionization balanced by radiative recombination
Plasma is optically thin
$\Longrightarrow$ Cooling by line emission and thermal bremsstrahlung.

Coronal Plasmas

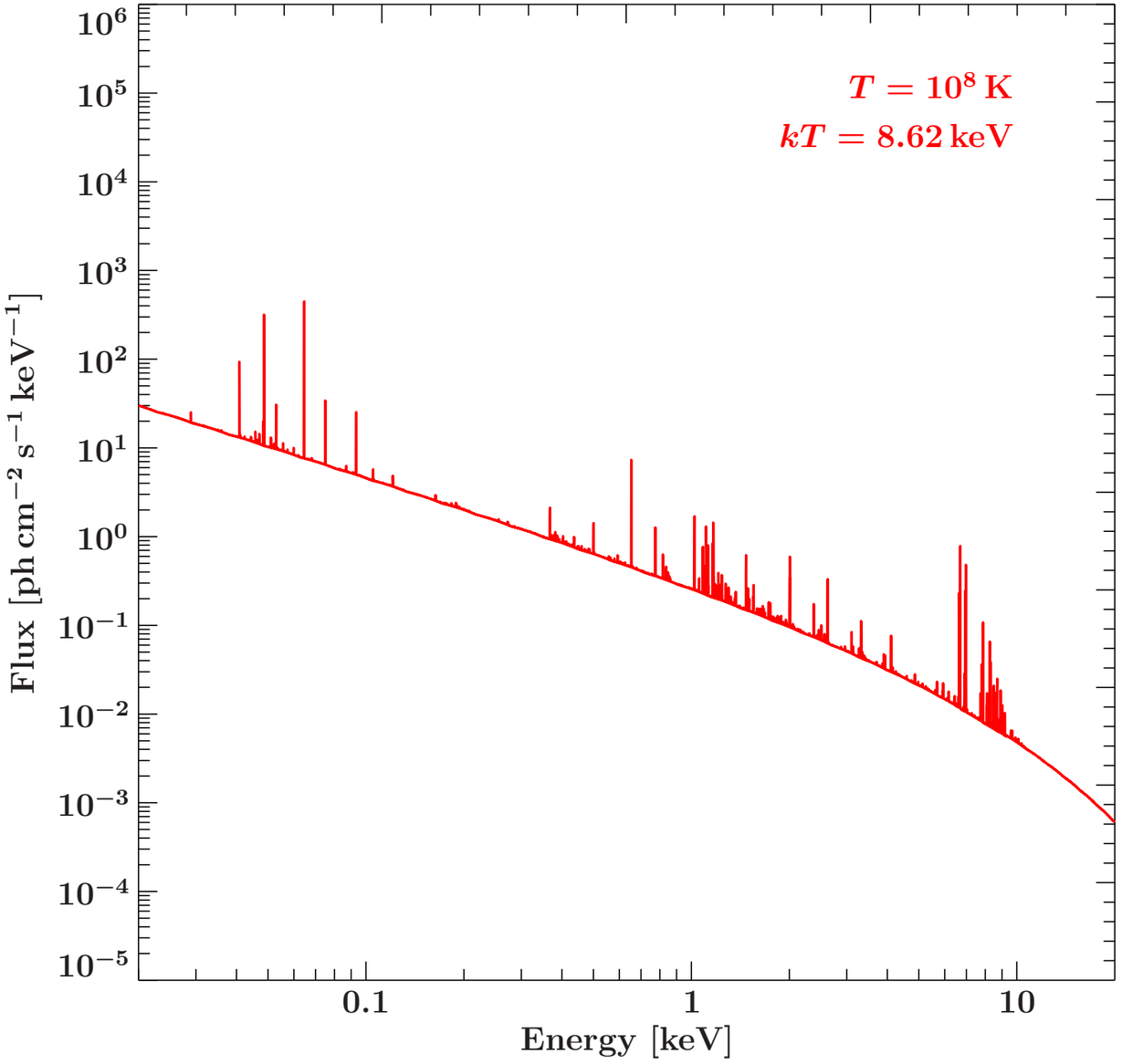

Physics of Corona: Coronal Plasma
(CIE: Coronal Ionization Equilibrium).
Basic assumption: collisional ionization balanced by radiative recombination
Plasma is optically thin
$\Longrightarrow$ Cooling by line emission and thermal bremsstrahlung.

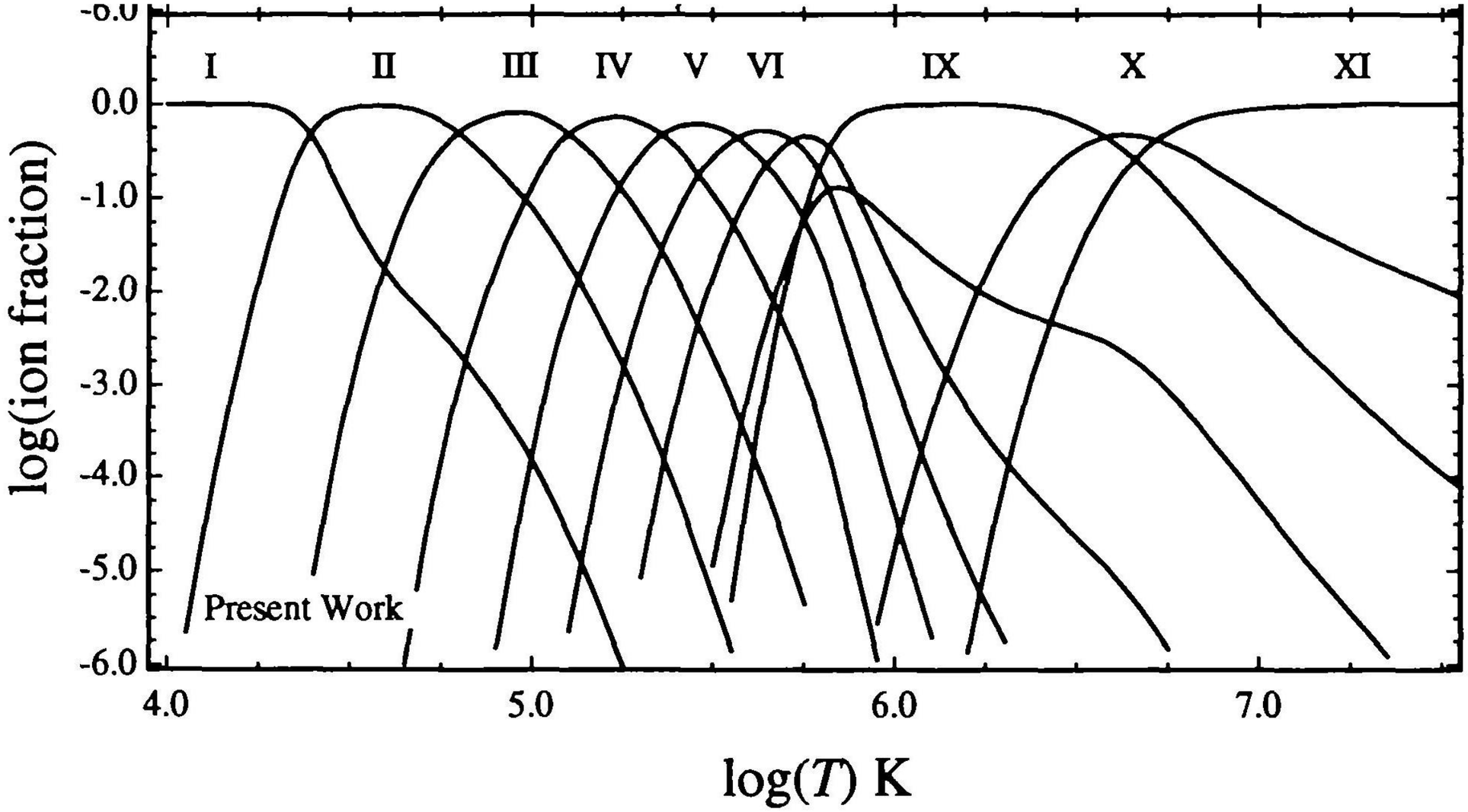

Sutherland & Dopita (1993), Fig. 4

Ionization balance of Neon as a function of temperature in coronal equilibrium.

Only two or three ionization stages are present at each given temperature.

Coronal Plasmas

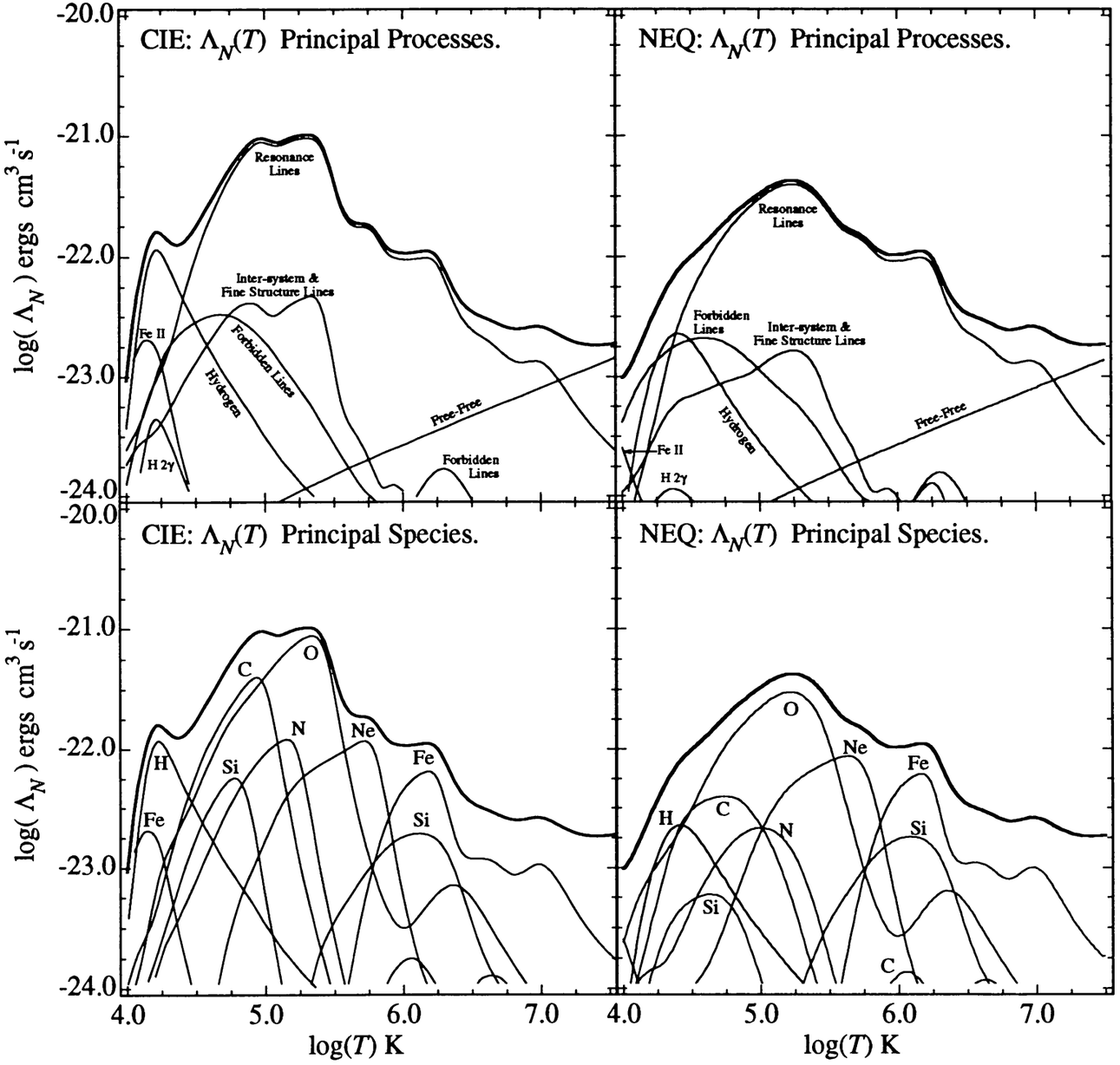

Depending on temperature, different species dominate the cooling

$\Longrightarrow$ Temperature diagnostics.

In addition, using X-ray lines, temperature and density diagnostics become possible (see later, chapter on supernova remnants).

Sutherland & Dopita (1993, Fig. 18)

Line Diagnostics

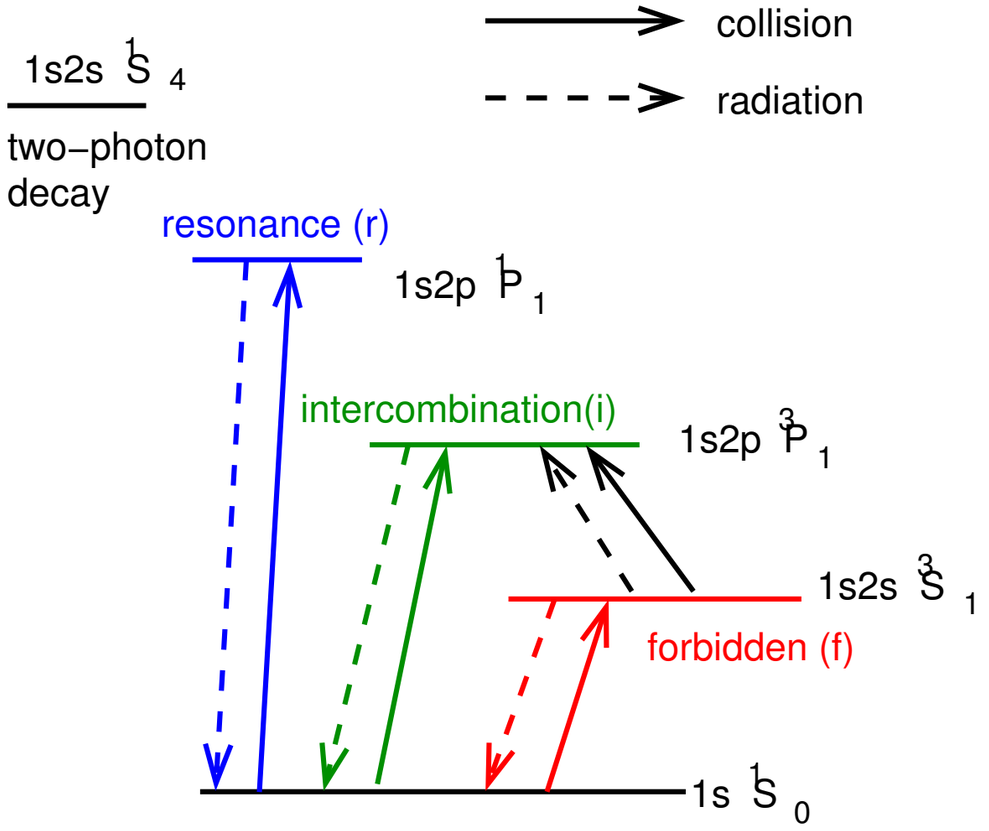

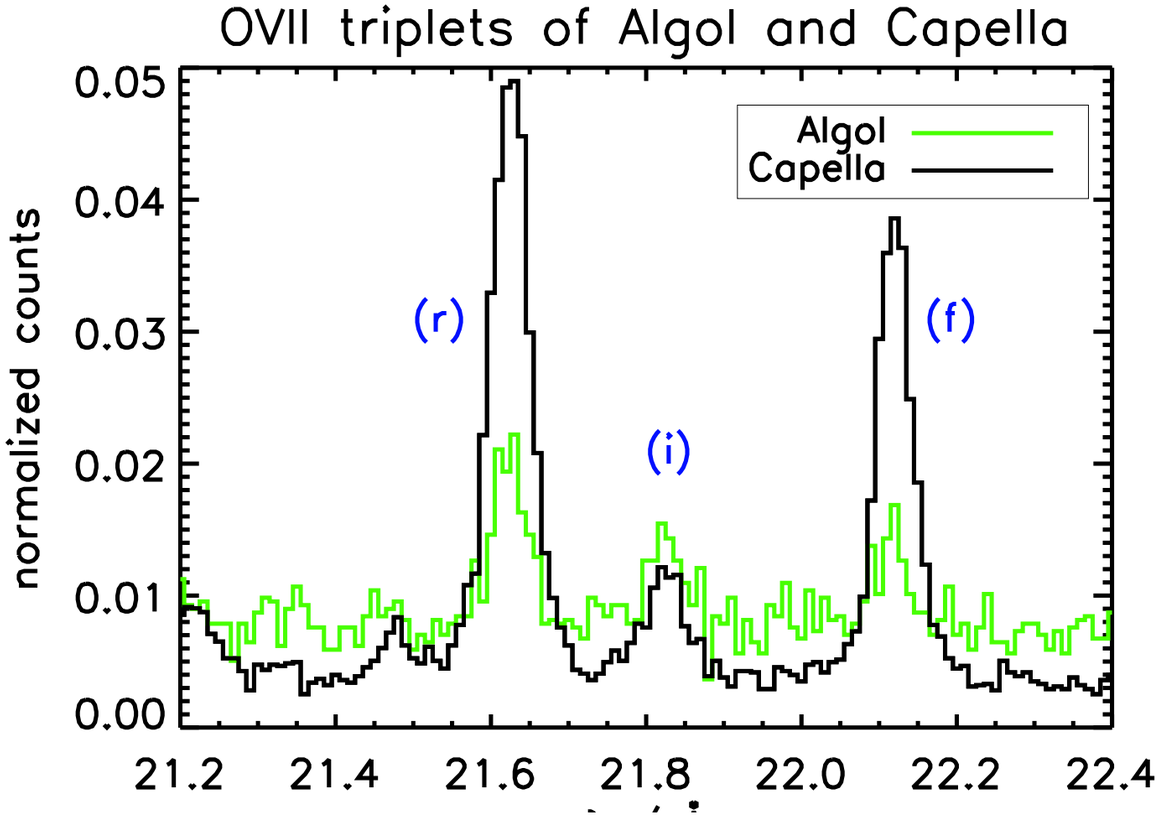

(Güdel, 2004, after J.U. Ness)

He-like triplets (e.g., C V, N VI, O VII, ..., Si XIII) allow us to measure coronal density: Flux ratio of forbidden and intercombination line:

$$R = \frac{R_0}{1 + n_e/N_c} = \frac{f}{i}$$

where R_0: intensity at low n_e, N_c: critical density (around $10^{10}\,\mathrm{cm}^{-3}$).

need to know photospheric radiation field since this enhances $^3S_1 - {}^3P_{1,2}$ transitions – compare Algol (suppressed) and Capella (normal)!

Line Diagnostics

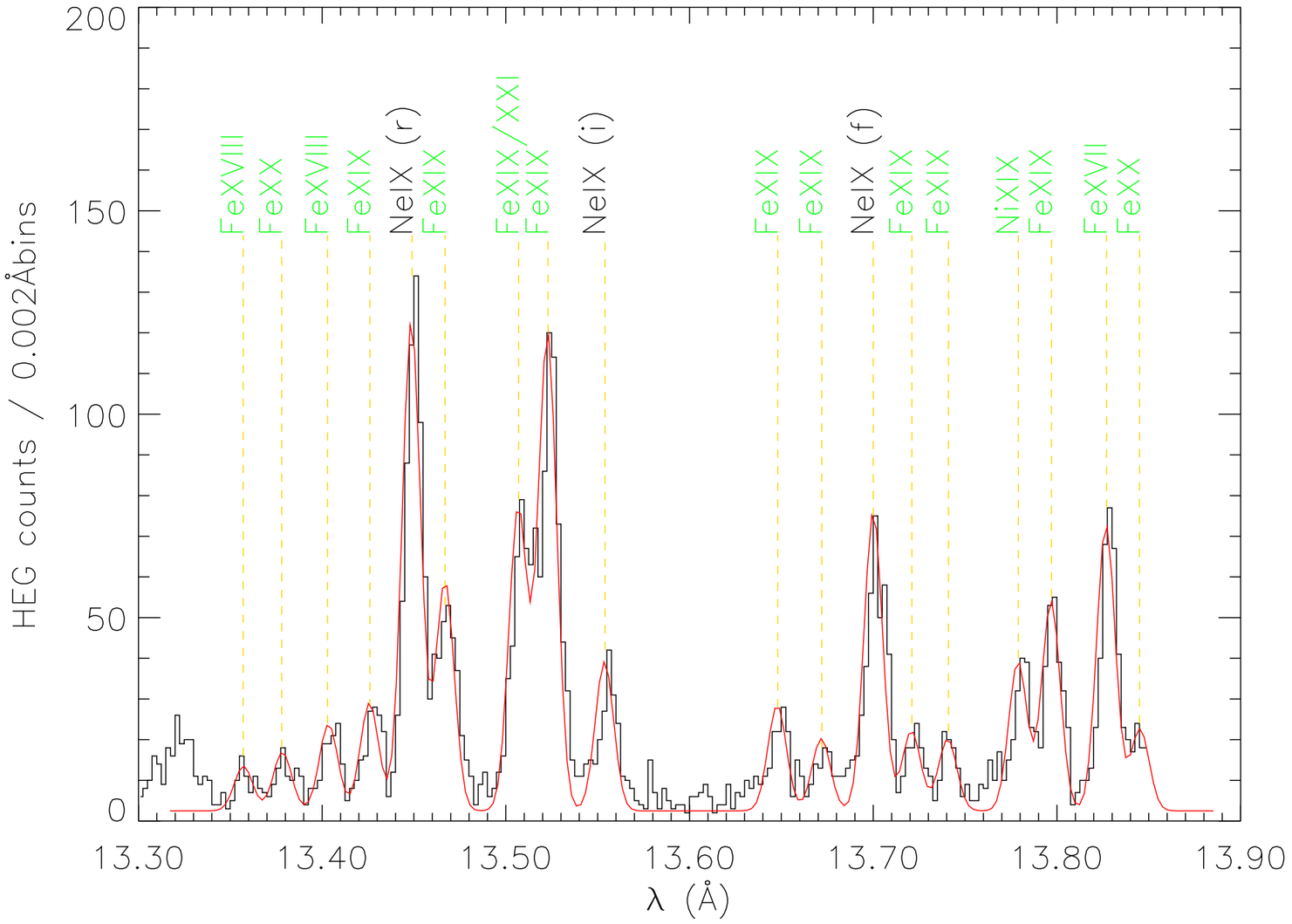

A problem in the analysis of He-like ions is blending with lines Fe lines $\Longrightarrow$ danger for instruments with lower resolution!

(Güdel, 2004, after J.U. Ness)

Typical densities found: Inactive stars have $n_e < 10^{10}\,\mathrm{cm}^{-3}$, and active stars have $n_e \sim$ several $\times\, 10^{10}\,\mathrm{cm}^{-3}$.

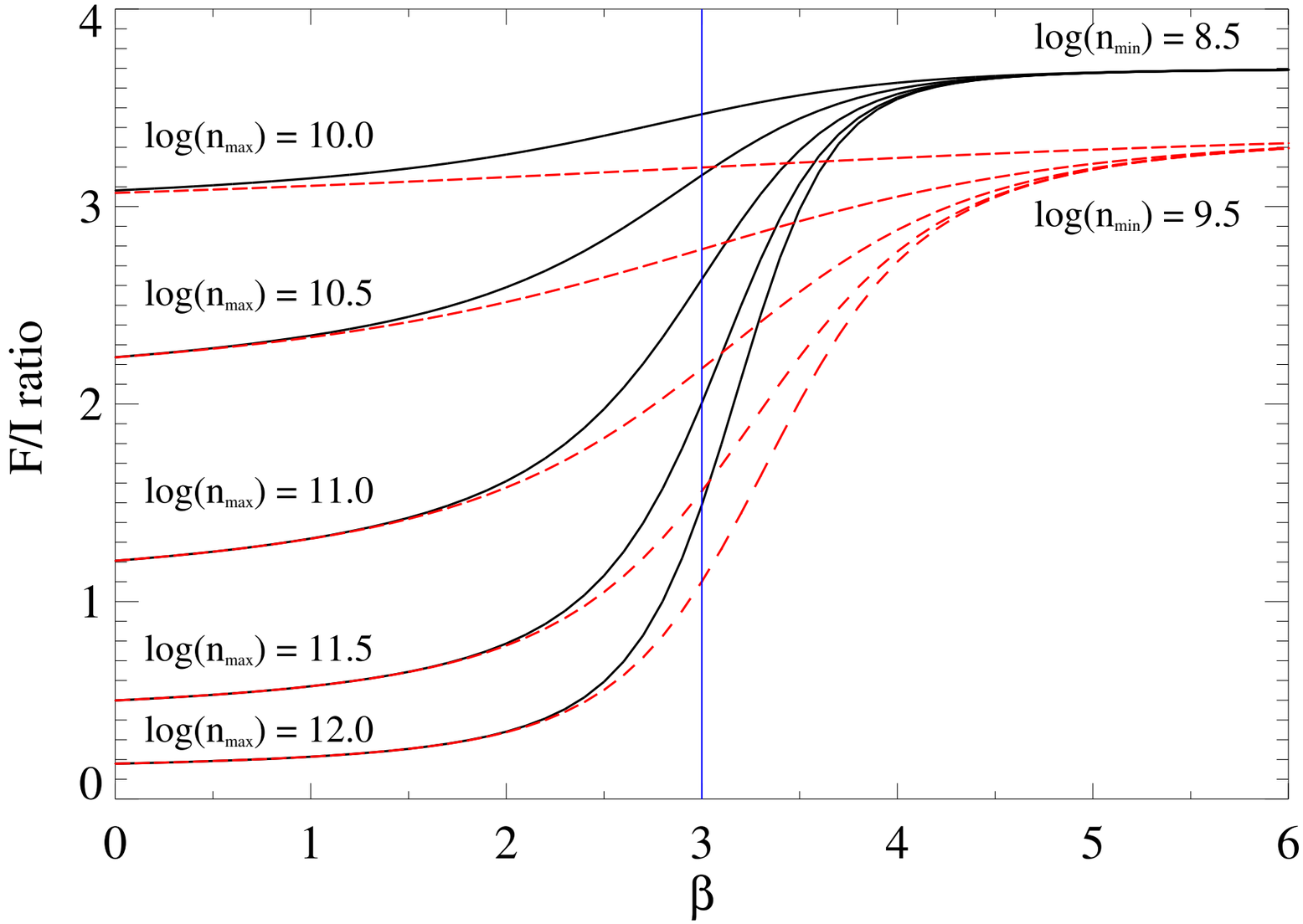

(Güdel, 2004, Fig. 13 (top))

Inhomogeneity also influences diagnostics: Change of f/i-ratio for O VII in inhomogeneous plasma with electron volume density distribution $dV/dn_e \propto n_e^{-\beta}$

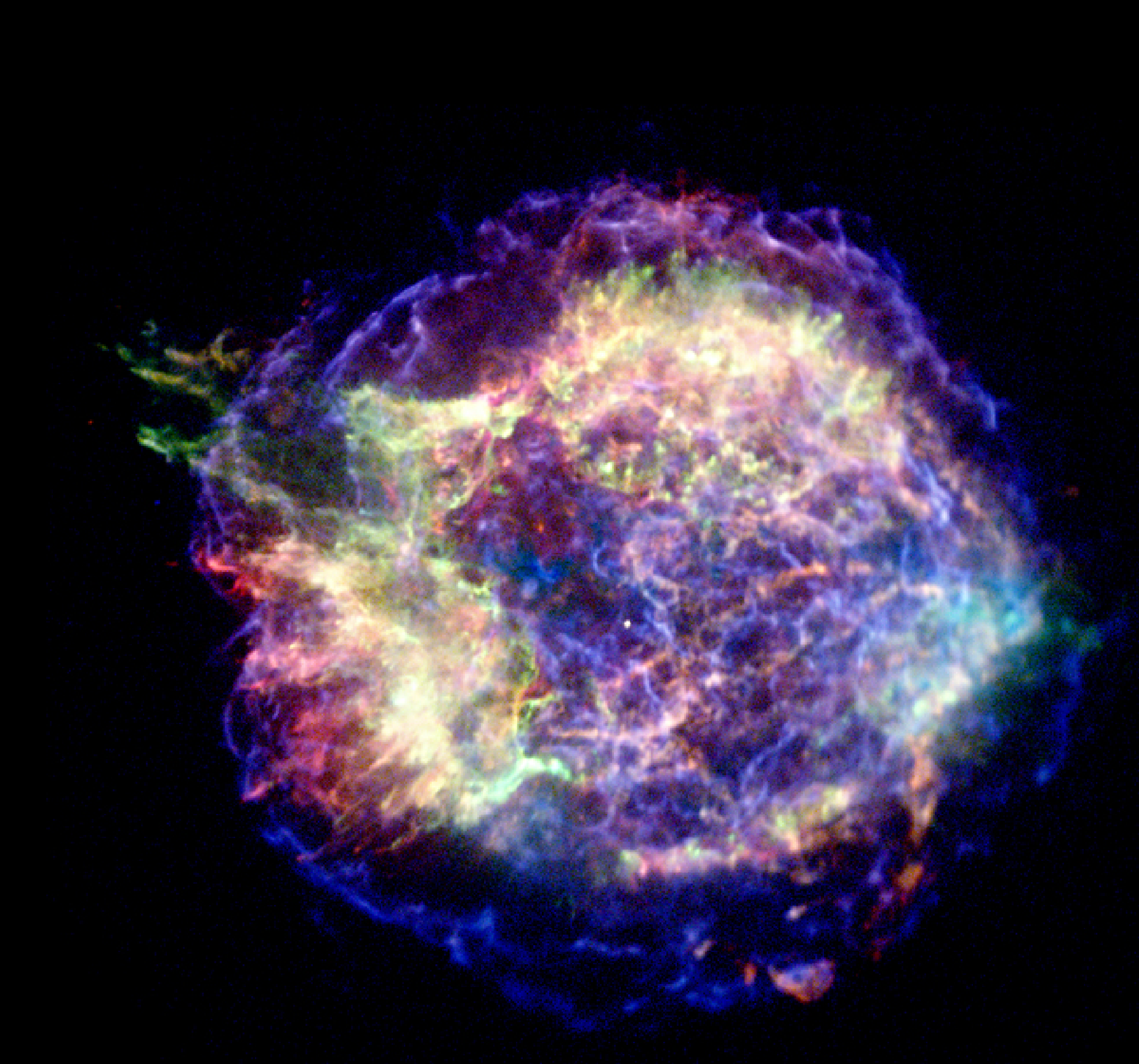

Cassiopeia A: Young remnant (∼1670), no optical explosion observed
Mass of ejected material 10–15 $M_\odot$ $\Longrightarrow$ possibly type II?

Type II are also fainter, explaining why explosion has not been reported.

2000: Chandra discovers point-source in center
$\Longrightarrow$ neutron star

Beyond the coronal model

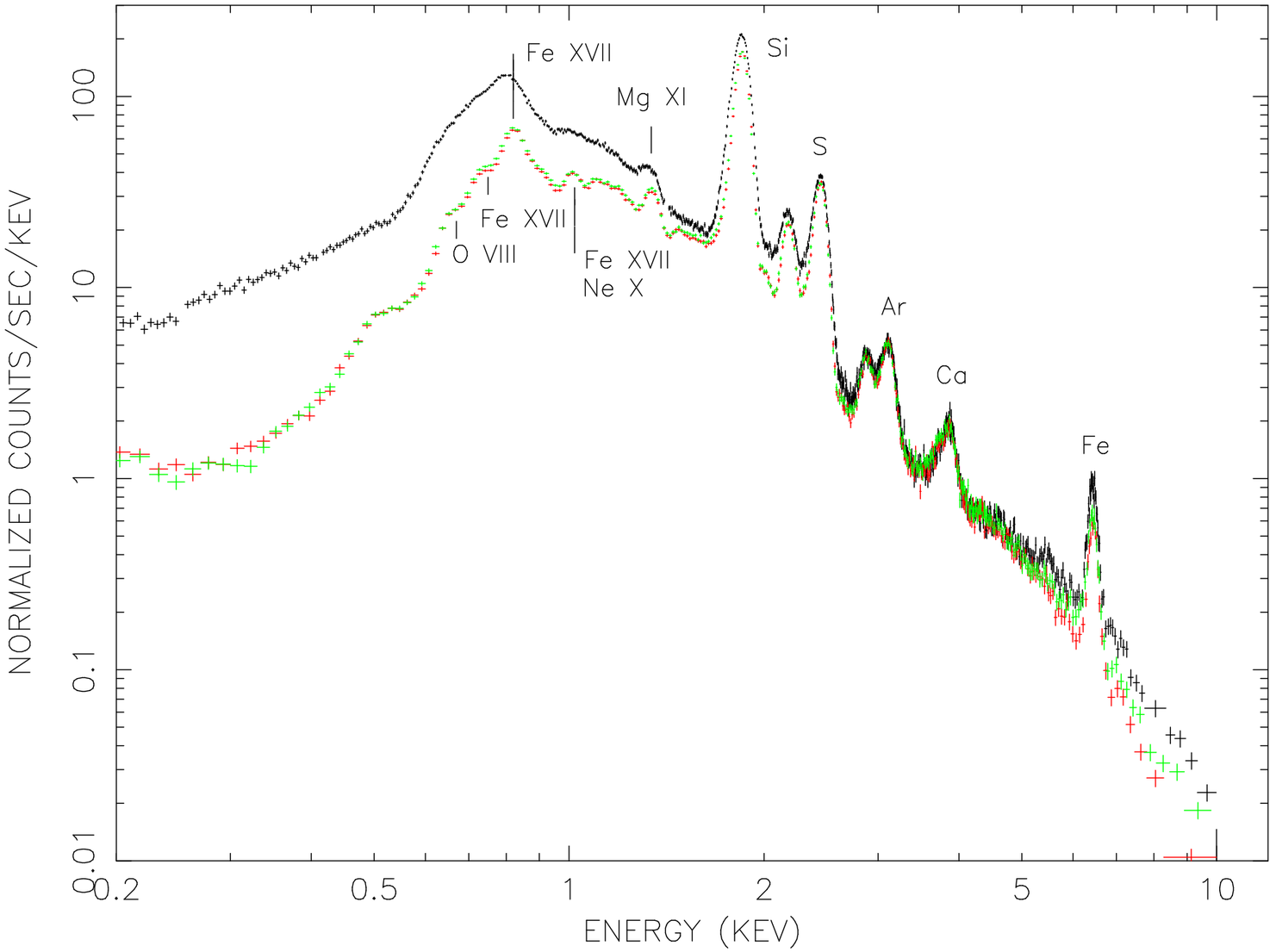

Tycho's SNR: Low-energy X-ray spectrum is line dominated

$\Longrightarrow$ interior emission from shock excited plasma of stellar debris; outer rim from continuum emission.

Mass estimate from X-ray spectroscopy and radio:

$1 \ldots 2\,M_\odot \Longrightarrow \sim 1.4\,M_\odot$?!?

$\Longrightarrow$ remnant of type I explosion?

No central X-ray source!

XMM EPIC spectrum of Tycho's SNR
(Decourchelle et al., 2001, Fig. 1a)

Beyond the coronal model

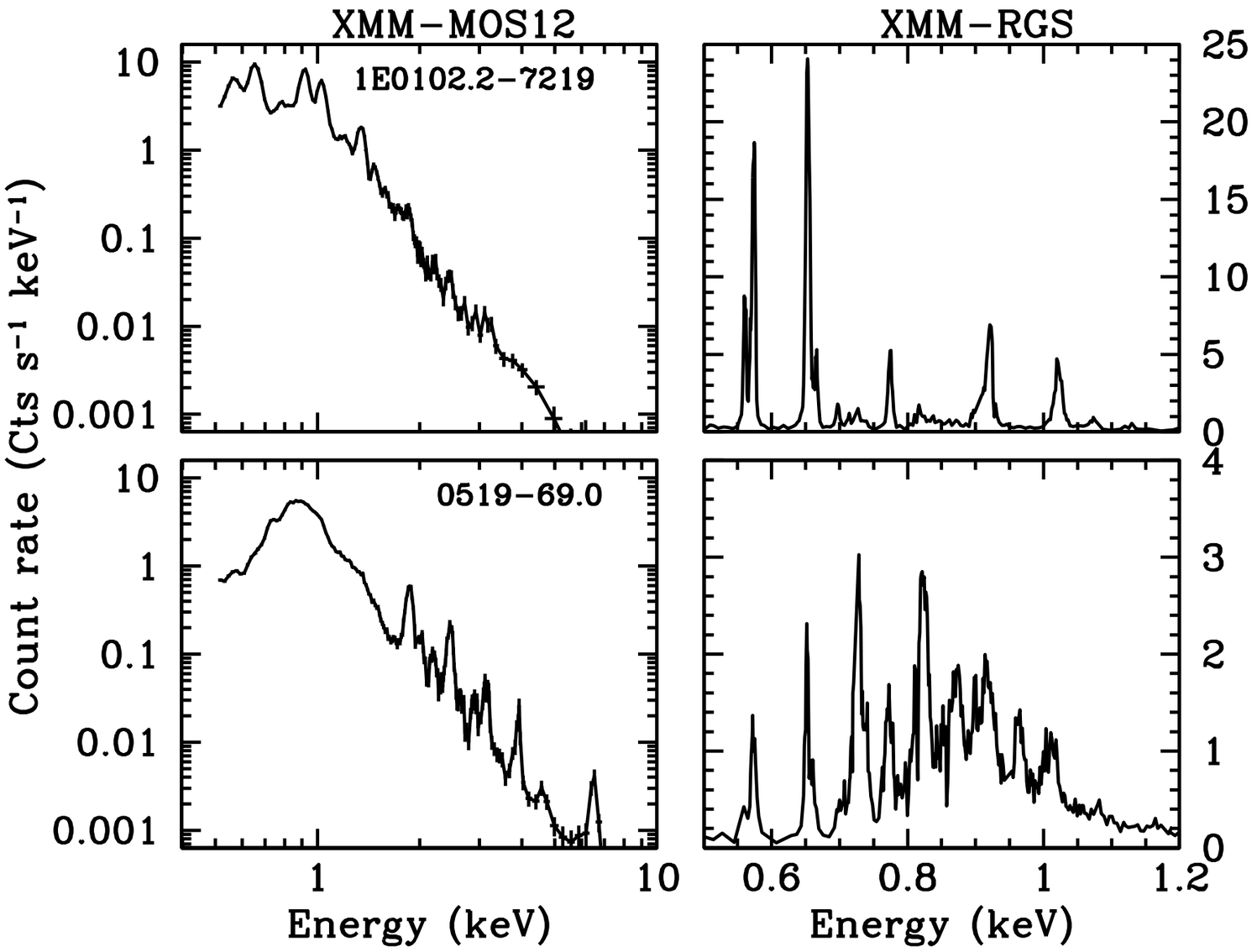

(Vink, 2012, Fig. 17)

gratings resolution needed to resolve low energy line forests

Beyond the coronal model

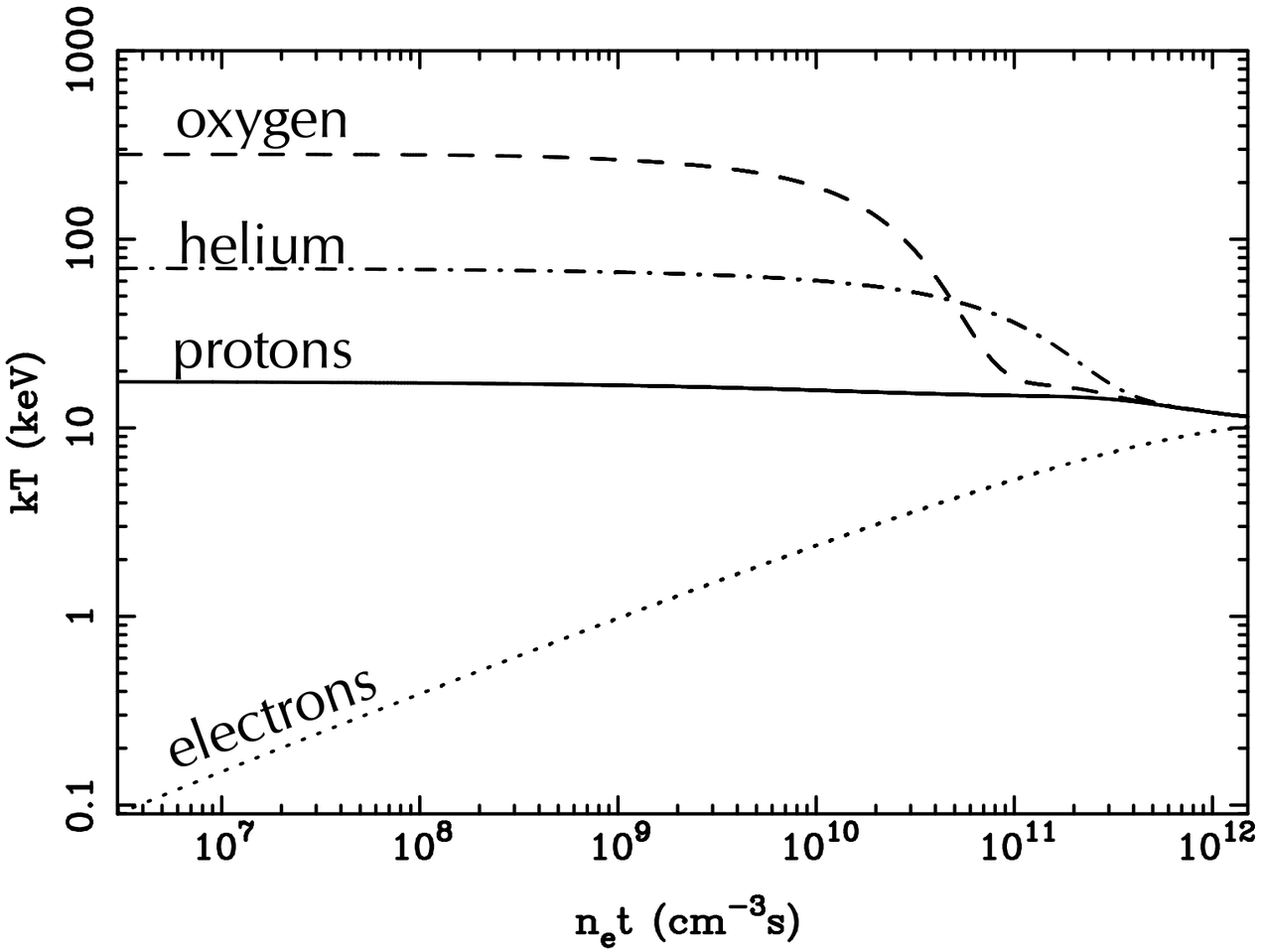

(temperature evolution of shocked plasma as function of time $n_e t$; Vink, 2012, Fig. 9)

Spectral shape reminiscent of collisional ionization equilibrium (CIE), *but*: plasma is *not* in thermodynamic equilibrium: non-equilibrium ionization (NEI)

Reason: Plasma is very tenuous $\Longrightarrow$ time scale for reaching thermodynamic equilibrium is very long (and $\propto m Z^2$, so faster for more massive elements).

measure time in $n_e t$, where n_e: particle density of plasma.

Beyond the coronal model

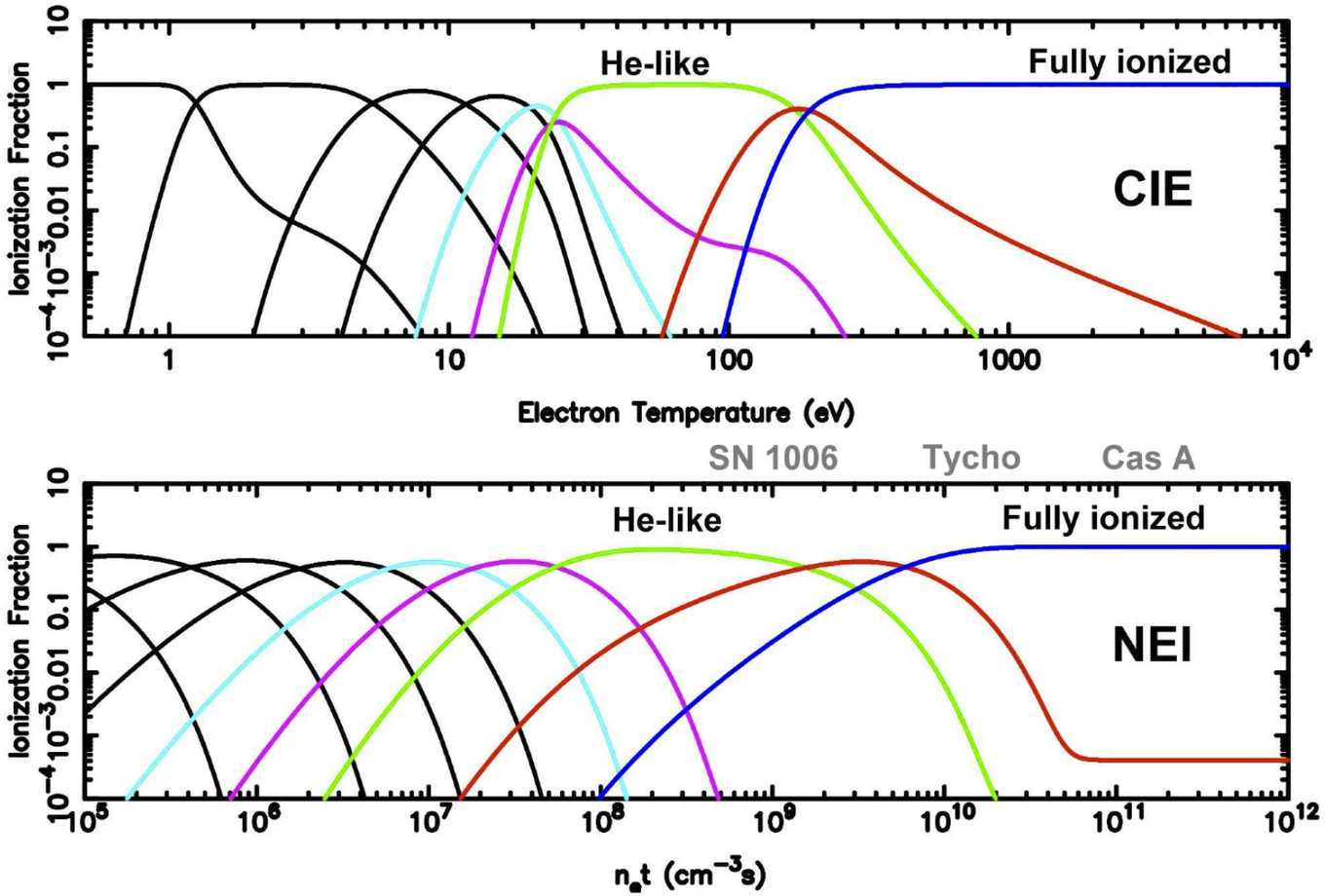

(ionization structure for CIE and NEI – note different x-axes! Vink, 2012, Fig. 11)

Spectral shape reminiscent of collisional ionization equilibrium (CIE), *but*: plasma is *not* in thermodynamic equilibrium: non-equilibrium ionization (NEI)

Reason: Plasma is very tenuous $\Longrightarrow$ time scale for reaching thermodynamic equilibrium is very long (and $\propto$ mZ^2, so faster for more massive elements).

measure time in $n_e t$, where n_e: particle density of plasma.

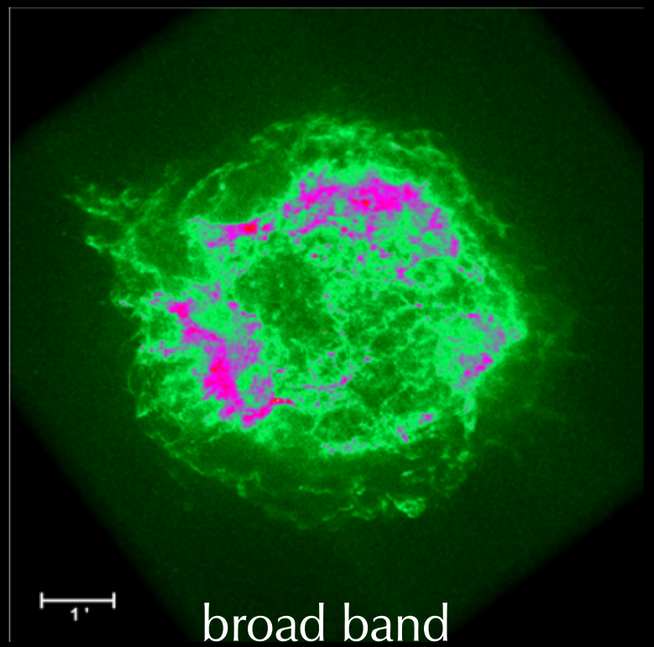

broad band

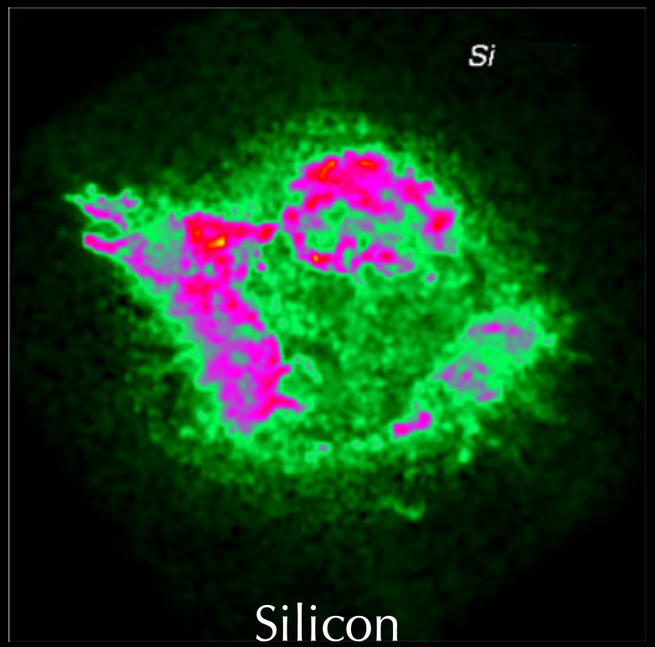

Silicon

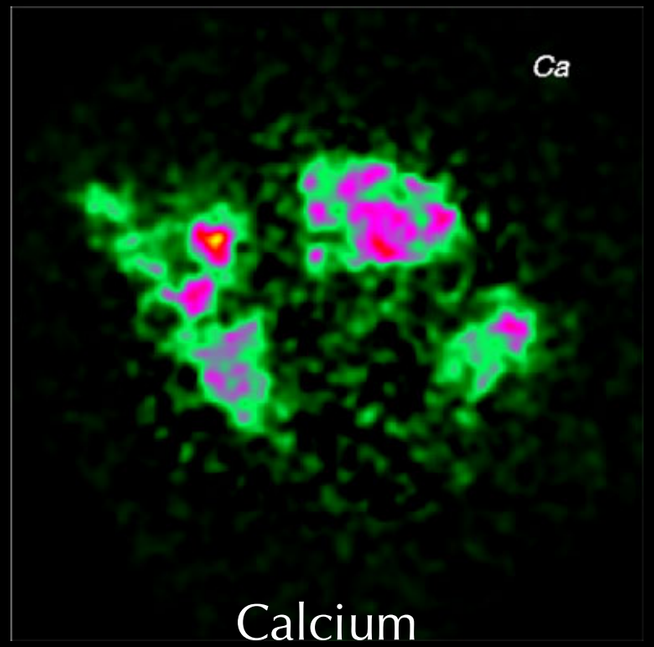

Calcium

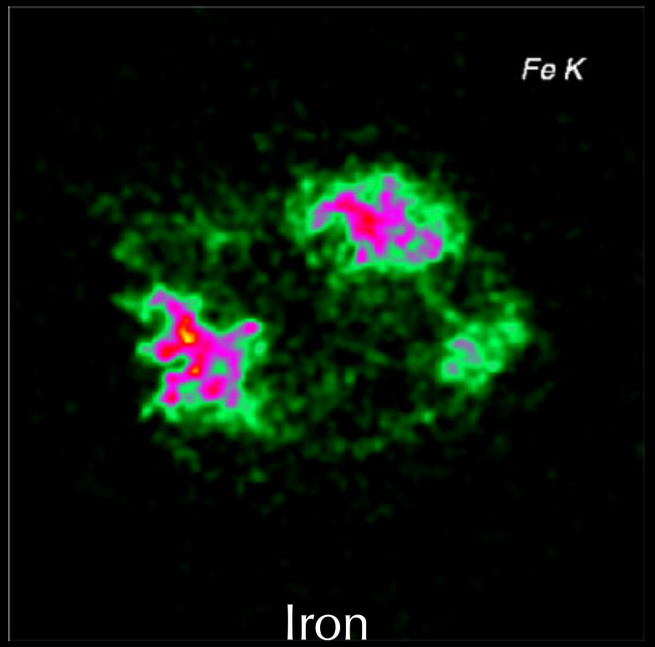

Iron

Beyond the coronal model

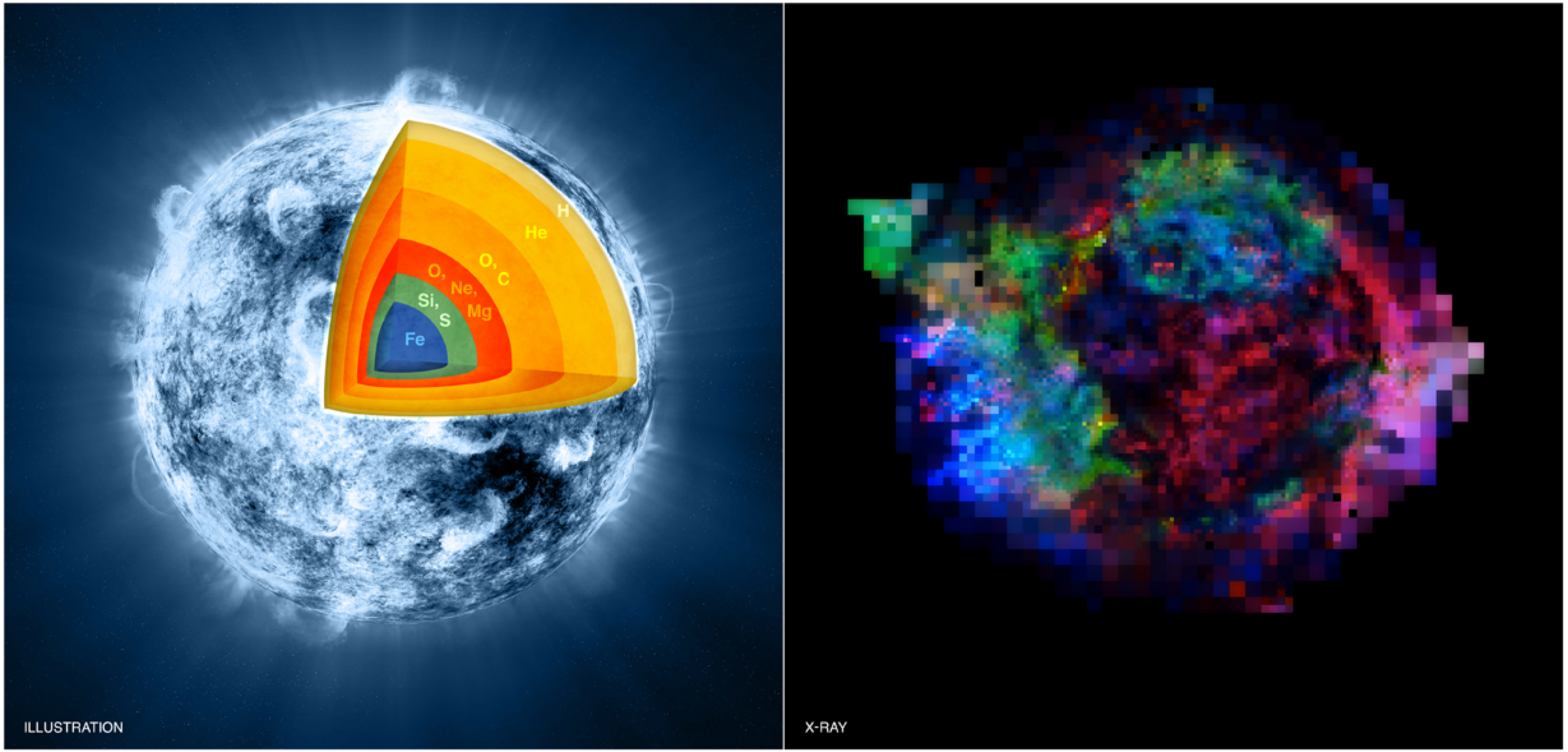

NASA/CXC/GSFC/U.Hwang & J.Laming

Elemental mapping is used to try understanding structure of progenitor.

X-ray Astronomy Today

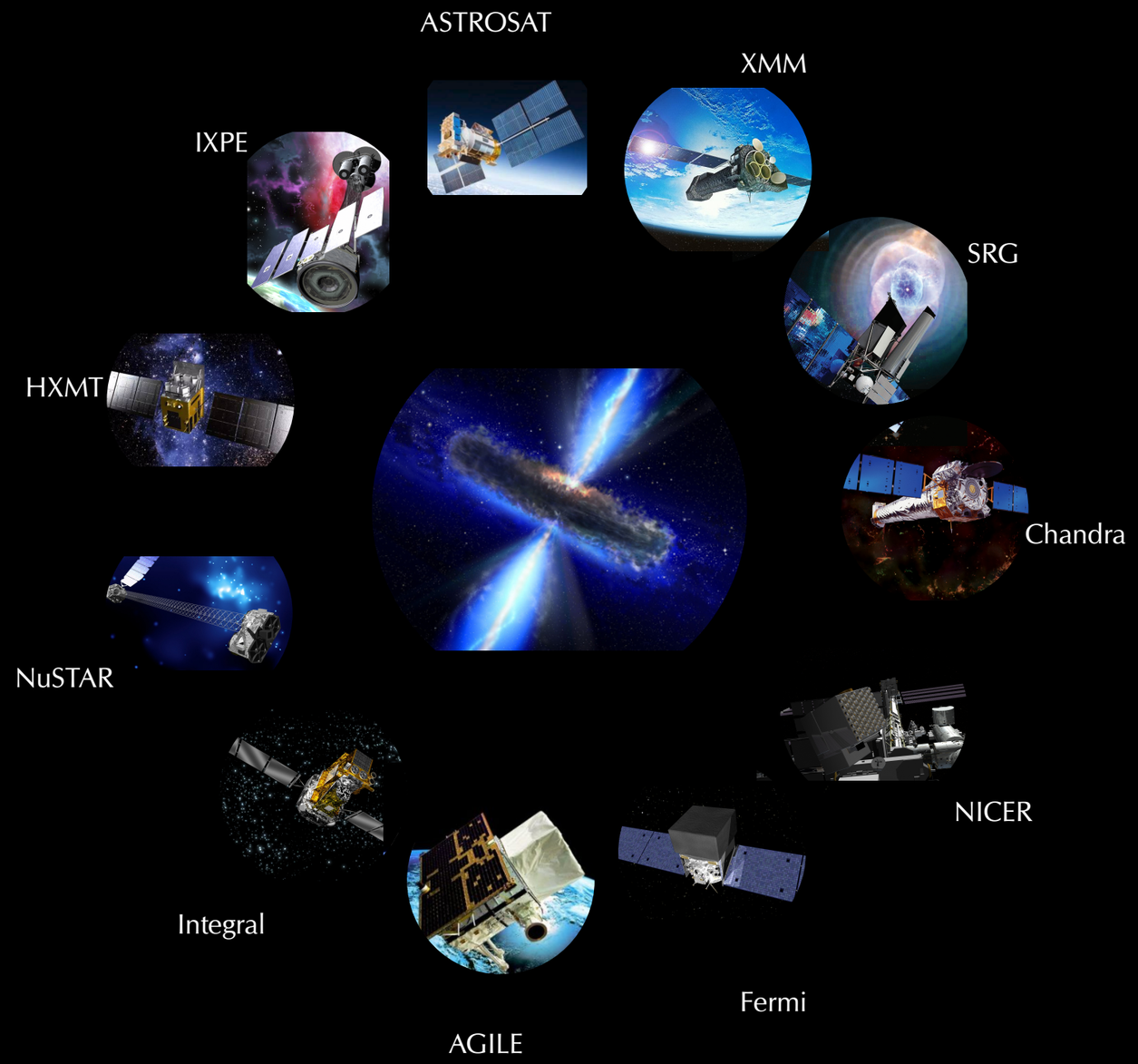

High-Resolution X-ray Astronomy Today

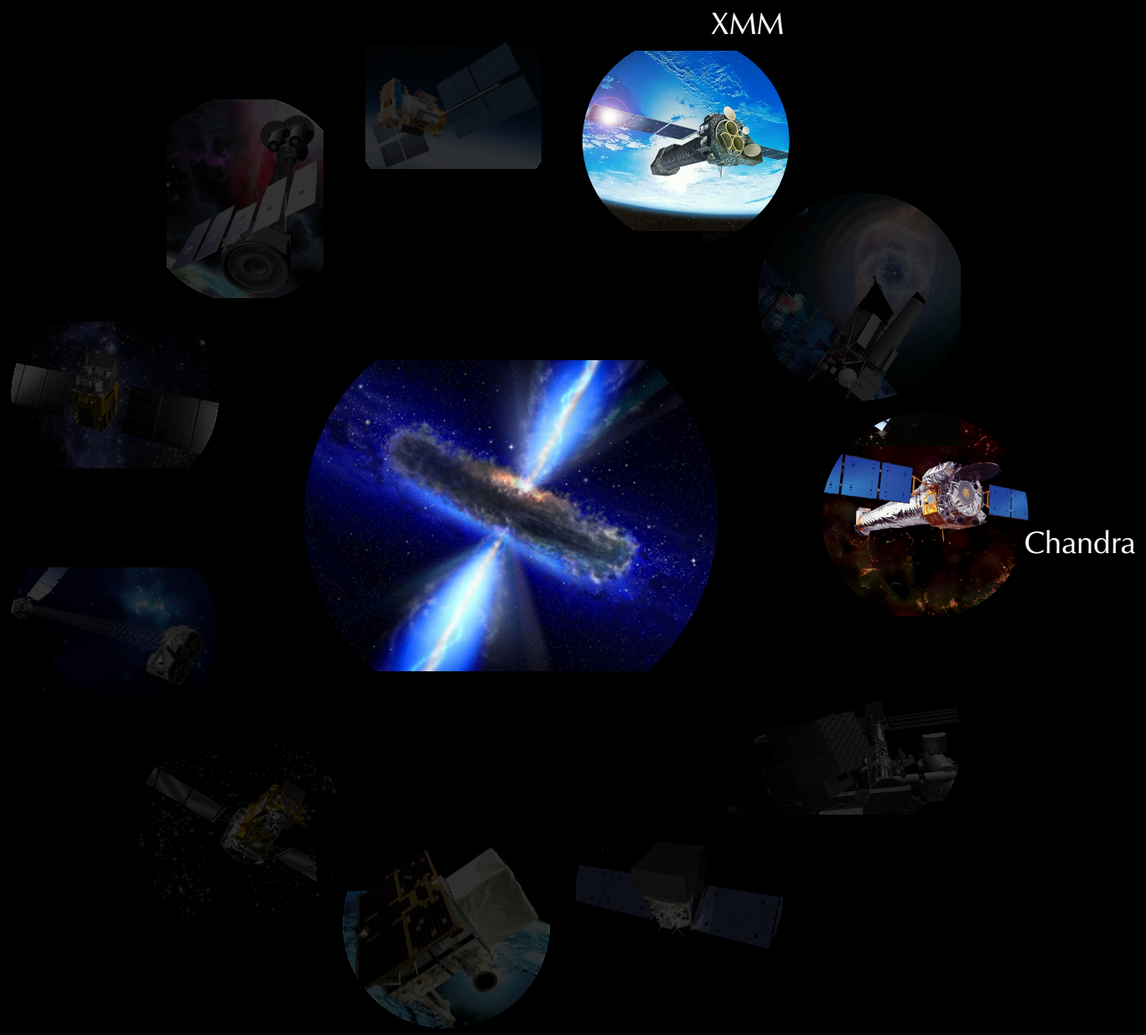

Gratings Spectrometers

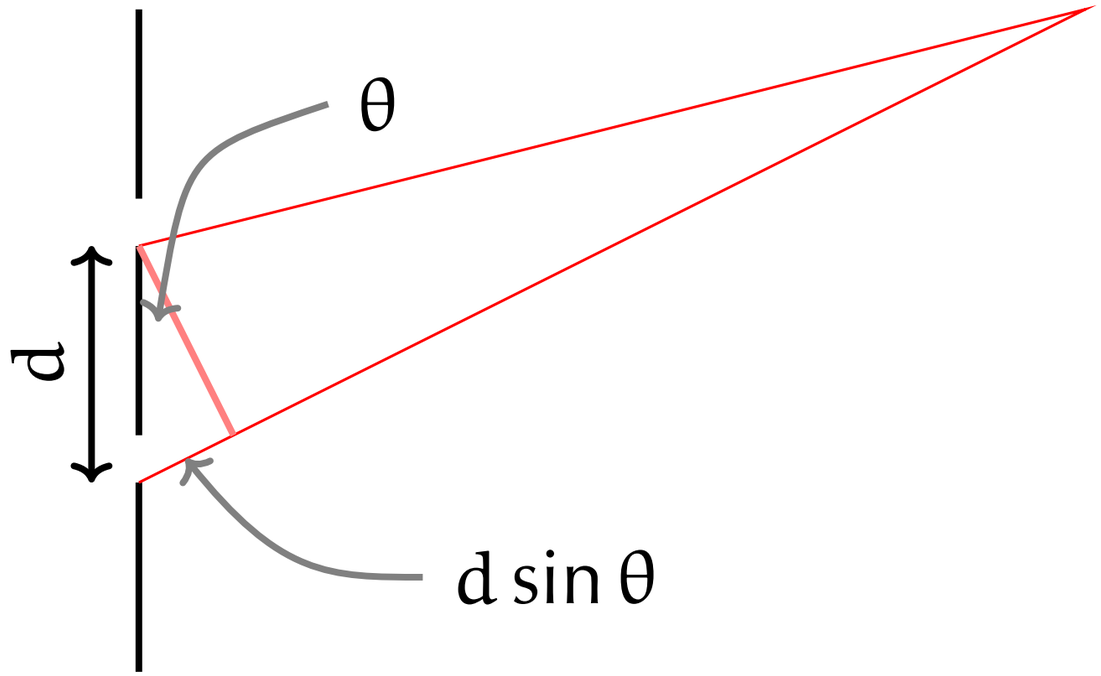

For light of wavelength λ: constructive interference for

$$d \sin\theta \stackrel{!}{=} m\lambda$$

(dispersion equation), where $m \in \mathbb{N}$, and therefore the angular dispersion

$$D := \frac{d\theta}{d\lambda} = \frac{m}{d\cos\theta}$$

i.e., angular separation between maxima for λ and $\lambda + \Delta\lambda$:

$$\Delta\theta = \frac{m\Delta\lambda}{d\cos\theta}$$

such that the resolving power is

$$R := \frac{\lambda}{\Delta\lambda} = \frac{m\lambda}{d\cos\theta\Delta\theta} = \frac{m\lambda N d\cos\theta}{d\cos\theta\lambda} = mN = \frac{mL}{d}$$

where L width of grating.

Gratings Spectrometers

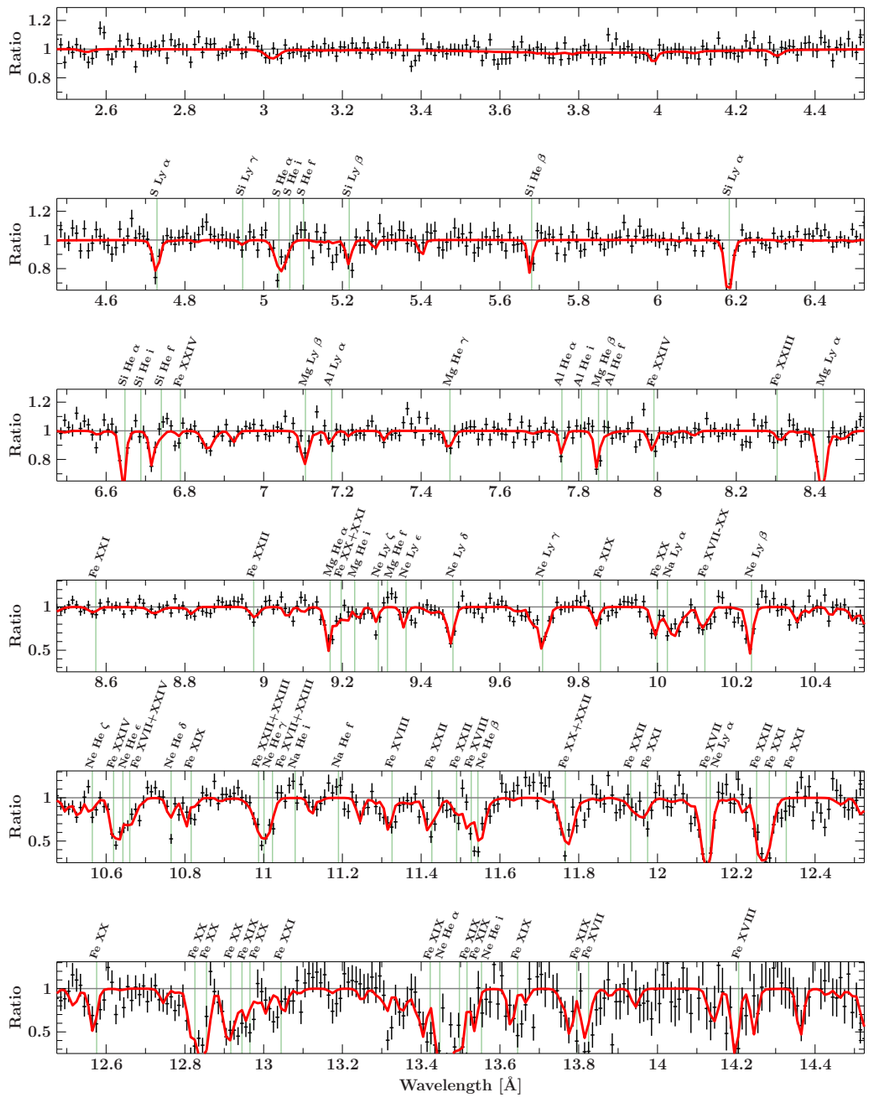

Typical good quality X-ray spectrum of a black hole binary (Cyg X-1): Line series of H- and He-like ions (Miškovičová et al., 2016)

Implementation

- Crystal spectrometers (rare, only one flown on *Einstein*)
- Gratings spectrometers:
  - transmission spectrometers: *Chandra*-HETGS and-LETGS
  - reflection spectrometer: *XMM-Newton*-RGS

Typical resolution of gratings spectrometers:

- *Chandra*-HETGS:
  $E/\Delta E \sim 800$ at 1.5 keV, ~200 at 6 keV
- *Chandra*-LETGS:
  $E/\Delta E > 1000$ in 0.07–0.2 keV
- *XMM-Newton*-RGS:
  $E/\Delta E$: 150–800 in 0.33–2.5 keV

Note: $|\lambda/\Delta\lambda| = |E/\Delta E|$

Reminder: CCDs: $E/\Delta E \sim 40$

$\Longrightarrow$ extreme diagnostic power!

T, n,...

Example: Chandra HETGS

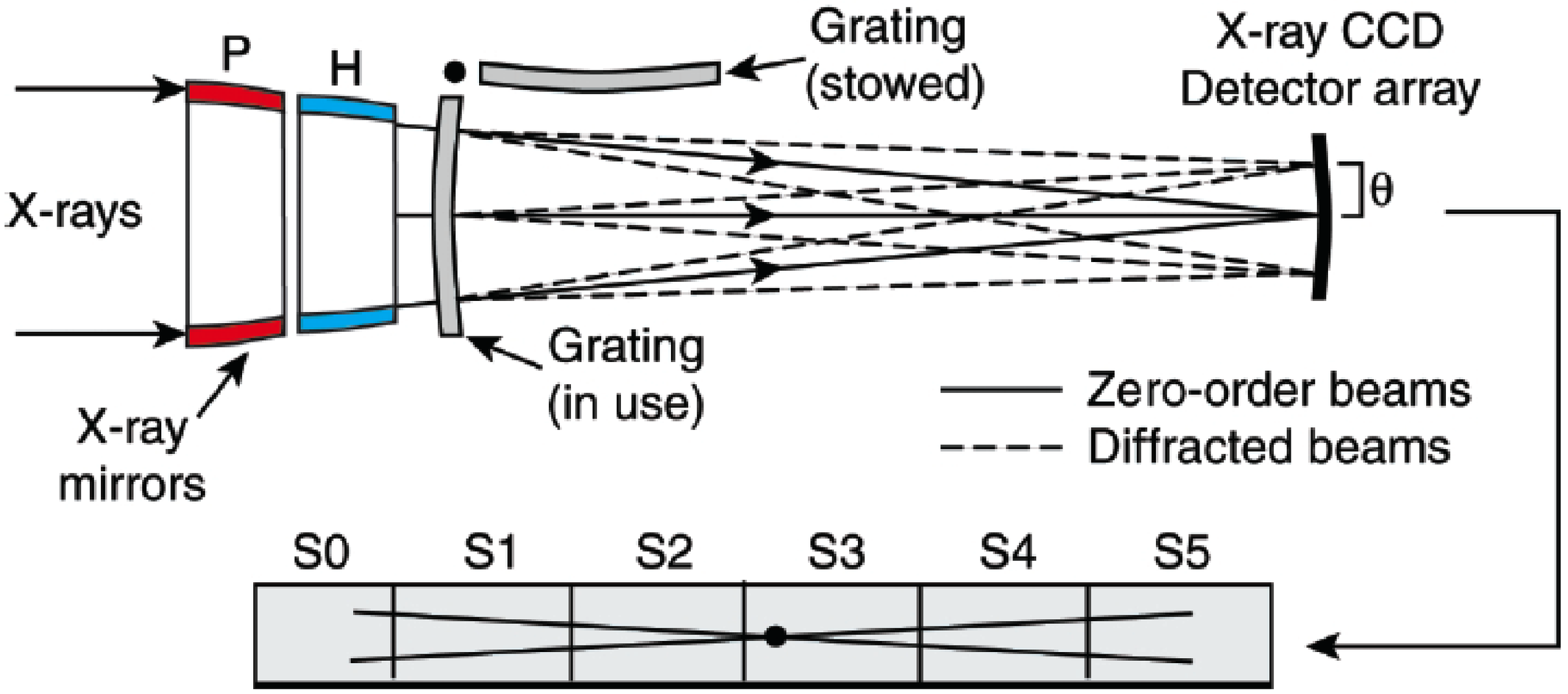

(Canizares et al., 2005)

Chandra High Energy Transmission Gratings Spectrometer

Example: Chandra HETGS

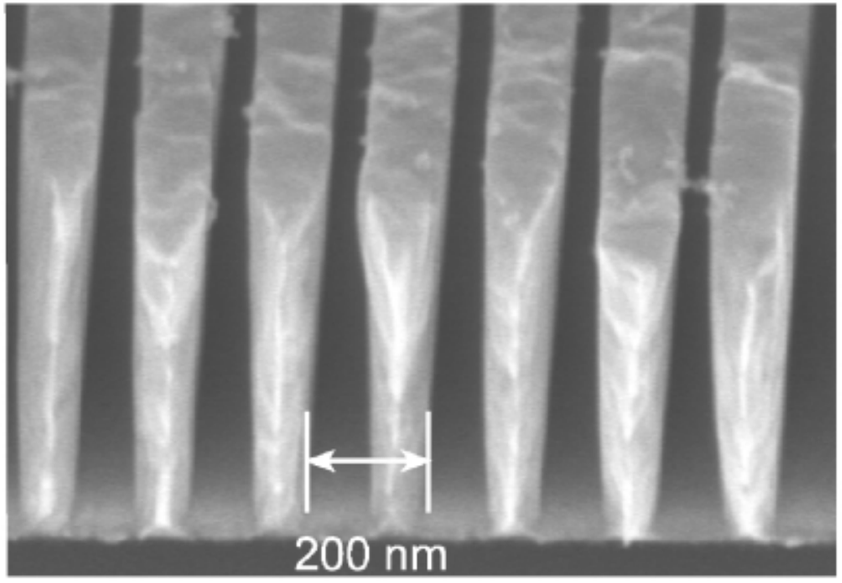

(a) High Energy Grating (HEG).

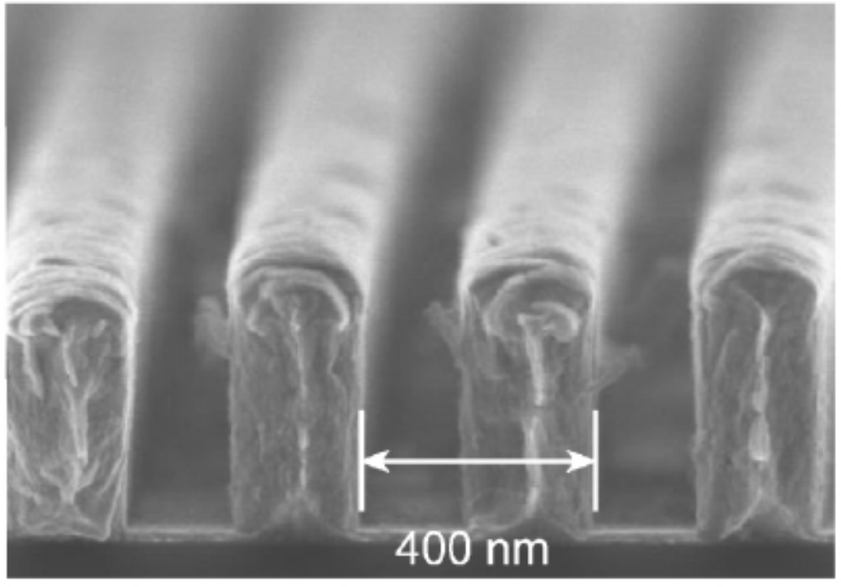

(b) Medium Energy Grating (MEG).

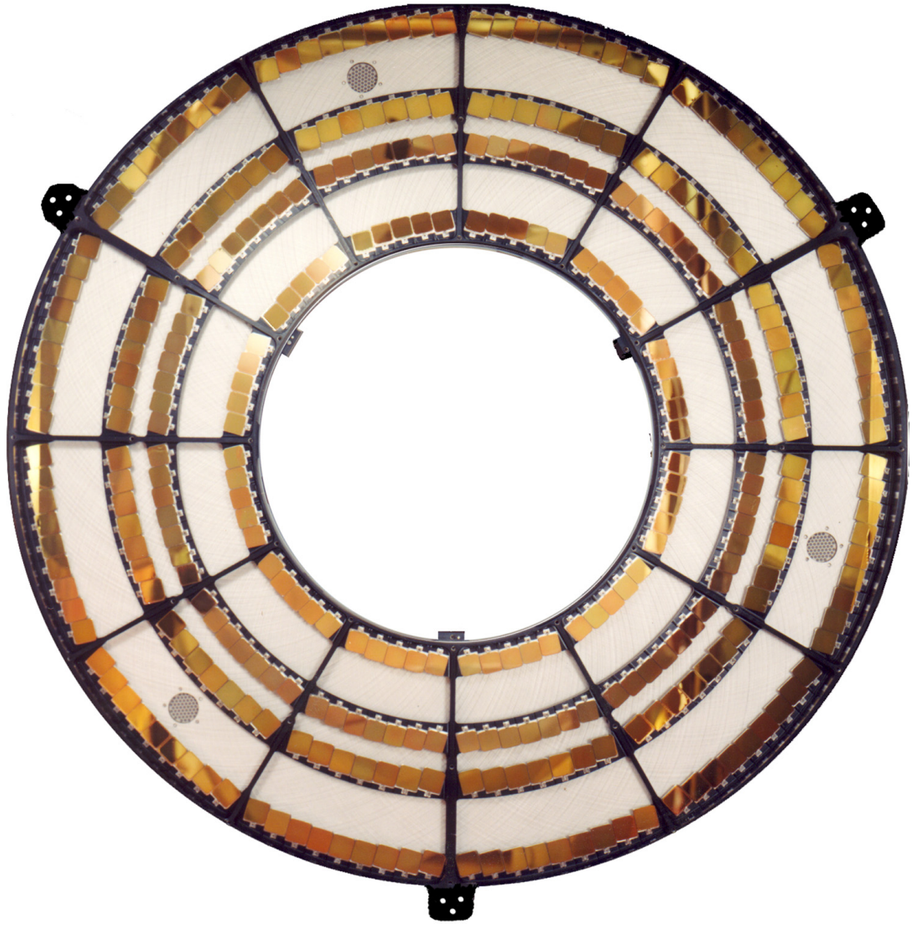

HETGS (built by MIT): Two tiled gratings

- HEG: 120 nm×510 nm Au bars, period $p = 200\,\text{nm}$
- MEG: 208 nm×360 nm Au bars, period $p = 400\,\text{nm}$

both on facets of $25 \times 25\,\text{mm}^2$ size

Example: Chandra HETGS

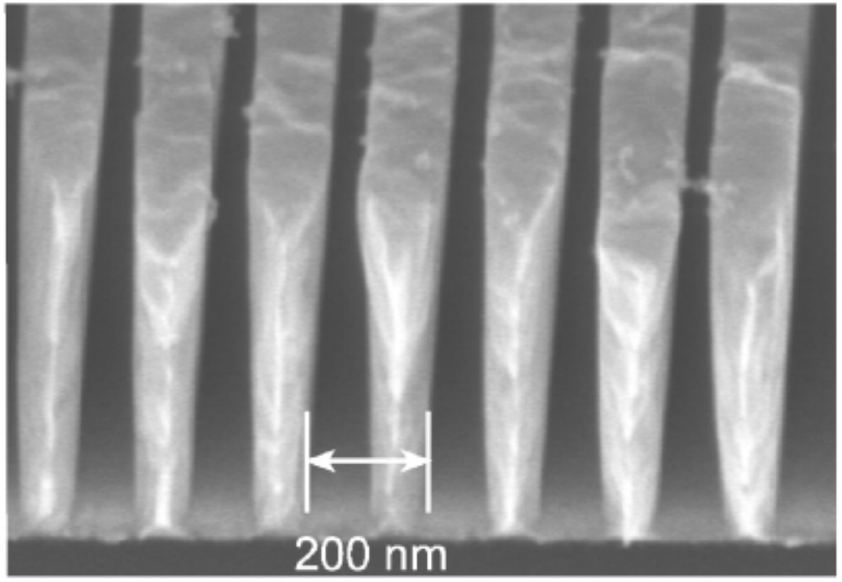

(a) High Energy Grating (HEG).

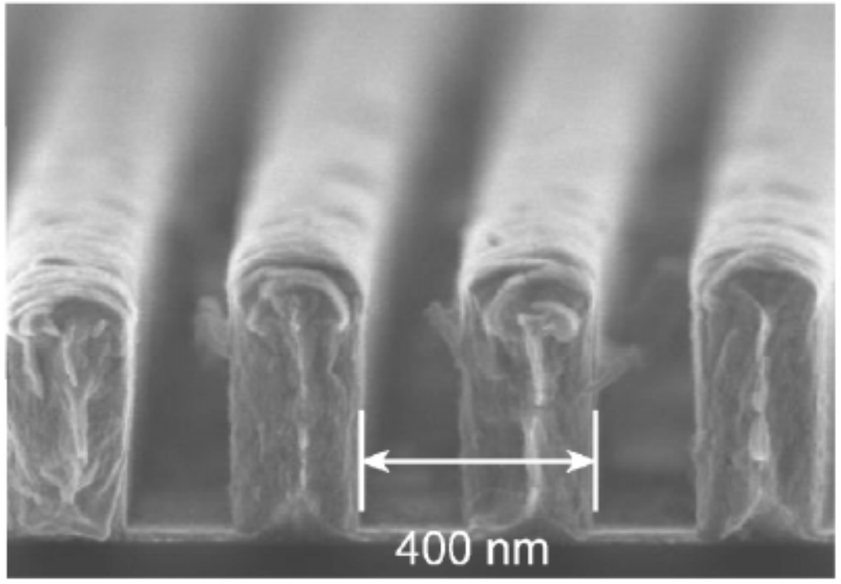

(b) Medium Energy Grating (MEG).

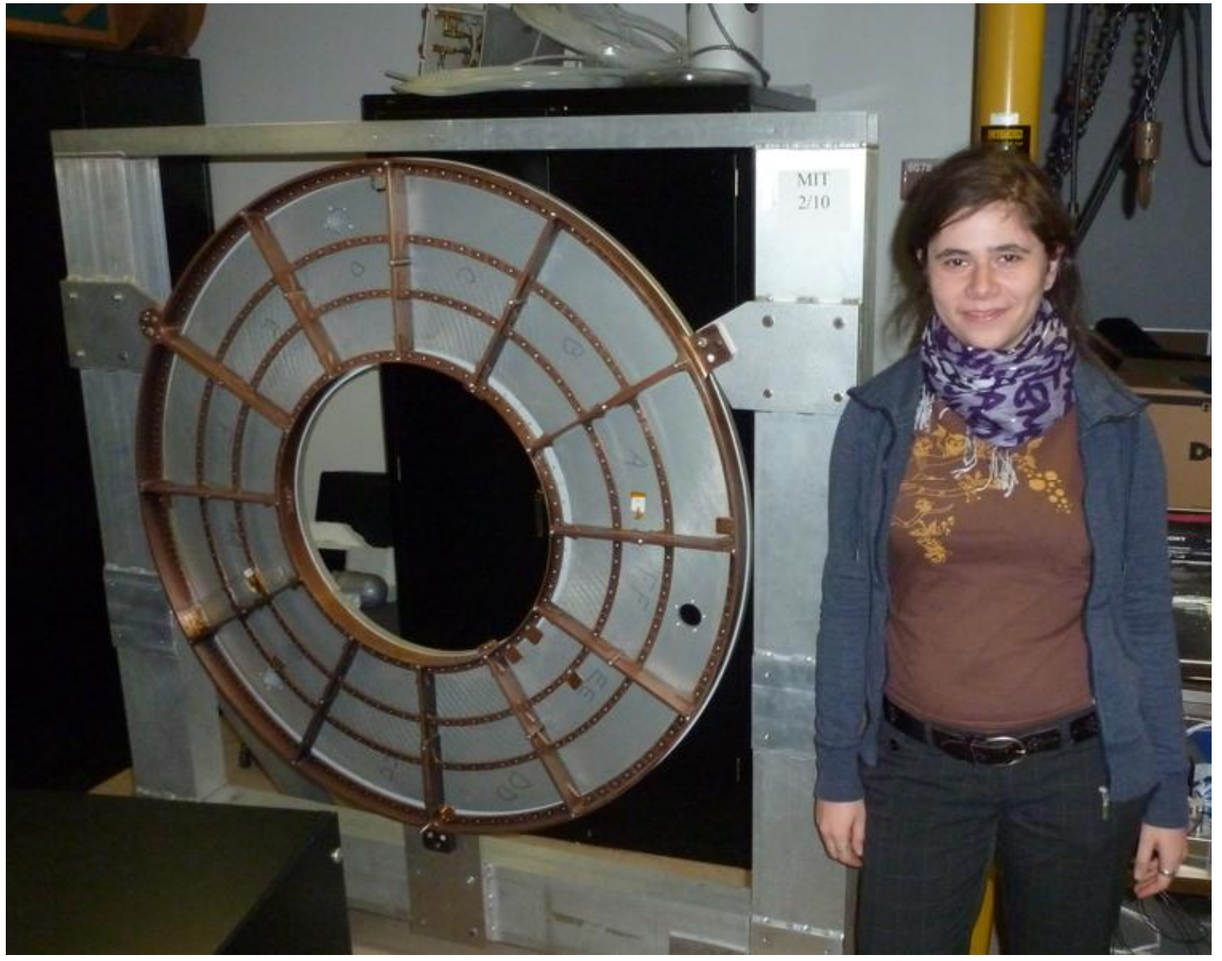

HETGS (built by MIT): Two tiled gratings

- HEG: 120 nm×510 nm Au bars, period $p = 200\,\text{nm}$
- MEG: 208 nm×360 nm Au bars, period $p = 400\,\text{nm}$

both on facets of $25 \times 25\,\text{mm}^2$ size

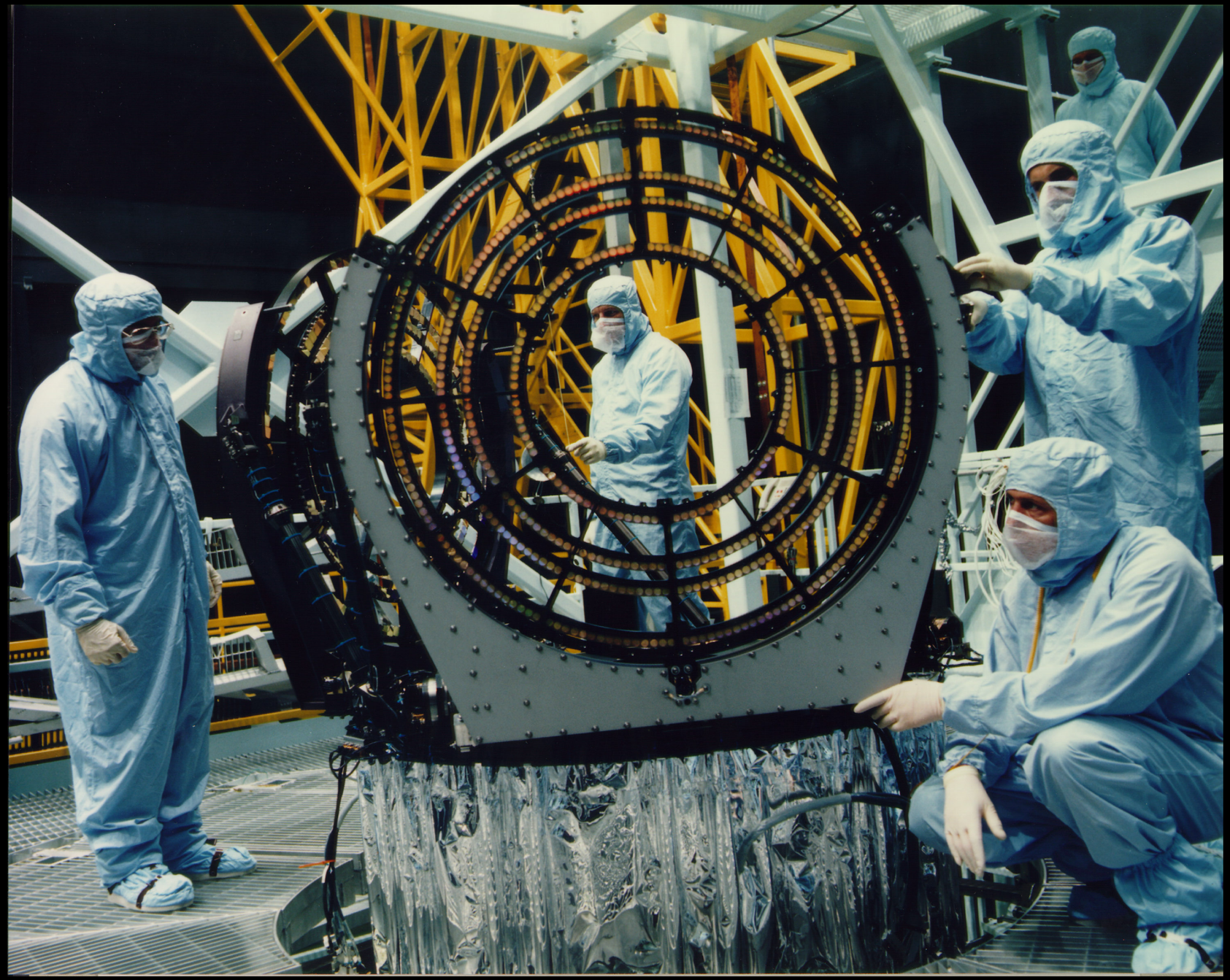

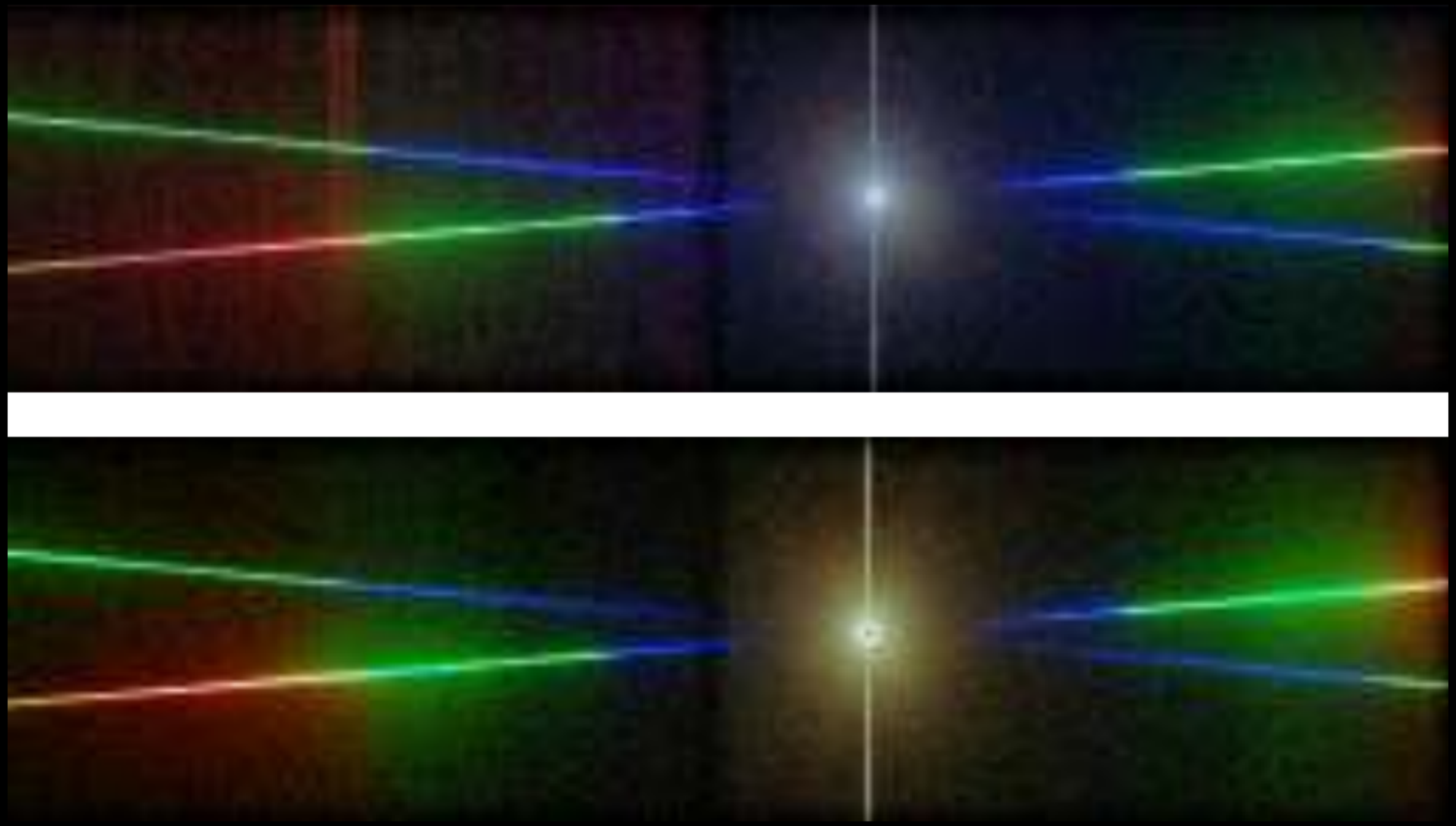

M. Hanke

Dispersion directions of MEG and HEG tilted by ~10°
$\Longrightarrow$ simultaneous measurement of HEG and MEG data.

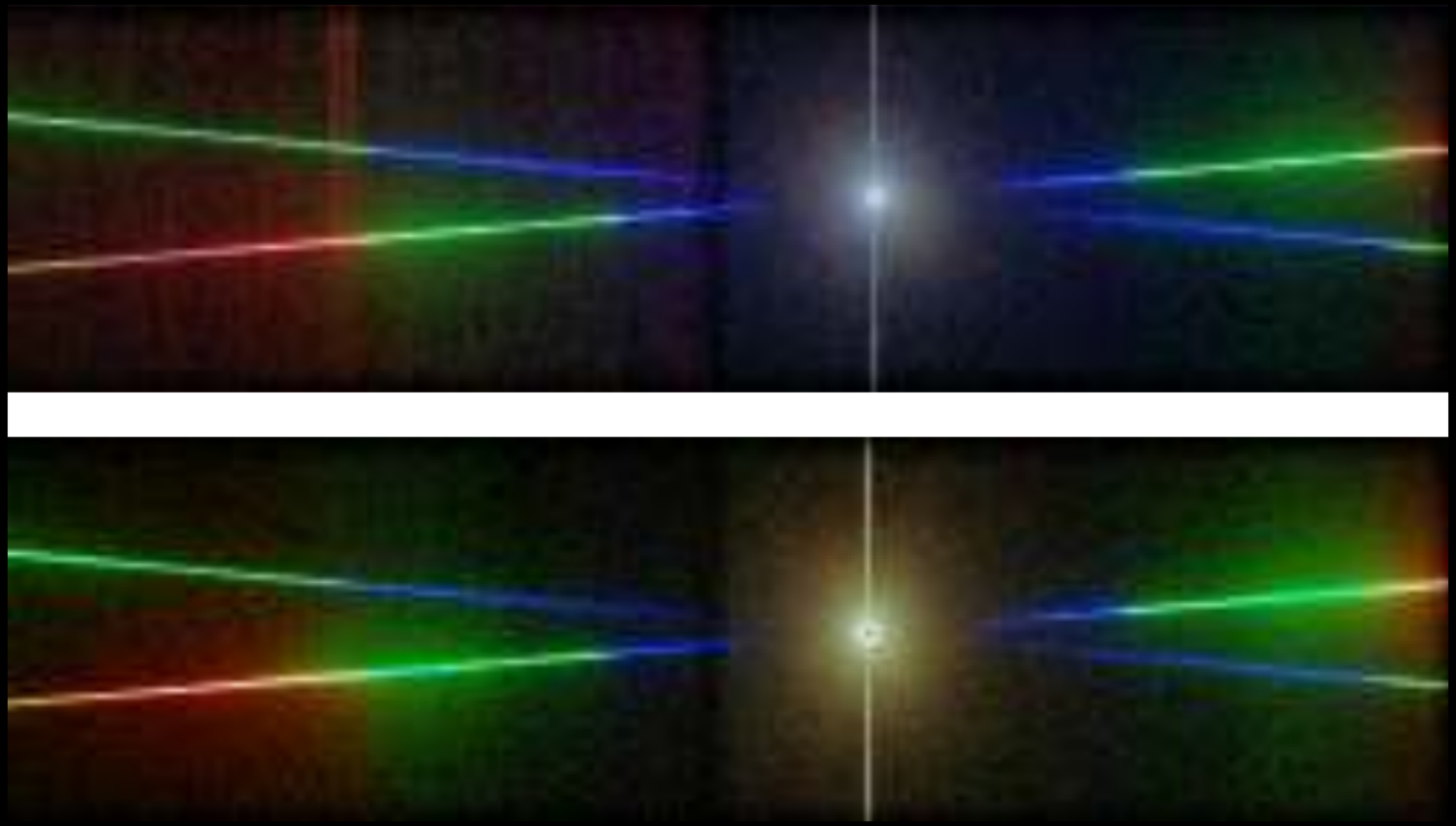

M. Hanke

Dispersion directions of MEG and HEG tilted by $\sim 10^\circ$

$\Longrightarrow$ simultaneous measurement of HEG and MEG data.

Note: X-ray dust scattering halo at 0th order, “out of time events”/“readout strip”.

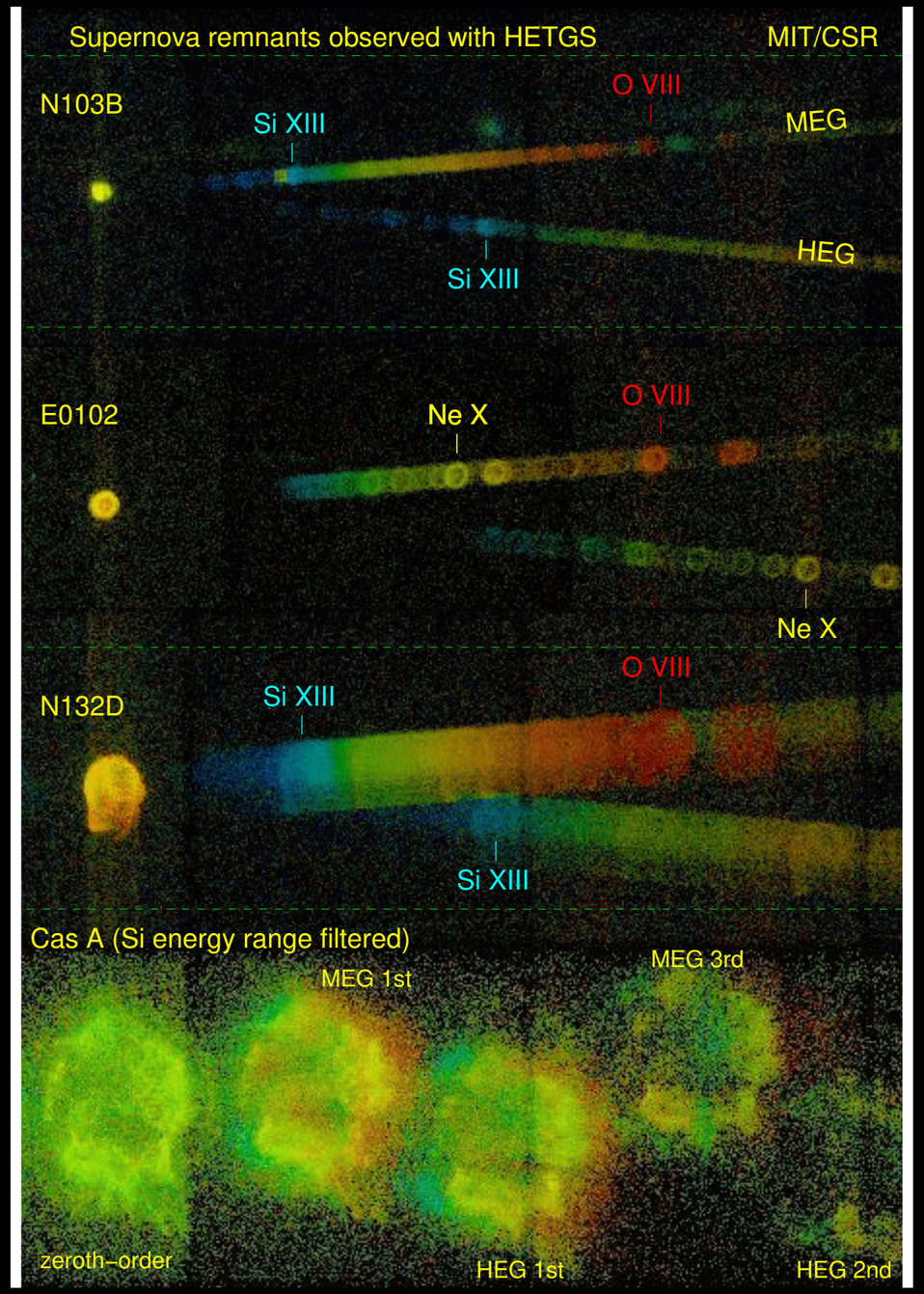

Chandra gratings spectra (0th and 1st order) of several SNRs

$\Longrightarrow$ because spectra are line dominated, elemental mapping is also possible with gratings (but technically very difficult)

Example: Chandra HETGS

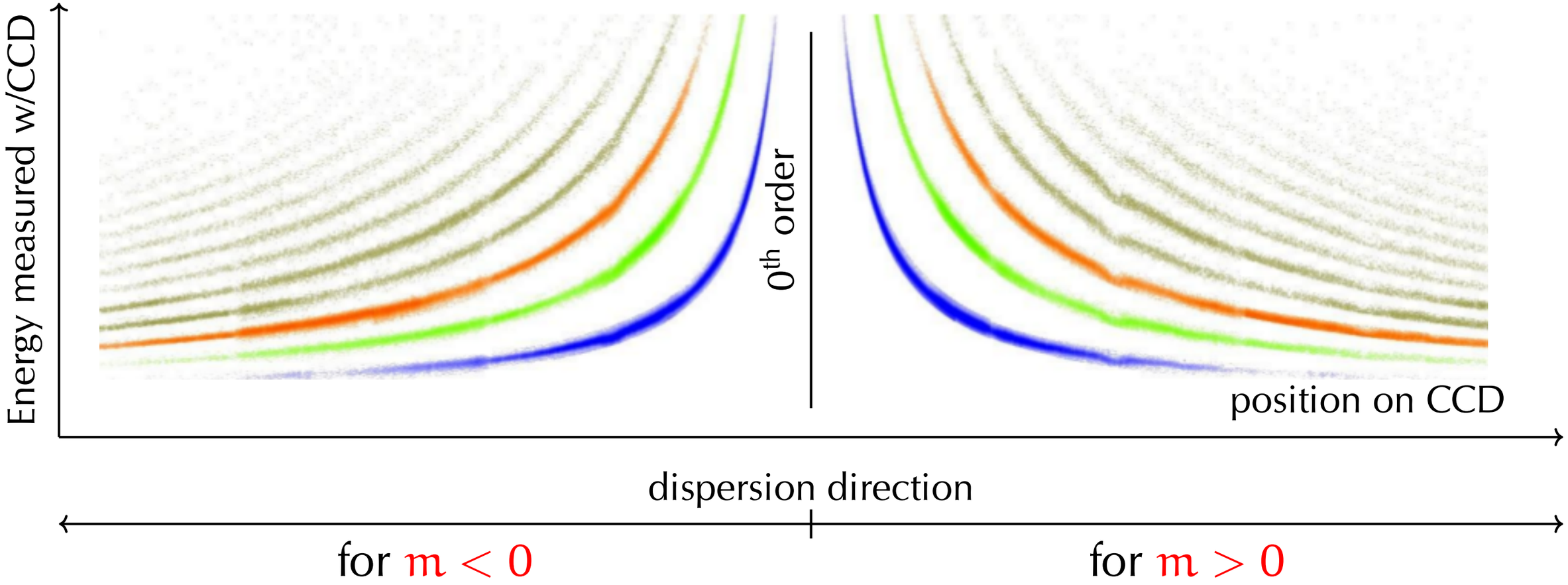

"banana plot"; after M. Hanke

Gratings are built such that gratings orders overlap

$\Longrightarrow$ use coarse energy measurement of ACIS CCDs to assign orders

Example: XMM RGS

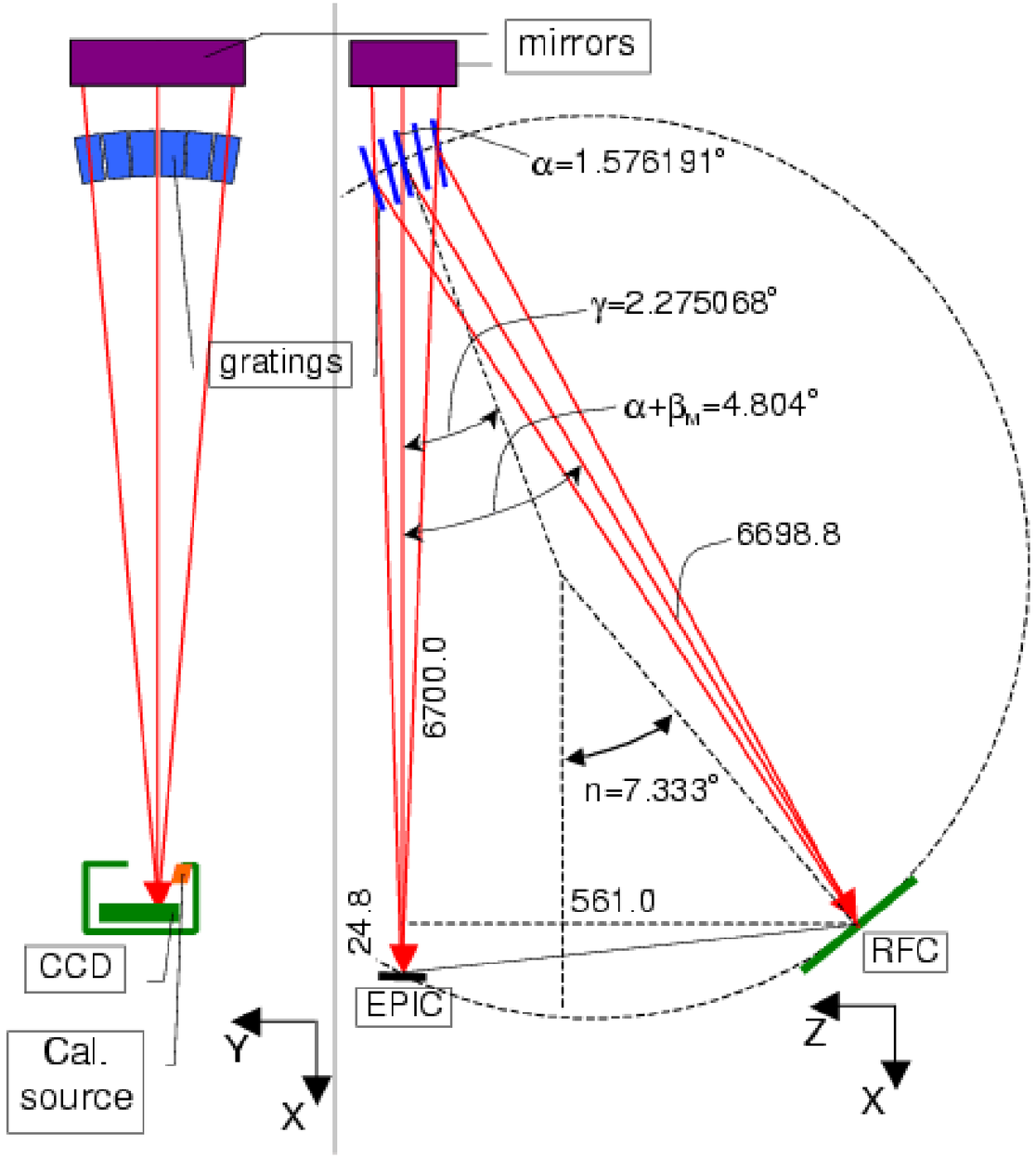

XMM-Newton Reflection Gratings Spectrometer: much larger effective area than *Chandra*, but lower resolution.

(den Herder et al., 2001)

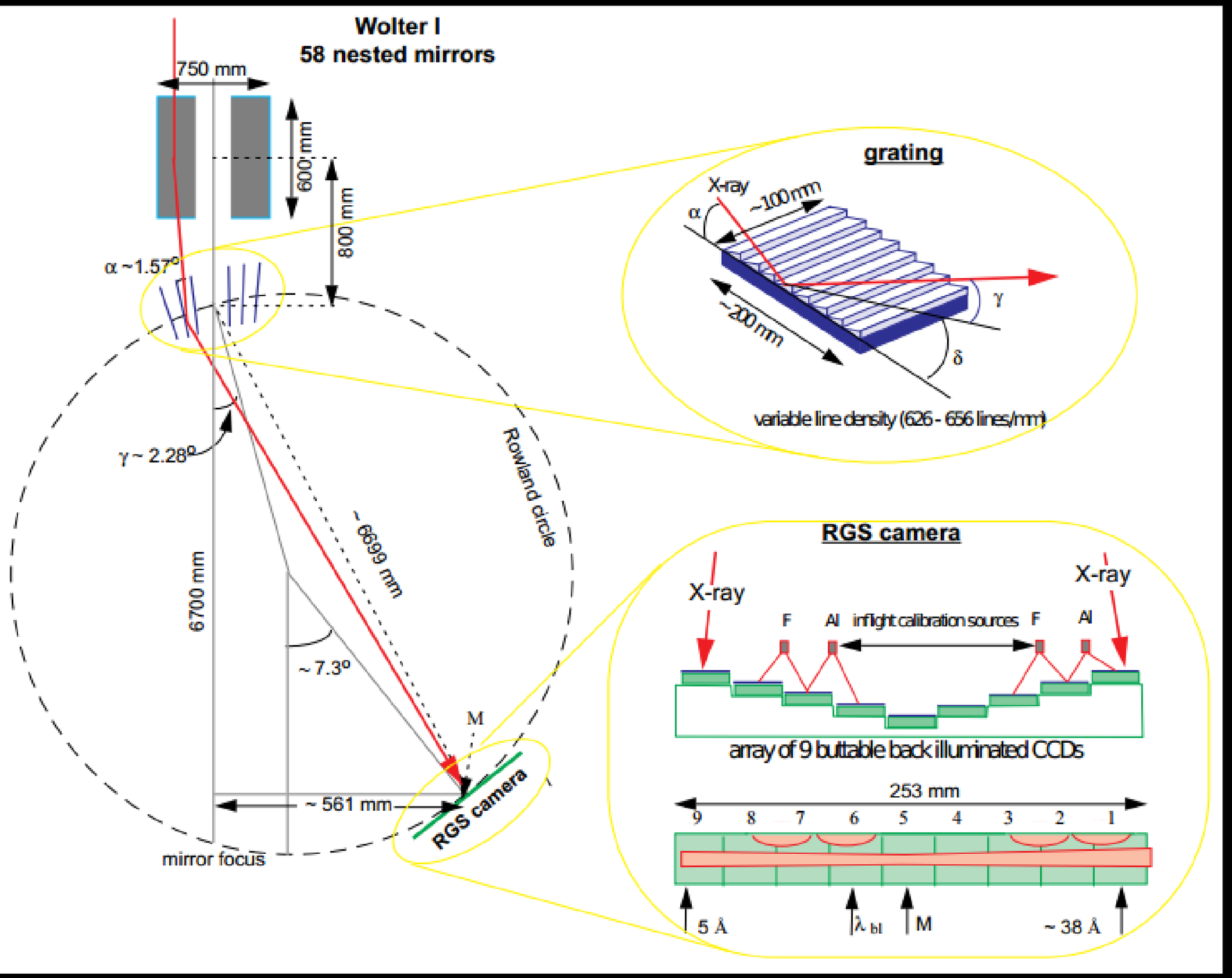

Brinkman et al., 1999, 1st XMM science workshop

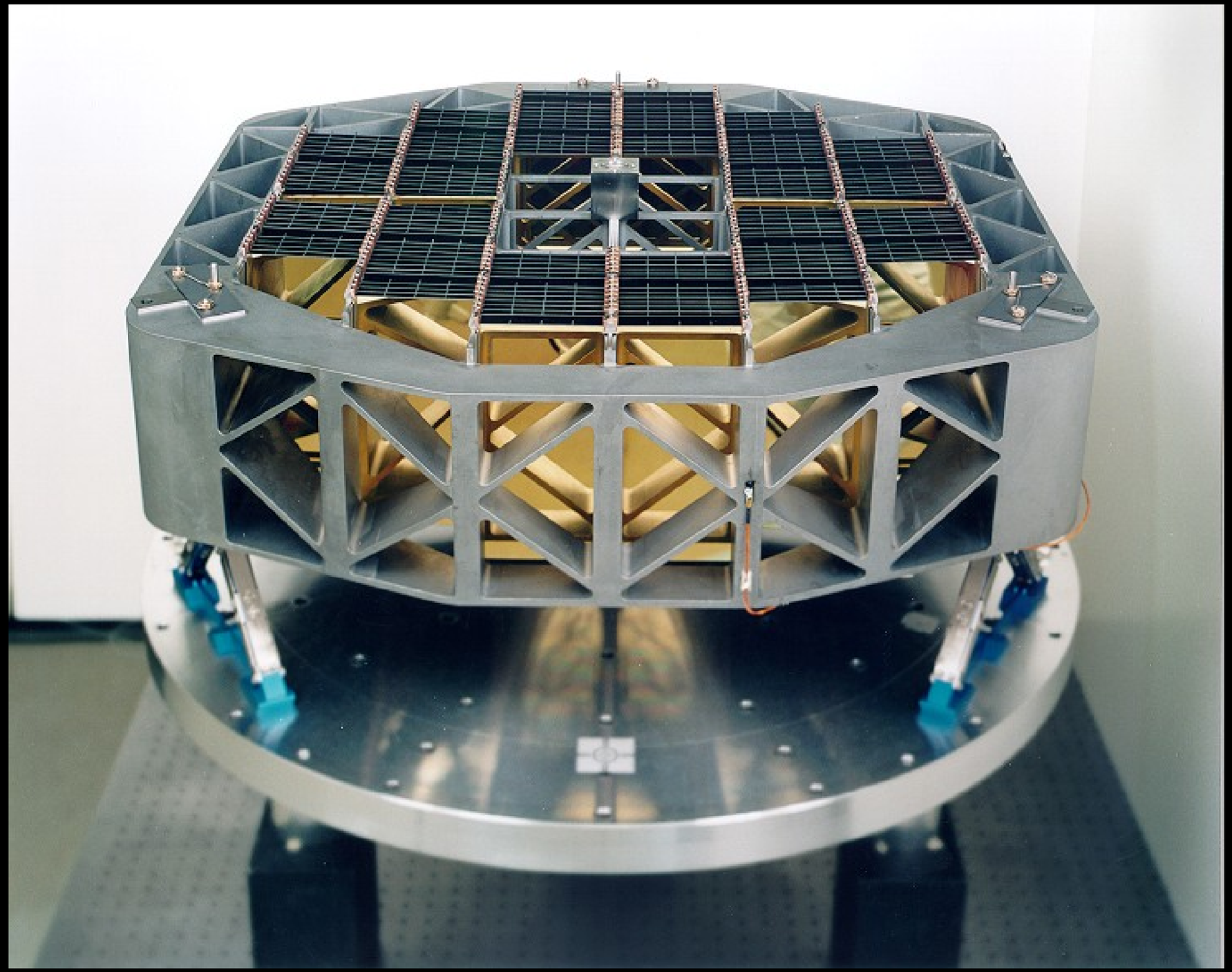

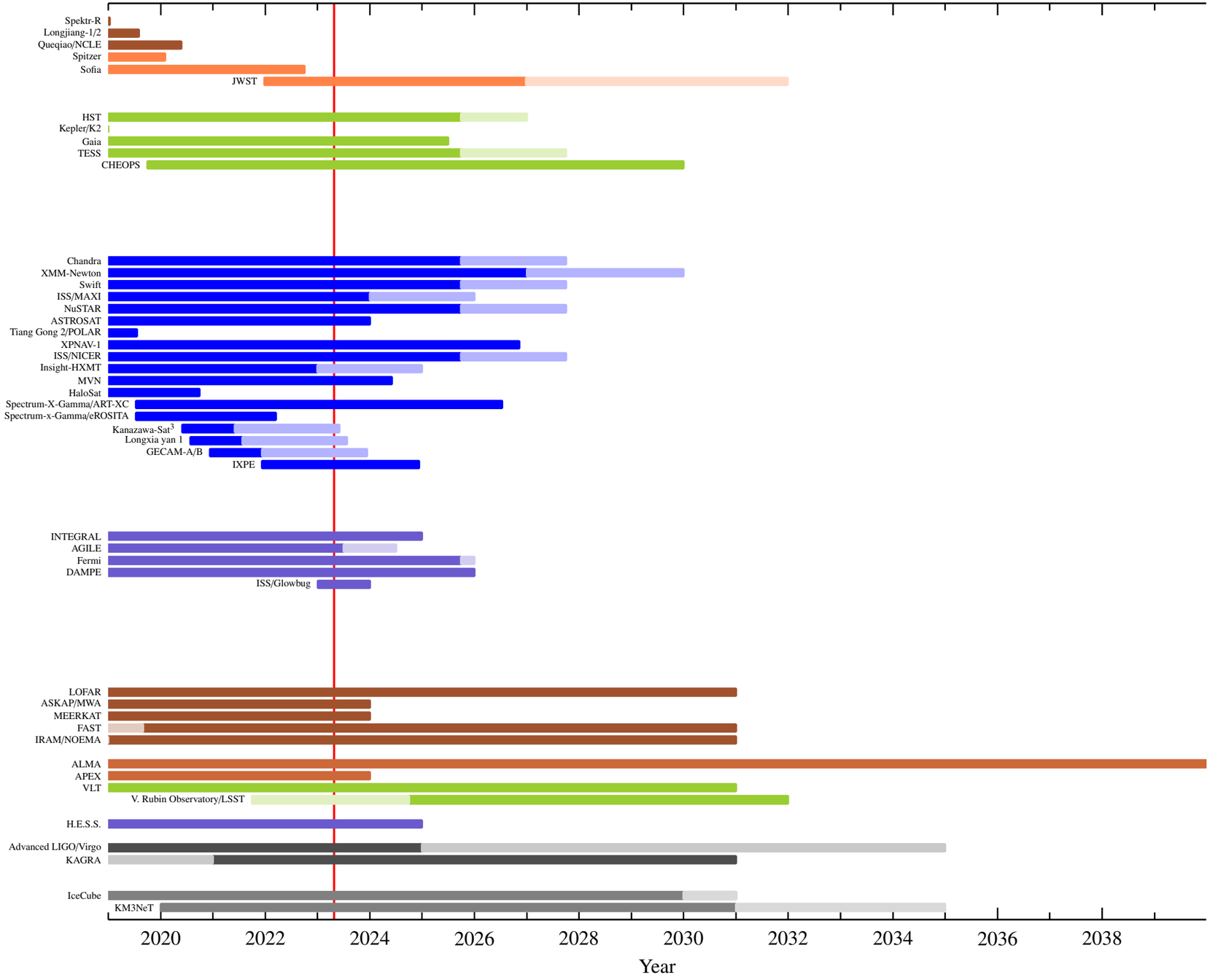
Spektr-R
Longjiang-1/2
Queqiao/NCLE
Spitzer
Sofia
JWST
HST
Kepler/K2
Gaia
TESS
CHEOPS
Chandra
XMM-Newton
Swift
ISS/MAXI
NuSTAR
ASTROSAT
Tiang Gong 2/POLAR
XPNAV-1
ISS/NICER
Insight-HXMT
MVN
HaloSat
Spectrum-X-Gamma/ART-XC
Spectrum-x-Gamma/eROSITA
Kanazawa-Sat3
Longxia yan 1
GECAM-A/B
IXPE
INTEGRAL
AGILE
Fermi
DAMPE
ISS/Glowbug
LOFAR
ASKAP/MWA
MEERKAT
FAST
IRAM/NOEMA
ALMA
APEX
VLT
V. Rubin Observatory/LSST
H.E.S.S.
Advanced LIGO/Virgo
KAGRA
IceCube
KM3NeT
2020
2022
2024
2026
2028
2030
2032
2034
2036
2038
Year

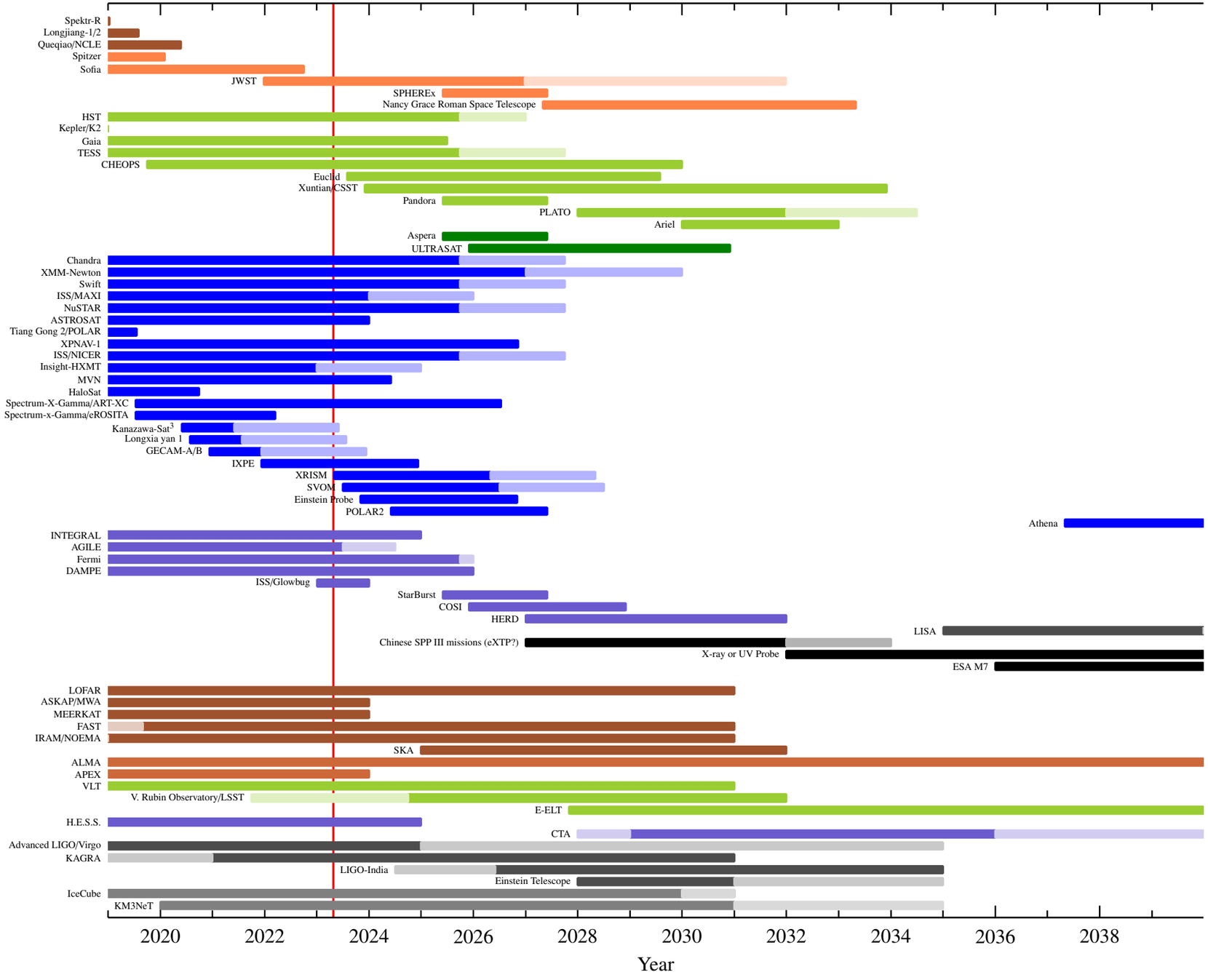
Spektr-R
Longjiang-1/2
Queqiao/NCLE
Spitzer
Sofia
JWST
SPHEREx
Nancy Grace Roman Space Telescope
HST
Kepler/K2
Gaia
TESS
CHEOPS
Euclid
Xuntian/CSST
Pandora
PLATO
Ariel
Aspera
ULTRASAT
Chandra
XMM-Newton
Swift
ISS/MAXI
NuSTAR
ASTROSAT
Tiang Gong 2/POLAR
XPNAV-1
ISS/NICER
Insight-HXMT
MVN
HaloSat
Spectrum-X-Gamma/ART-XC
Spectrum-x-Gamma/eROSITA
Kanazawa-Sat3
Longxia yan 1
GECAM-A/B
IXPE
XRISM
SVOM
Einstein Probe
POLAR2
Athena
INTEGRAL
AGILE
Fermi
DAMPE
ISS/Glowbug
StarBurst
COSI
HERD
LISA
Chinese SPP III missions (eXTP?)
X-ray or UV Probe
ESA M7
LOFAR
ASKAP/MWA
MEERKAT
FAST
IRAM/NOEMA
SKA
ALMA
APEX
VLT
V. Rubin Observatory/LSST
E-ELT
H.E.S.S.
CTA
Advanced LIGO/Virgo
KAGRA
LIGO-India
Einstein Telescope
IceCube
KM3NeT
2020
2022
2024
2026
2028
2030
2032
2034
2036
2038
Year

Calorimeters

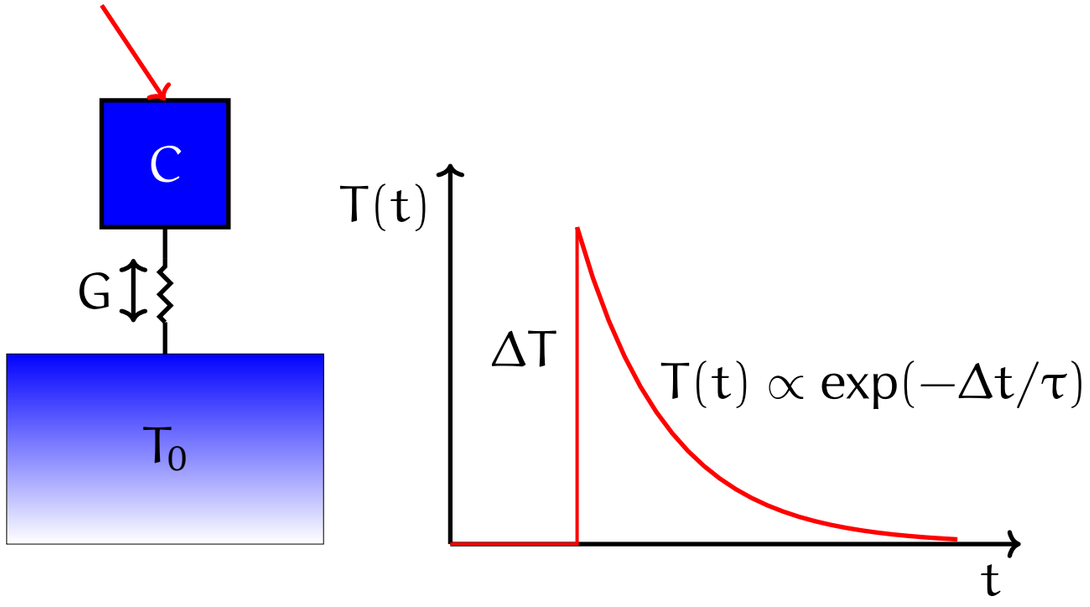

(after McCammon, 2005, Fig. 1)

Principle of calorimeter: Measure energy deposited by photon of energy E with a sensitive thermometer attached to a heat sink. Use ΔT to determine E: Temperature jump

$$\Delta T = E/c_V$$

where c_V: heat capacity

$\Longrightarrow$ the smaller c_V, the better

Calorimeters

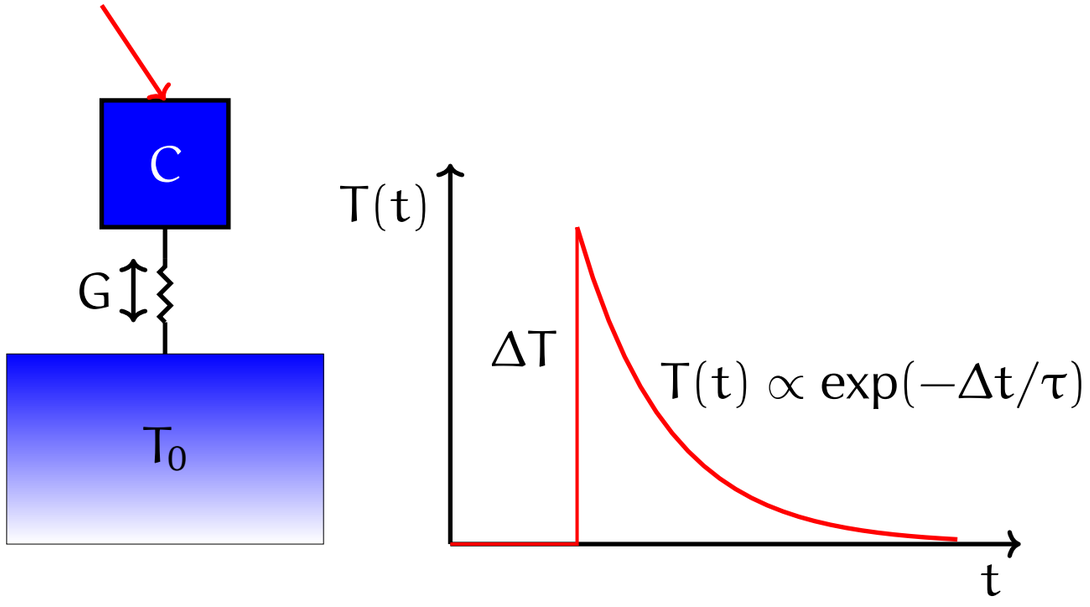

(after McCammon, 2005, Fig. 1)

Principle of calorimeter: Measure energy deposited by photon of energy E with a sensitive thermometer attached to a heat sink. Use ΔT to determine E: Temperature jump

$$\Delta T = E/c_V$$

where c_V: heat capacity
$\Longrightarrow$ the smaller c_V, the better

Normal material:

$$c_V \sim 3Nk$$

where N: number of atoms, k: Boltzmann.
Example: 1 mm^3 of Si: $N = 5 \times 10^{19}$ atoms, $c_V = 2 \times 10^4\,\mathrm{erg\,K^{-1}}$.
Therefore for E = 1 keV: $\Delta T = 8 \times 10^{-14}\,\mathrm{K}$

Calorimeters

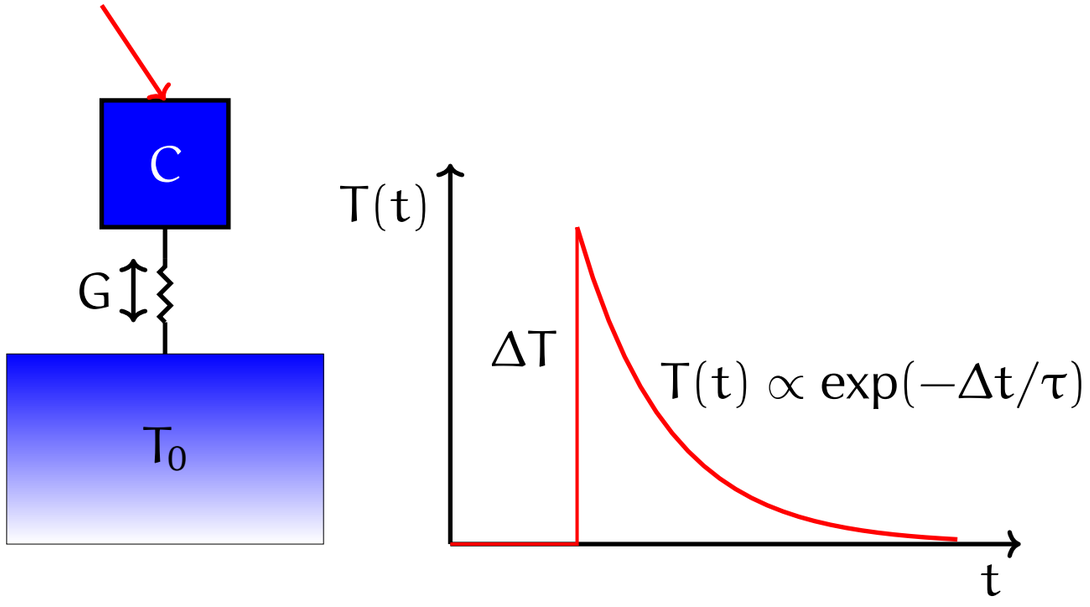

(after McCammon, 2005, Fig. 1)

Principle of calorimeter: Measure energy deposited by photon of energy E with a sensitive thermometer attached to a heat sink. Use ΔT to determine E: Temperature jump

$$\Delta T = E/c_V$$

where c_V: heat capacity
$\Longrightarrow$ the smaller c_V, the better

Low temperature: most particles in ground state, c_V collapses. Debye:

$$c_V \sim \frac{12\pi^4}{5} Nk \left(\frac{T}{\Theta}\right)^3$$

where Θ: Debye temperature
($k\Theta \sim \hbar\omega$ with ω: highest vibrational frequency of a crystal)

Example: Si: $\Theta = 640\,\mathrm{K} \Longrightarrow$ for $T = 0.1\,\mathrm{K}$: $c_V \sim 10^{-9}\,\mathrm{erg\,K^{-1}}$
and therefore for $E = 1\,\mathrm{keV}$: $\Delta T = 0.1\,\mathrm{K}$

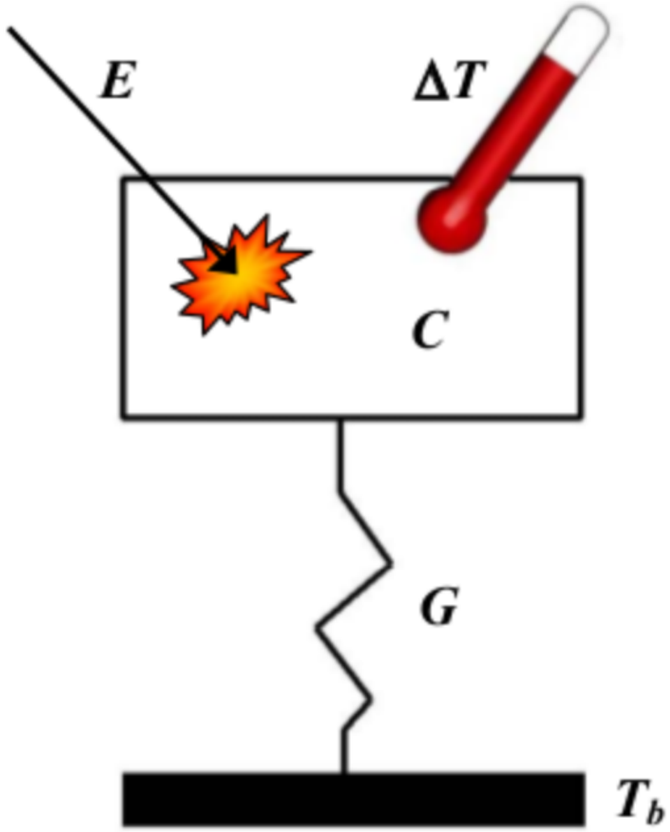

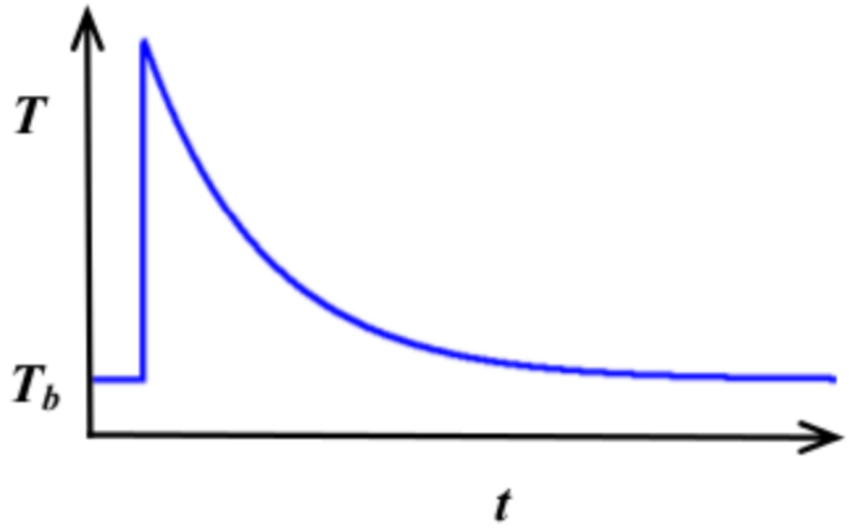

Smith (2006 PhD Leicester)

Calorimeter: measure temperature change in device with temperature T_0 connected to heat bath with temperature T_S.
Joule heating by current through device $\Longrightarrow T_0 > T_S$
Absorption: temperature rises: $\Delta T = E_\gamma / C$
C: heat capacity

Relaxes back to T_0. Typical timescale: $\tau = C/G$.
Resolution given by thermal fluctuations: $\Delta E = 2.35\sqrt{kT^2C}$
$\Longrightarrow$ Small (few eV) for T small (mK)

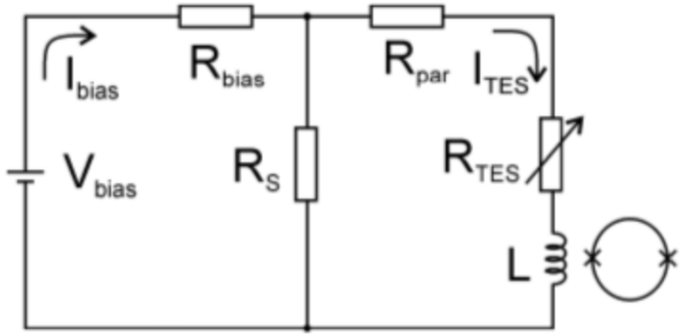

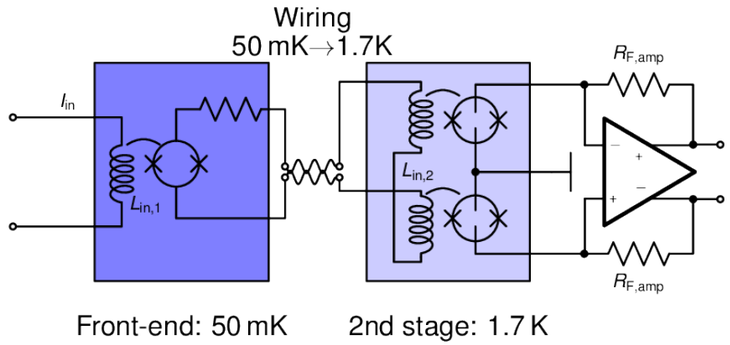

Kinnunen (2011, PhD Jyväskylä)

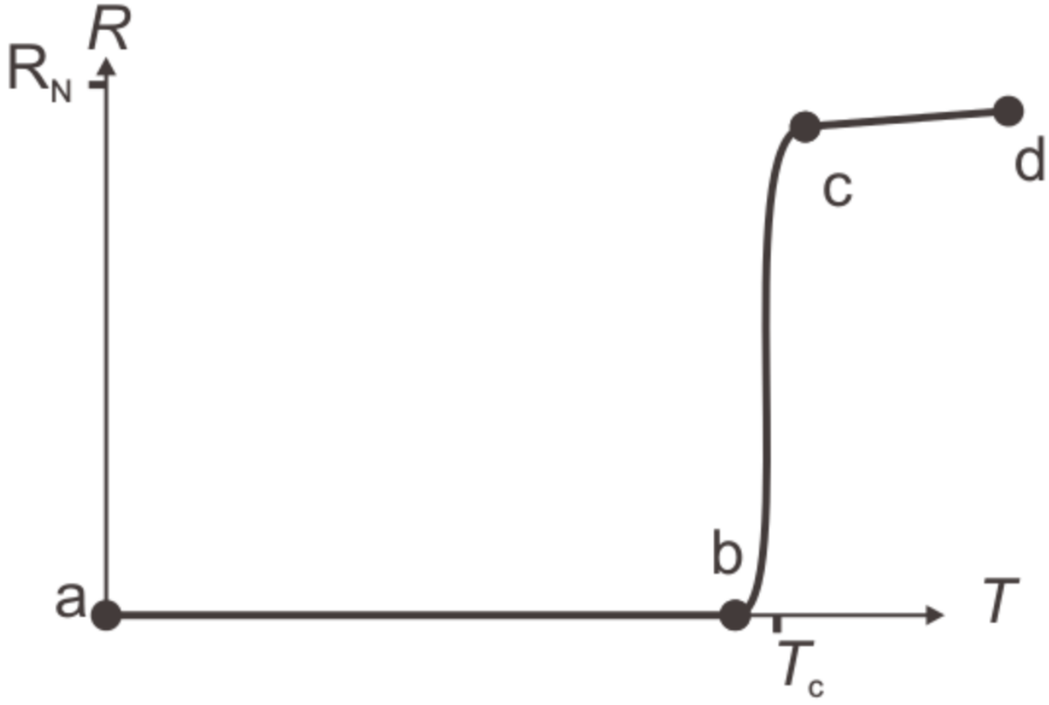

negative electrotermal feedback: Operate circuit at Transition Edge between superconduction and normal conduction, voltage bias circuit:

absorption $\Longrightarrow$ R $\nearrow$

$\Longrightarrow$ Joule power $P_J = I^2R$ $\searrow$

$\Longrightarrow$ faster cooling than for R = const

Typical time constants 75 µs...400 µs

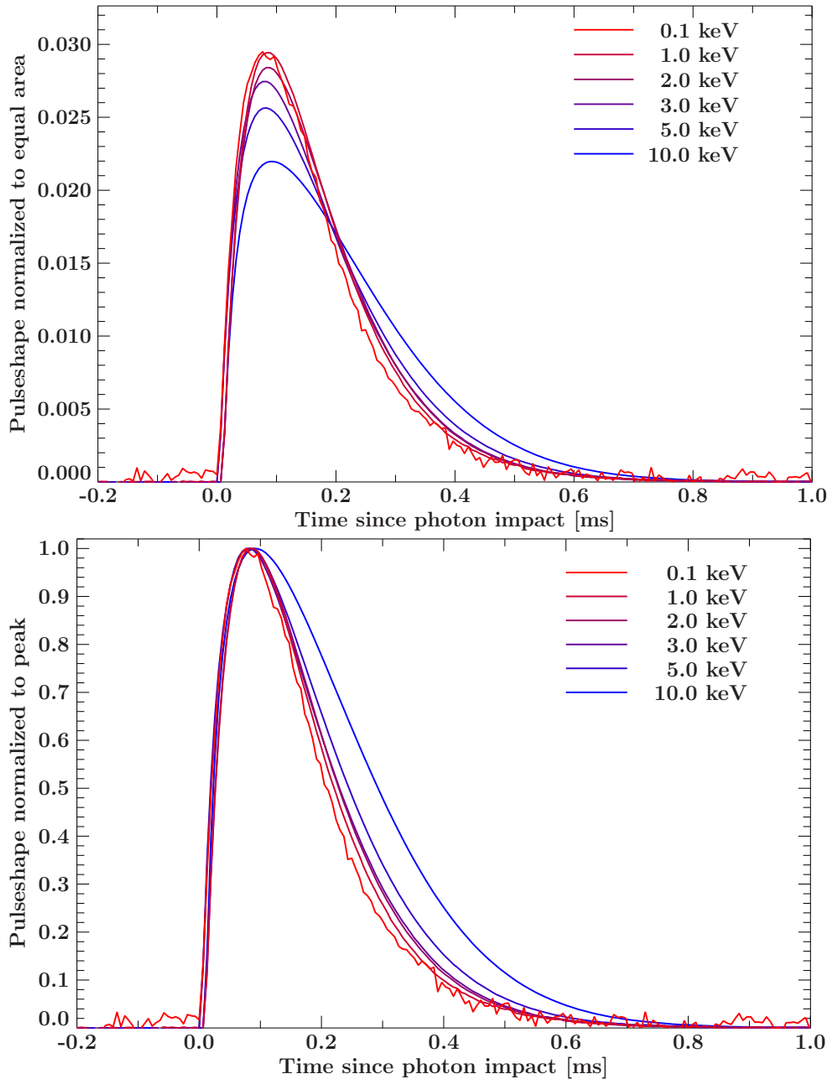

Typical pulse shapes for 0.1, 1, 2, 3, 5, 10 keV, normalized to top: equal area, bottom: peak current.

- Time dependence of TES
  (e.g., Irwin & Hilton, 2005

$$C\frac{dT}{dt} = -P_b + P_J + P + \text{Noise}$$

$$L\frac{dI}{dt} = V - IR_L - IR(T, I) + \text{Noise}$$

- often used linear resistance model, $R(T, I; \alpha, \beta)$
- noise treatment: Johnson of circuit, bath, excess noise
- input parameters: C, G_b, n, α, β, m, R_0, T_0, T_b, L_{crit}

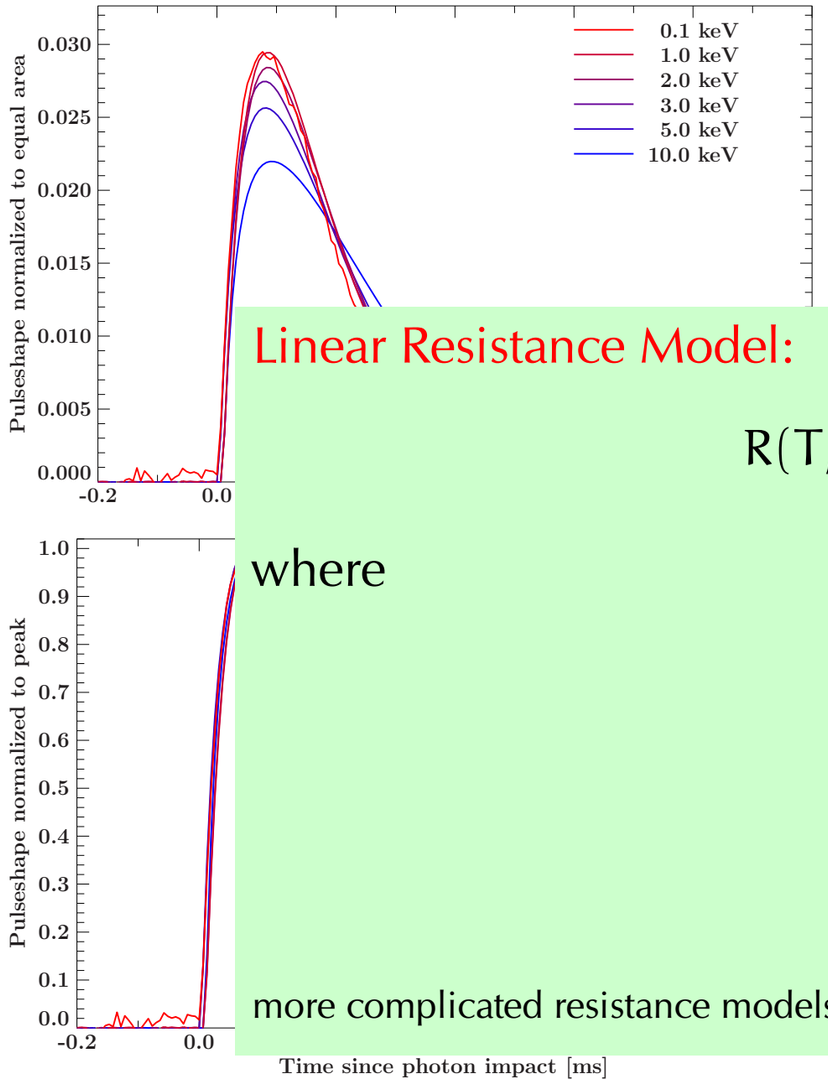

Linear Resistance Model:

$$R(T, I) = R_0 + \left.\frac{\partial R}{\partial T}\right|_{I_0} (T - T_0) + \left.\frac{\partial R}{\partial I}\right|_{T_0} (I - I_0) \tag{1}$$

where

$$\alpha = \left.\frac{\partial \log R}{\partial \log T}\right|_{I_0} = \frac{T_0}{R_0} \left.\frac{\partial R}{\partial T}\right|_{I_0} \tag{2}$$

$$\beta = \left.\frac{\partial \log R}{\partial \log I}\right|_{T_0} = \frac{I_0}{R_0} \left.\frac{\partial R}{\partial I}\right|_{T_0} \tag{3}$$

more complicated resistance models used in real work (“cross talk”)

Typical pulse shapes for 0.1, 1, 2, 3, 5, 10 keV, normalized to top: equal area, bottom: peak current.

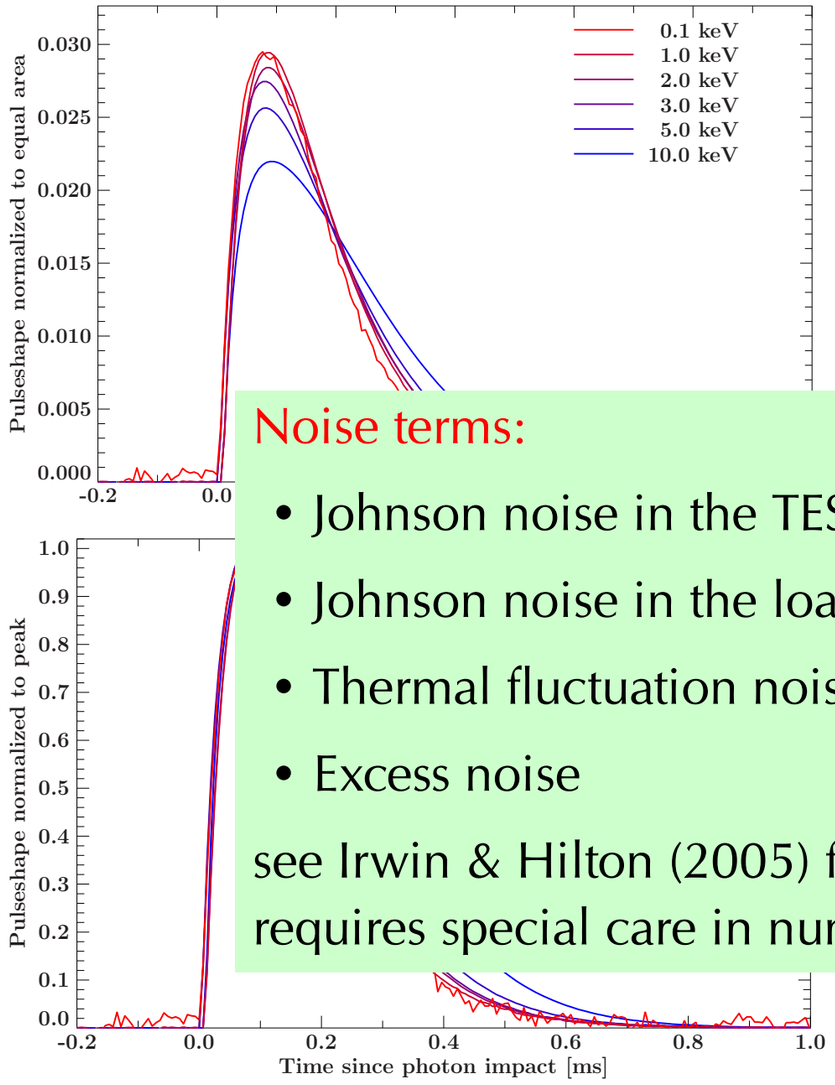

Typical pulse shapes for 0.1, 1, 2, 3, 5, 10 keV, normalized to top: equal area, bottom: peak current.

Noise terms:

- Johnson noise in the TES
- Johnson noise in the load resistor
- Thermal fluctuation noise
- Excess noise

see Irwin & Hilton (2005) for details
requires special care in numerical integrator

- input parameters: C, G_b, n, α, β, m, R_0, T_0, T_b, L_{crit}

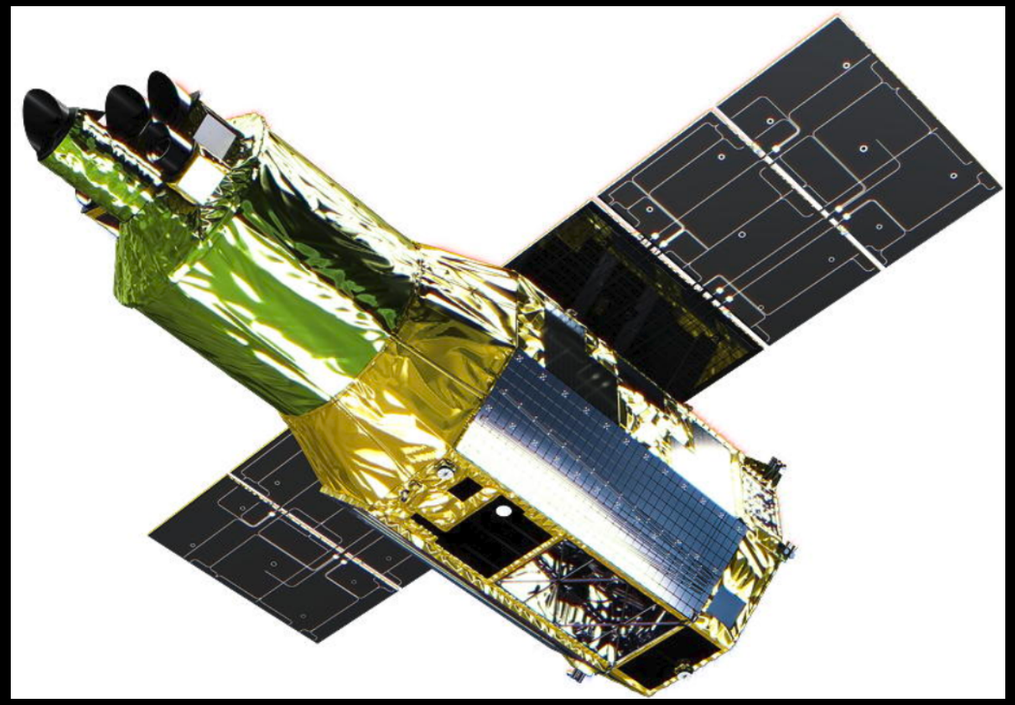

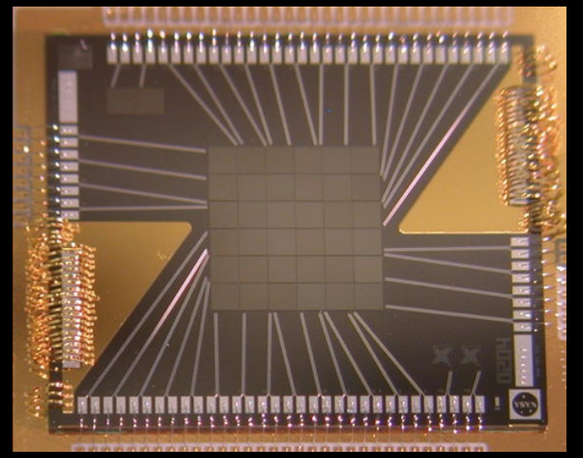

XRISM: Launch in August 2023 – microcalorimetry

successor to failed Hitomi mission

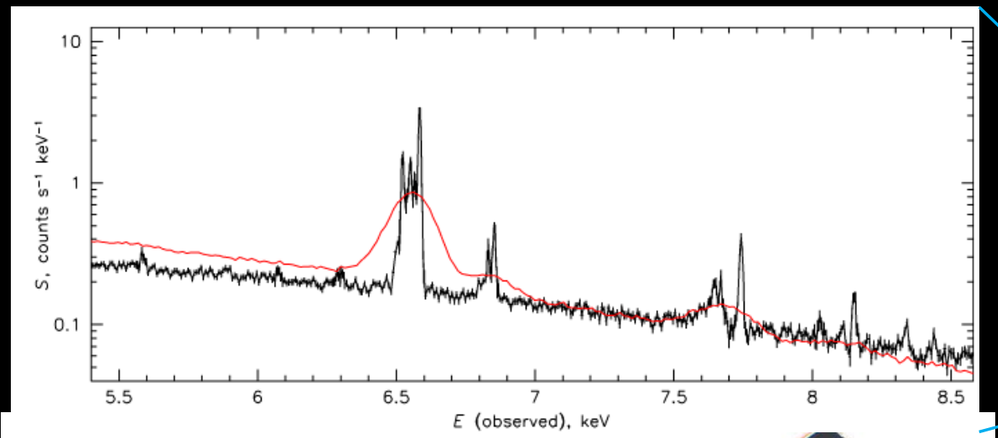

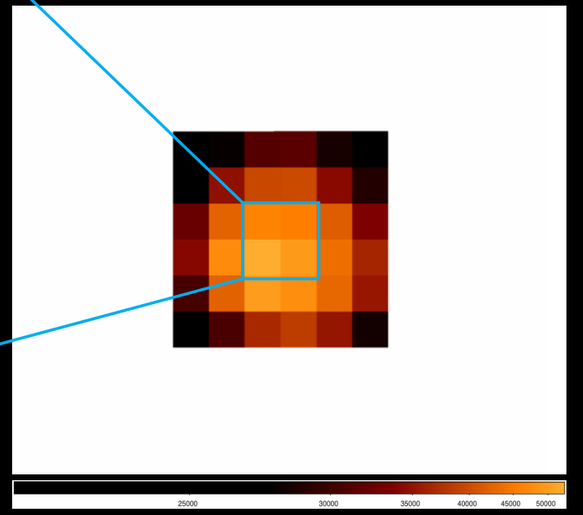

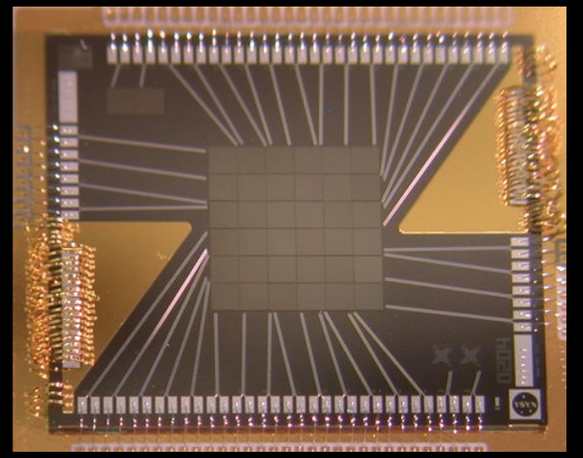

XRISM: Launch in August 2023 – microcalorimetry

successor to failed Hitomi mission

Effective Areas

Si-type resolution

(Fano – ΔE ~ 150 eV at 5.9 keV, R ~ 40)

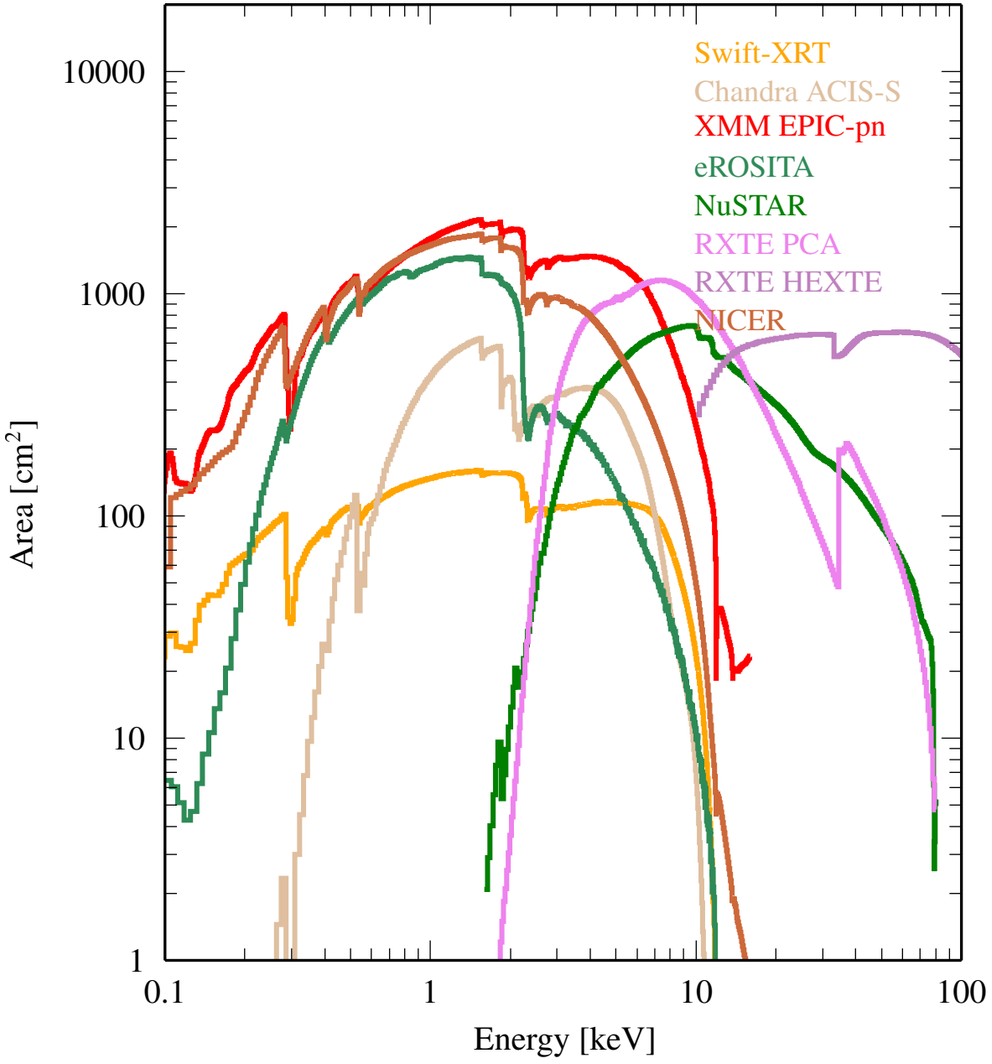

Gratings

(R ~ 1000)

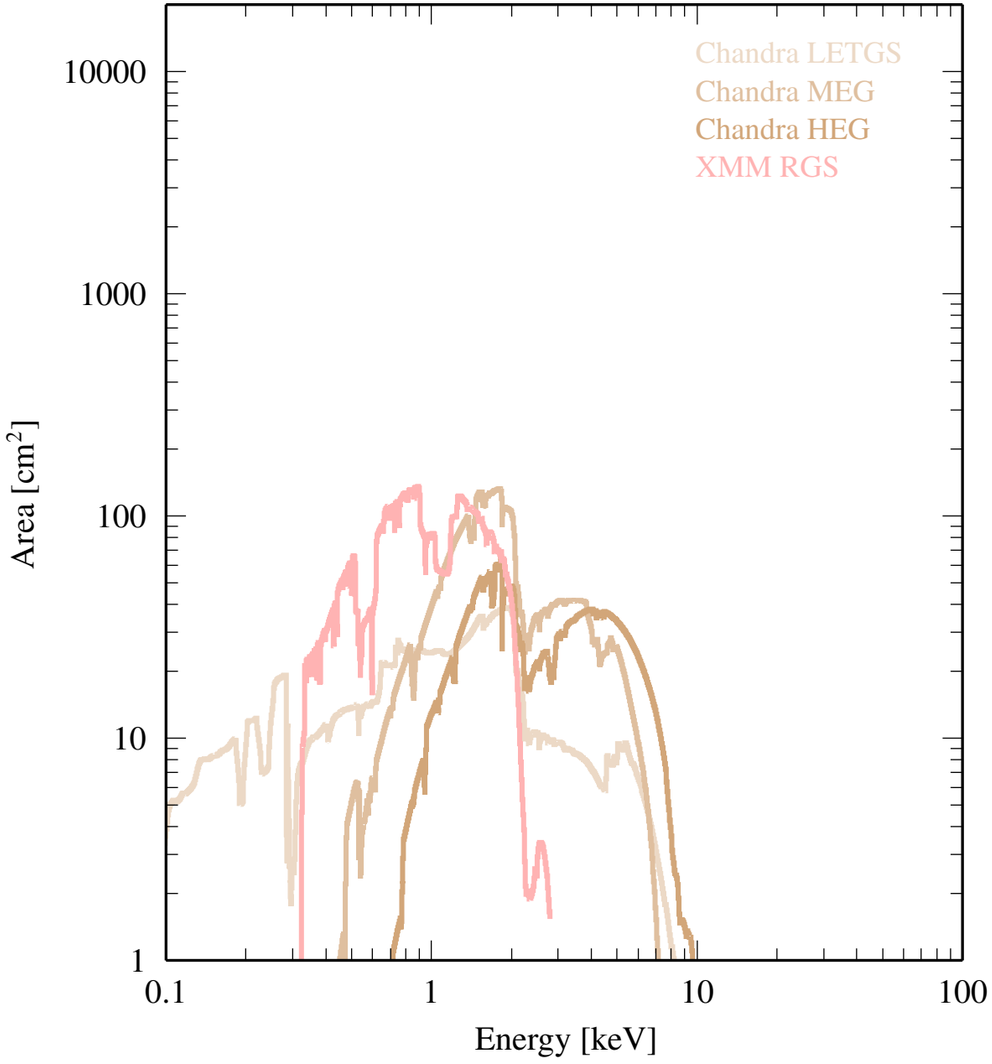

Si-type resolution

(Fano – ΔE ~ 150 eV at 5.9 keV, R ~ 40)

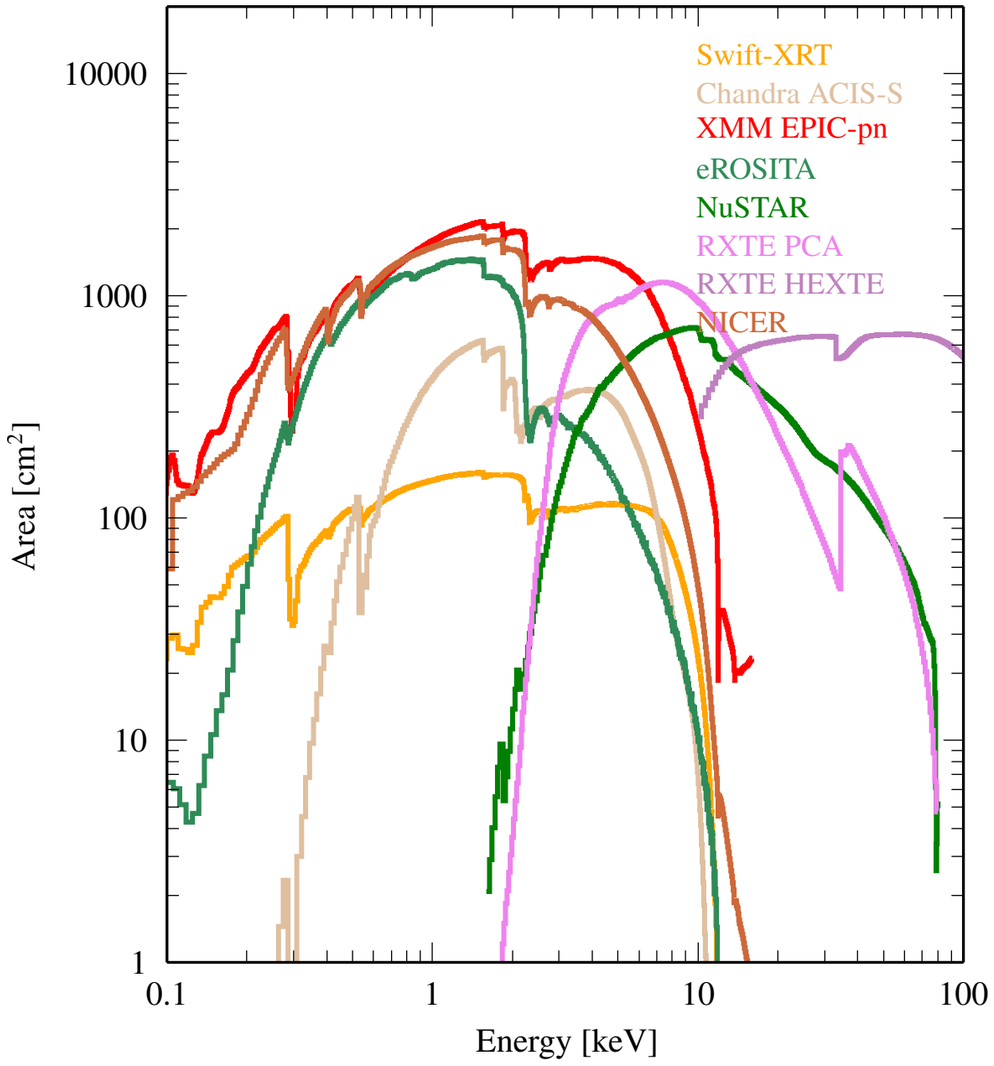

Gratings & Microcalorimeters

(R ~ 1000, R ~ 70 . . . 4000)

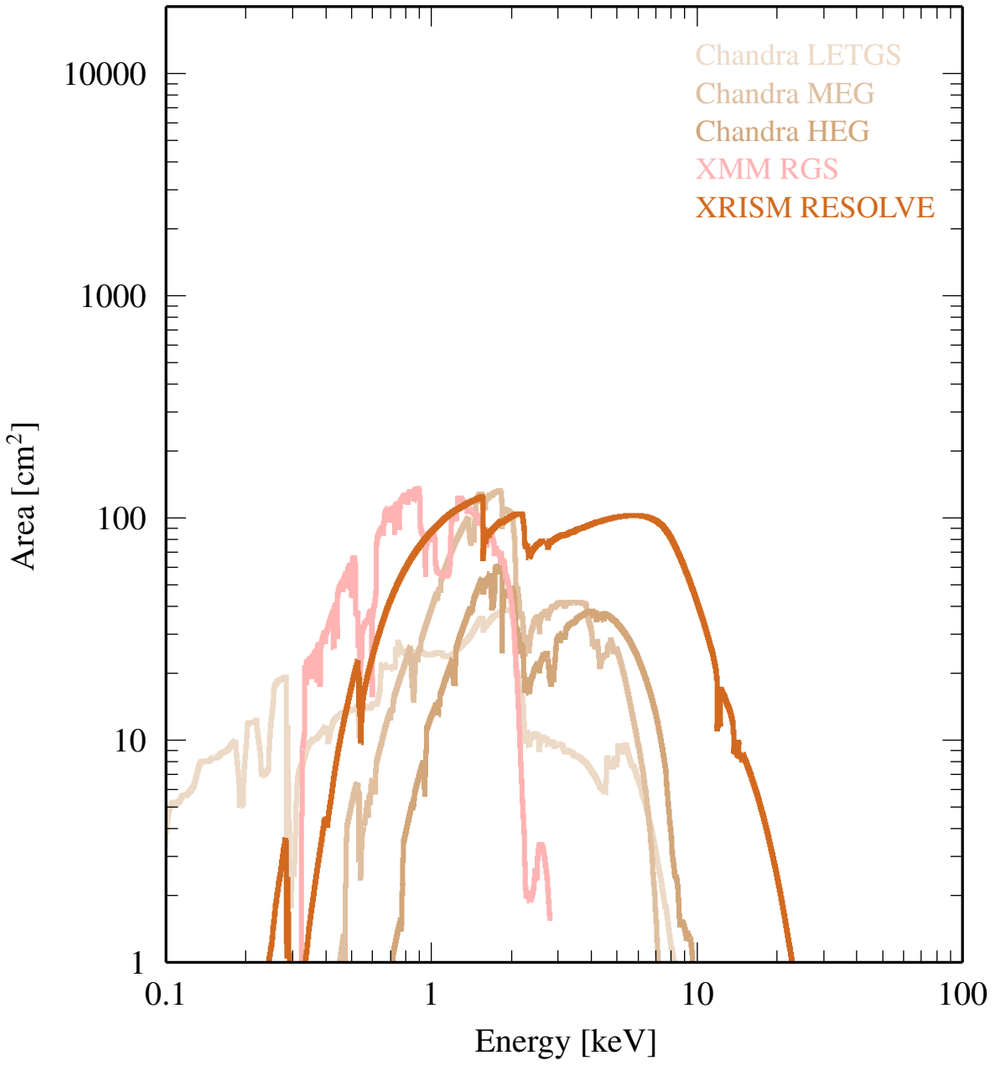

Si-type resol… …Microcalorimeters

(Fano – ΔE ~ 150 eV a… …0, R ~ 70 . . . 4000)

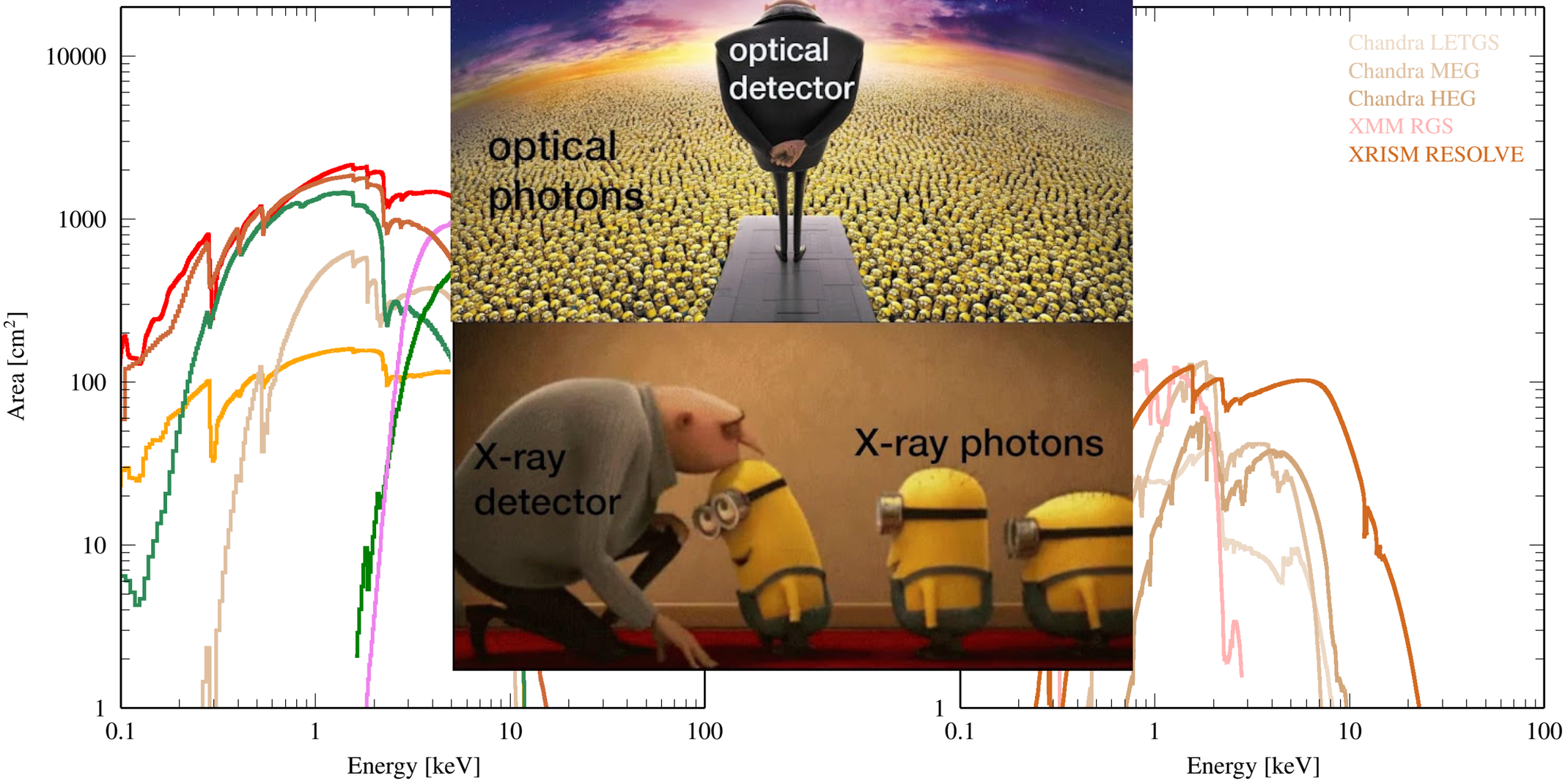

Si-type resolution

(Fano – ΔE ~ 150 eV at 5.9 keV, R ~ 40)

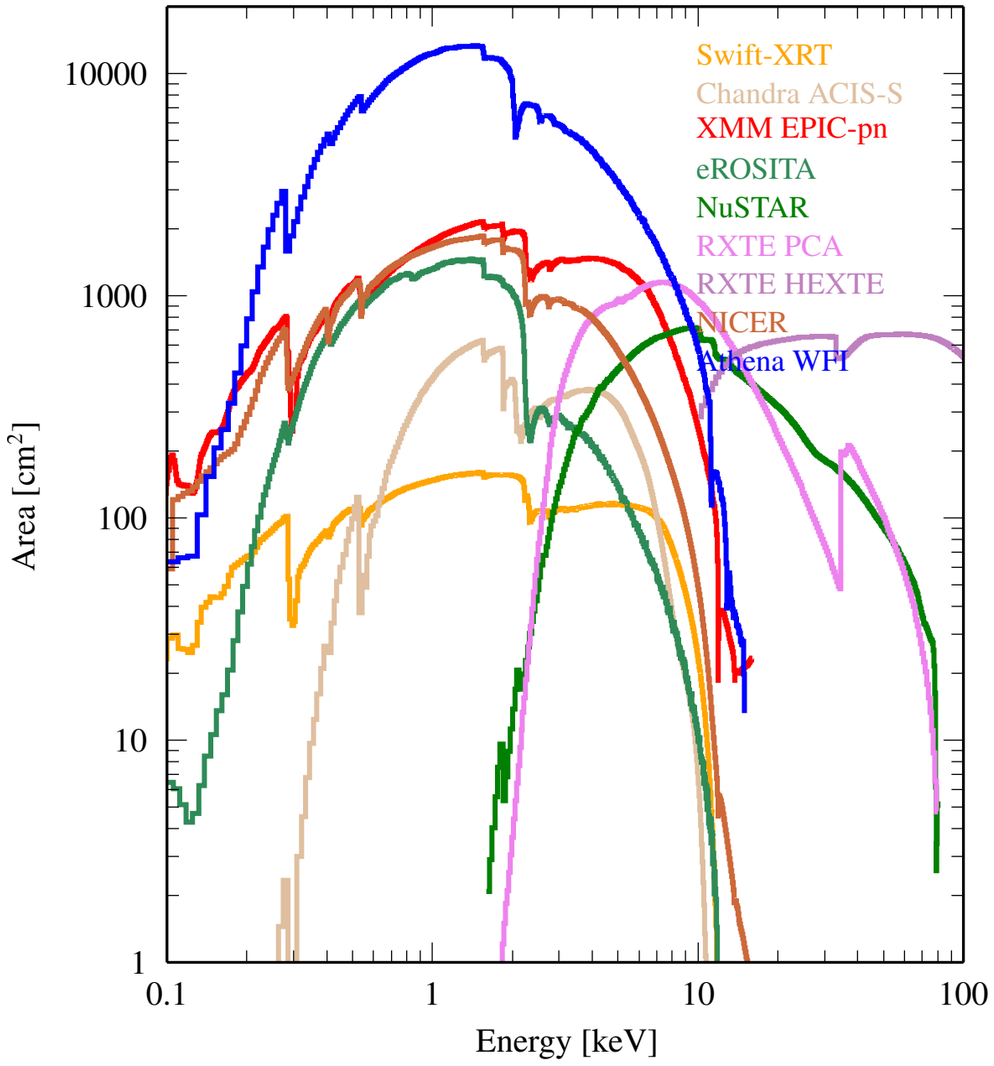

Gratings & Microcalorimeters

(R ~ 1000, R ~ 70 . . . 4000)

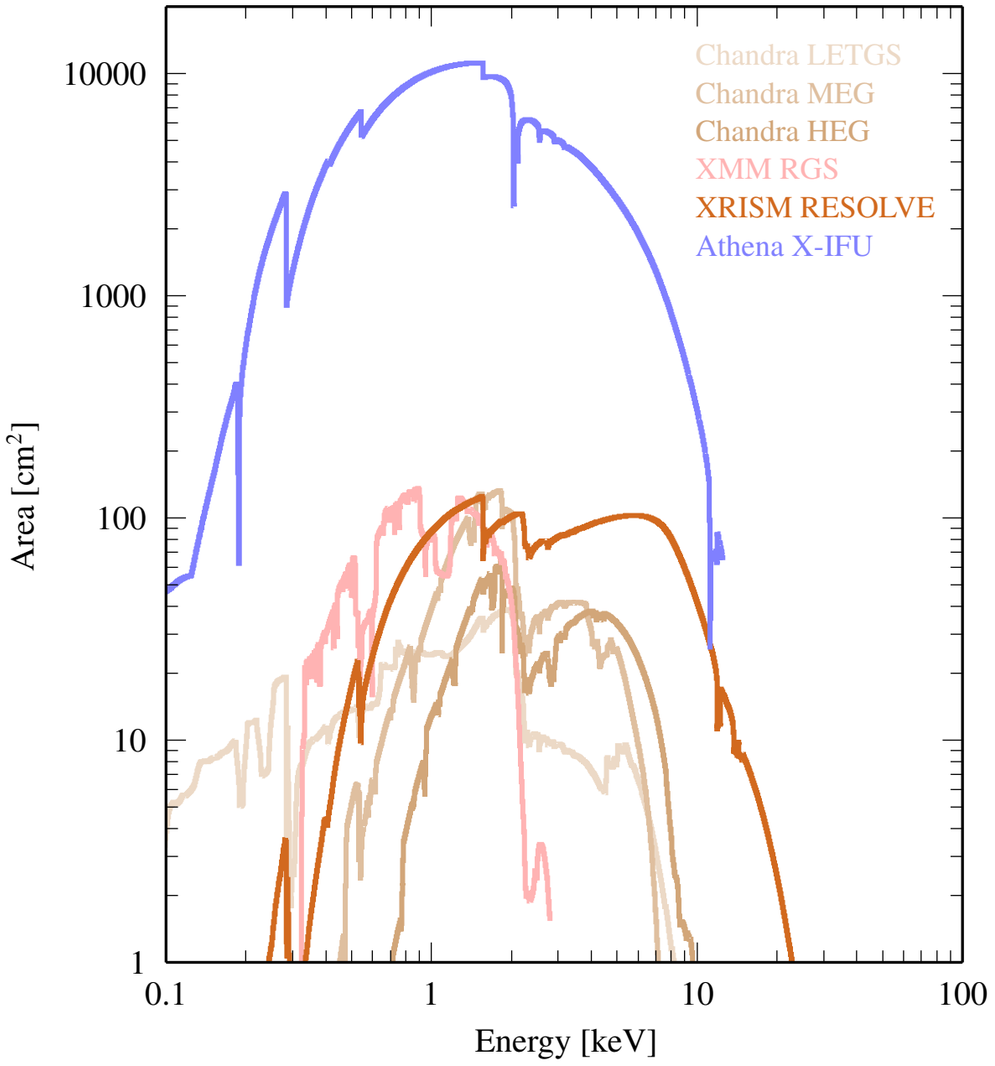

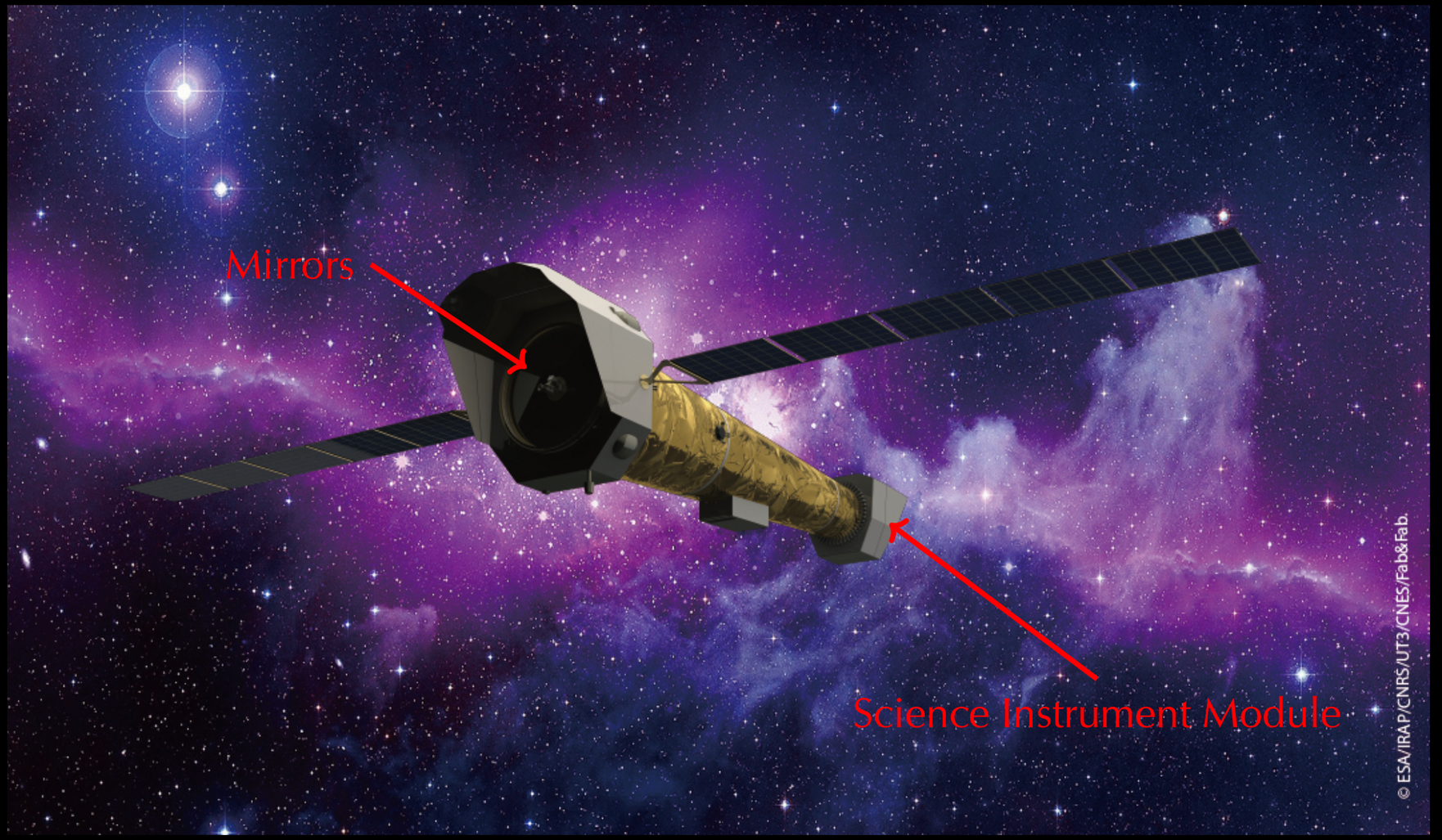
Mirrors
Science Instrument Module
© ESA/IRAP/CNRS/UT3/CNES/Fab&Fab.

Mirrors: Silicon pore optics (Cosine, Leiden)

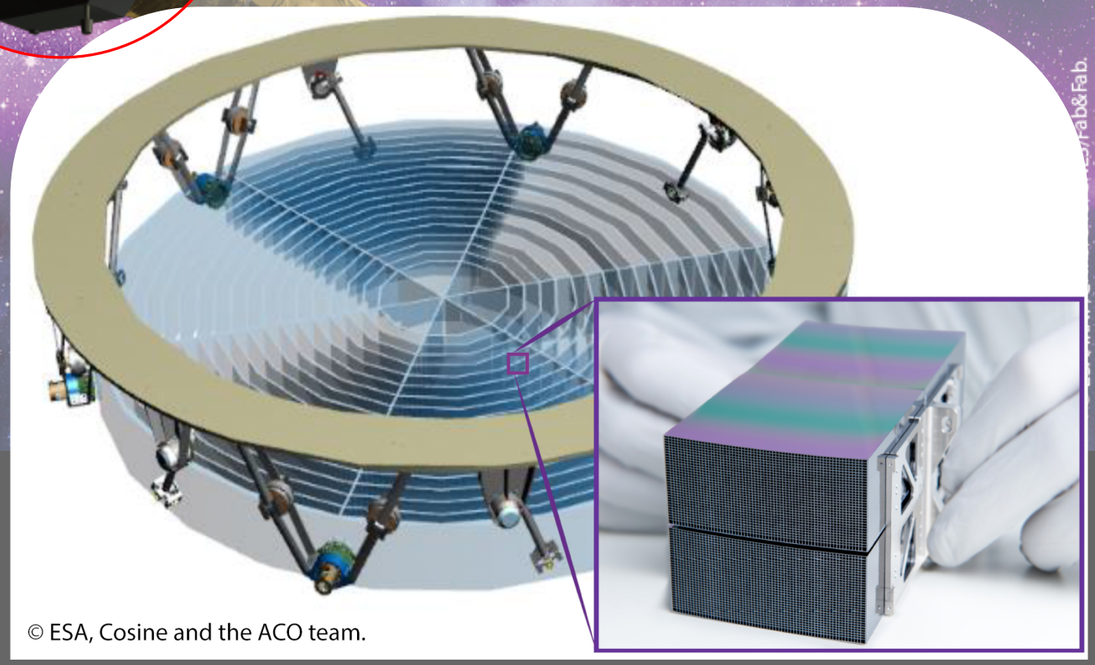

© ESA, Cosine and the ACO team.

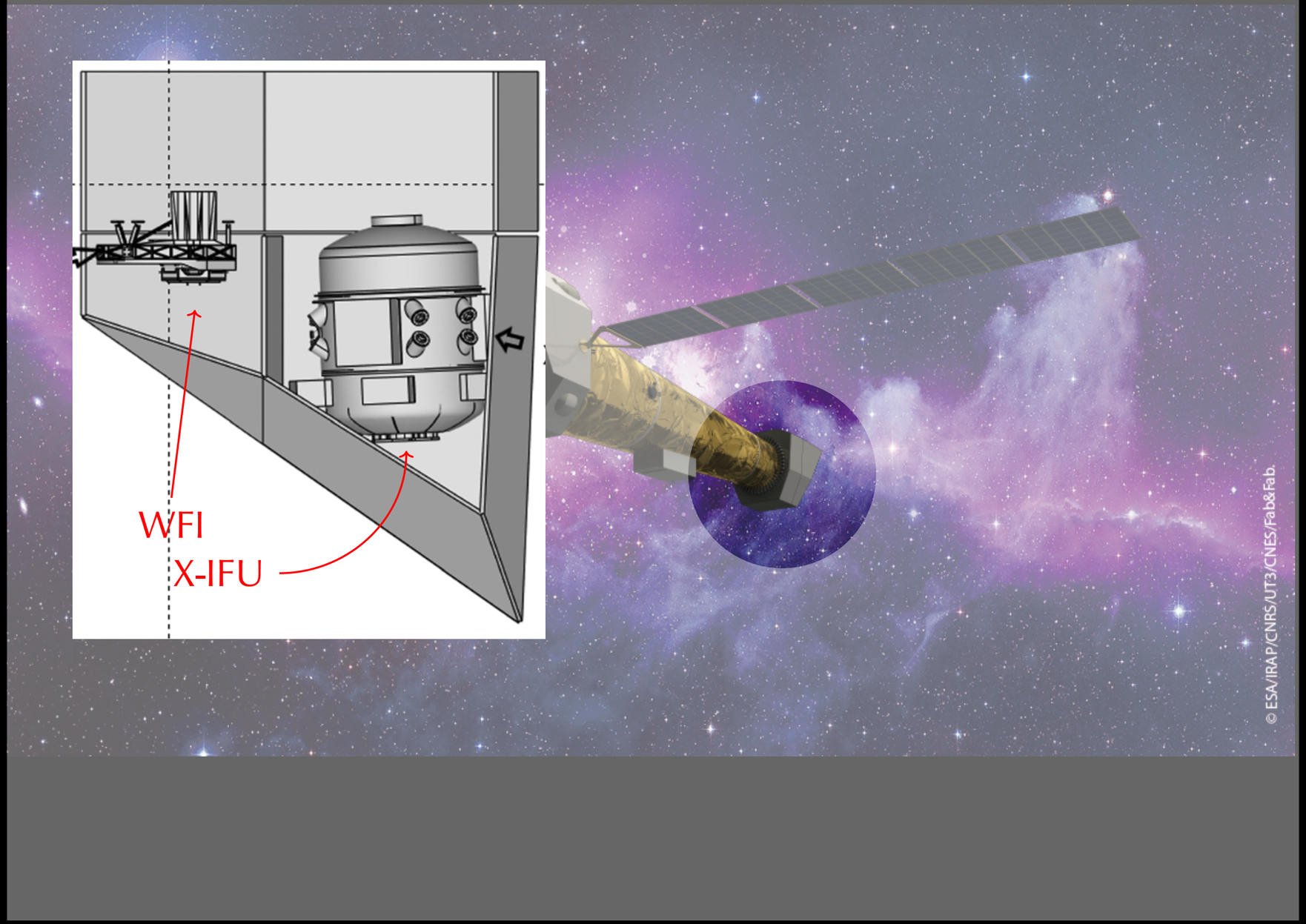
WFI
X-IFU
© ESA/IRAP/CNRS/UT3/CNES/Fab&Fab.

X-IFU

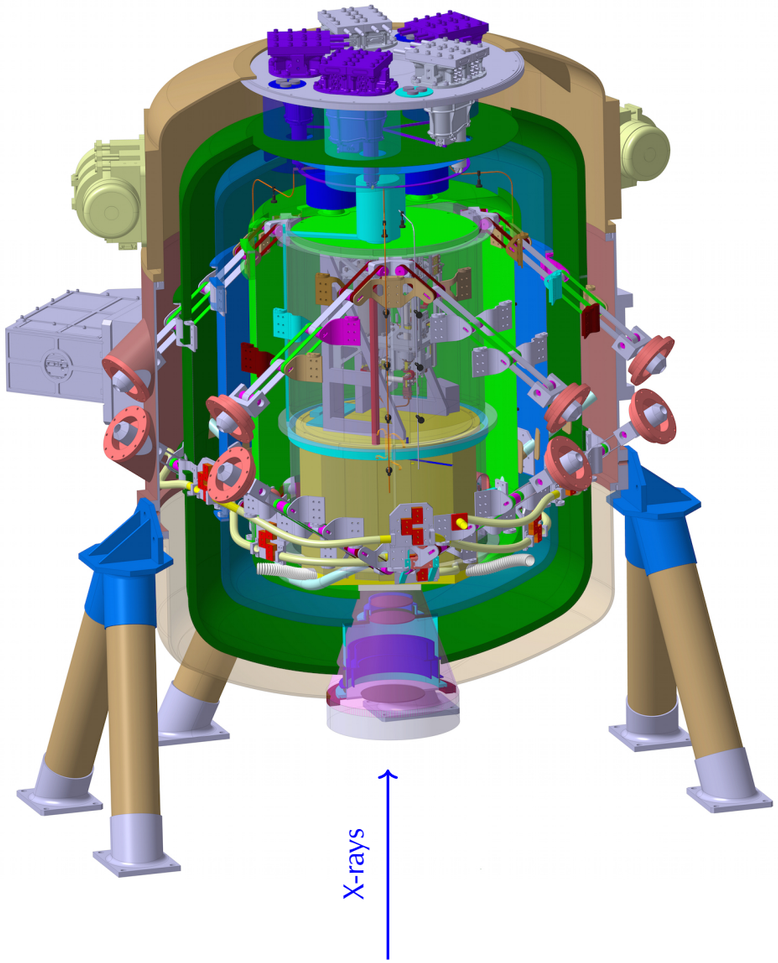

- 3840 TES
- operated at 50 mK
- Energy resolution 2.5 eV
- 5′ field of view
- PI: D. Barret (IRAP, F)

X-IFU

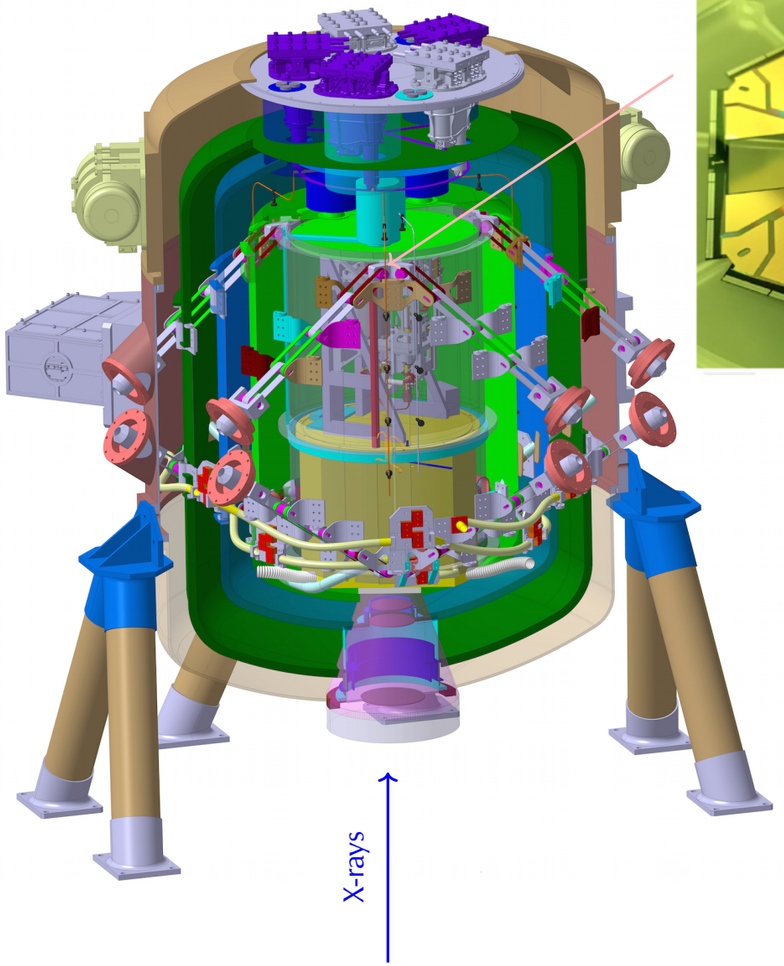

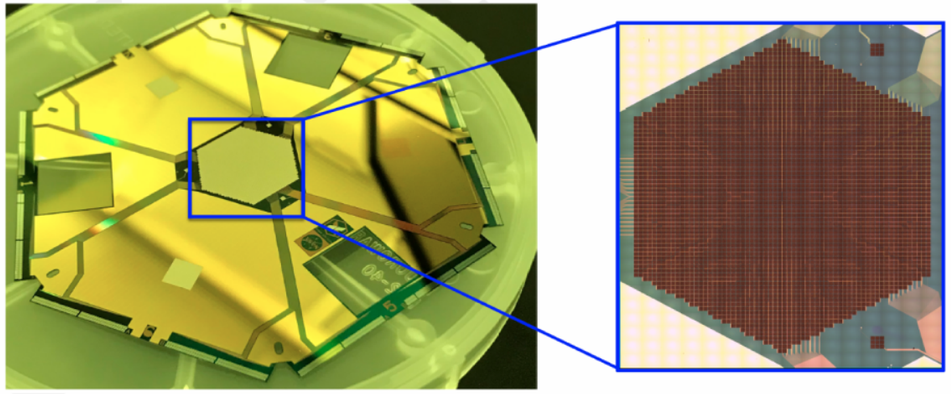

- 3840 TES
- operated at 50 mK
- Energy resolution 2.5 eV
- 5′ field of view
- PI: D. Barret (IRAP, F)

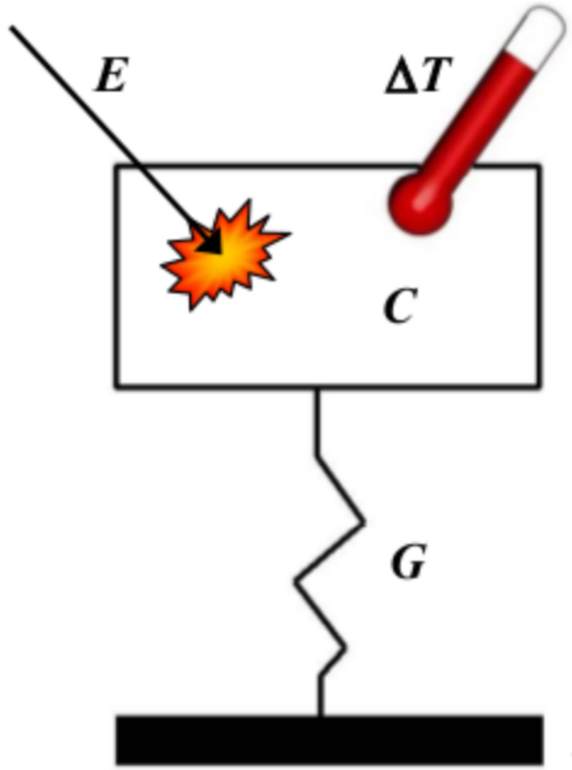

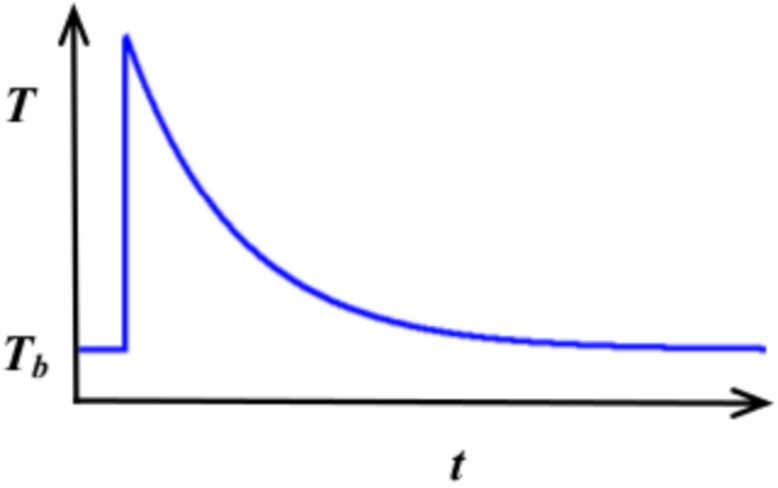

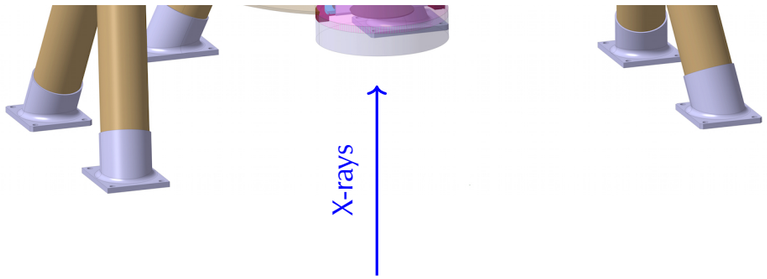

- Energy resolution 2.5 eV
- 5′ field of view
- PI: D. Barret (IRAP, F)

X-IFU

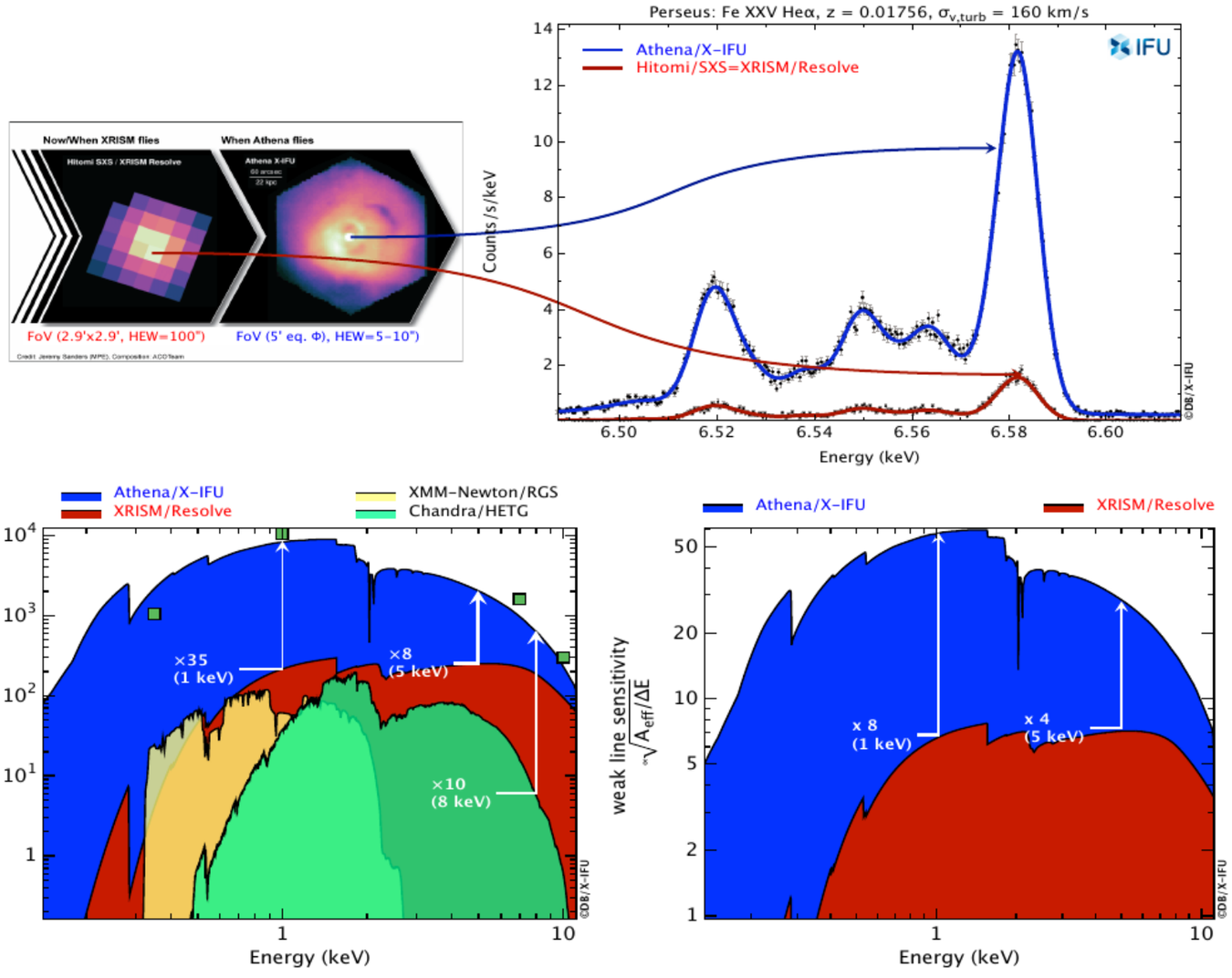

D. Barret

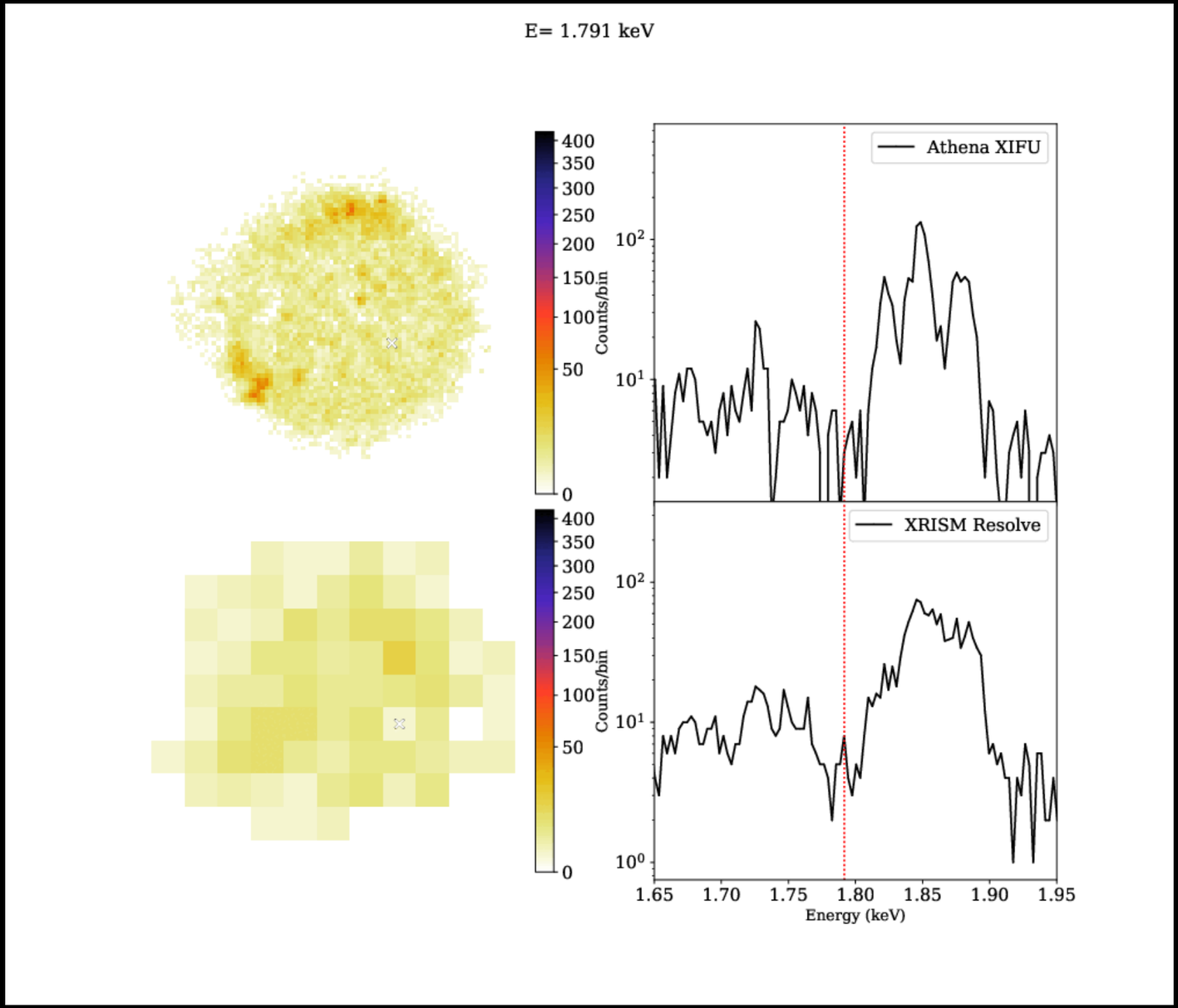

Cas A (F. Acero, A. Decourchelle [CEA], C. Kirsch, J. Wilms, T. Dauser [ECAP])

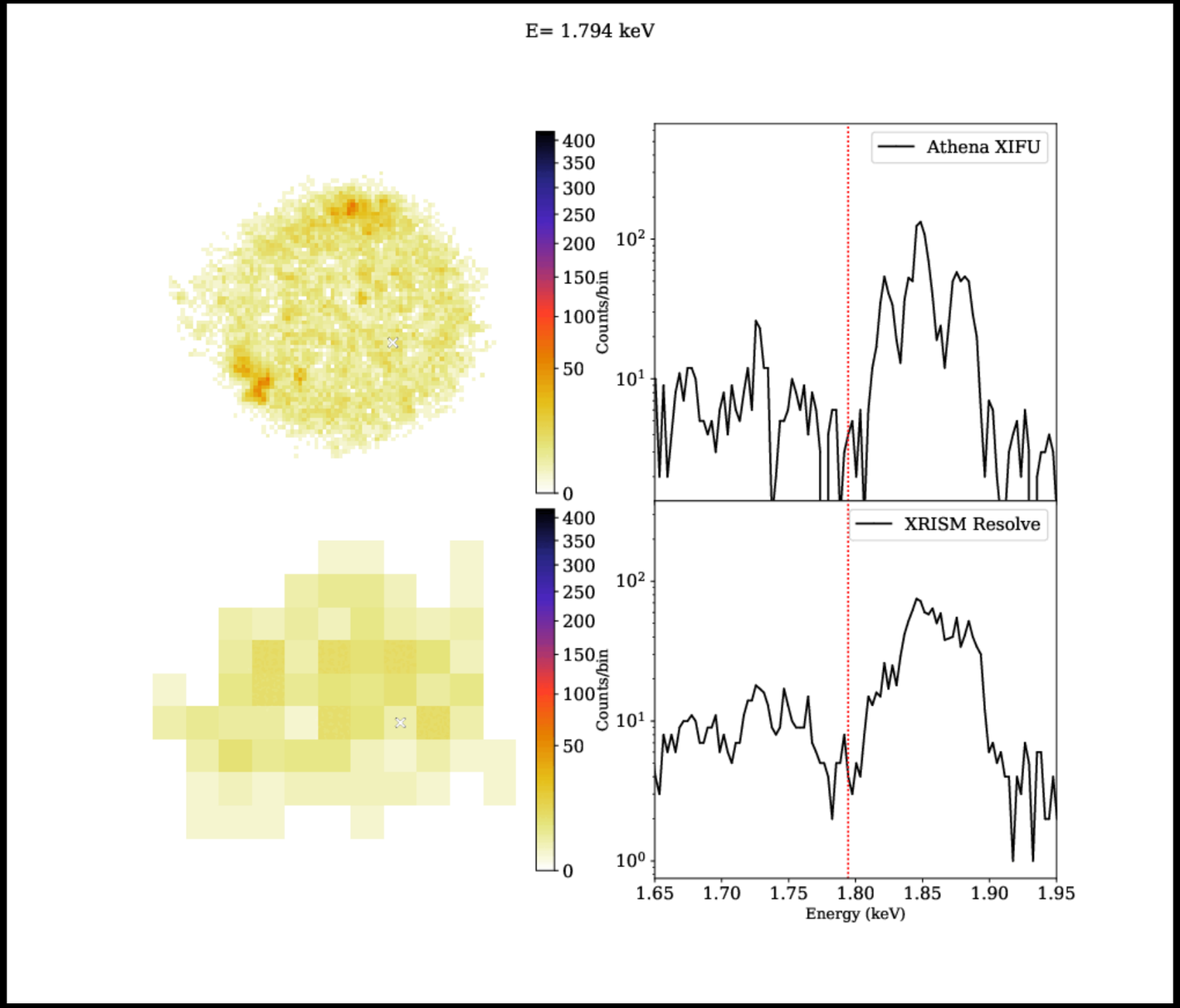

Cas A (F. Acero, A. Decourchelle [CEA], C. Kirsch, J. Wilms, T. Dauser [ECAP])

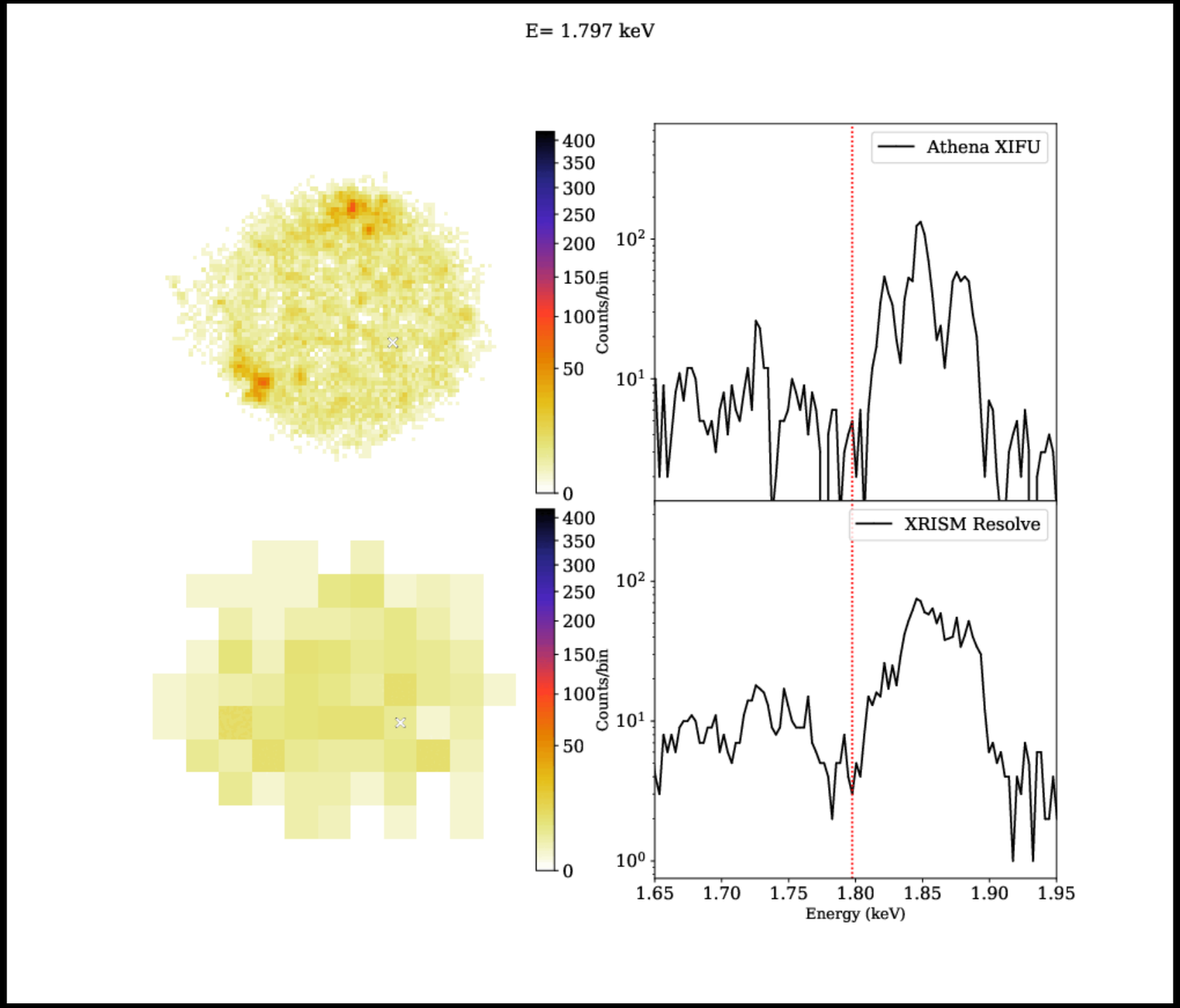

Cas A (F. Acero, A. Decourchelle [CEA], C. Kirsch, J. Wilms, T. Dauser [ECAP])

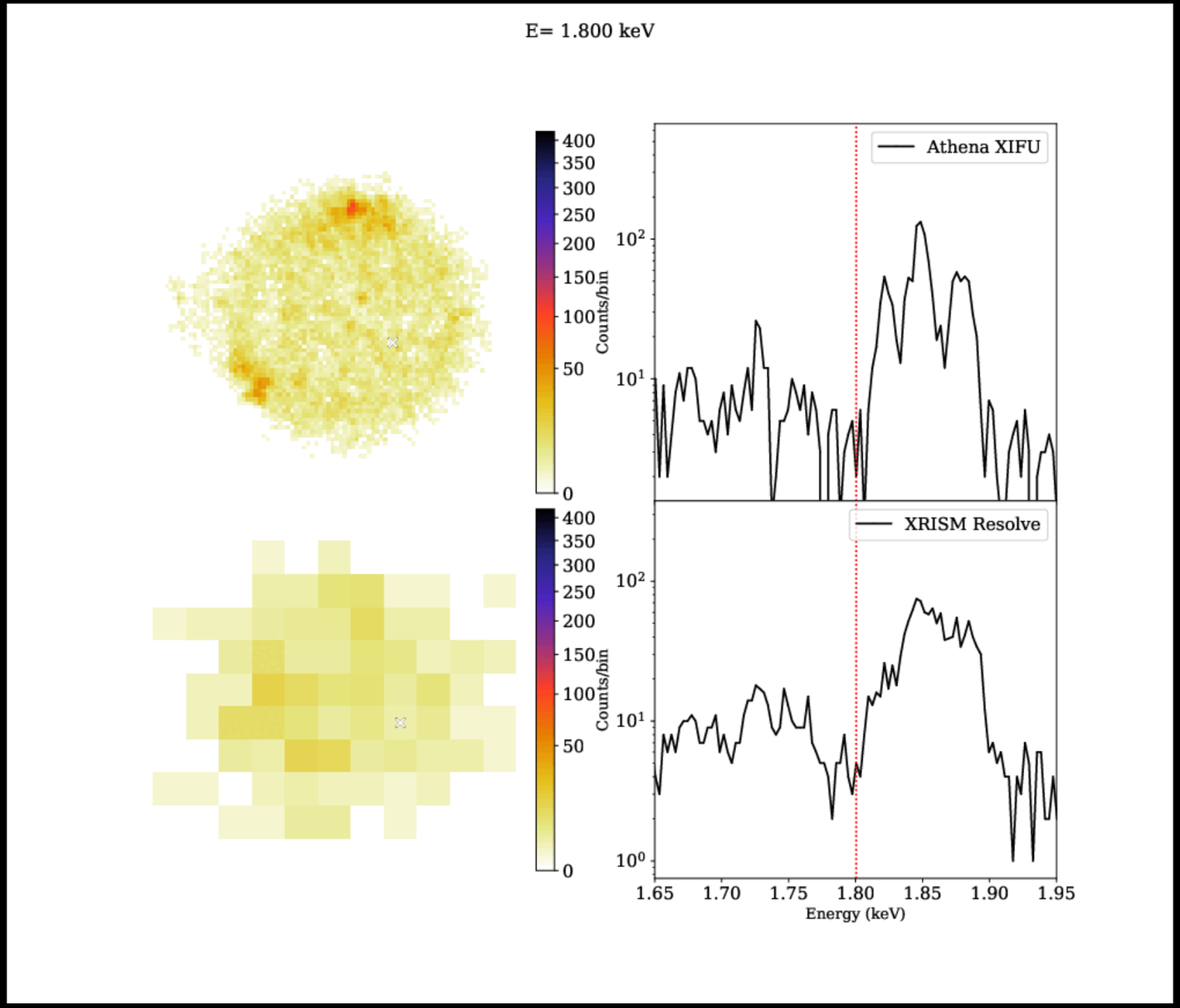

Cas A (F. Acero, A. Decourchelle [CEA], C. Kirsch, J. Wilms, T. Dauser [ECAP])

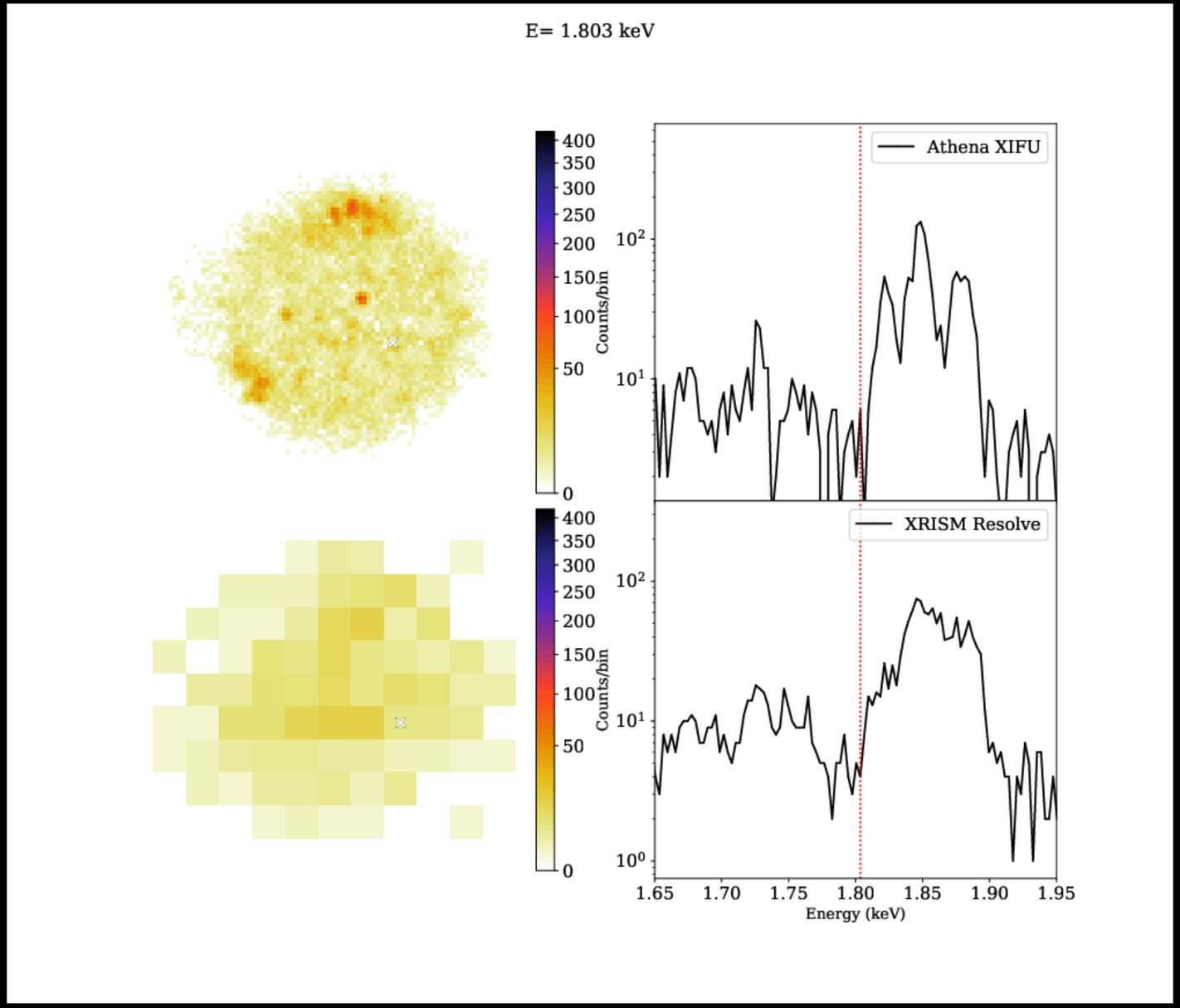

Cas A (F. Acero, A. Decourchelle [CEA], C. Kirsch, J. Wilms, T. Dauser [ECAP])

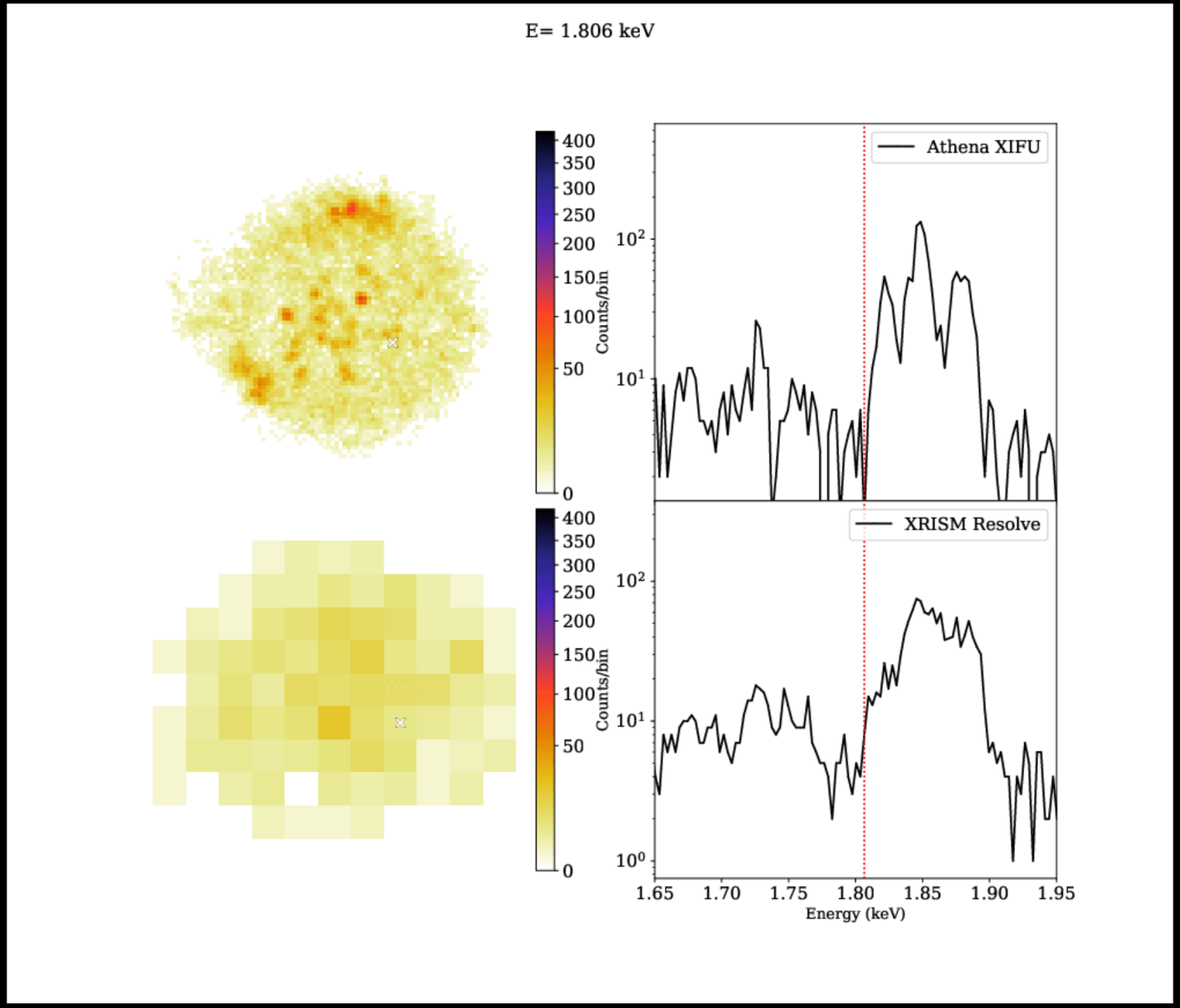

Cas A (F. Acero, A. Decourchelle [CEA], C. Kirsch, J. Wilms, T. Dauser [ECAP])

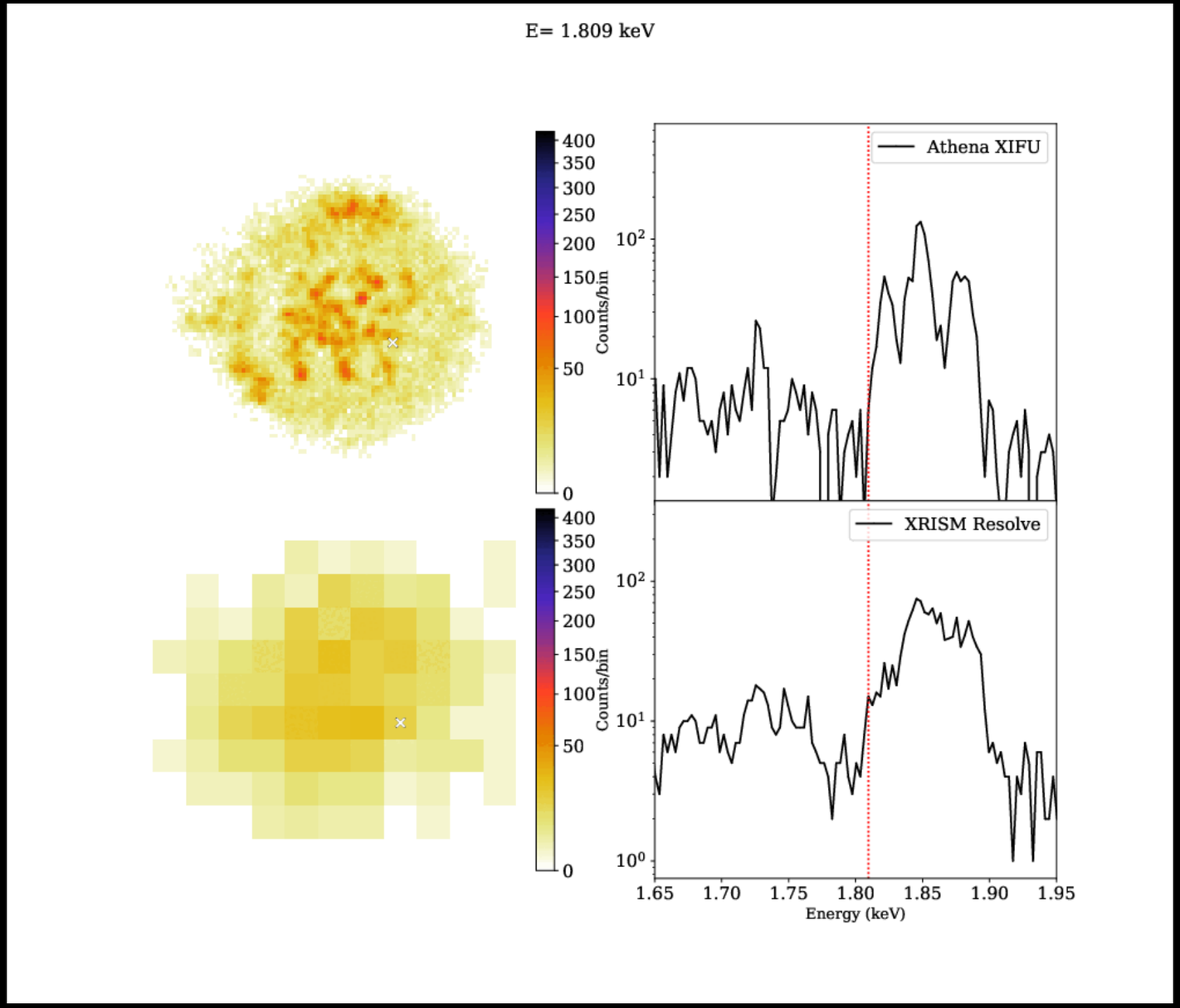

Cas A (F. Acero, A. Decourchelle [CEA], C. Kirsch, J. Wilms, T. Dauser [ECAP])

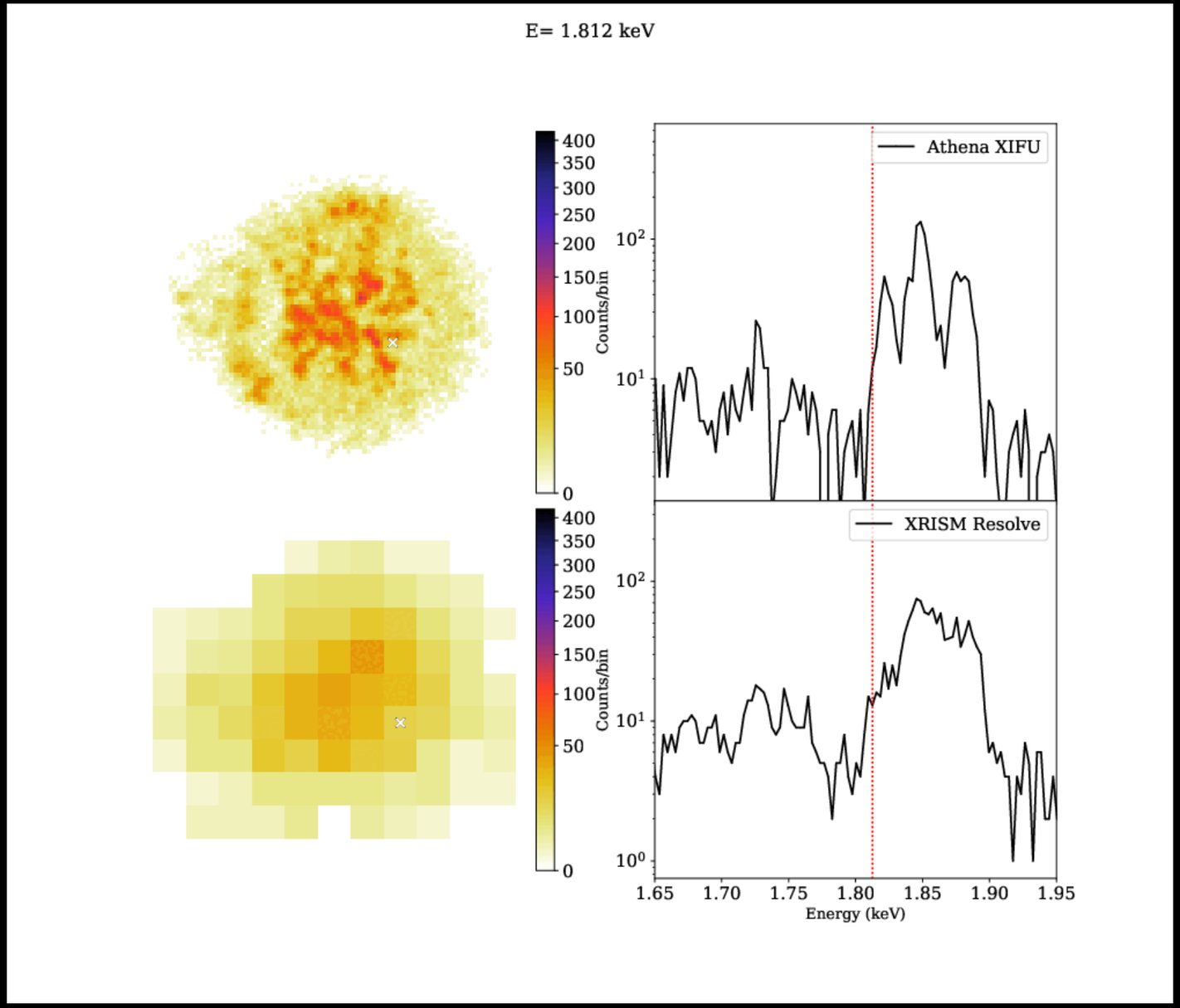

Cas A (F. Acero, A. Decourchelle [CEA], C. Kirsch, J. Wilms, T. Dauser [ECAP])

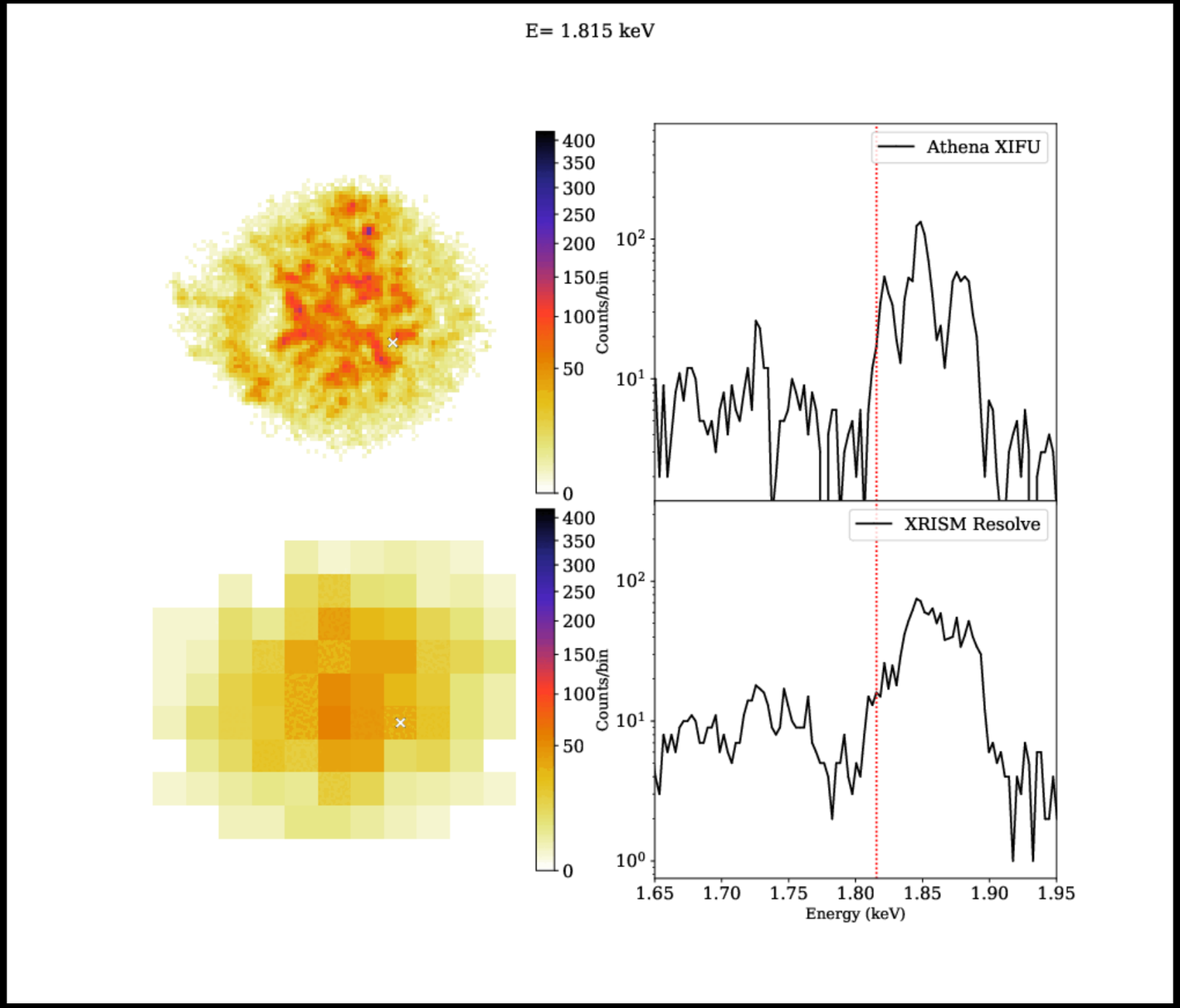

Cas A (F. Acero, A. Decourchelle [CEA], C. Kirsch, J. Wilms, T. Dauser [ECAP])

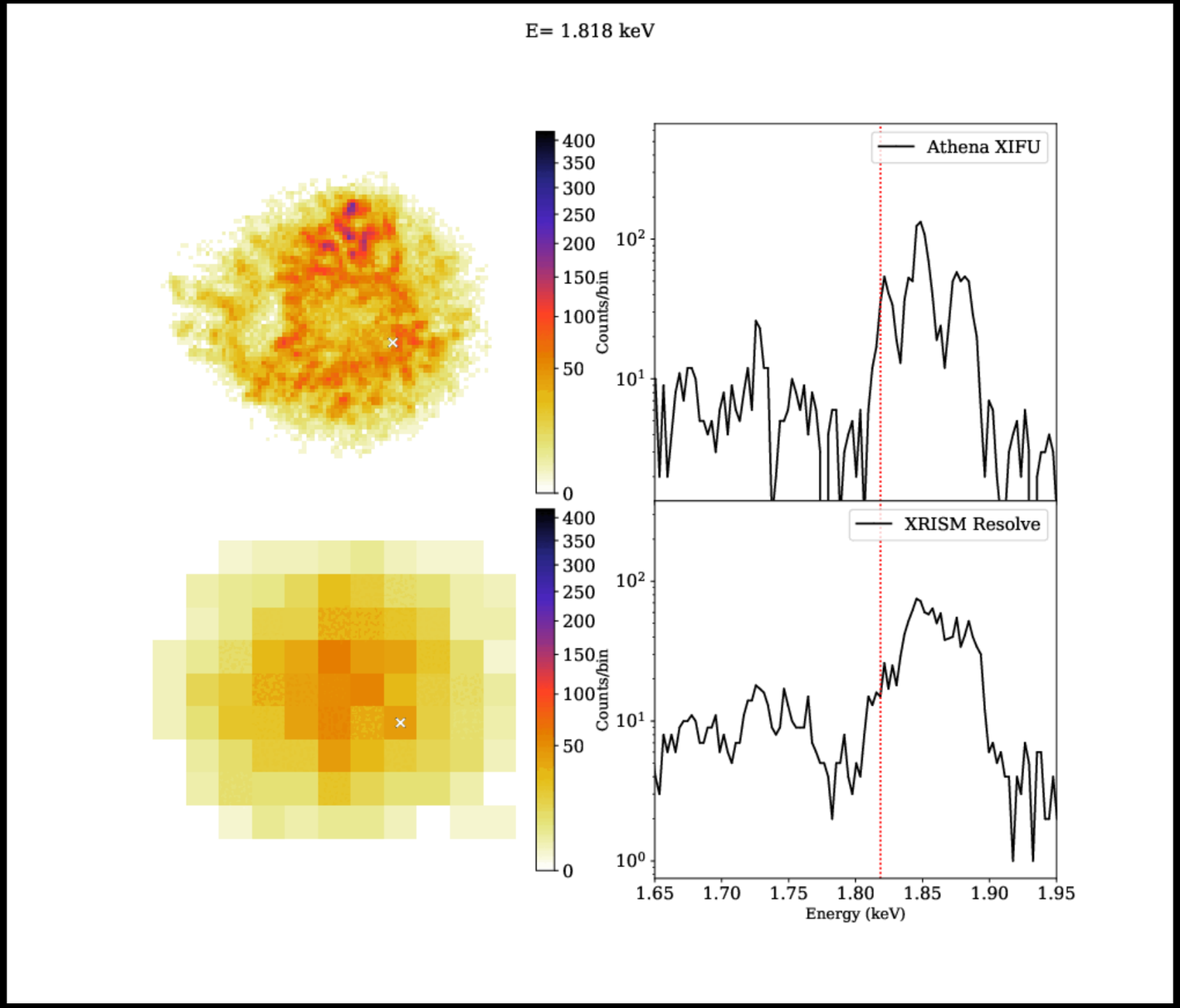

Cas A (F. Acero, A. Decourchelle [CEA], C. Kirsch, J. Wilms, T. Dauser [ECAP])

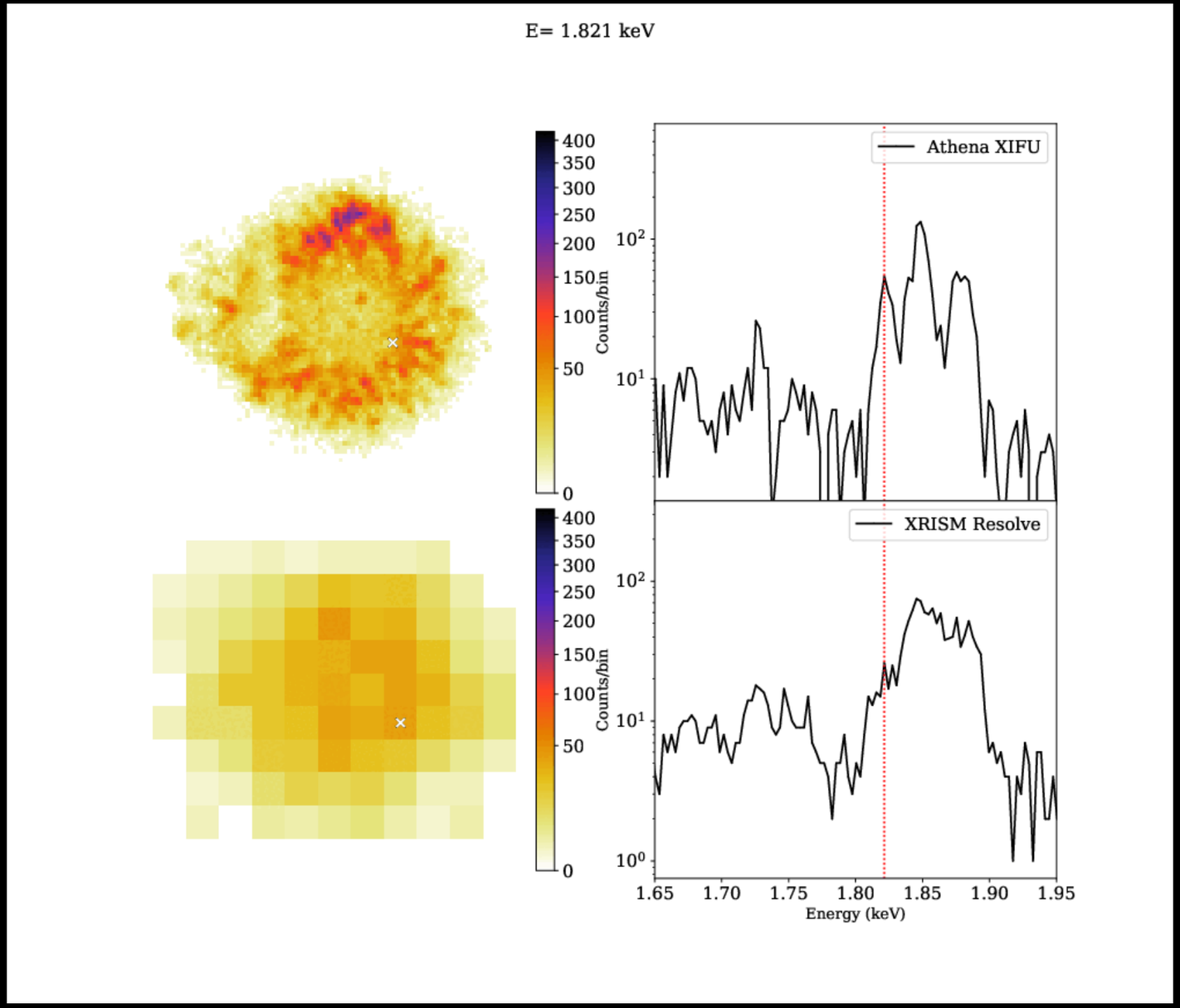

Cas A (F. Acero, A. Decourchelle [CEA], C. Kirsch, J. Wilms, T. Dauser [ECAP])

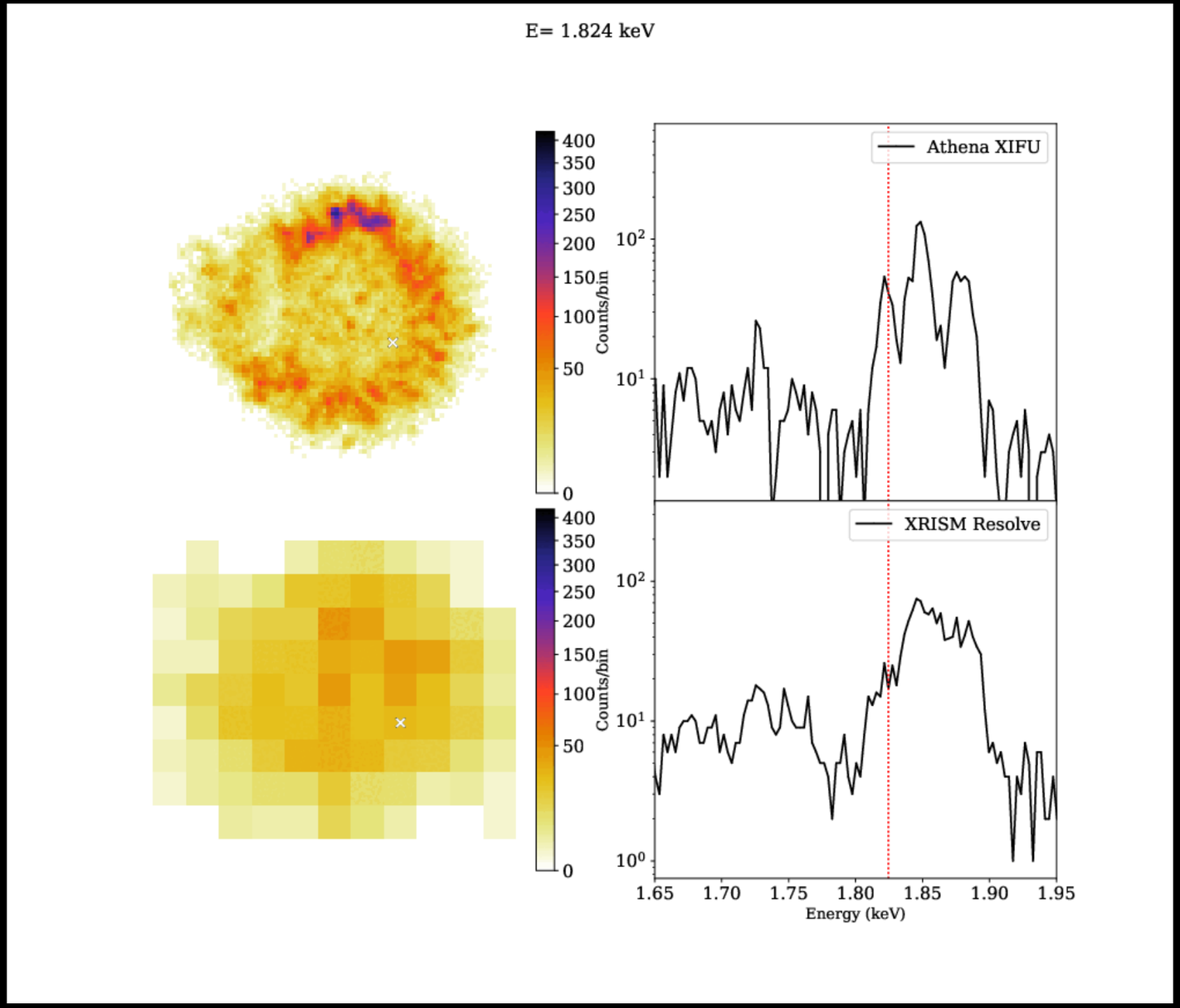

Cas A (F. Acero, A. Decourchelle [CEA], C. Kirsch, J. Wilms, T. Dauser [ECAP])

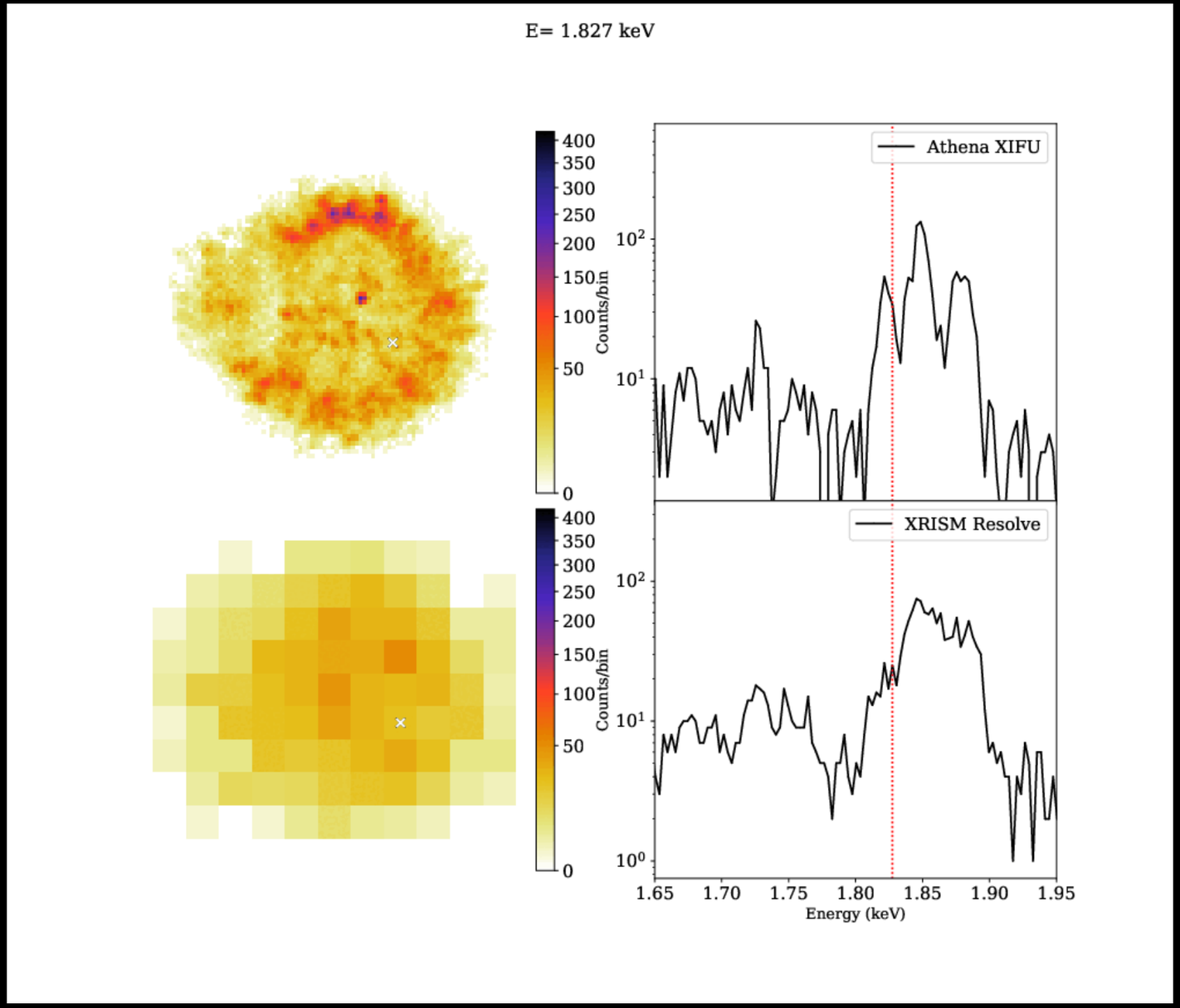

Cas A (F. Acero, A. Decourchelle [CEA], C. Kirsch, J. Wilms, T. Dauser [ECAP])

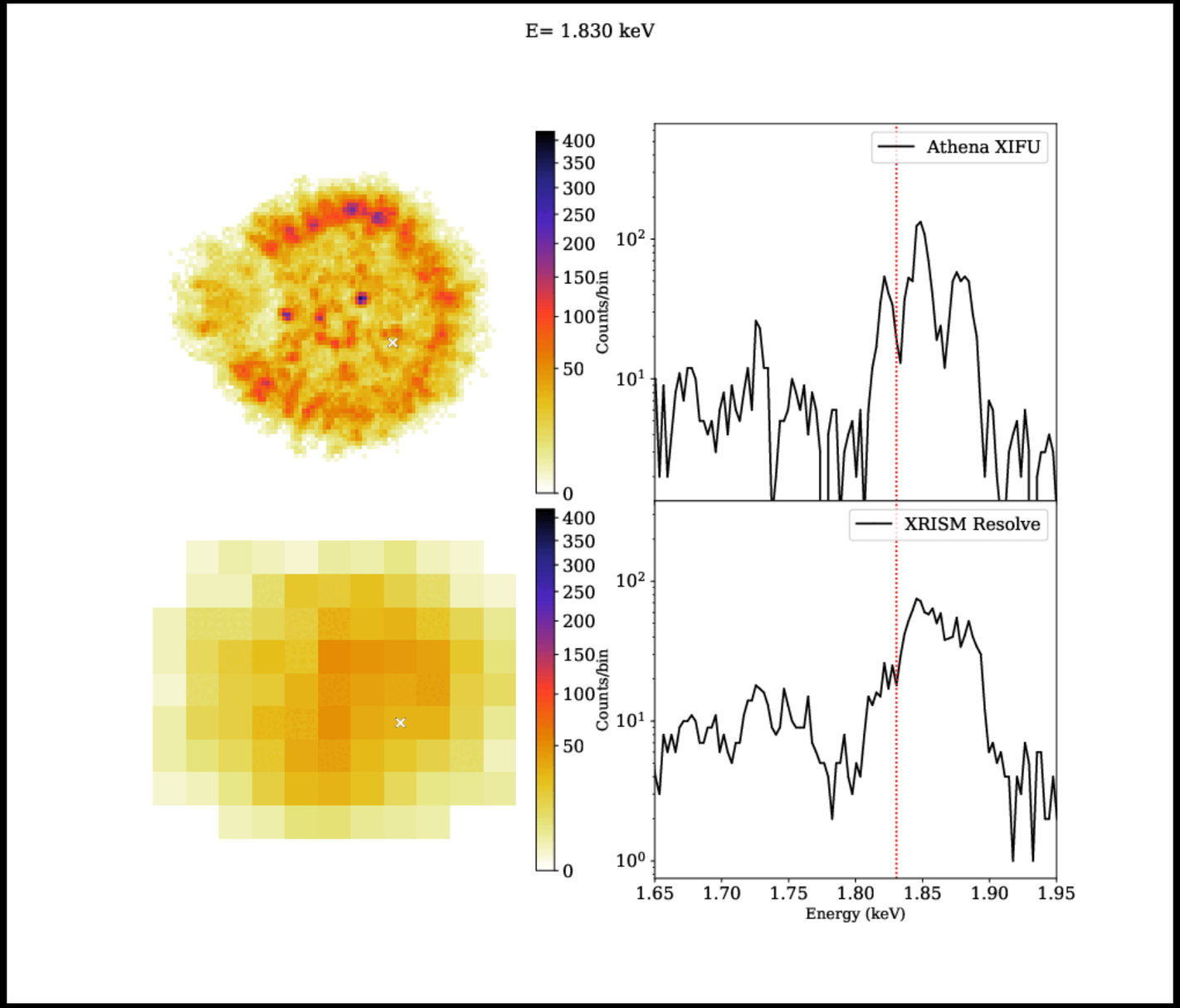

Cas A (F. Acero, A. Decourchelle [CEA], C. Kirsch, J. Wilms, T. Dauser [ECAP])

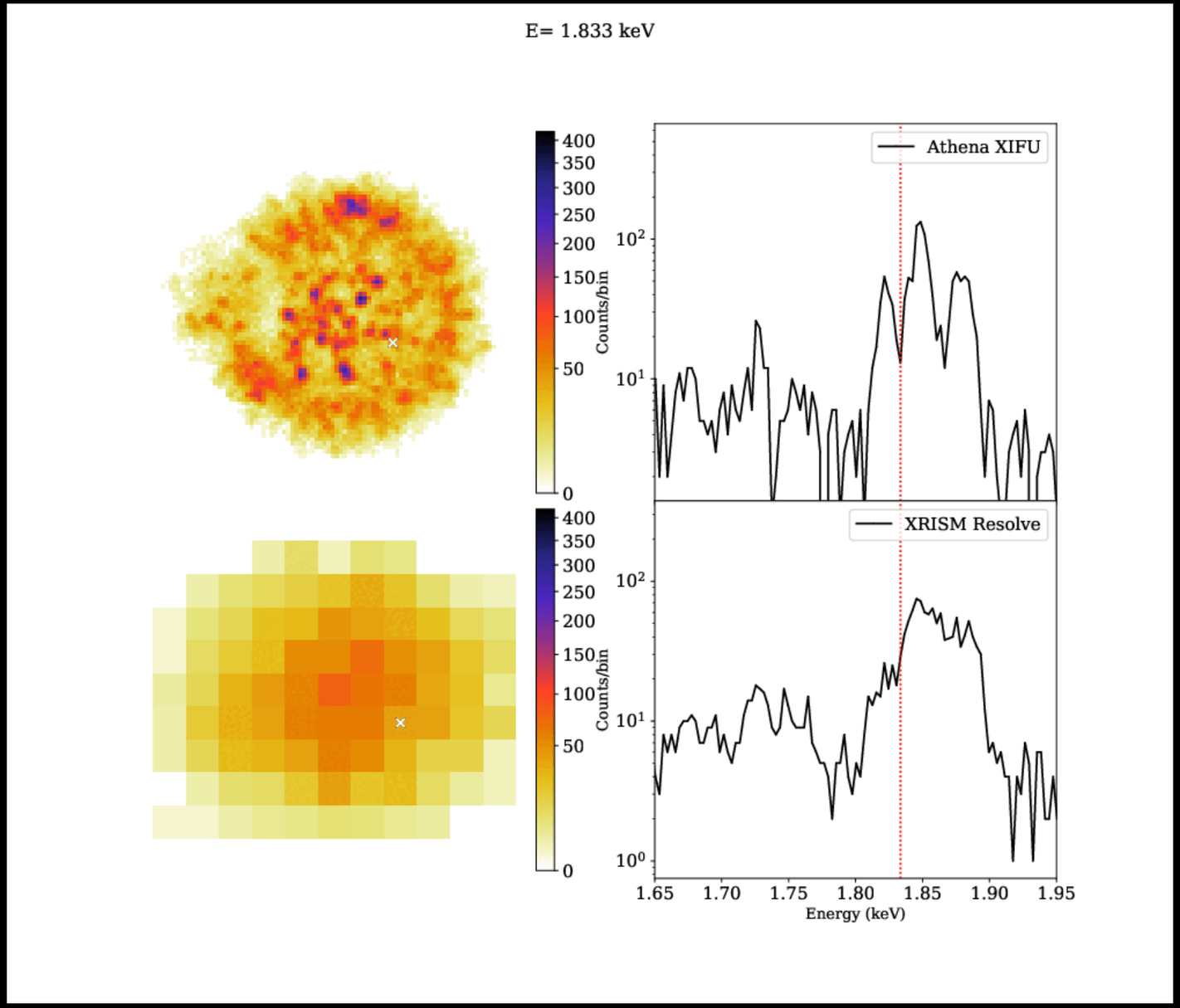

Cas A (F. Acero, A. Decourchelle [CEA], C. Kirsch, J. Wilms, T. Dauser [ECAP])

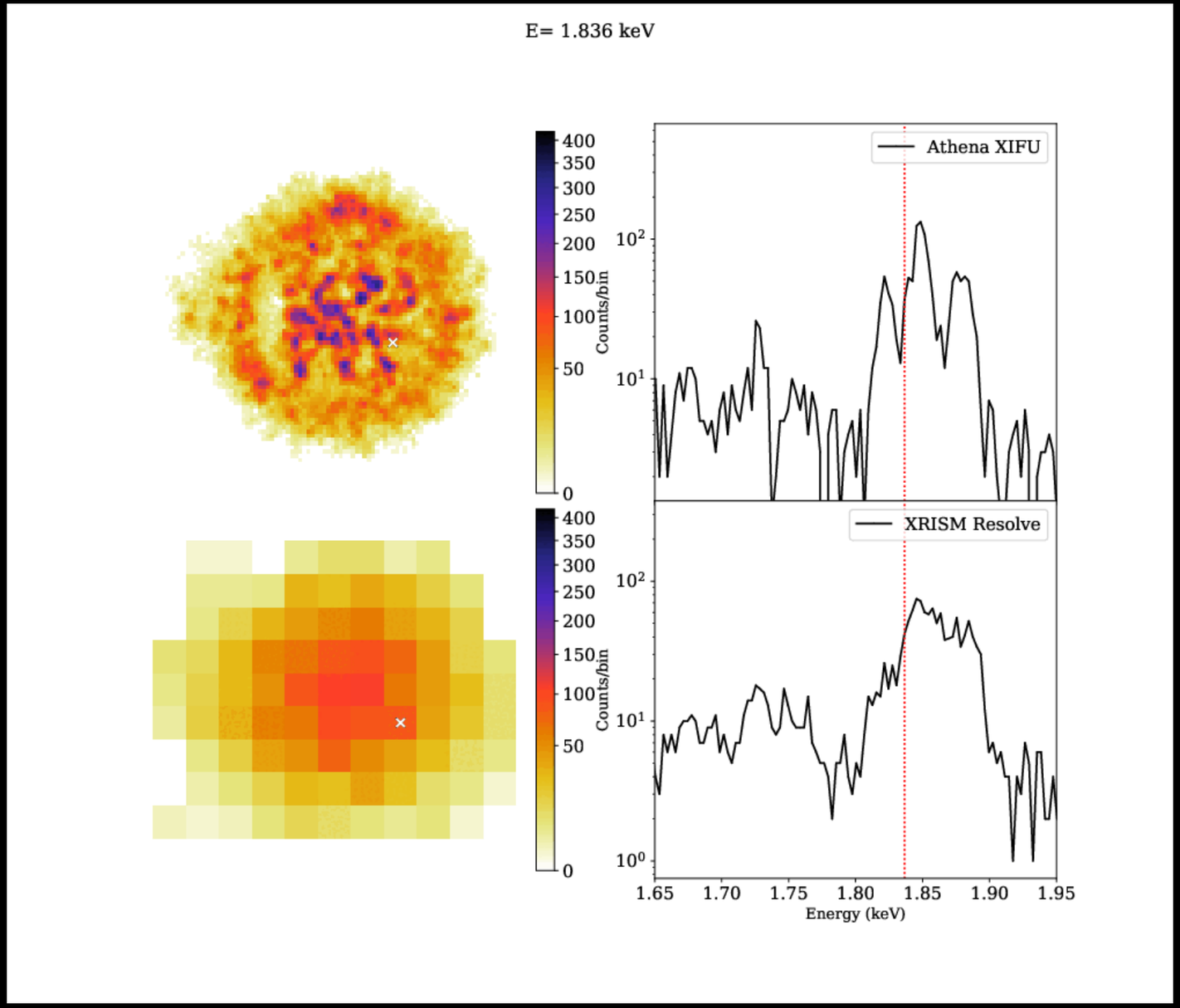

Cas A (F. Acero, A. Decourchelle [CEA], C. Kirsch, J. Wilms, T. Dauser [ECAP])

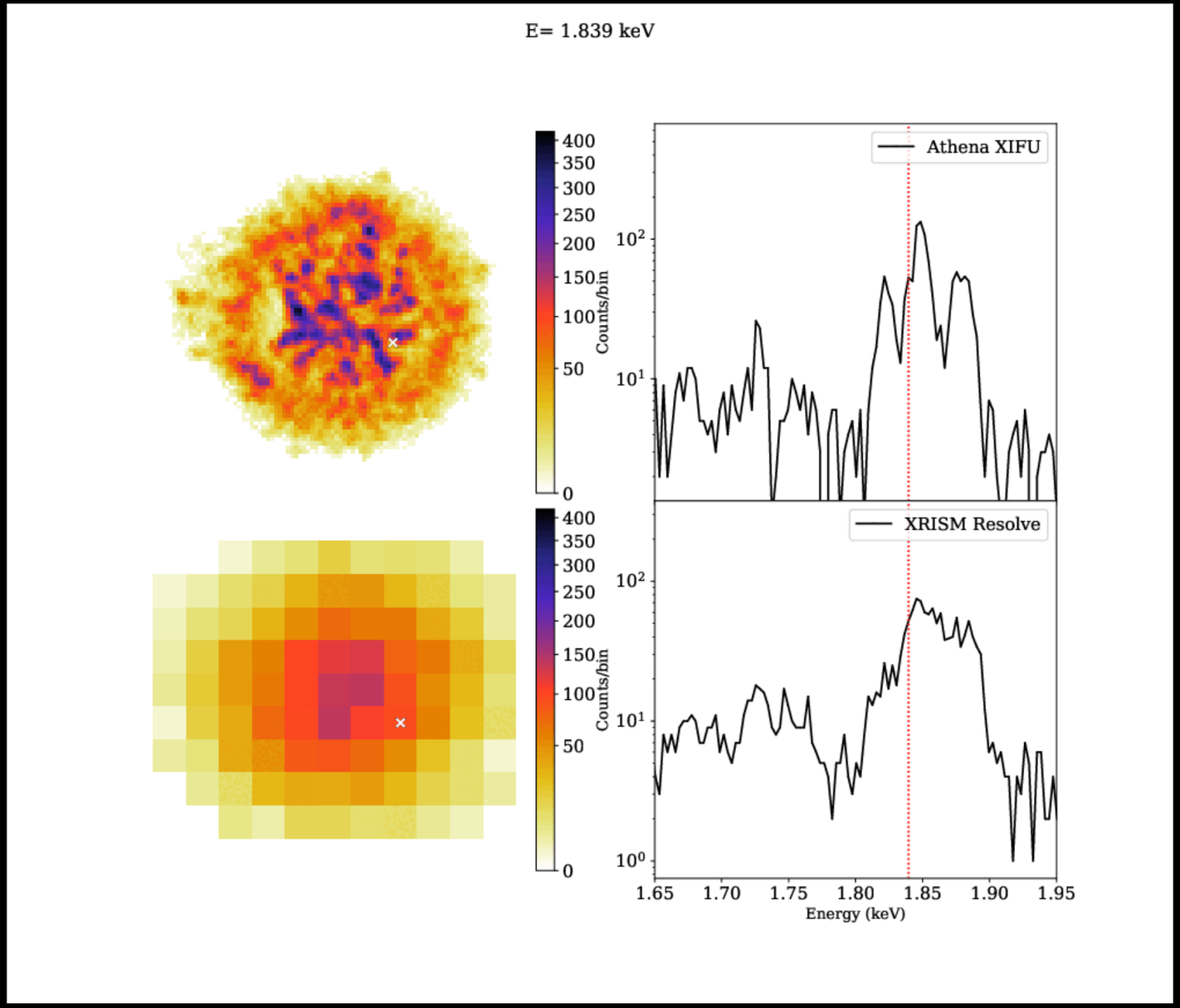

Cas A (F. Acero, A. Decourchelle [CEA], C. Kirsch, J. Wilms, T. Dauser [ECAP])

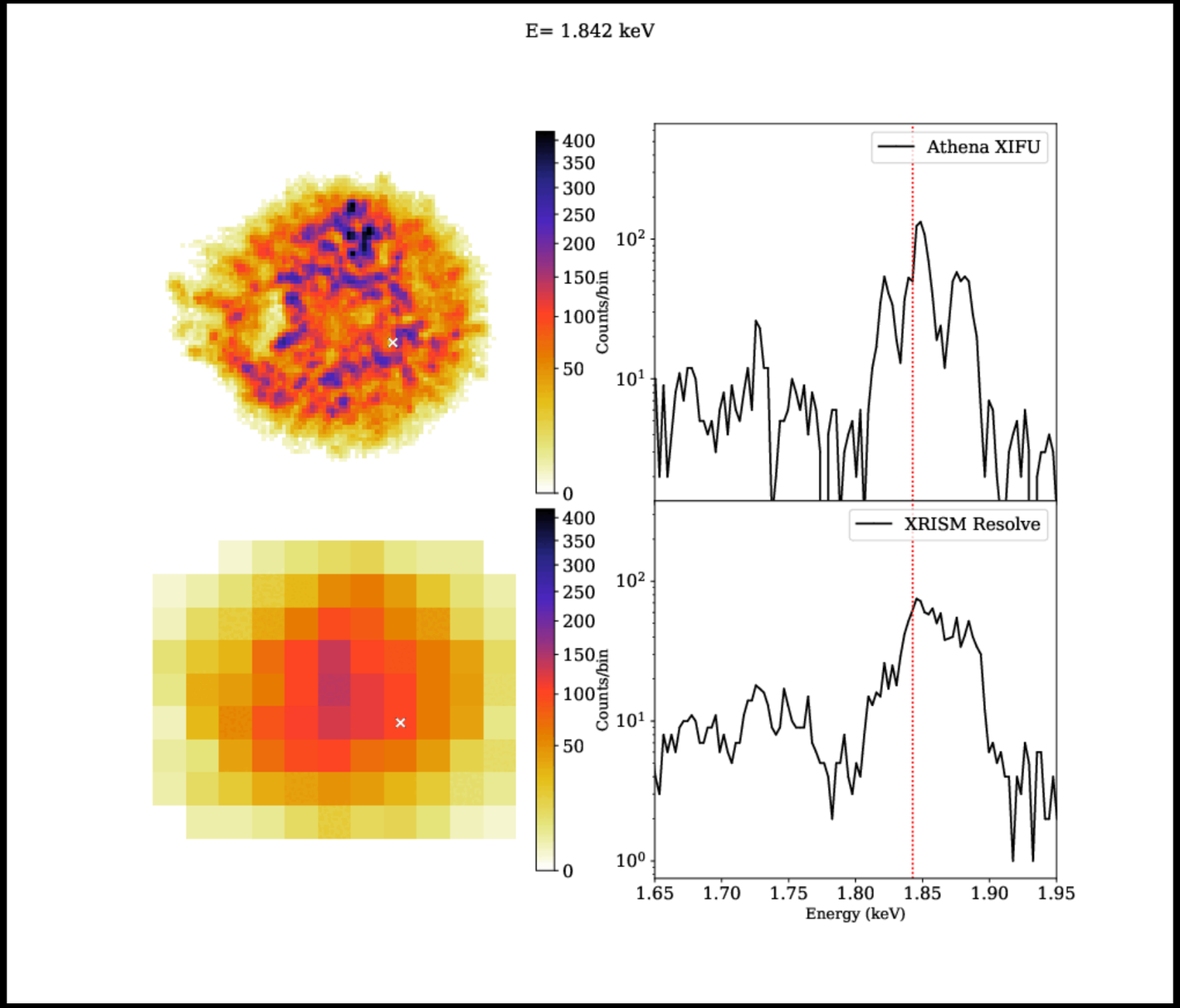

Cas A (F. Acero, A. Decourchelle [CEA], C. Kirsch, J. Wilms, T. Dauser [ECAP])

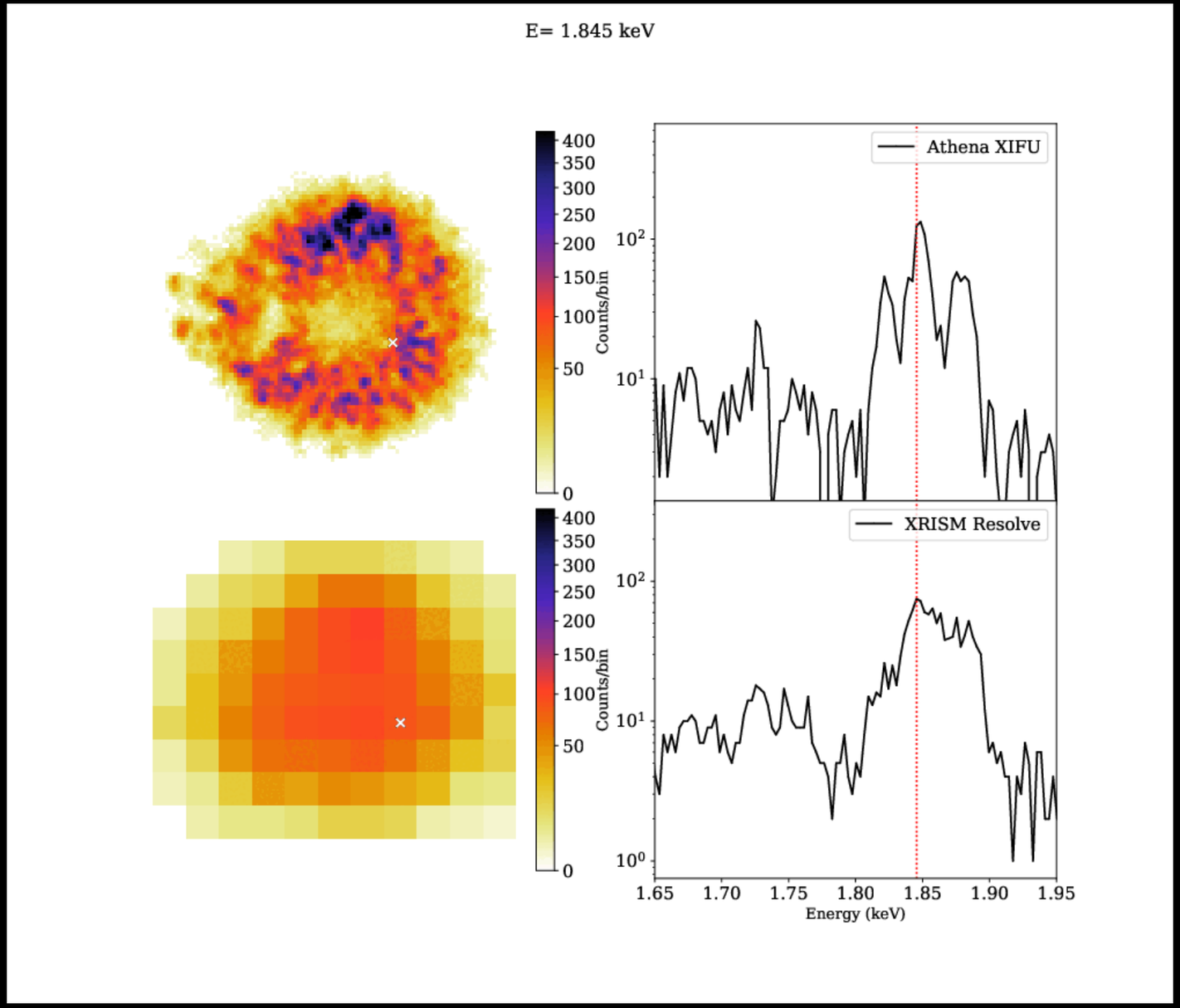

Cas A (F. Acero, A. Decourchelle [CEA], C. Kirsch, J. Wilms, T. Dauser [ECAP])

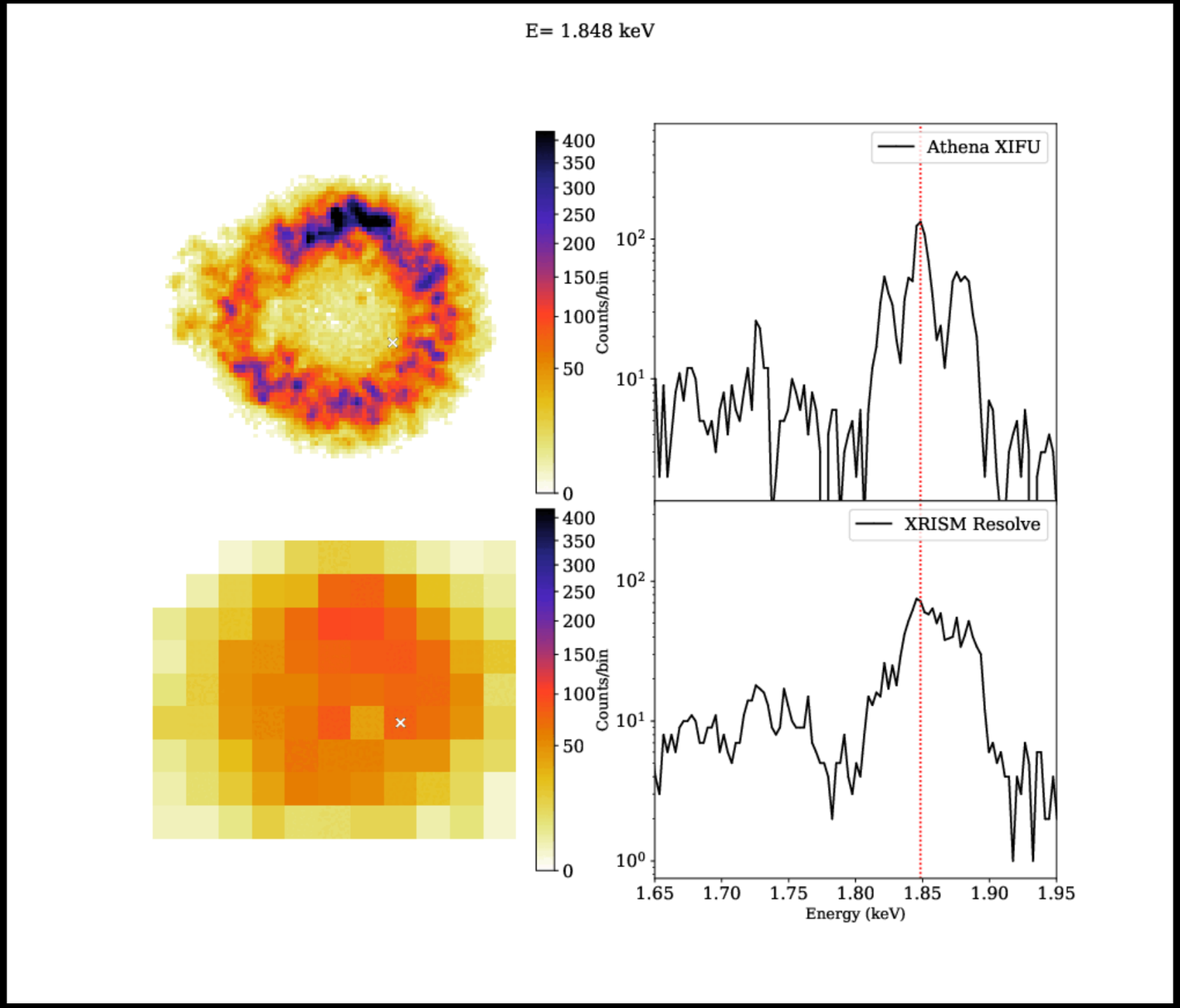

Cas A (F. Acero, A. Decourchelle [CEA], C. Kirsch, J. Wilms, T. Dauser [ECAP])

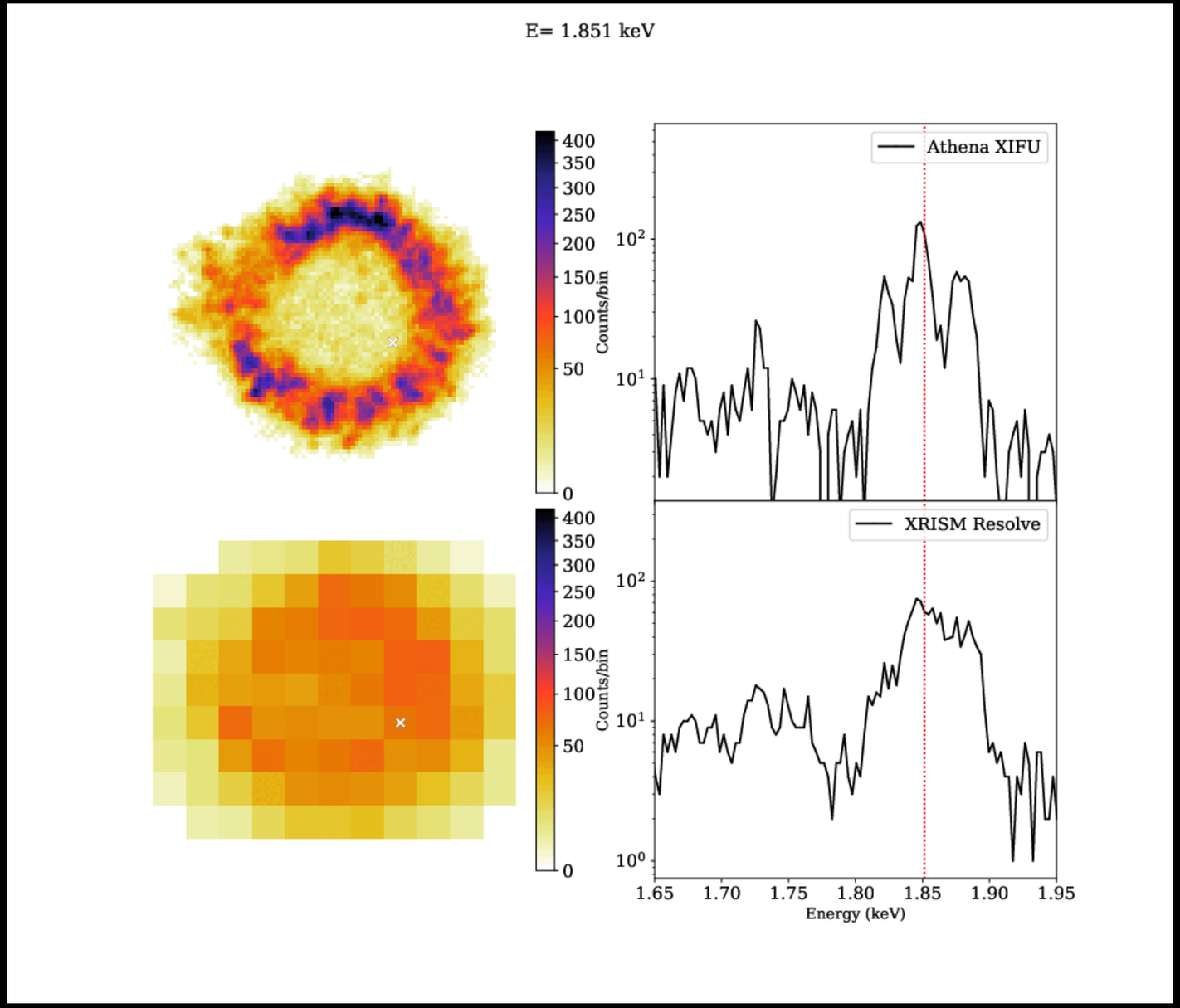

Cas A (F. Acero, A. Decourchelle [CEA], C. Kirsch, J. Wilms, T. Dauser [ECAP])

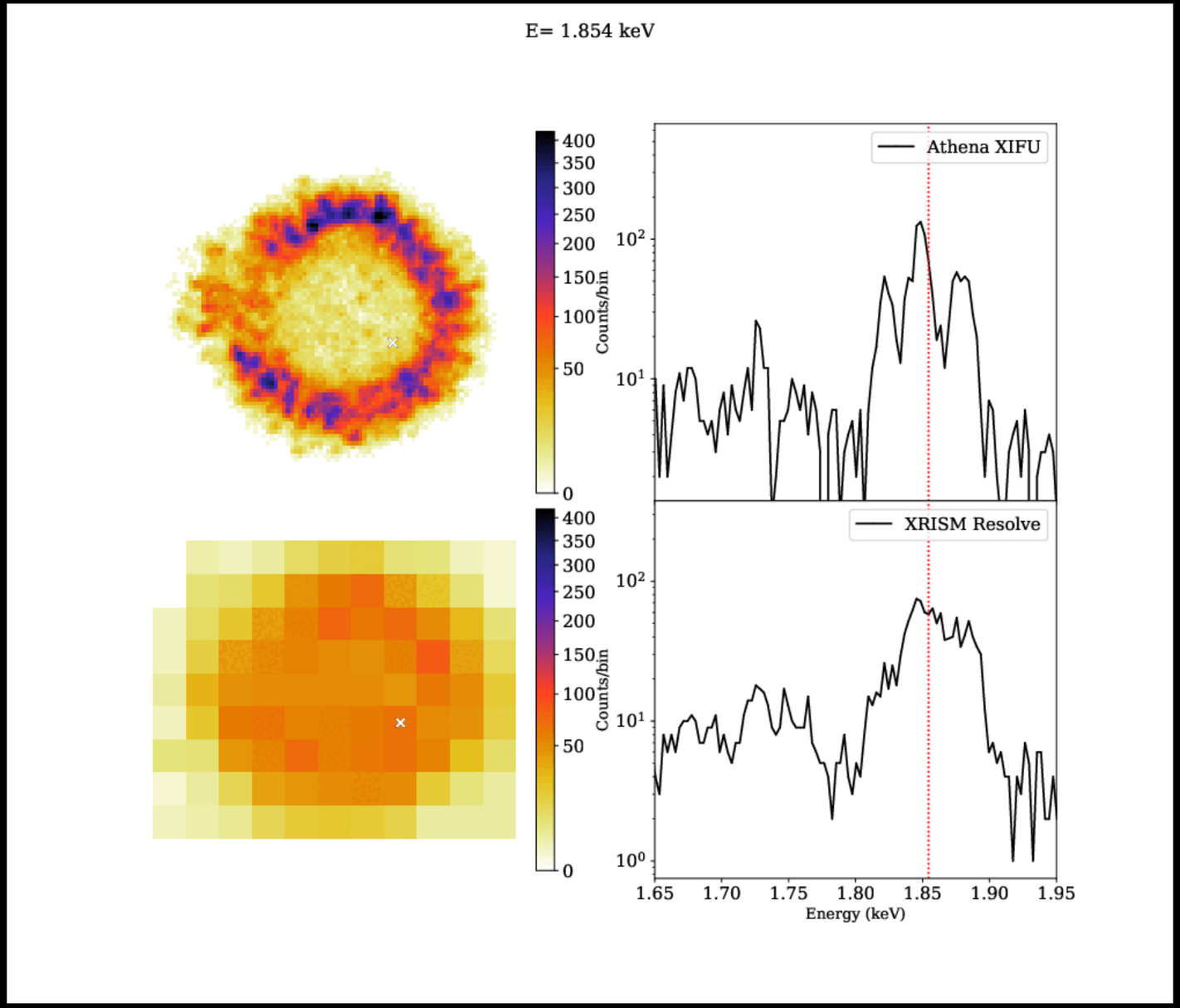

Cas A (F. Acero, A. Decourchelle [CEA], C. Kirsch, J. Wilms, T. Dauser [ECAP])

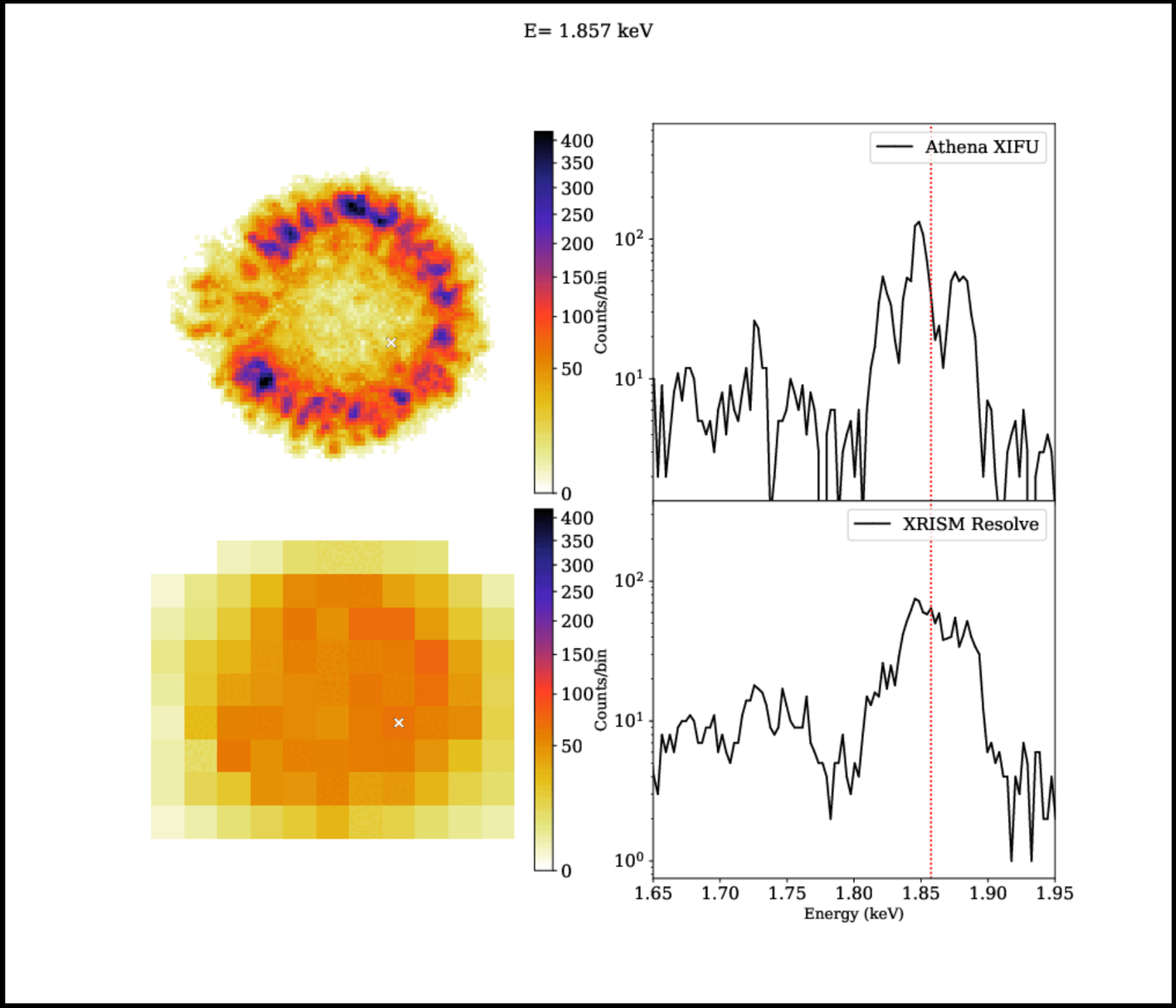

Cas A (F. Acero, A. Decourchelle [CEA], C. Kirsch, J. Wilms, T. Dauser [ECAP])

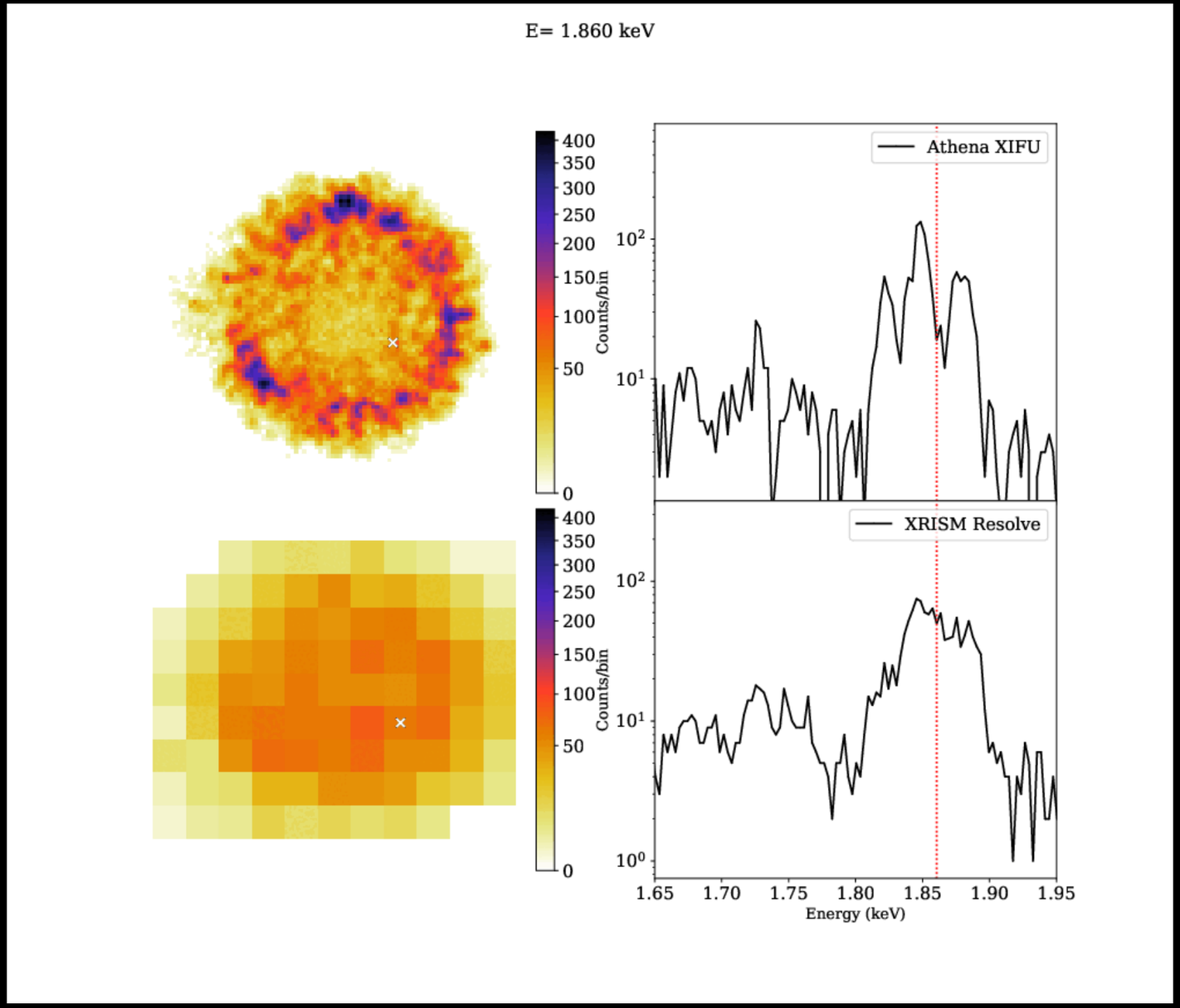

Cas A (F. Acero, A. Decourchelle [CEA], C. Kirsch, J. Wilms, T. Dauser [ECAP])

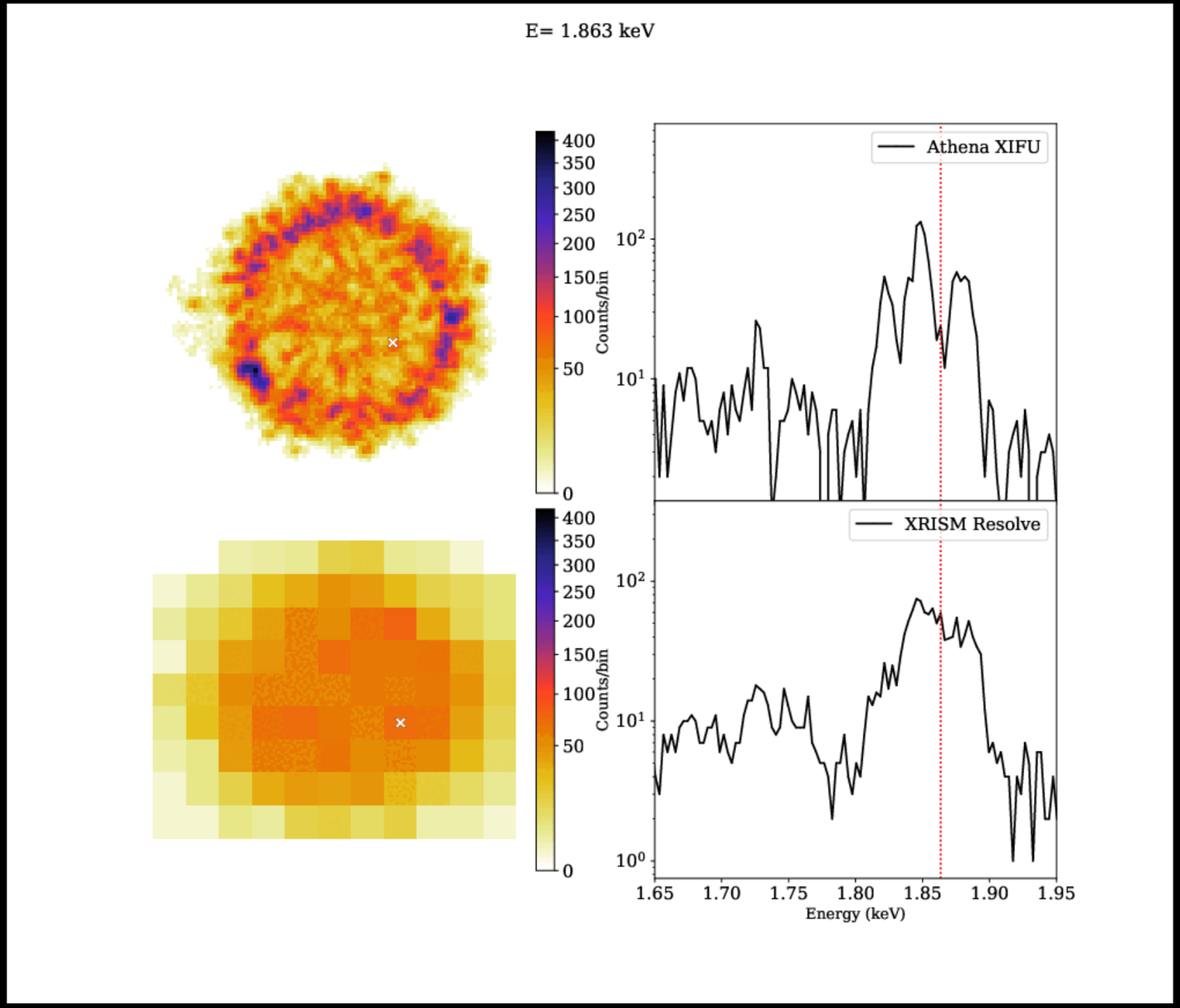

Cas A (F. Acero, A. Decourchelle [CEA], C. Kirsch, J. Wilms, T. Dauser [ECAP])

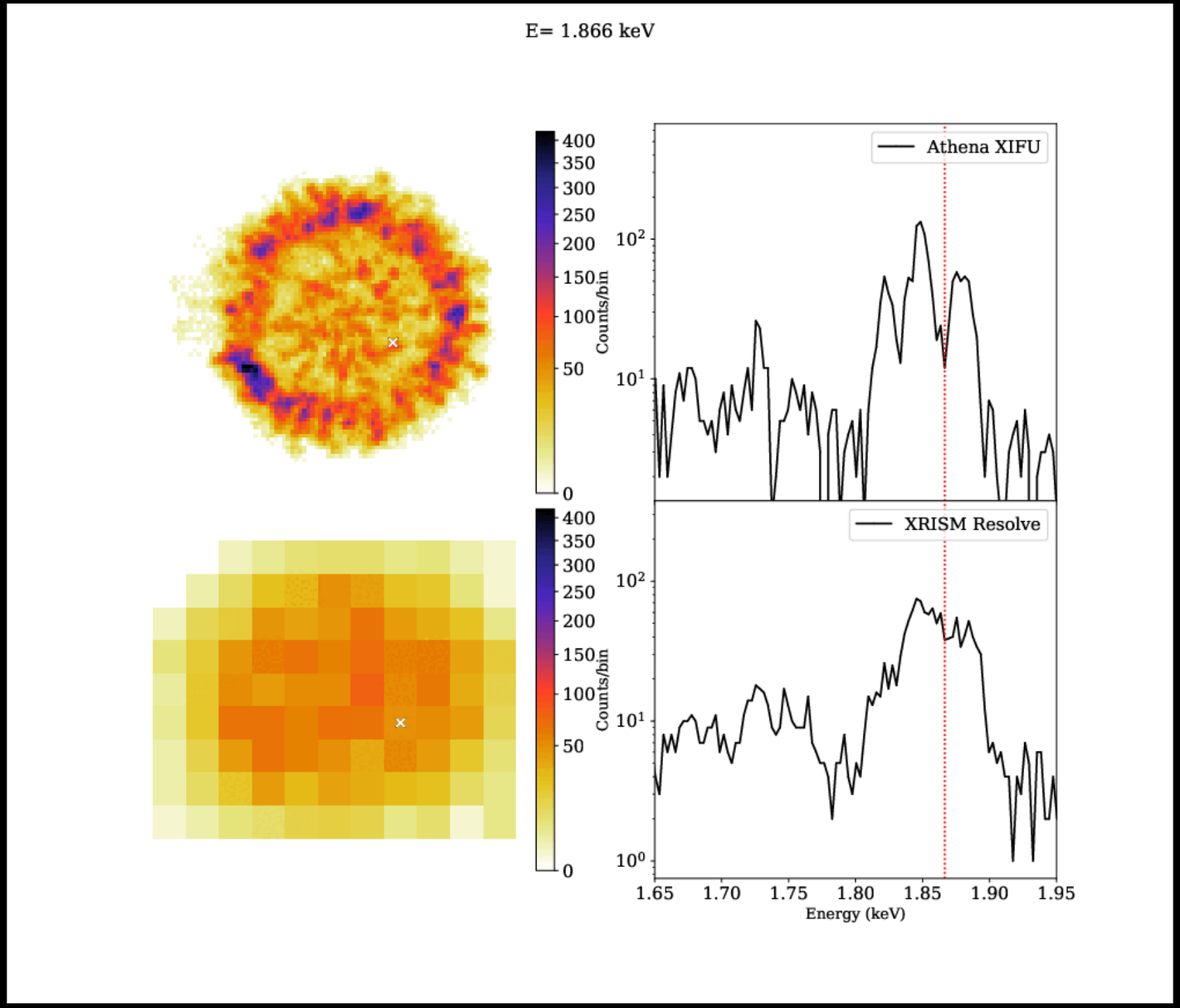

Cas A (F. Acero, A. Decourchelle [CEA], C. Kirsch, J. Wilms, T. Dauser [ECAP])

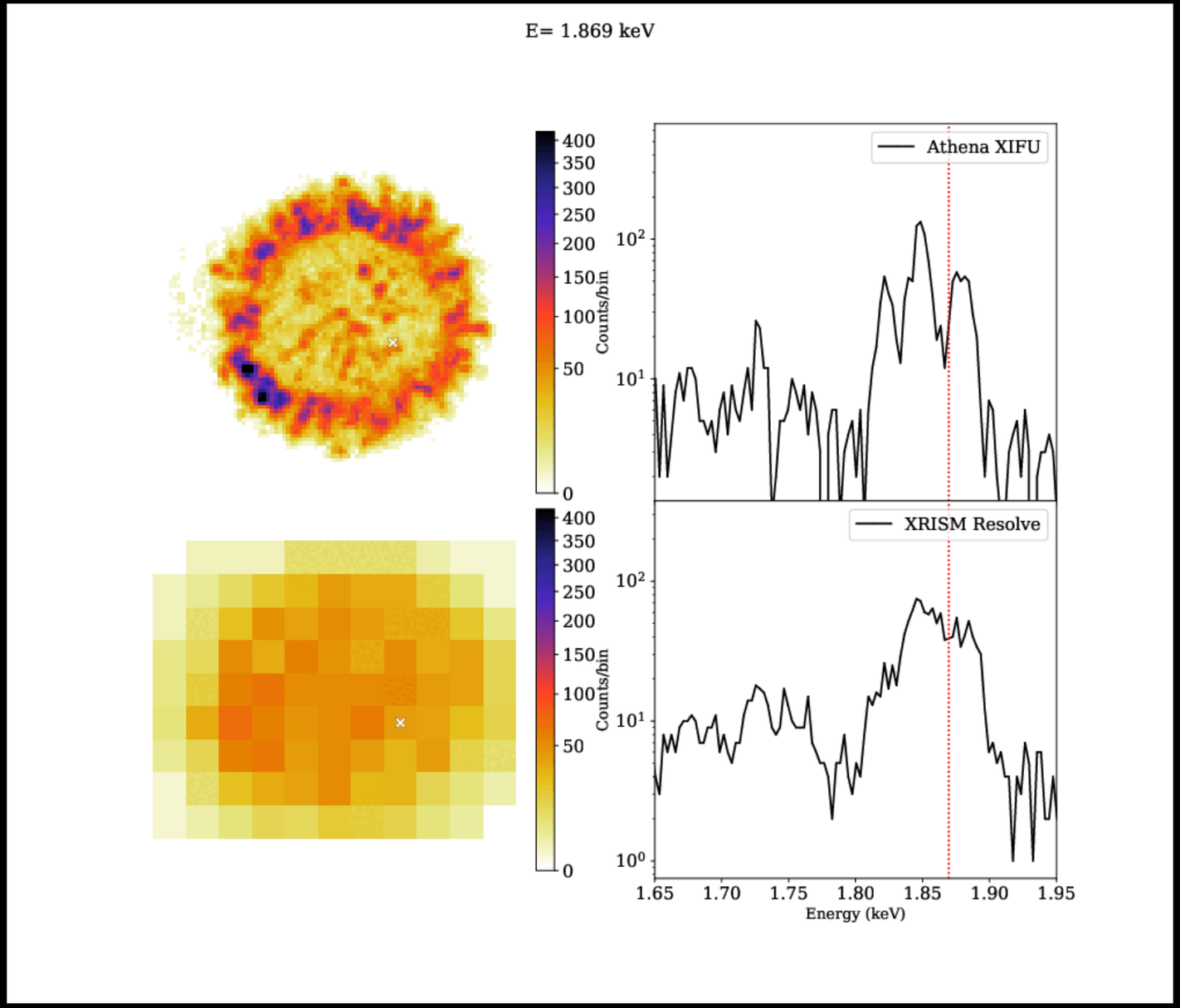

Cas A (F. Acero, A. Decourchelle [CEA], C. Kirsch, J. Wilms, T. Dauser [ECAP])

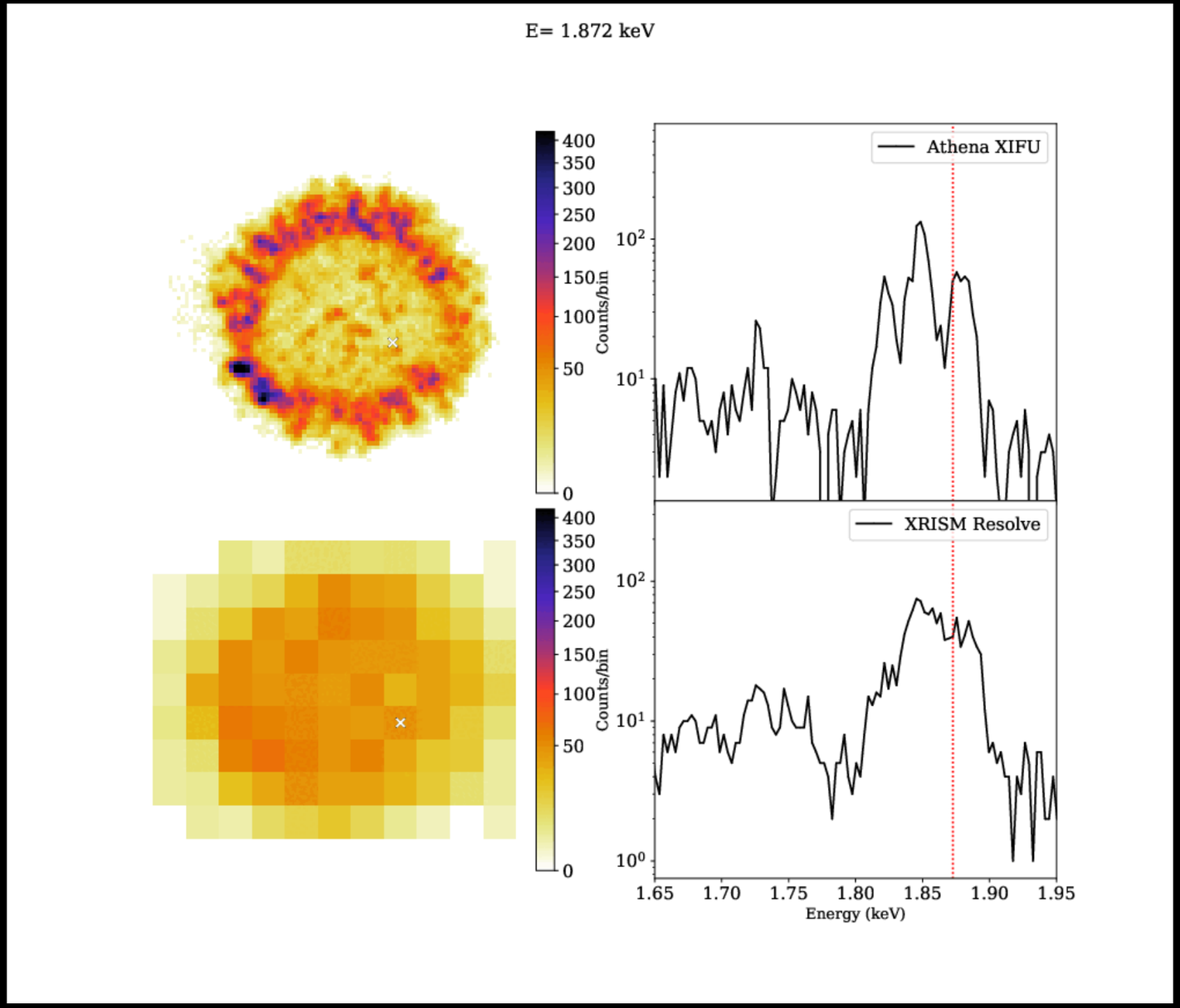

Cas A (F. Acero, A. Decourchelle [CEA], C. Kirsch, J. Wilms, T. Dauser [ECAP])

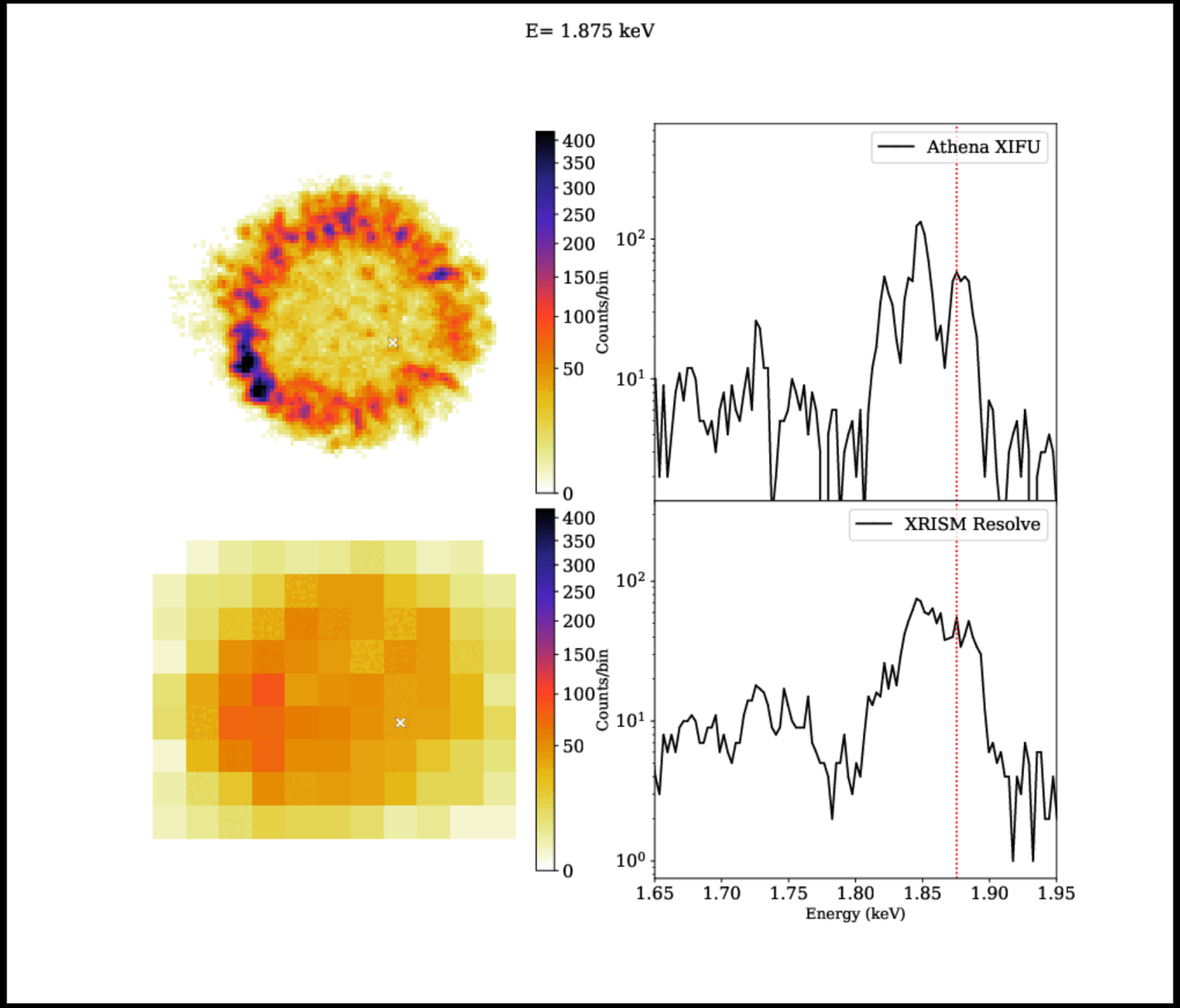

Cas A (F. Acero, A. Decourchelle [CEA], C. Kirsch, J. Wilms, T. Dauser [ECAP])

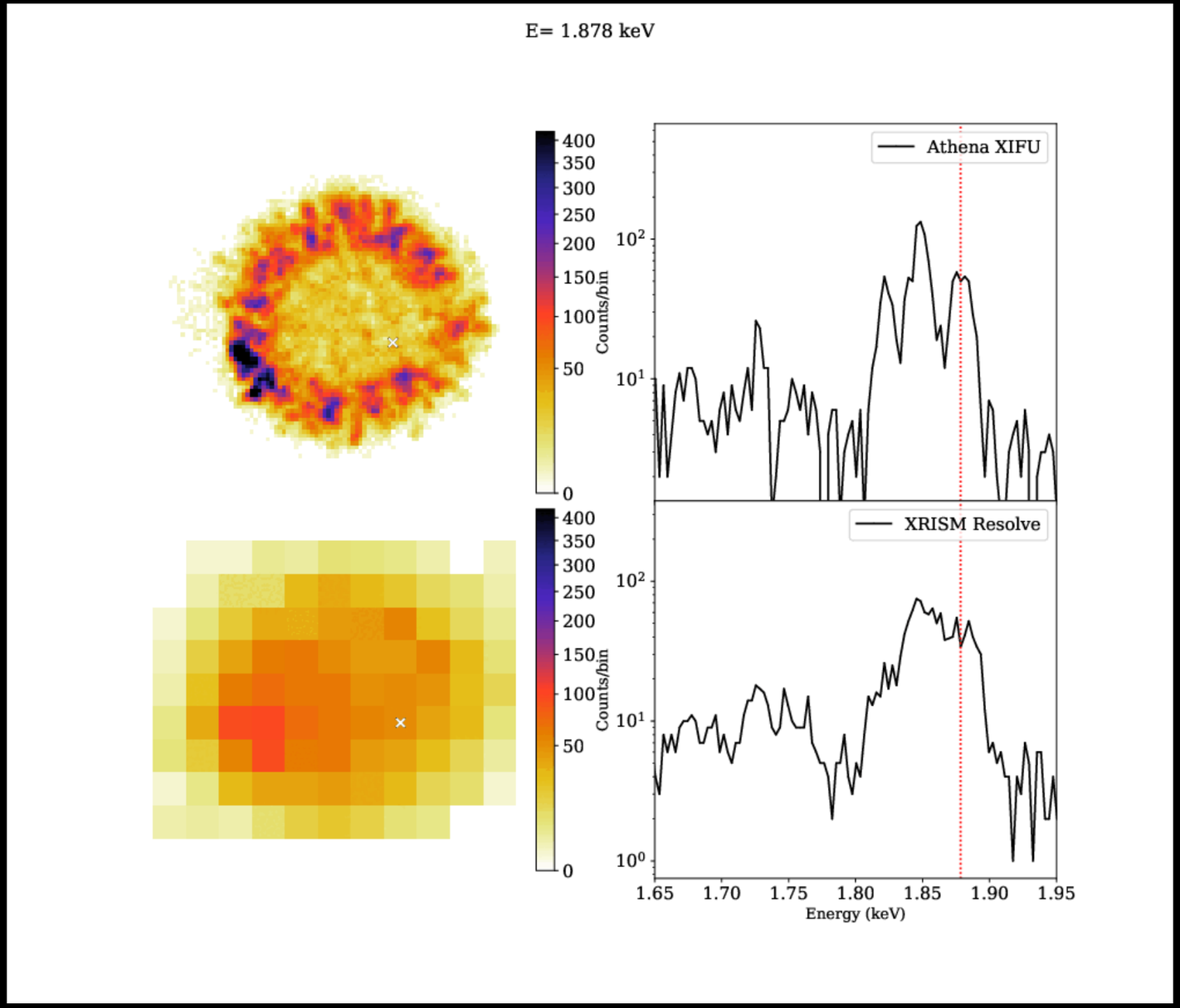

Cas A (F. Acero, A. Decourchelle [CEA], C. Kirsch, J. Wilms, T. Dauser [ECAP])

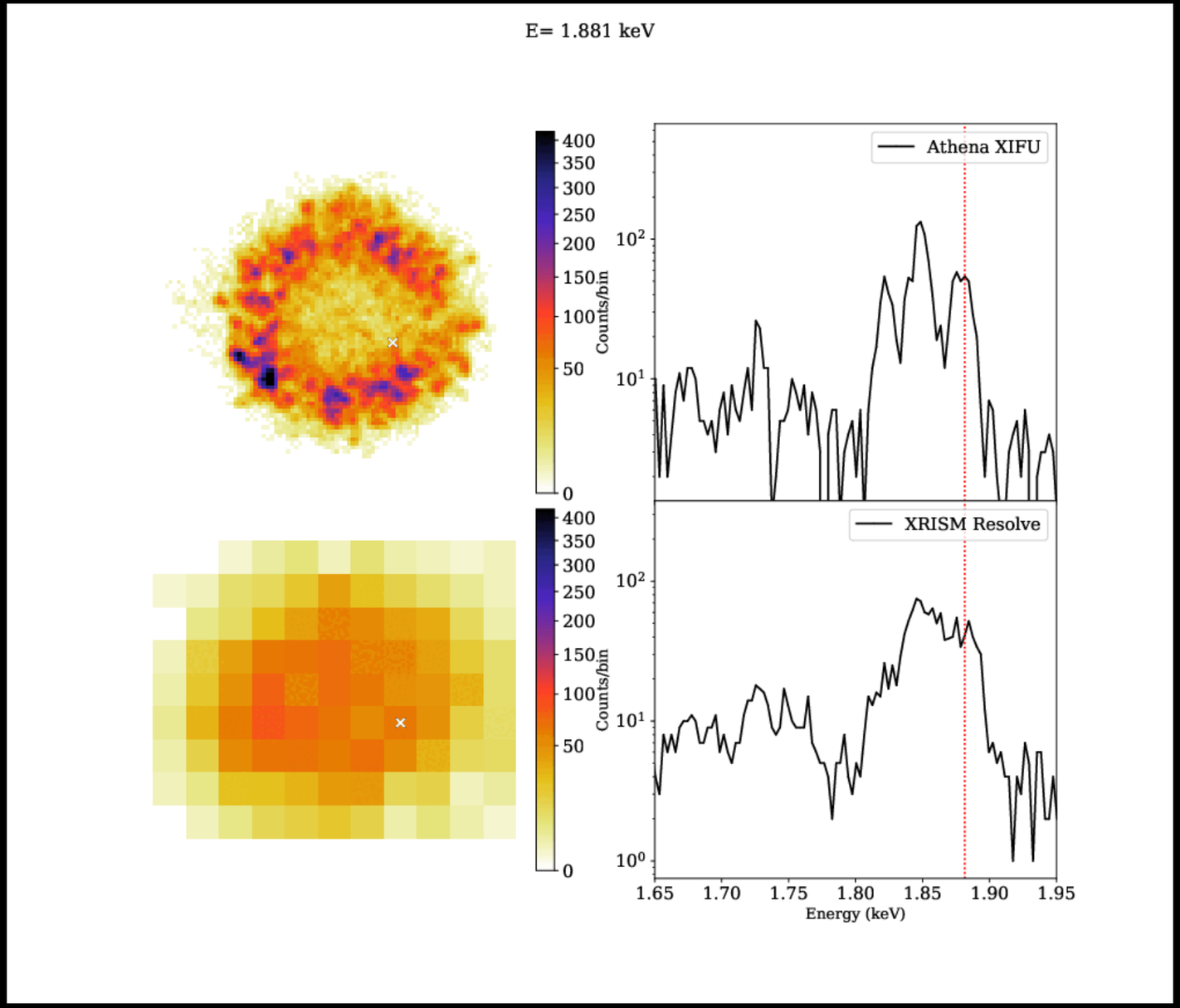

Cas A (F. Acero, A. Decourchelle [CEA], C. Kirsch, J. Wilms, T. Dauser [ECAP])

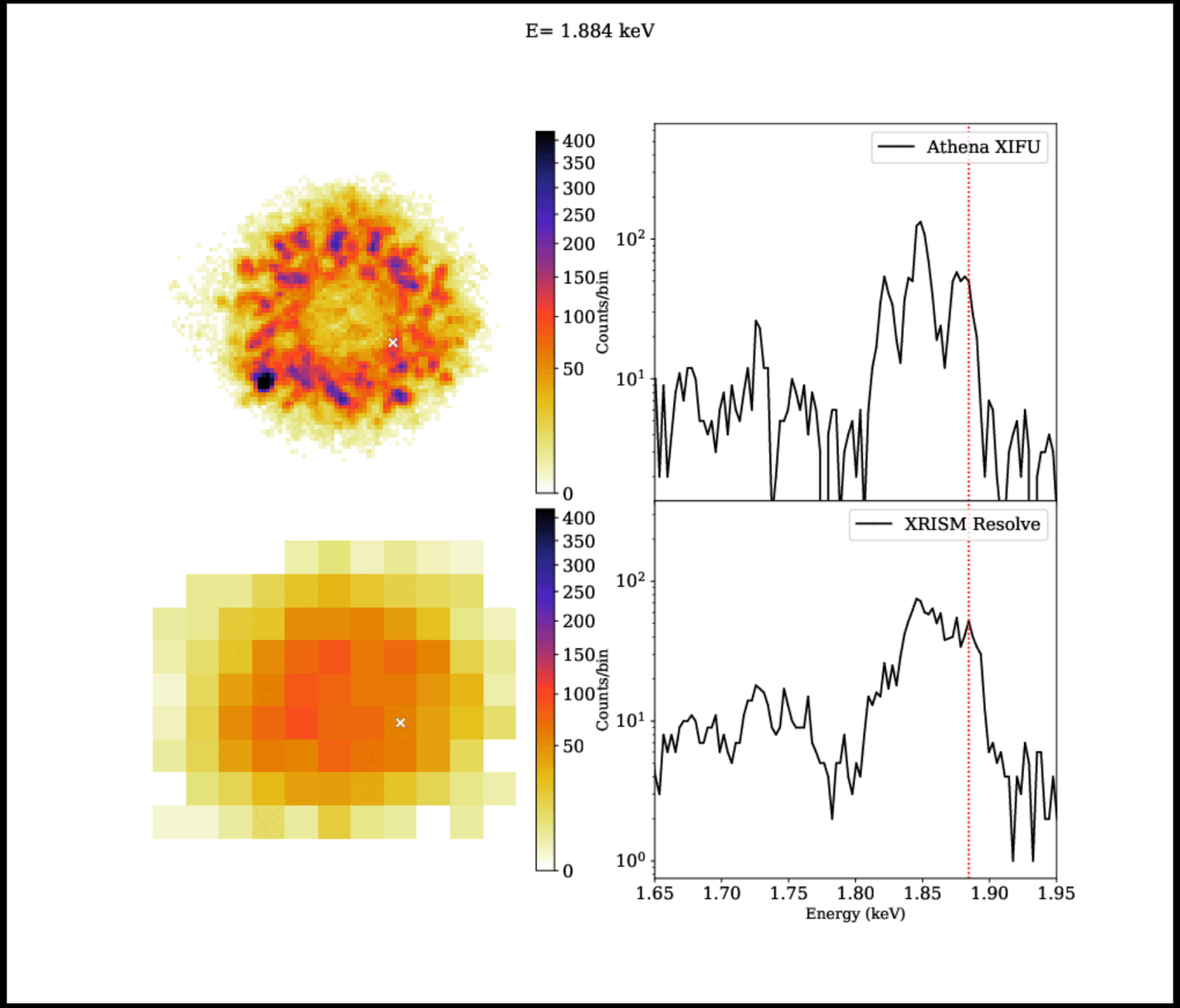

Cas A (F. Acero, A. Decourchelle [CEA], C. Kirsch, J. Wilms, T. Dauser [ECAP])

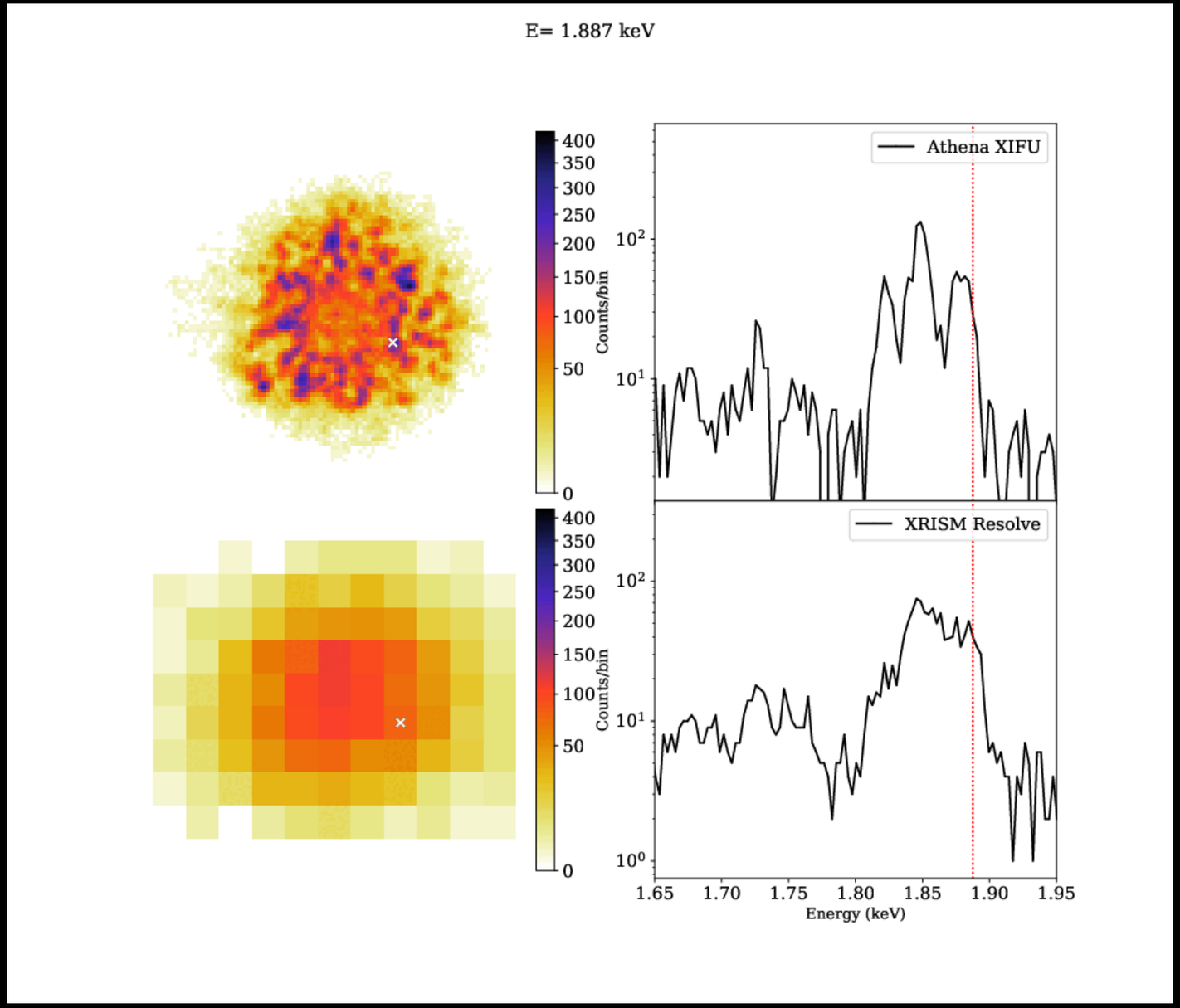

Cas A (F. Acero, A. Decourchelle [CEA], C. Kirsch, J. Wilms, T. Dauser [ECAP])

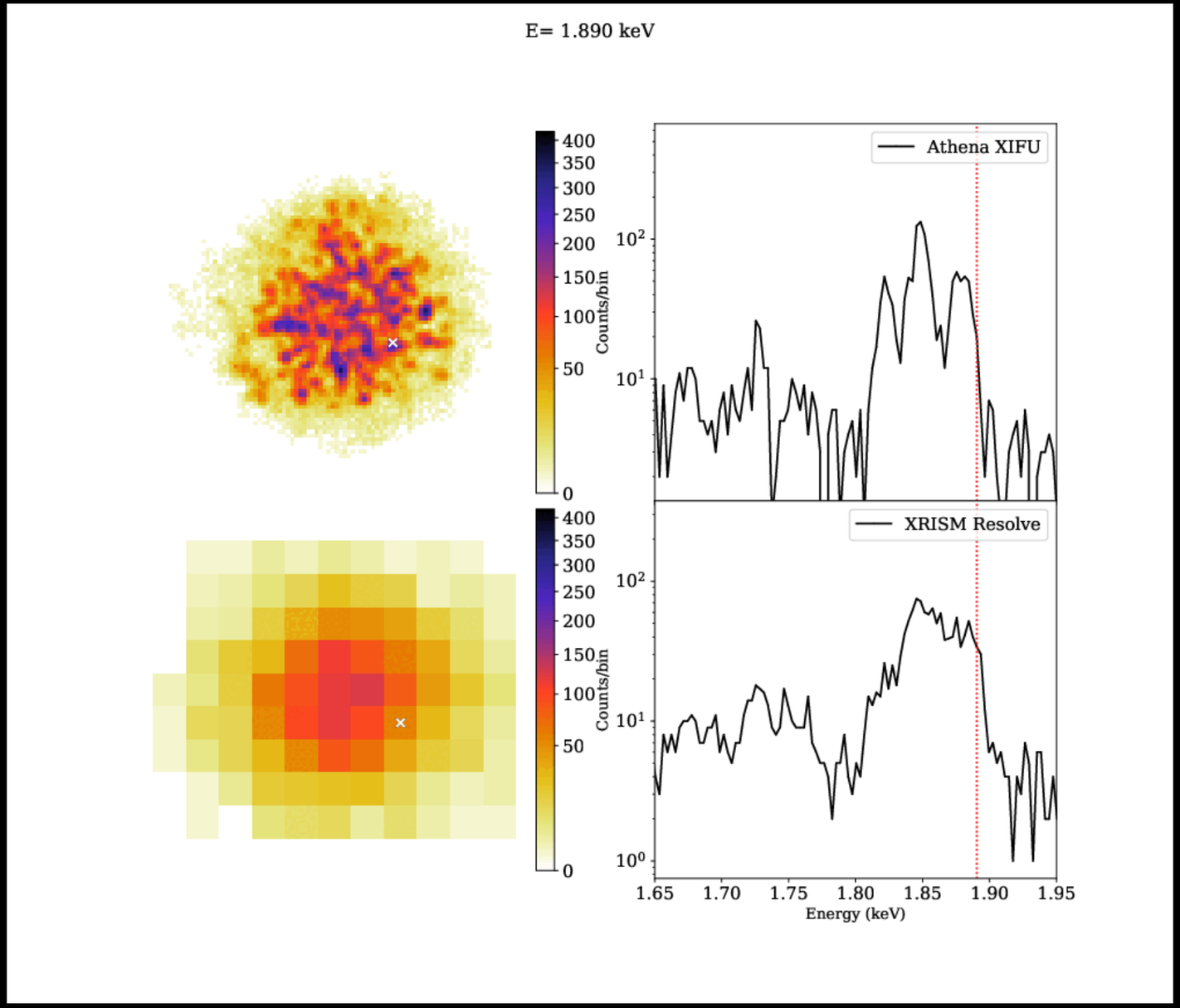

Cas A (F. Acero, A. Decourchelle [CEA], C. Kirsch, J. Wilms, T. Dauser [ECAP])

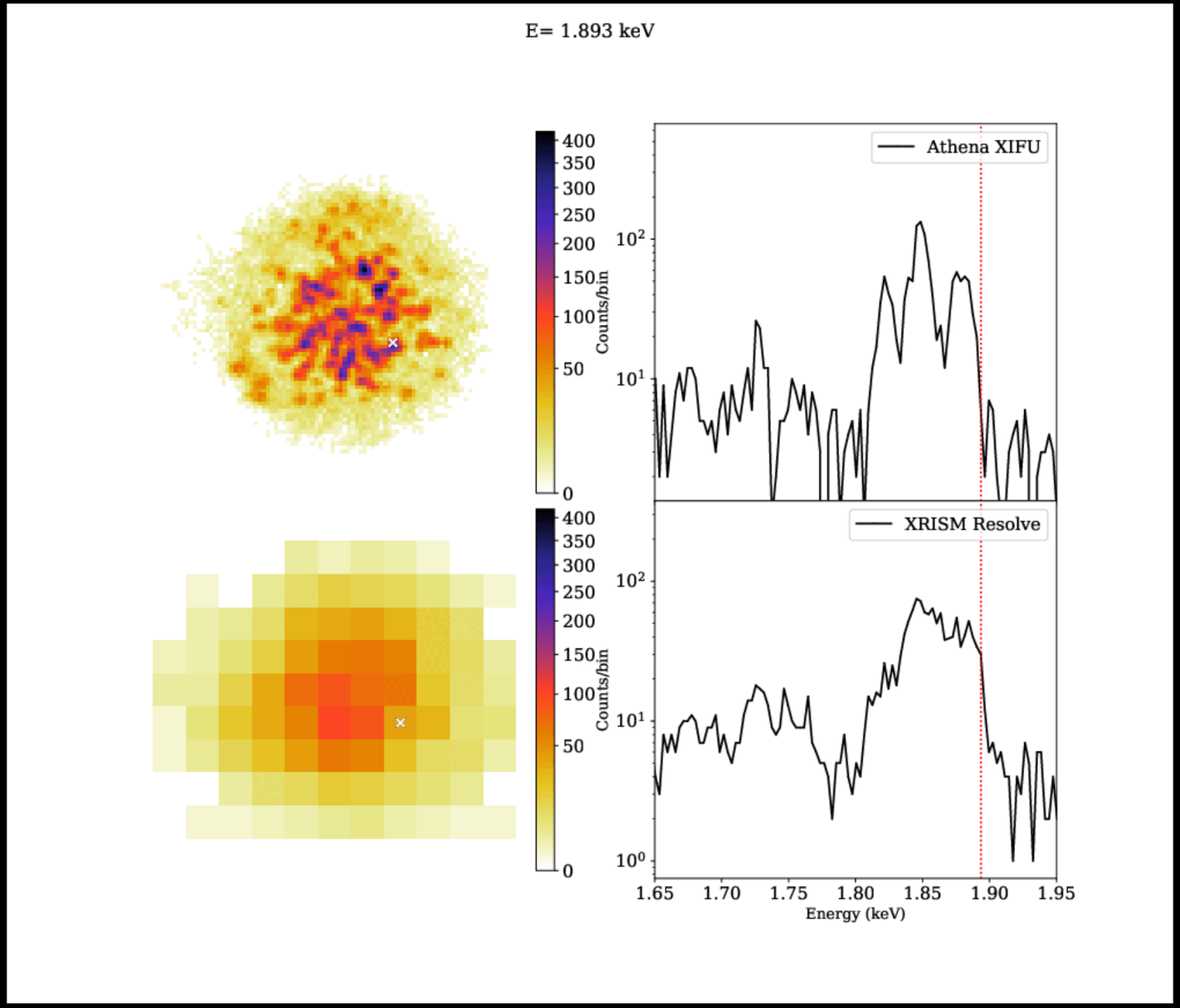

Cas A (F. Acero, A. Decourchelle [CEA], C. Kirsch, J. Wilms, T. Dauser [ECAP])

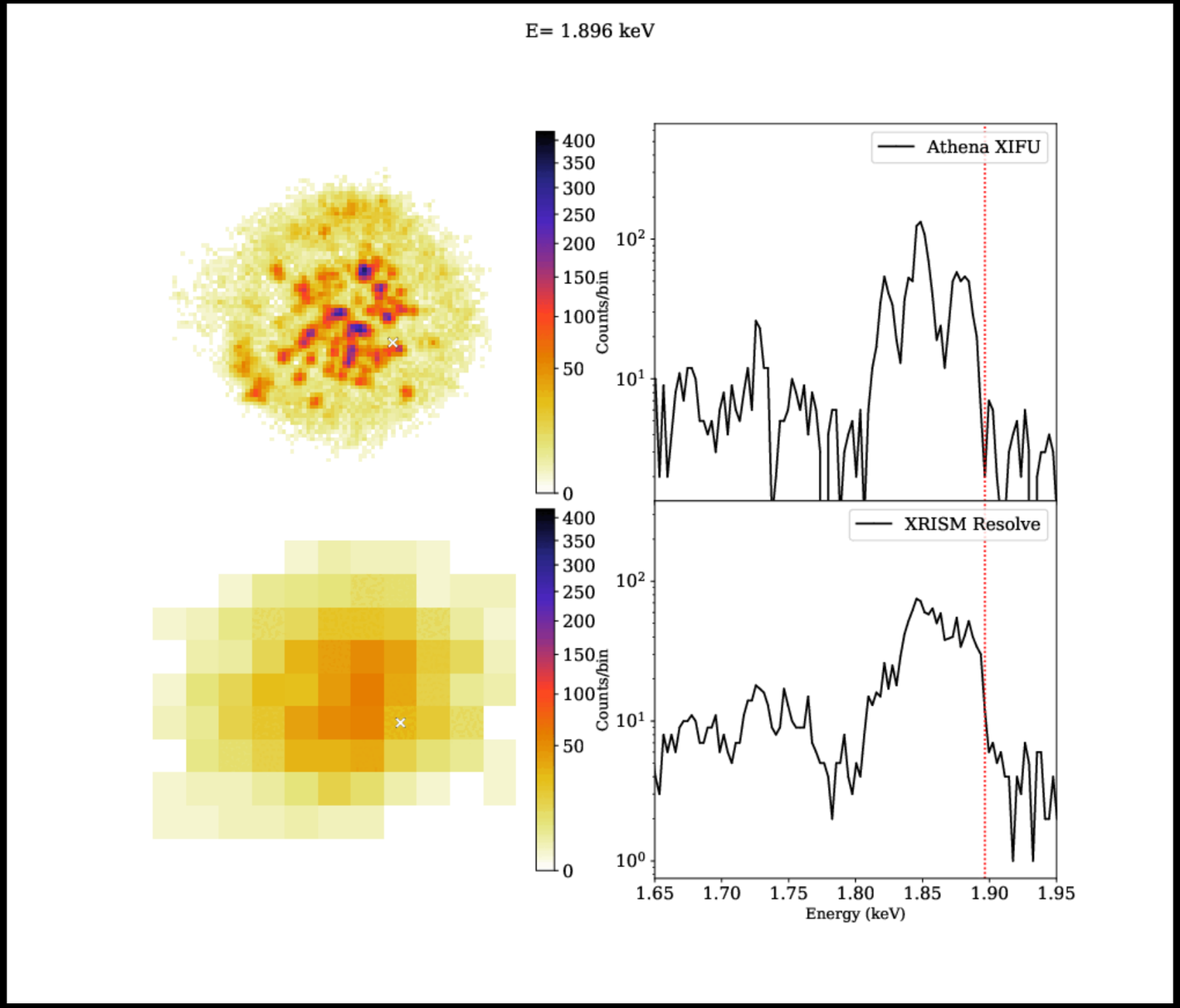

Cas A (F. Acero, A. Decourchelle [CEA], C. Kirsch, J. Wilms, T. Dauser [ECAP])

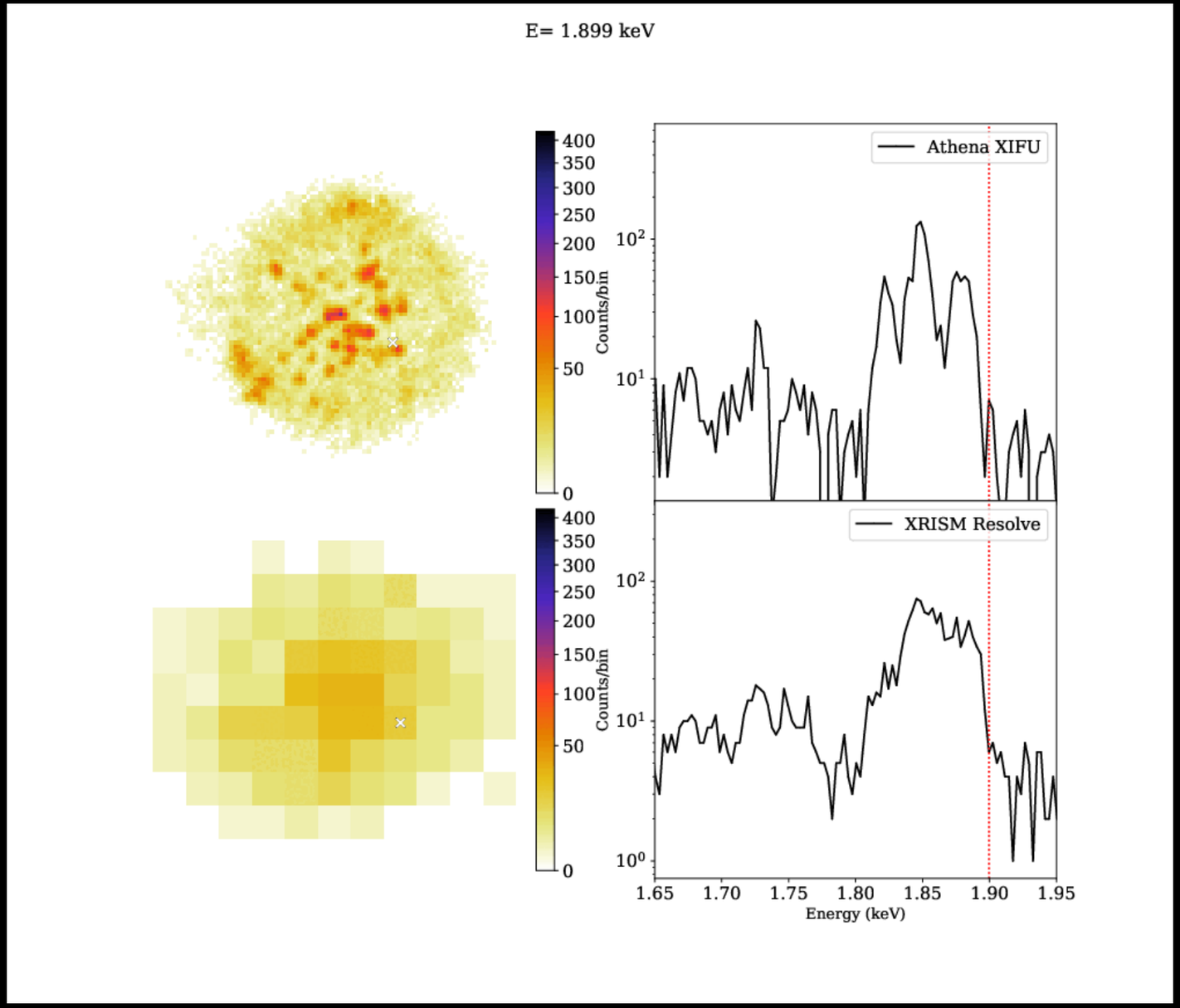

Cas A (F. Acero, A. Decourchelle [CEA], C. Kirsch, J. Wilms, T. Dauser [ECAP])

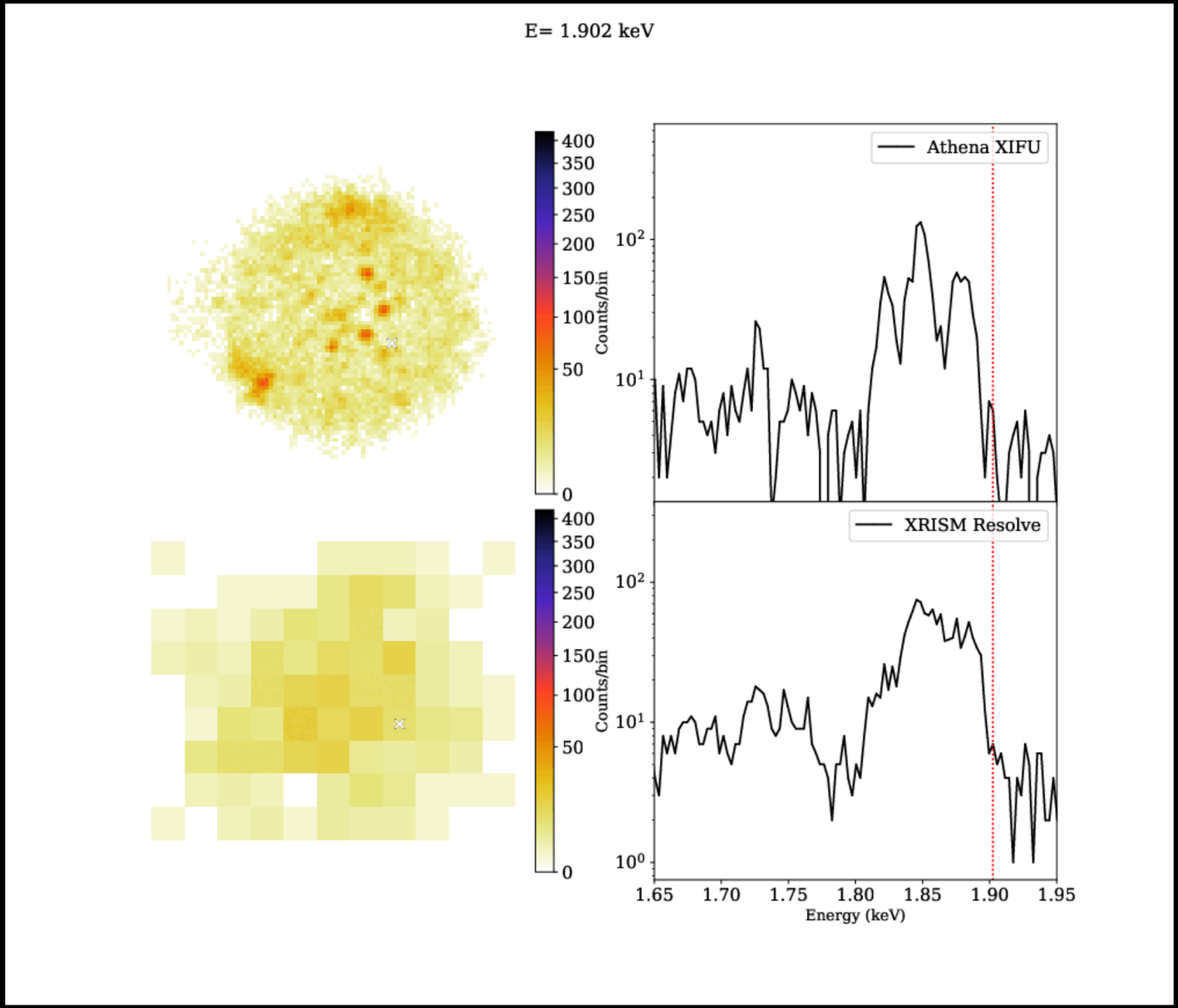

Cas A (F. Acero, A. Decourchelle [CEA], C. Kirsch, J. Wilms, T. Dauser [ECAP])

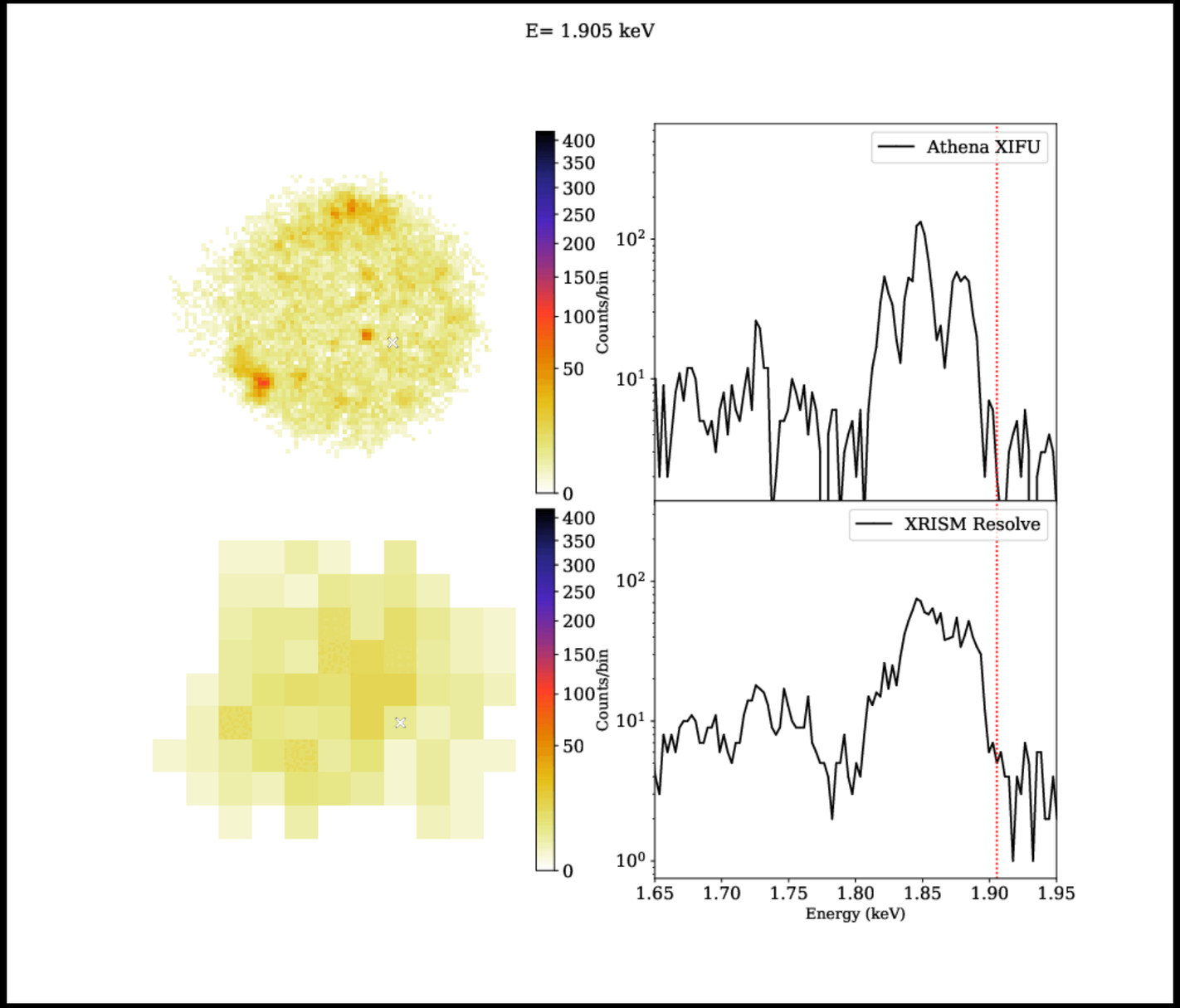

Cas A (F. Acero, A. Decourchelle [CEA], C. Kirsch, J. Wilms, T. Dauser [ECAP])

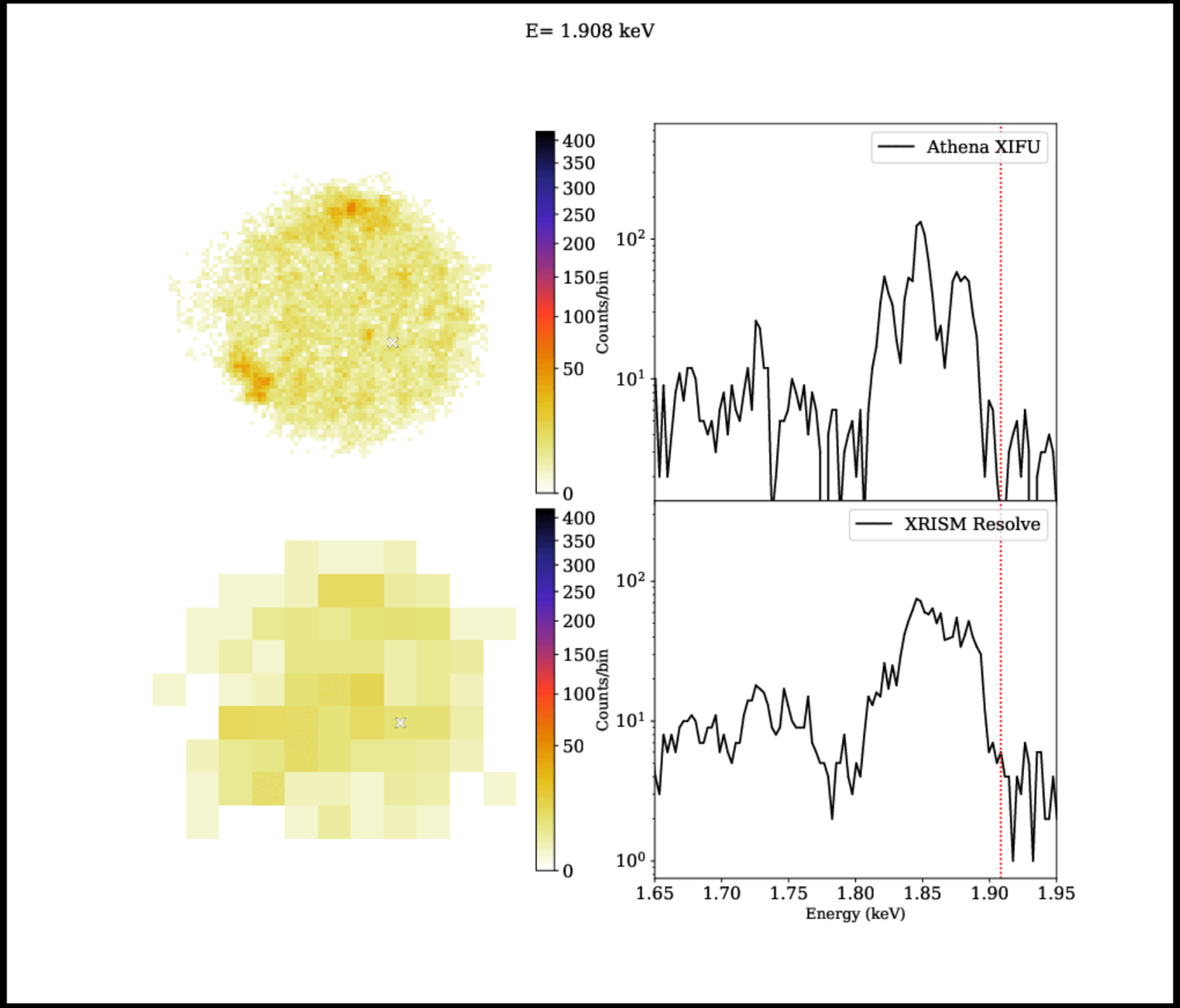

Cas A (F. Acero, A. Decourchelle [CEA], C. Kirsch, J. Wilms, T. Dauser [ECAP])

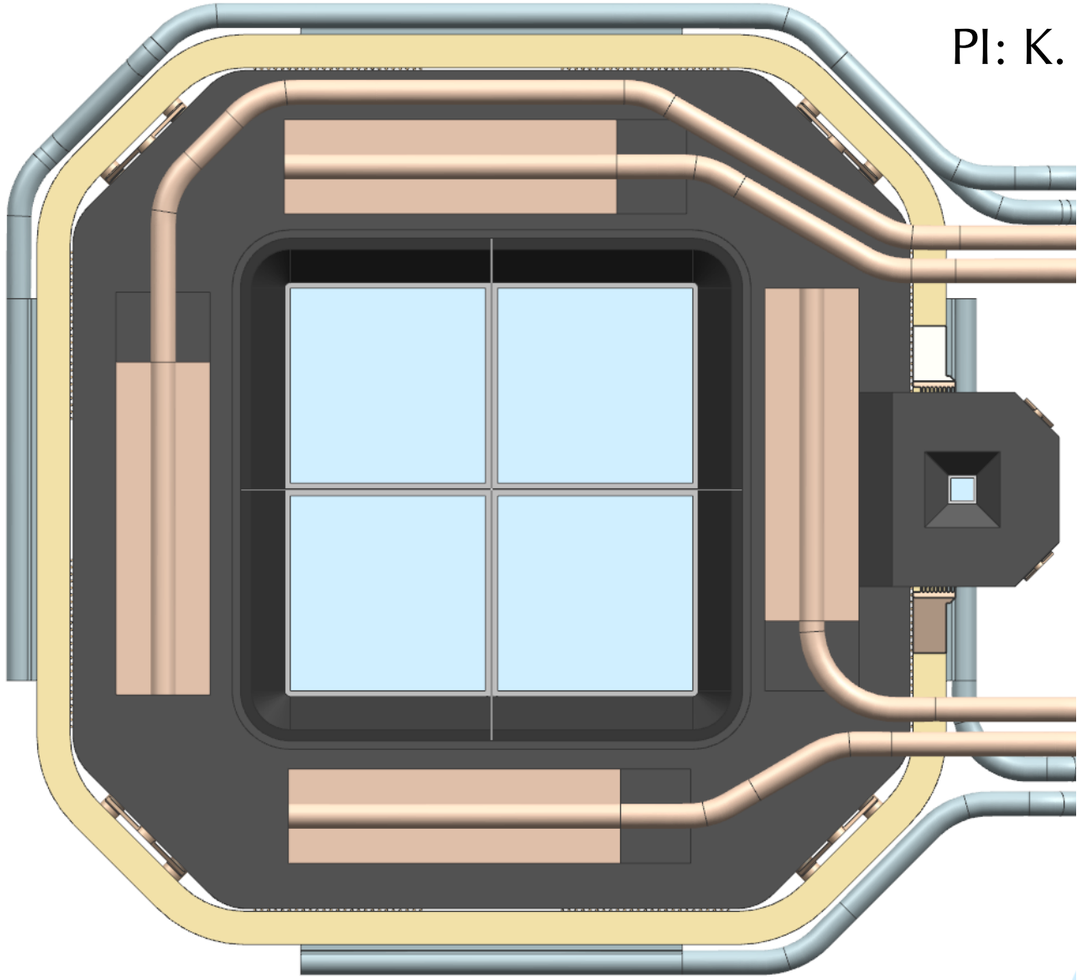

PI: K. Nandra (MPE, D)

Large Detector Array
- 40'x40
- 4x512x512 pxl
- <5ms/frame
  <10µs/row

Fast Detector
- defocused
- 64x64(/2) pxl
- <80µs/frame
  <2.5µs/row

Both
- 130µmx130µm
- DEPFET technology

A. Rau

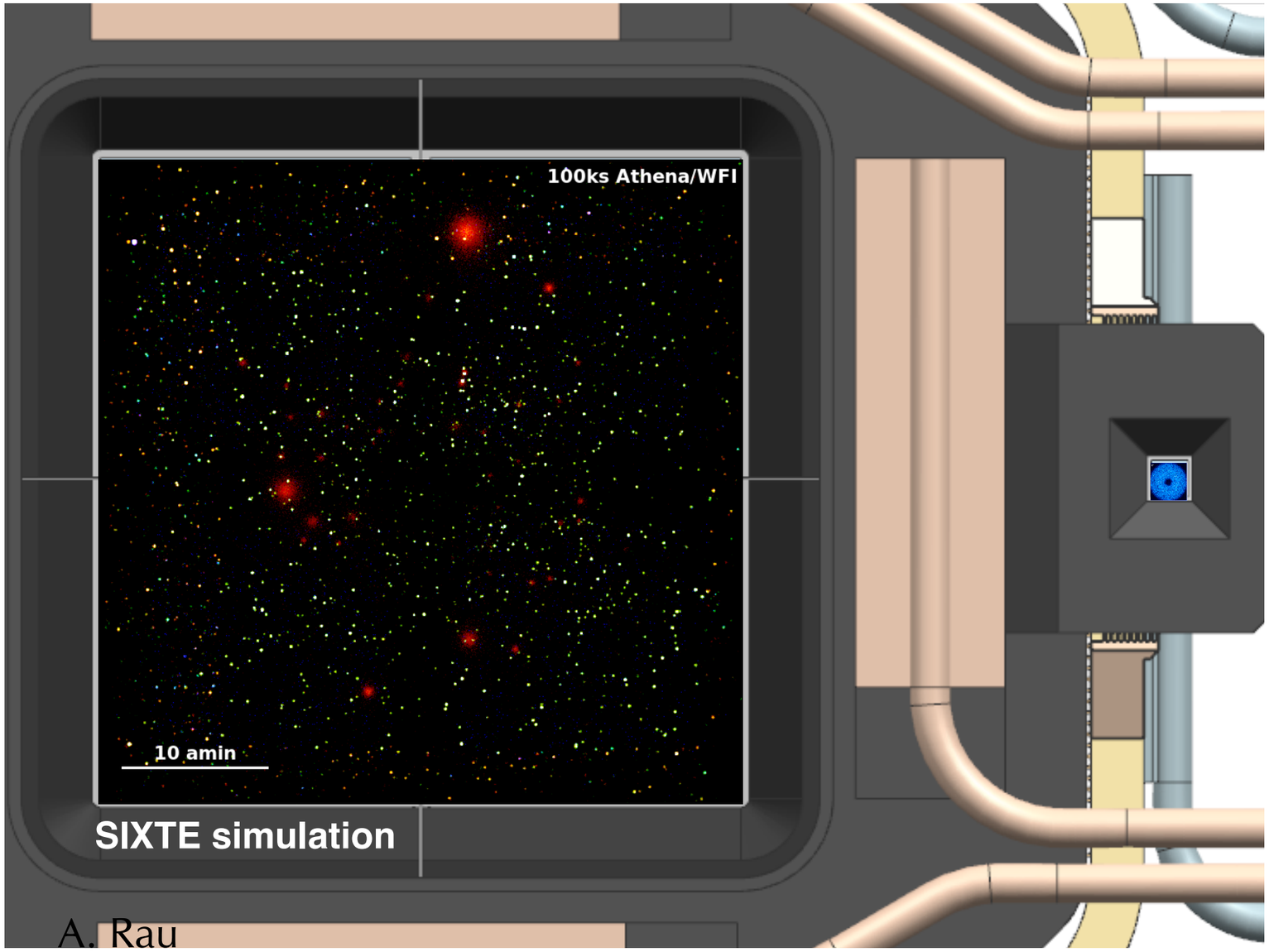
100ks Athena/WFI
10 amin
SIXTE simulation

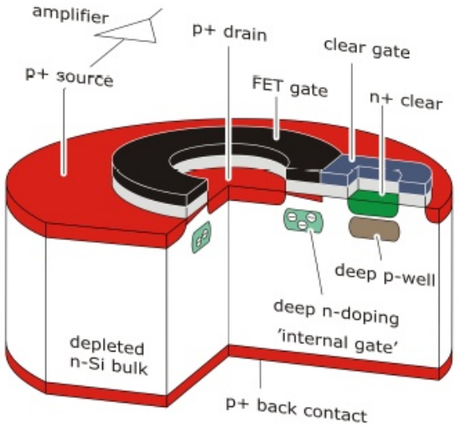

WFI: 1024 × 1024 Array of DEPFET-Sensors (active pixel sensors)
µs time resolution...

energy resolution at theoretical (Fano) limit (~150 eV at 6 keV).

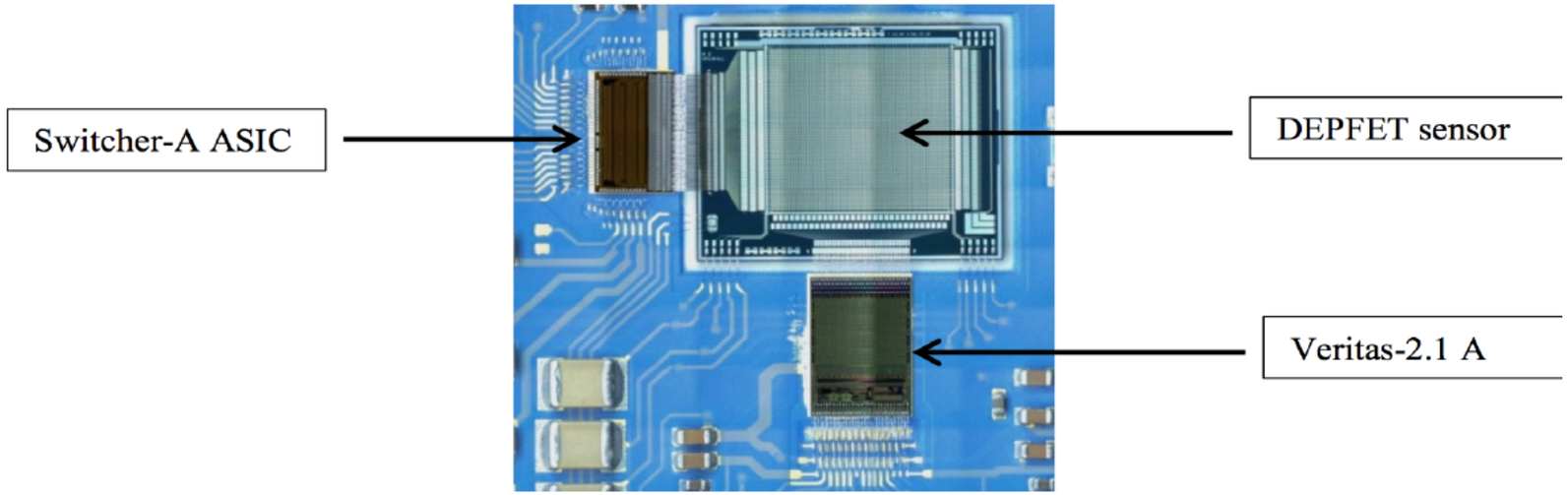

BSc M. Rohe (Remeis/ECAP/FAU)

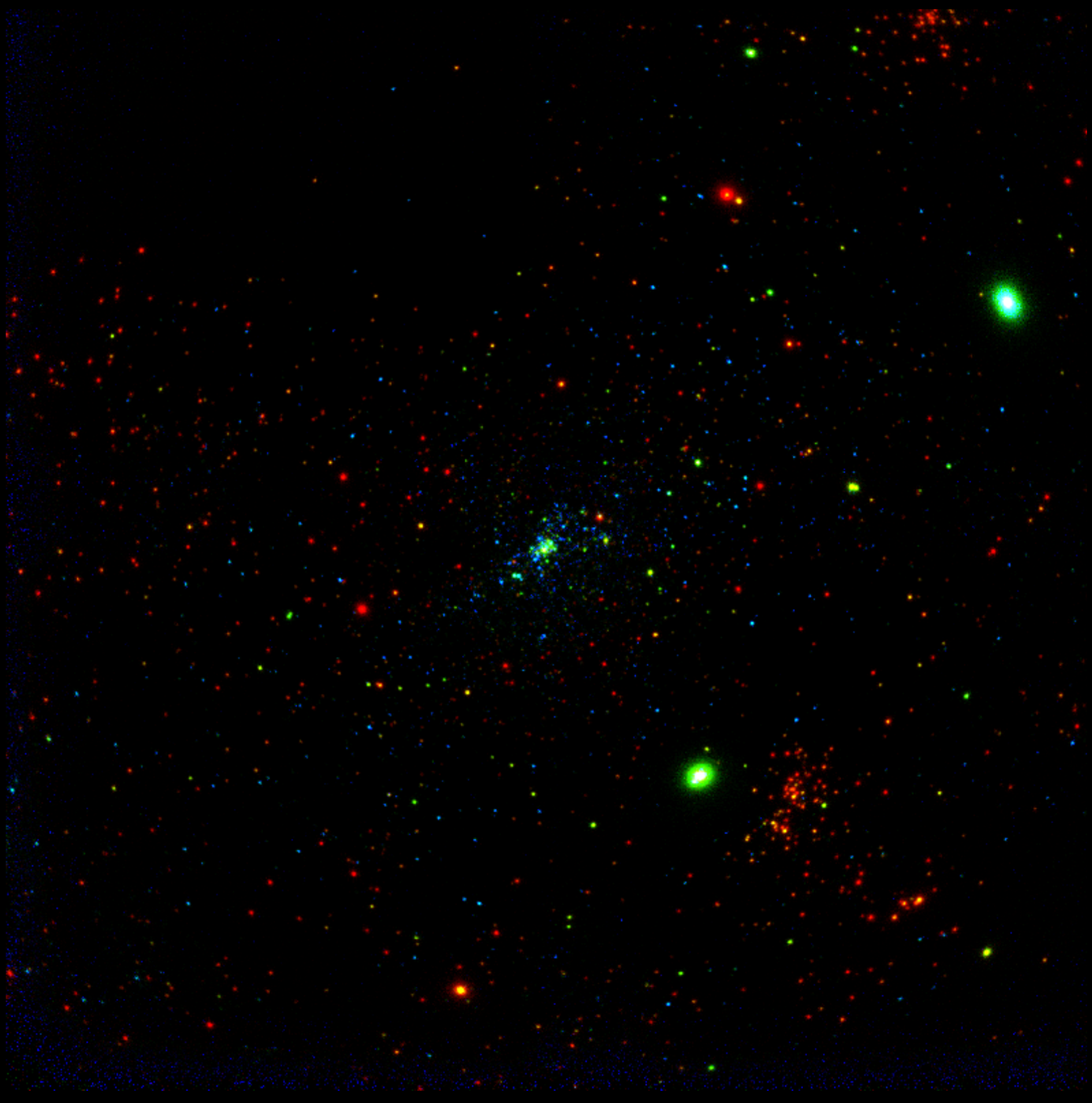

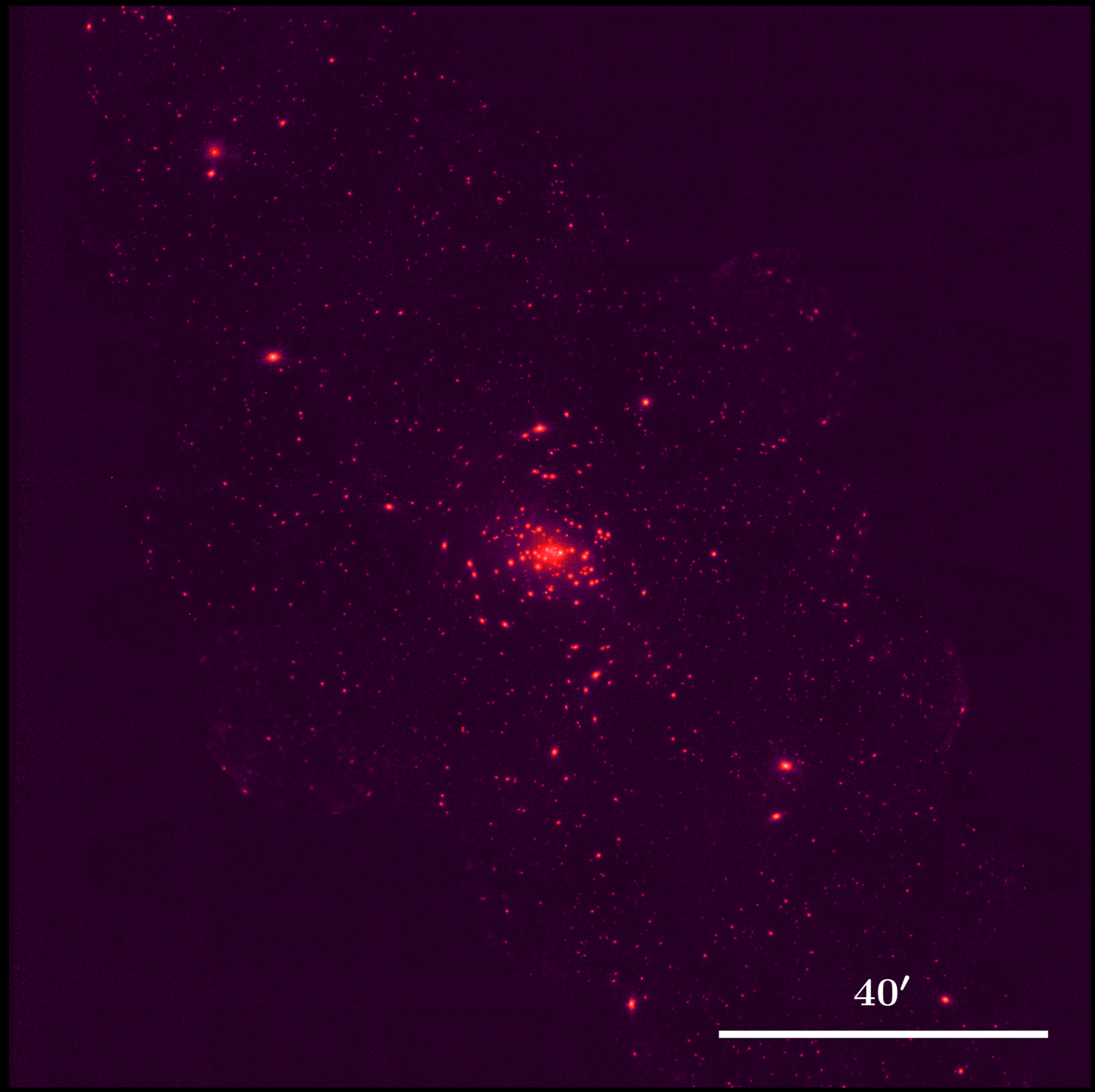

T. Dauser (Remeis/ECAP/FAU), N. Vulic (GSFC)

Atomic Data

rel. difference between A coeffs

AtomDB vs. SPEX

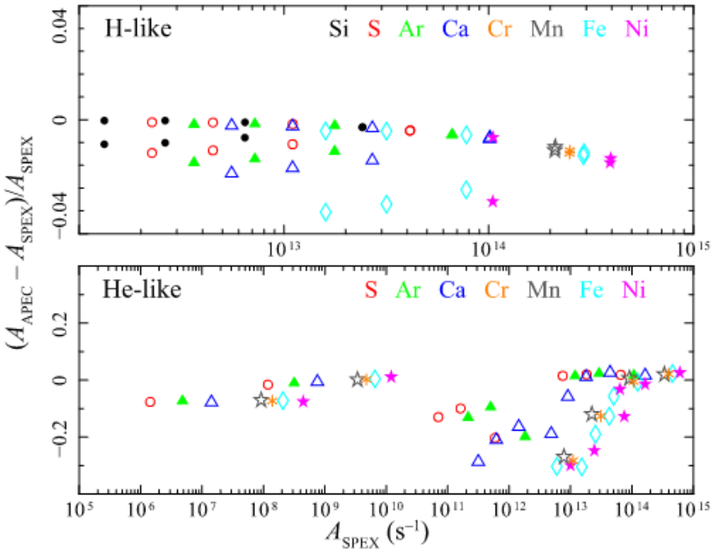

CHIANTI vs. SPEX

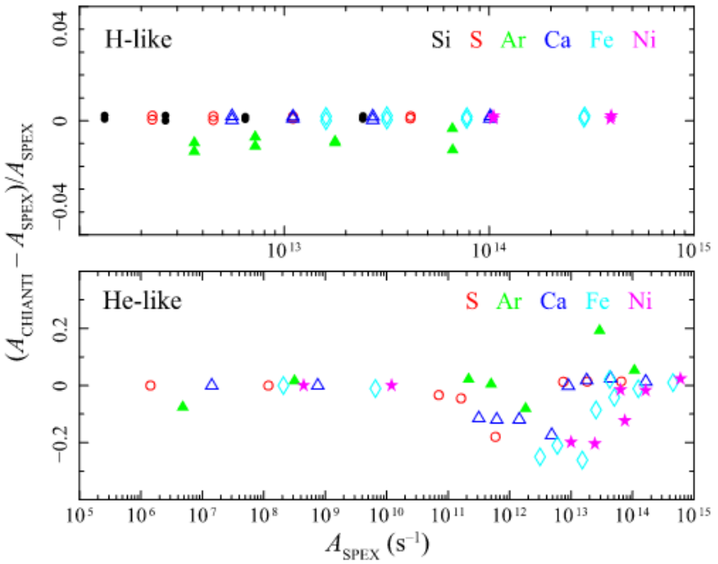

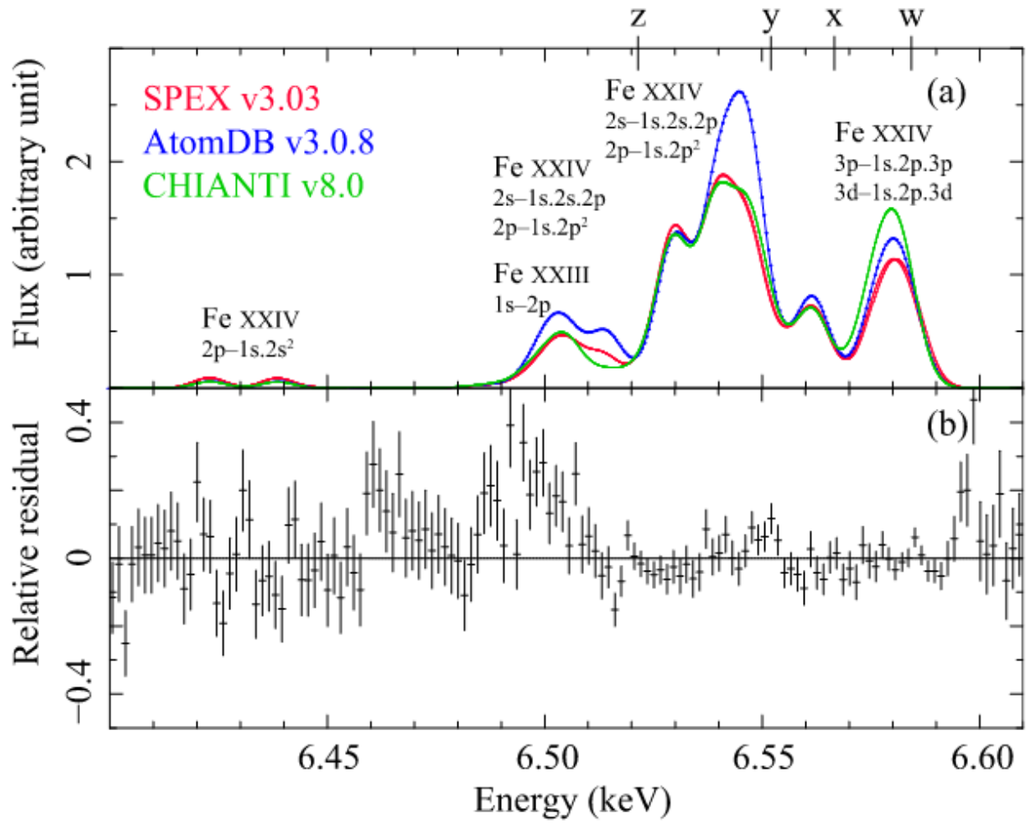

Uncertainties in atomic physics data strongly limit the scientific interpretation of microcalorimeter data.

(Aharonian et al., 2018, Publ. Astron. Soc. Japan 70, 12)

HDE 226868/Cyg X-1: Friend & Castor (1982), Gies et al. (2008): clumpy stellar wind/flow.

$10^{10}\,\mathrm{cm}^{-3} \leqslant n_{\mathrm{H}} \leqslant 10^{11}\,\mathrm{cm}^{-3}$

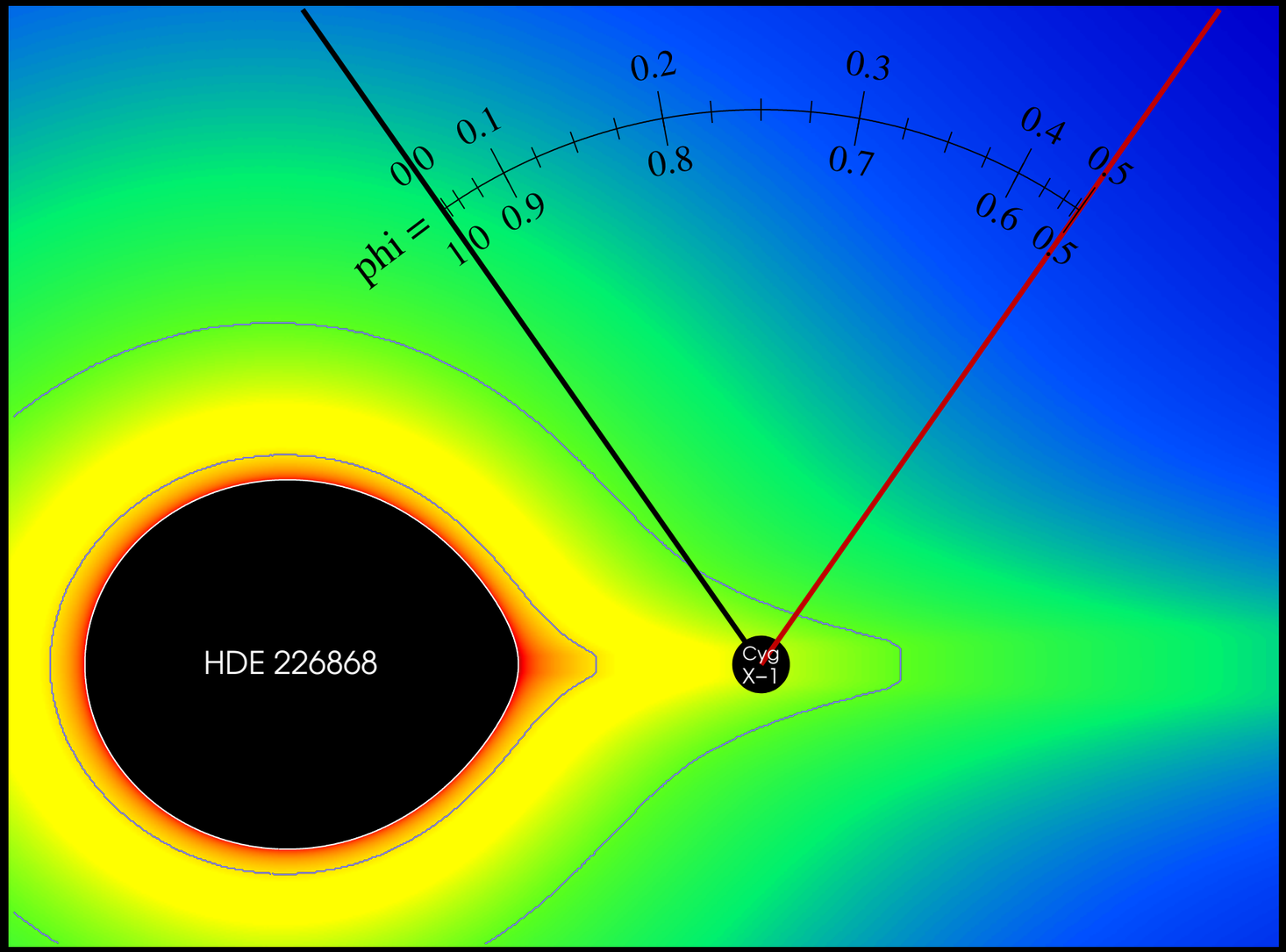

HDE 226868/Cyg X-1: Friend & Castor (1982), Gies et al. (2008): clumpy stellar wind/flow.

$10^{10}\,\mathrm{cm}^{-3} \leqslant n_{\mathrm{H}} \leqslant 10^{11}\,\mathrm{cm}^{-3}$

Clumps in Cyg X-1

Spectra: Profiles of Si XIV, Mg XII, Ne X

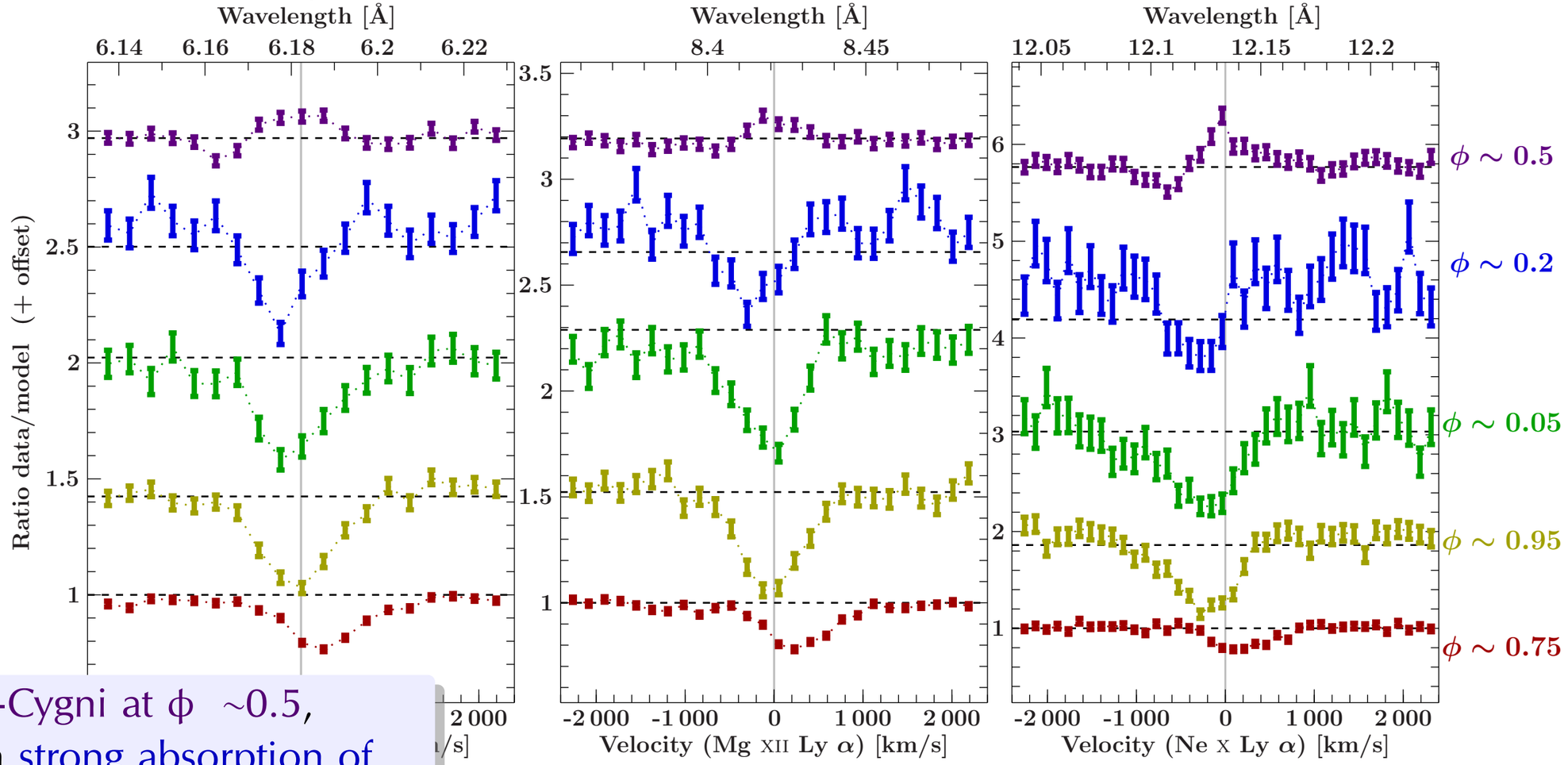

From P-Cygni at ϕ ∼0.5, through strong absorption of low blueshift at ϕ ∼0 – 0.2, to redshifted absorption at ϕ ∼0.75.

Clumps in Cyg X-1

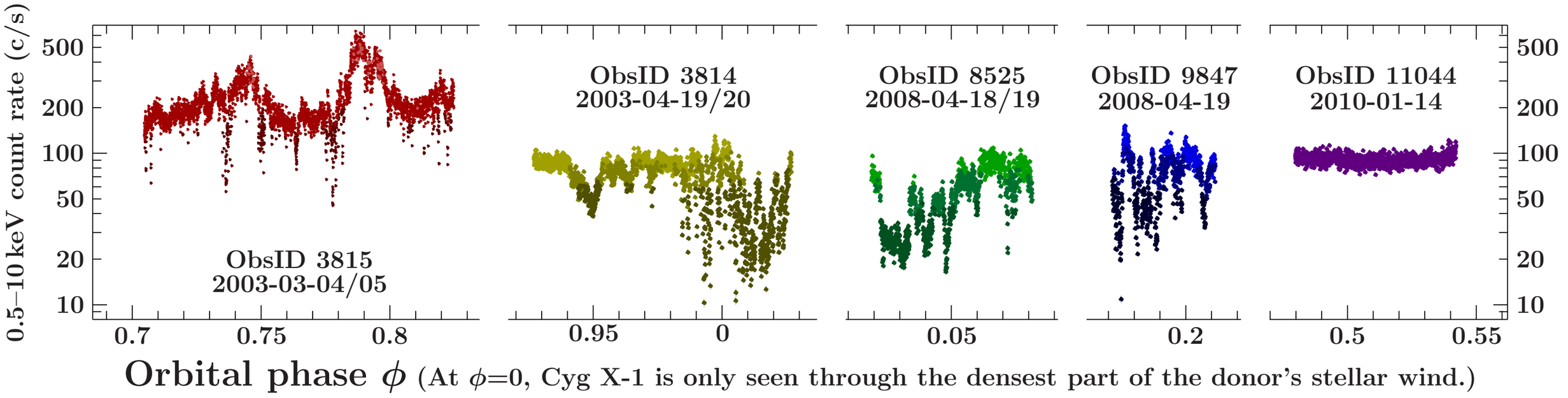

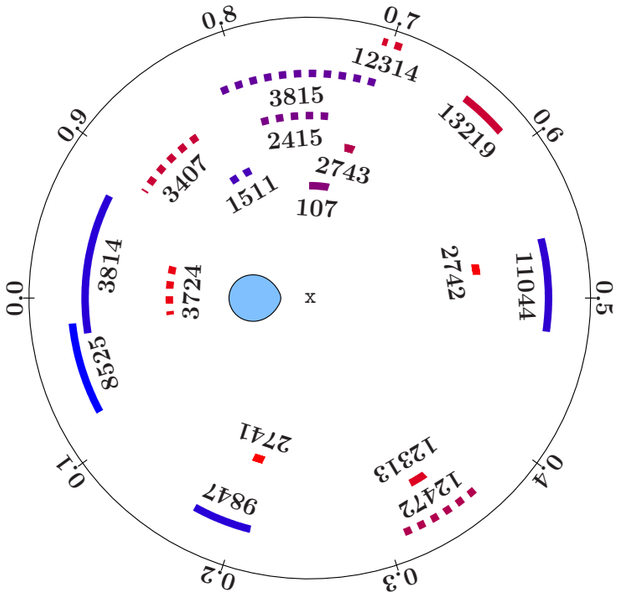

Dipping: strongest when looking through focused stream, not present at lower conjunction of BH

Clumps in Cyg X-1

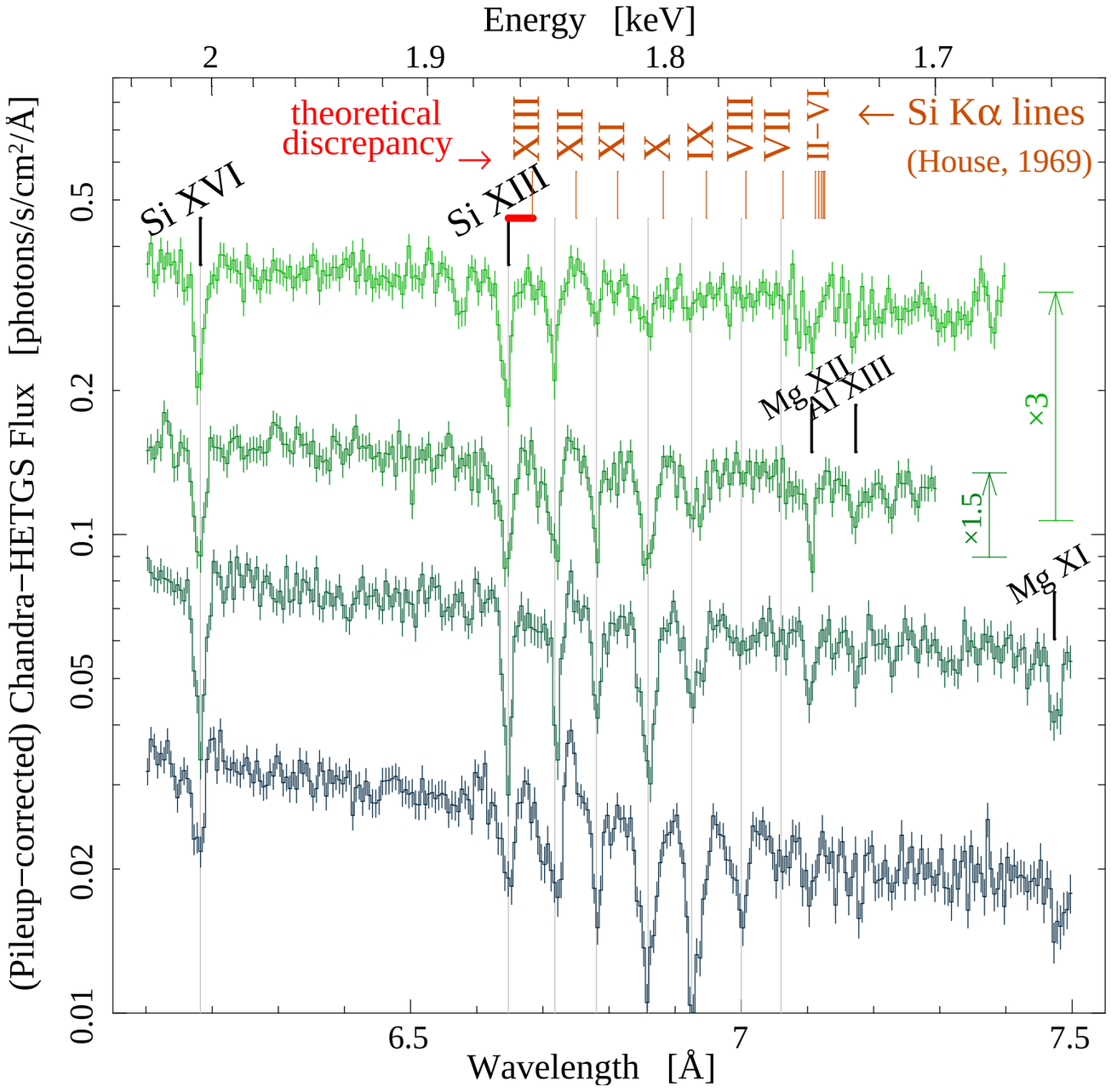

Dips: absorption lines allow to study ionization structure of dipping material

Deepest dip probing densest regions: lower ionization

>10 keV data: absorbing material embedded in Compton-thick medium

$E_{obs} - E_{lit} \neq 0$: Doppler shift or atomic physics?

Hell et al. (2013)

Electron Beam Ion Trap

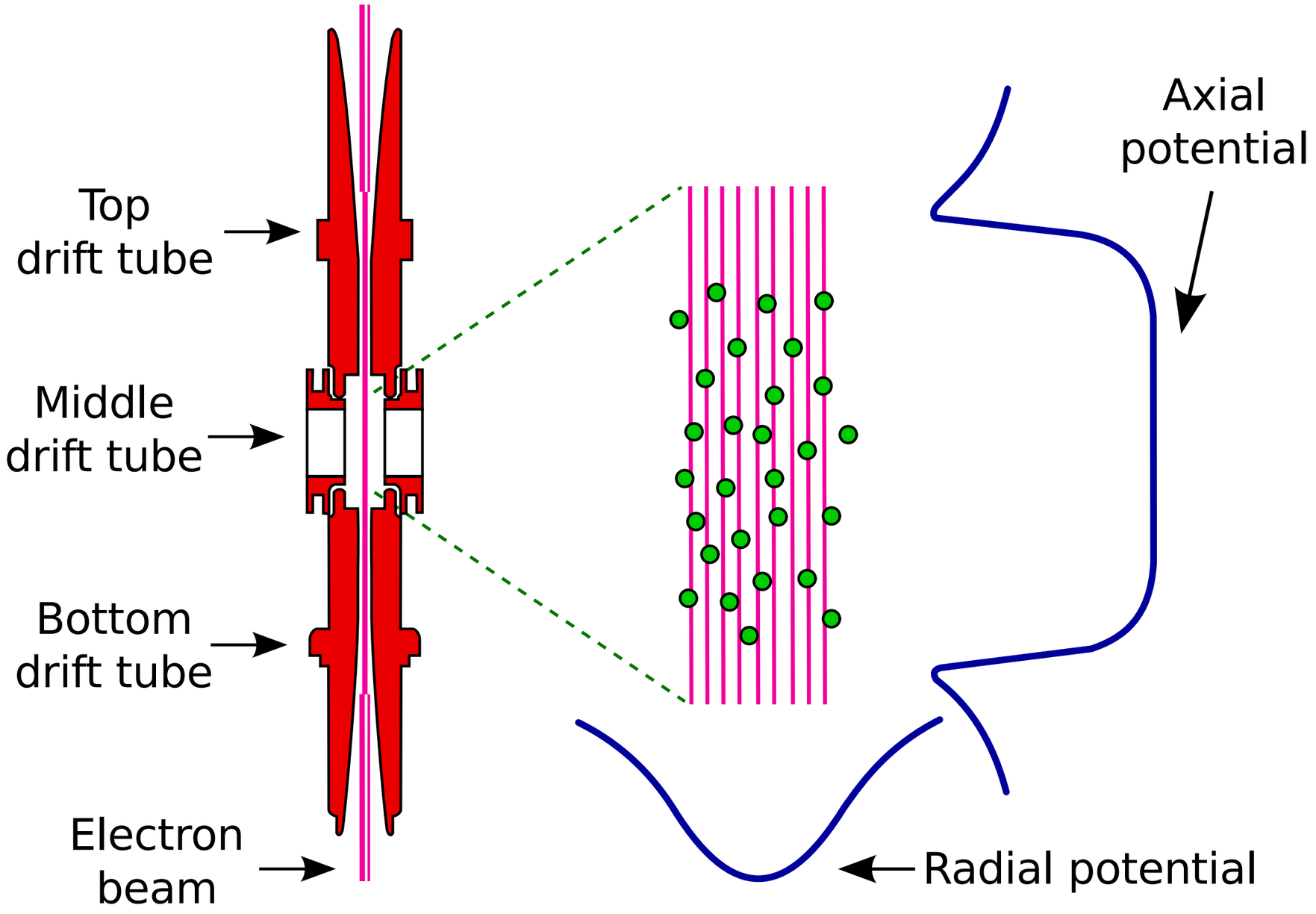

https://ebit.llnl.gov/overviewEBIT.html

Electron Beam Ion Trap

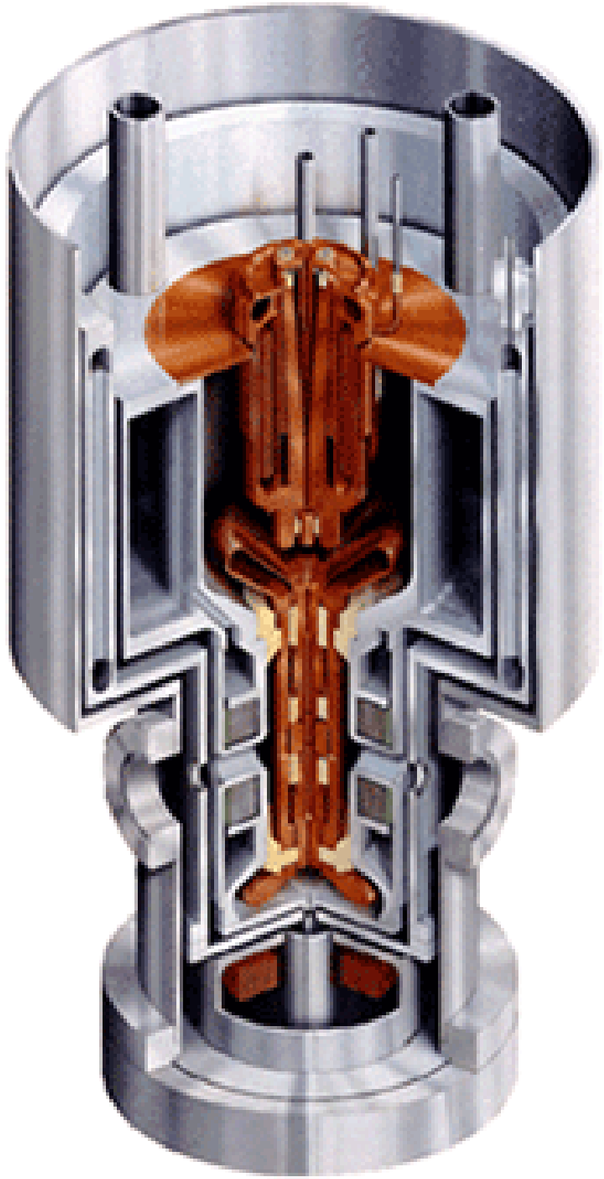

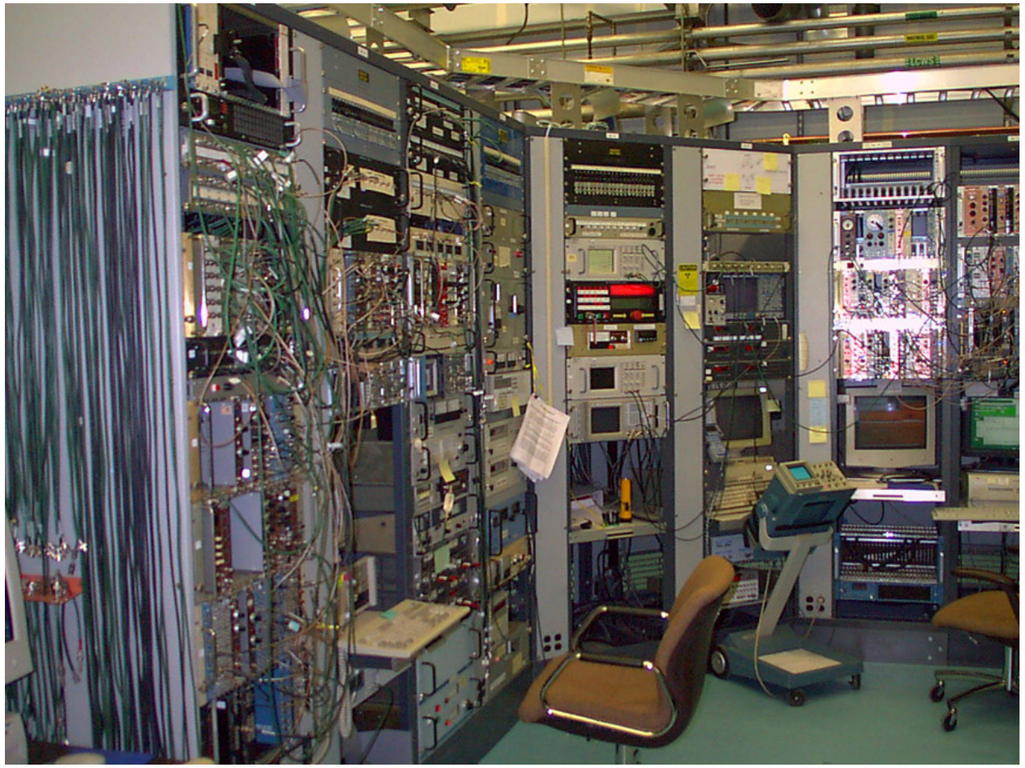

Use EBIT-I at LLNL

(also available as Super EBIT; up to bare Uranium, U^{92+}!)

Electron Beam Ion Trap

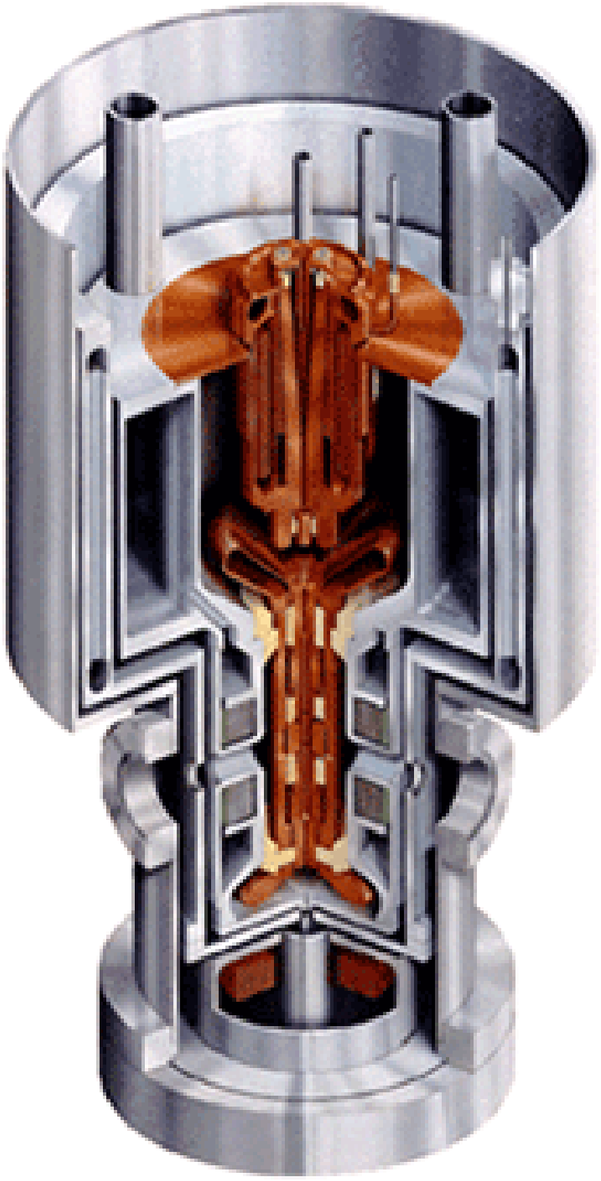

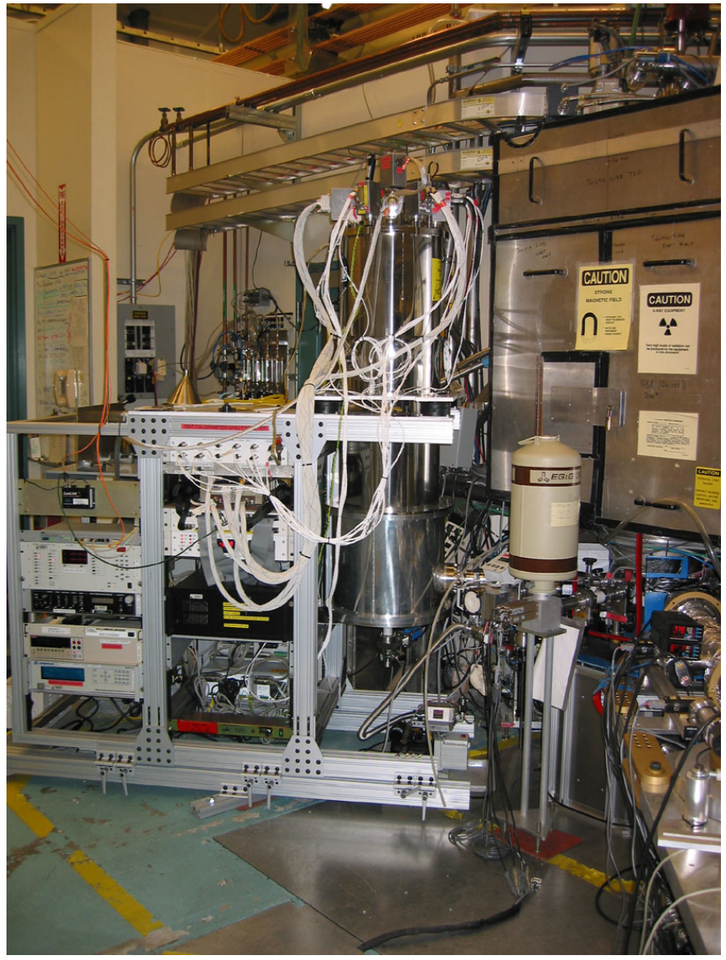

https://ebit.llnl.gov/EBITPhotoGallery.html

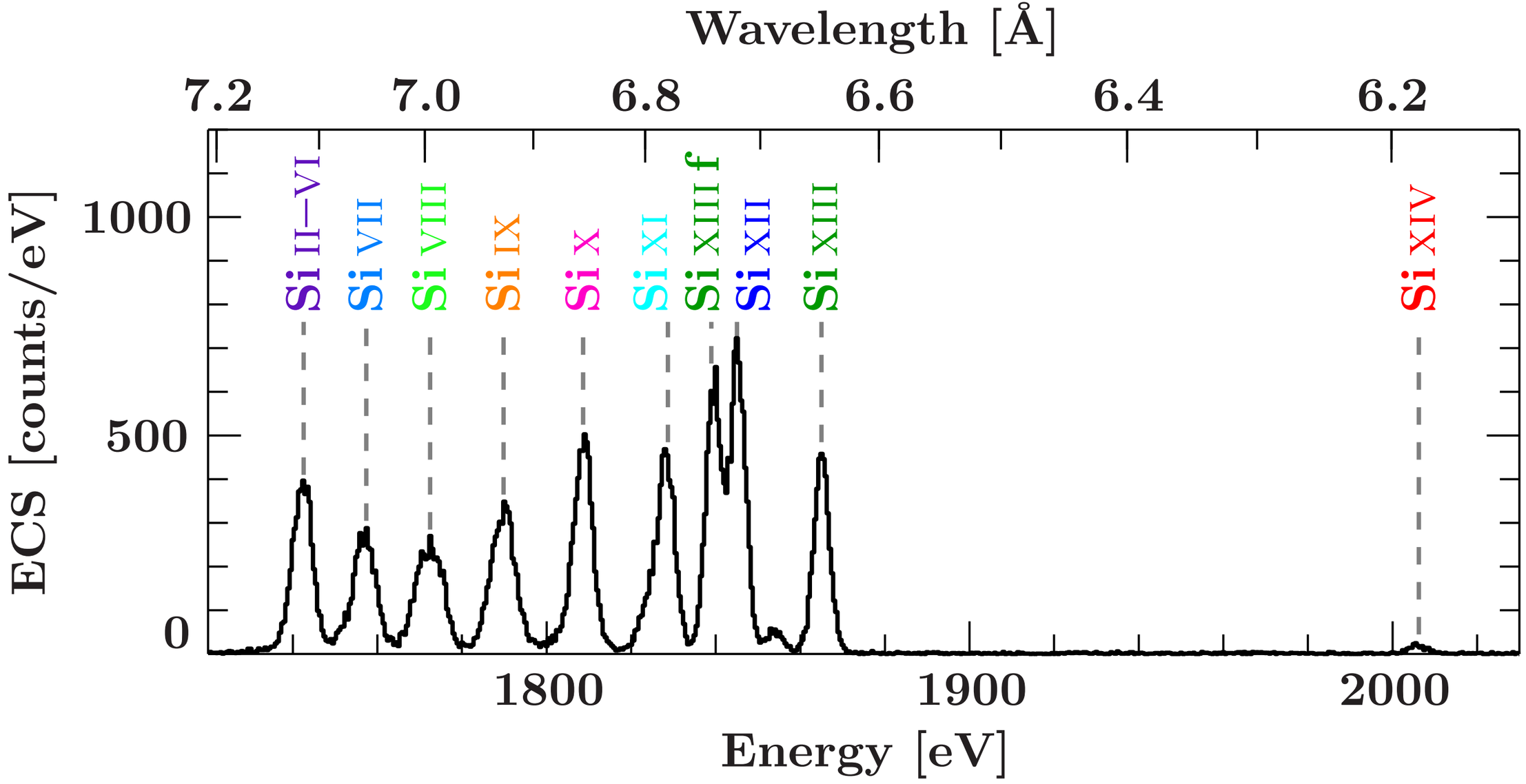
Wavelength [Å]
7.2
7.0
6.8
6.6
6.4
6.2
ECS [counts/eV]
1000
500
0
Si II–VI
Si VII
Si VIII
Si IX
Si X
Si XI
Si XIII f
Si XII
Si XIII
Si XIV
1800
1900
2000
Energy [eV]

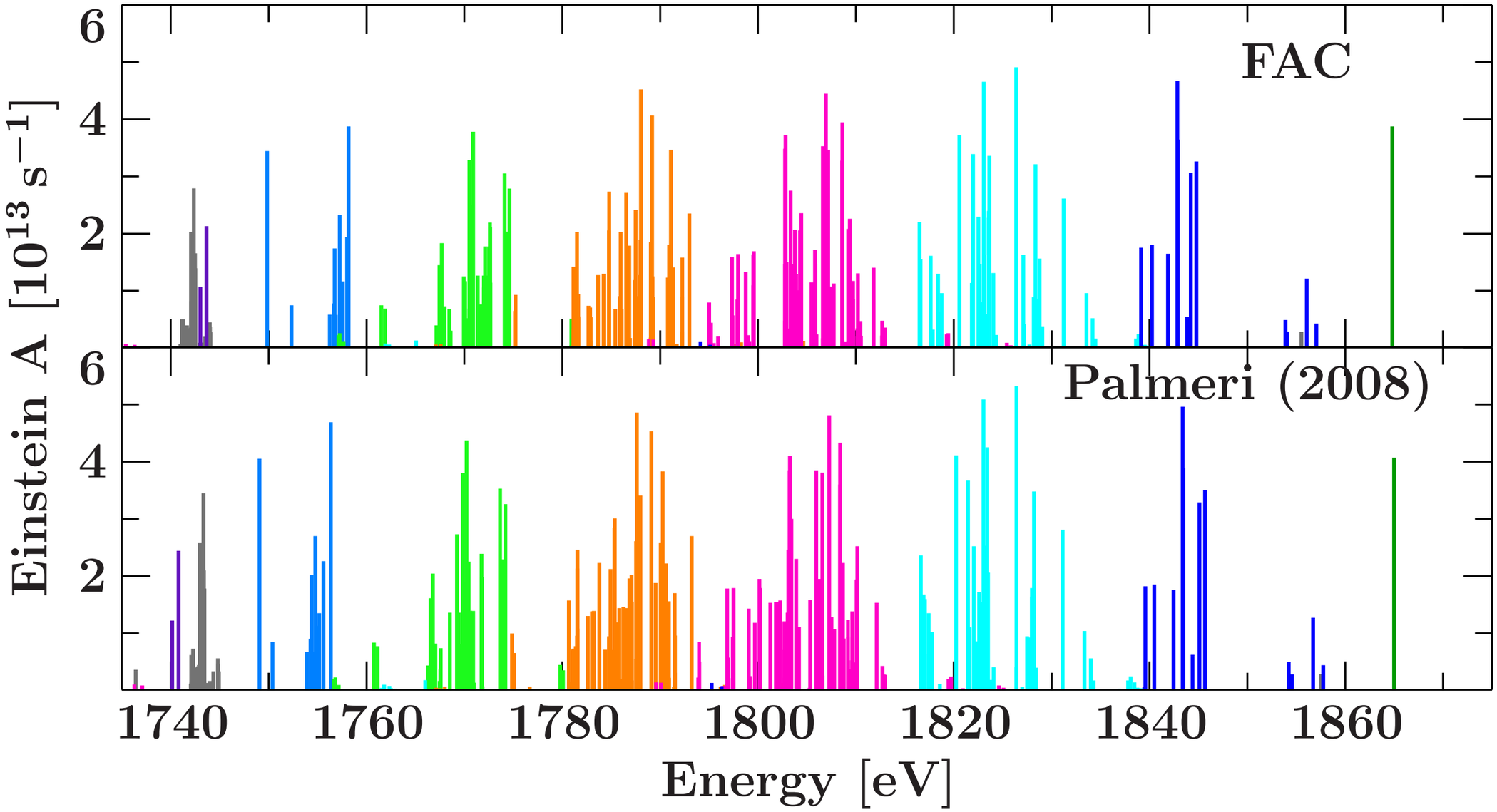

Comparison of jj-coupling (FAC; Gu, 2008) and LS-coupling calculations (Autostructure; Palmeri et al., 2008)

$\Longrightarrow$ Significant differences!

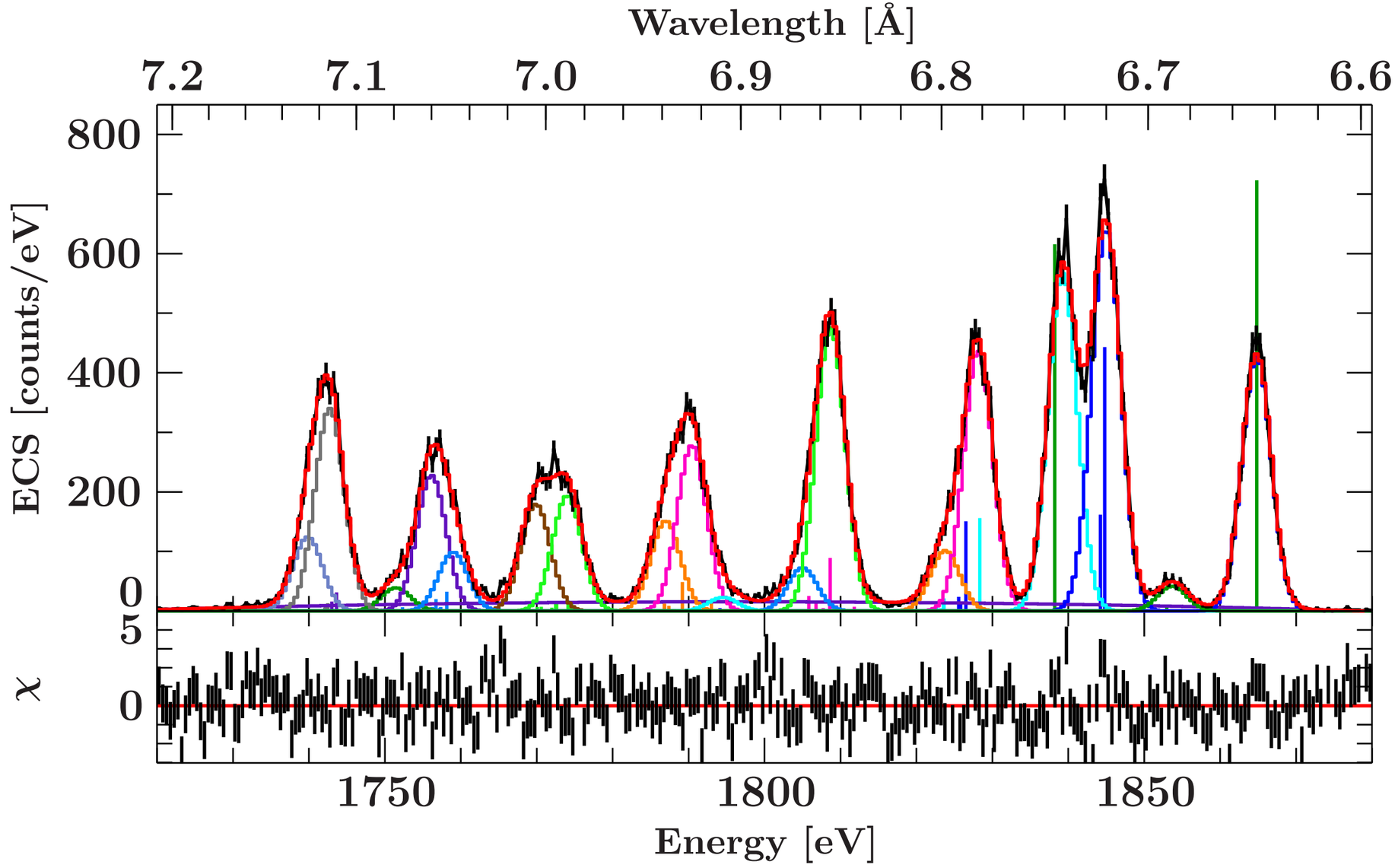

Comparison data – FAC *after* theory shift (0.32 eV).

Electron Beam Ion Trap

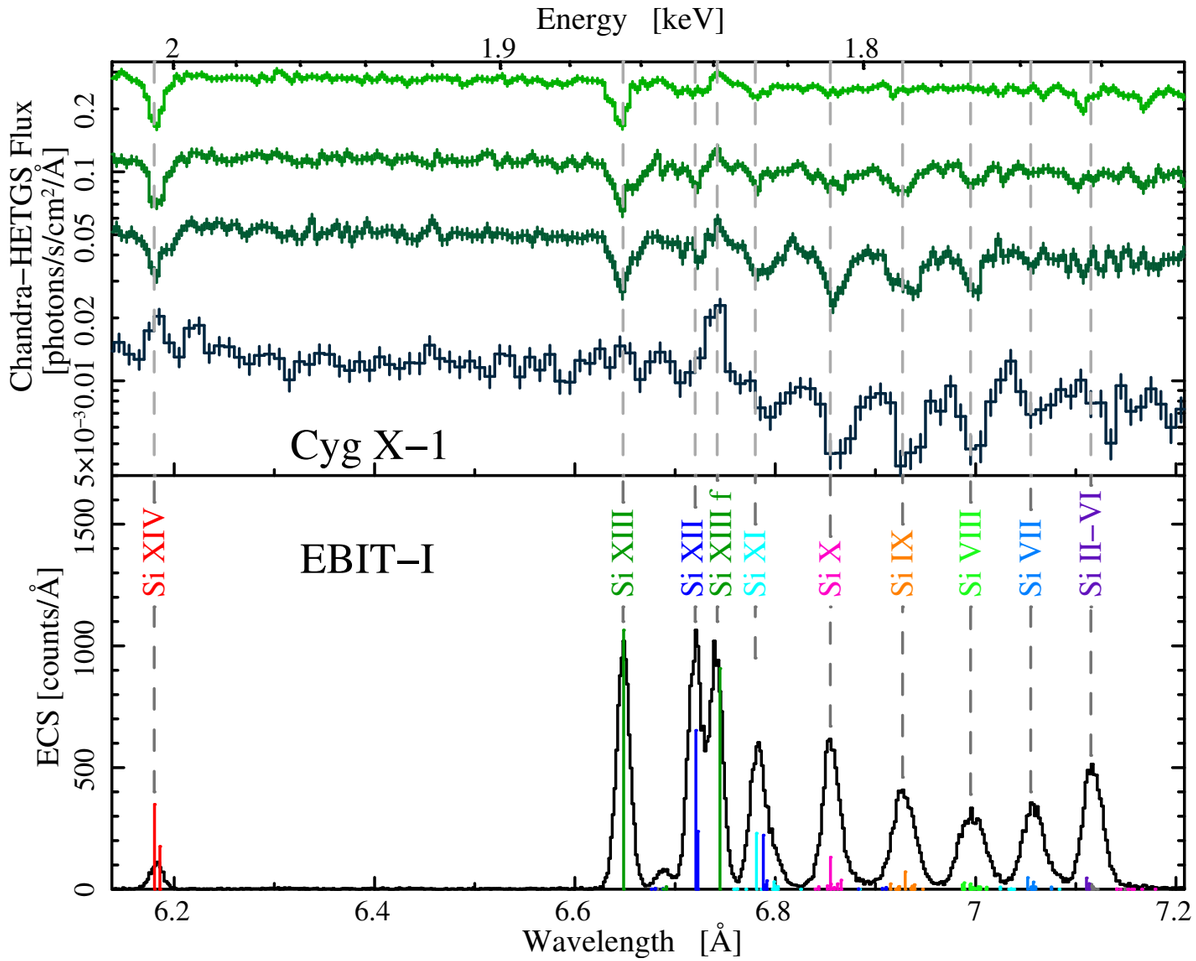

Hell, priv. comm.

For XRISM and Athena: availability of better atomic physics calculations and verified with laboratory measurements will be crucial!

Electron Beam Ion Trap

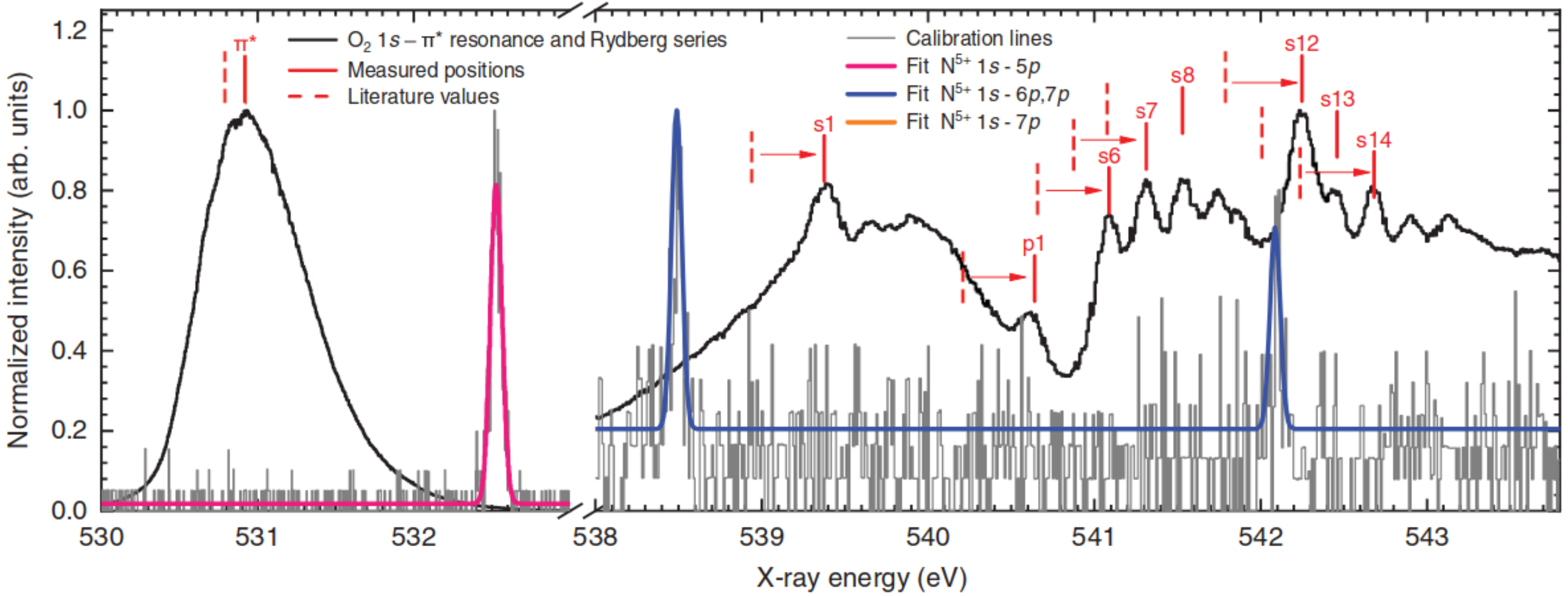

Leutenegger et al., 2020

For XRISM and Athena: availability of better atomic physics calculations and verified with laboratory measurements will be crucial!

Summary

- Most X-ray astronomical observations really are multi-color photometry; mainly: continua, plus some bright lines

  but provide good timing, imaging,...

- High resolution X-ray spectroscopy:
  - high diagnostic power $\Longrightarrow$ n, T, Doppler,...
  - today: no real imaging possible, photon starved, mainly soft X-rays
- Later this year: XRISM
  - launch this August – start thinking about proposals now
  - good resolution, Fe band very interesting
- Mid-2030s: ATHENA: Real imaging spectroscopy

  potentially: US X-ray probes such as ARCUS or LEM

- crucial for all of us X-ray people:
  - Learn your atomic physics
  - Push for improvements in atomic databases

    If you think that atomic physics is understood, think again

Bibliography

Canizares, C., et al. 2005, PASP, 117, 1144

den Herder, J. W., Brinkman, A. C., Kahn, S. M., et al. 2001, A&A, 365, L7

Friend, D. B., & Castor, J. I. 1982, ApJ, 261, 293

Gies, D. R., Bolton, C. T., Blake, R. M., et al. 2008, ApJ, 678, 1237

Gu, M.-F., 2008, Can. J. Phys., 86, 675

Güdel, M., 2004, Astron. Astrophys. Rev., 12, 71

Hanke, M., 2011, Ph.D. thesis, Friedrich-Alexander-Universität Erlangen-Nürnberg, Erlangen

McCammon, D., 2005, in Cryogenic Particle Detection, ed. C. Enss, Topics in Applied Physics 99, (Heidelberg: Springer), Chapt. 1, 1

Miškovičová, I., Hell, N., Hanke, M., et al. 2016, A&A, 590, 114

Palmeri, P., Quinet, P., Mendoza, C., et al. 2008, ApJS, 177, 408

Sutherland, R. S., & Dopita, M. A. 1993, ApJS, 88, 253

Vink, J., 2012, Astron Astrophys Rev, 20, 49